EDITORIAL BOARD OF THE JOURNAL OF AGRICULTURE AND DEVELOPMENT

EDITORIAL SECRETARIAT

Contact information:
Nong Lam University
Room 404, Thien Ly Building
Linh Trung Ward, Thu Duc City, Ho Chi Minh City, Vietnam
Tel: (84-28)37245670
Email: jad@hcmuaf.edu.vn

The Journal of Agriculture and Development
Volume 23 - Specical Issue 2 (2024)
pISSN 2615-9503
eISSN 2615-949X

CONTENT

Current situation and solutions for efficient use of dragon fruit planting land in Bac Binh district, Binh Thuan province

Phuong T. B. Nguyen[1]*, Lam N. Le[1], Hung D. Tran[1], Quyet T. Nguyen[1], & Cang V. Nguyen[2]

[1]Faculty of Land and Real Estate Management, Nong Lam University, Ho Chi Minh City, Vietnam

[2]Office of The District Party Committee of Bac Binh District, Binh Thuan, Vietnam

ARTICLE INFO

Research Paper

Received: September 09, 2024
Revised: October 22, 2024
Accepted: October 31, 2024

Keywords

Binh Thuan
Dragon fruit
Exported fruit
GAP
Land use

***Corresponding author**

Nguyen Thi Bich Phuong
Email:
phuong.nguyenthibich@hcmuaf.edu.vn

ABSTRACT

The objectives of the study were to evaluate the current state of land use for dragon fruit cultivation in Bac Binh district, Binh Thuan province, identify influencing factors, and propose solutions for the sustainable and effective use of this land. The study utilized survey data from dragon fruit growers and expert consultations to assess the current situation and development trends, serving as a basis for proposing solutions. The key findings were as follows: (1) The area planted with dragon fruit increased by 3,767 ha from 2010 to 2020, but it began to decrease sharply from 2021. By 2023, the cultivated area declined to 2,933 ha, a reduction of 1,718 ha (36.94%) compared to 2020. (2) Productivity remained relatively high, with an average output of about 25 - 30 tons/ha during the on-season and 20 tons/ha during the off-season. From 2010 to 2020, the average profit was approximately 6,000 - 6,800 USD/ha per year, but since 2021 profits had declined sharply, averaging only about 3,744 USD/ha per year, with a continued downward trend leading to a gradual reduction in dragon fruit cultivation. (3) The main factors contributing to the shrinking area of dragon fruit land included economic factors such as selling price, profit, and export challenges, as well as technical and production planning factors. (4) The study proposed solution groups, including organizing production based on the value chain, supporting the development of large-scale enterprises, policy solutions, and human resources solutions.

Cited as: Nguyen, P. T. B., Le, L. N., Tran, H. D., Nguyen, Q. T., & Nguyen, C. V. (2024). Current situation and solutions for efficient use of dragon fruit planting land in Bac Binh district, Binh Thuan province. *The Journal of Agriculture and Development* 23 (Special issue 2), 1-13.

1. Introduction

Dragon fruit belongs to the cactus family (Cactaceae), a plant originating from dry tropical regions, making it well-suited to withstand heat and drought. Currently, it is grown in many parts of the world, especially in Asia, including Vietnam, Thailand, Malaysia, Indonesia, and China. In Vietnam, dragon fruit is mainly cultivated in the provinces of Binh Thuan, Long An, and Tien Giang, which together account for nearly 85% of the country's dragon fruit cultivation area. Among these, Binh Thuan was once the largest dragon fruit-producing province, contributing 52% of the cultivation area and more than 50% of the total output nationwide (Vo et al., 2021). Dragon fruit is considered a key fruit crop in Vietnam and holds a competitive advantage in the global market. It is grown on a commercial scale with a total area of about 37,000 ha. By the end of 2020, Binh Thuan had approximately 33,730 ha under cultivation, yielding an output of 650,000 tons per year, which represents 80% of the country's total dragon fruit production (PCBTP, 2022). Dragon fruit from Binh Thuan is consumed in two forms: domestic consumption (about 15%) and export (about 85%), with the majority exported to China. Between 2016 and 2022, Binh Thuan province officially exported nearly USD 53 million worth of dragon fruit, equivalent to 43,748 tons. The remaining amount was sold abroad through unofficial channels via border gates. The value of these border exports contributed USD 2,637 million to Binh Thuan province, averaging about USD 376.7 million per year (SOB, 2022).

The export market for agricultural products is increasingly competitive, requiring high quality and strict adherence to food hygiene and safety standards. Since 2006, ASEAN has established a common GAP- Good Agricultural Practices process for member countries, and in 2008, the Ministry of Agriculture and Rural Development of Vietnam issued the VietGAP-Vietnamese Good Agricultural Practices standard to define the necessary criteria for agricultural products. This underscores the importance for Vietnamese agricultural products in general, and Binh Thuan dragon fruit in particular, to ensure high quality and food safety in order to expand export markets.

Bac Binh is a mountainous district of Binh Thuan province, located 68 km northeast of Phan Thiet city. The district's main economic activity is agricultural production, which accounts for 75% of its economy. The area planted with dragon fruit represents 12.04% of the total area in Binh Thuan province. However, in recent years, both the area and output have tended to decrease sharply.

Therefore, researching „Current situation and solutions for effective land use for dragon fruit cultivation in Bac Binh district, Binh Thuan province" is highly necessary.

2. Materials and Methods

2.1. Overview of the research area

Bac Binh is located in the north of Binh Thuan province, with the center being Cho Lau town. It covers a natural area of 1,865.76 km², making it the largest district in terms of area among the districts of Binh Thuan province.

Figure 1 shows that the geographic coordinates range from 108°06'30" to 108°37'34" East longitude and from 10°58'27" to 11°31'38" North latitude, with:

- East longitude and from.

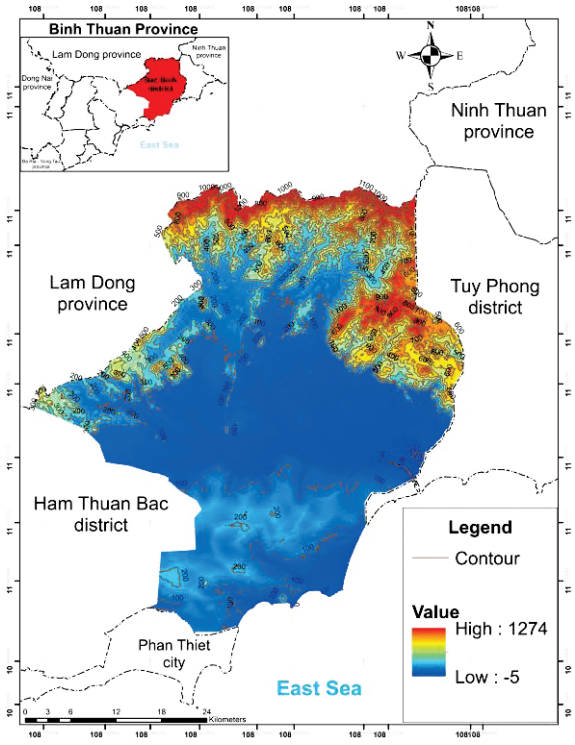

Figure 1. Digital elevation model map of study area.

- The West and Northwest bordering Ham Thuan Bac district and Di Linh district, Lam Dong province.

- The East and Northeast bordering Tuy Phong district.

- The Southeast bordering the East Sea.

- The South and Southwest bordering the East Sea and Phan Thiet city.

Bac Binh district has 16 communes and 2 towns, with diverse and potential natural resources. The terrain is complex, gradually tilting from Northwest to Southeast, with altitude decreasing towards the plains along the Luy River and Mao River.

The climate is tropical monsoon with low rainfall, which often results in droughts during the dry season and floods during the rainy season. The land resources of this district are highly specific, including 6 main soil groups, with the gray soil group accounting for the highest proportion at 56.77%. This soil is widely distributed in Phan Hoa, Phan Ri Thanh communes, Luong Son town, and other areas. Bac Binh district has land resources, water resources, and a climate that are very suitable for growing dragon fruit trees (SOB, 2022).

Socio-economically, the population of Bac Binh district is 131,680 people, with an average population density of 70.46 people/km^2, and rural areas account for 78.50% of the total population. The average income per capita is estimated at 1,707.2 USD/person per year. The economic structure among the sectors: Agriculture- Industry and Construction-Trade and Services was 29.61%, 20.69%, and 49.70%, respectively (PCBTP, 2022).

2.2. Materials and Methods

2.2.1. Materials

Documents and secondary data collected from relevant agencies are listed in Table 1 below:

Table 1. Secondary documents and data

No.	Documents/data	Place of supply
1	Data on natural conditions, natural resources and socio-economic development.	Statistics Department, Department of Agriculture and Rural Development, Department of Economics, People's Committee of Bac Binh district
2	Report on the socio-economic situation.	
3	Data on productivity, output and export of dragon fruit in Bac Binh district.	
4	Assessment of land adaptation in Bac Binh district; Land inventory results 2015, 2020, 2021, 2022	Bac Binh district Department of Resources and Environment.
5	Data on land use planning and agricultural planning.	Department of Agriculture and Rural Development; People's Committee of Bac Binh district.

2.2.2 Methods

Primary documents and data: Consulted with experts identified as managers in relevant fields, comprising 20 respondents including: agricultural officials in communes with relatively large dragon fruit growing areas, the Division of Agriculture and Rural Development, the Department of Natural Resources and Environment, enterprises and cooperatives purchasing dragon fruit.

In addition, the study conducted a survey of households directly growing dragon fruit. The number of survey questionnaires was determined using the formula proposed by Yamane (Yamane, 1967):

$$n = \frac{N}{1 + N \times e^2}$$

In there:

n: the number of household to be investigated;

N: the total number of households growing dragon fruit in the area;

e: the level of significance (with a confidence level of 90 to 99%).

According to the Statistical Yearbook of Bac Binh district in 2022, there are 3,800 households growing dragon fruit (N = 3,800), with a significance level of e = 0.1, n = 98 votes can be determined. The survey content mainly covers area, yield, selling price, use of seeds and fertilizers, profit efficiency, and jobs brought from growing dragon fruit trees.

- Method to evaluate economic efficiency: The economic efficiency of land used for growing dragon fruit is evaluated using the formula: Pr = GO - C

In there:

Pr: profit

GO: production value

C: the total cost

The assessment level hierarchy is presented in Table 2:

Table 2. Hierarchy of economic efficiency assessment

Rating level	Symbol	Total cost (million VND/ha per year)	Total revenue (million VND/ha per year)	Profit (millio VND/ha per year)	Rate (times)
Very high	VH	> 100	> 200	> 100	> 2.0
High	H	70 - 100	150 - 200	70 - 100	1.5 - 2.0
Medium	M	50 - 70	100 - 150	30 - 70	1.3 - 1.5
Short	L	< 50	< 100	< 30	< 1.2

Source: Sub-NIAPP (2020).

- Map construction method:

+ Digital elevation model (DEM) map: The DEM map shows the geographical position of Bac Binh district, and also shows the slope and convexity of the terrain, which are factors of interest in the arrangement of agricultural land use.

+ Thematic maps: This study employs Microstation and ArcGIS software to arrange and edit land use status maps. Dragon fruit land allocation map has been built using AcrGIS software on the basis of the current land use status map of Bac Binh district combined with the layer of current status of dragon fruit trees allocated in communes in 2022.

3. Results and Discussion

3.1. Current status of agricultural land use

3.1.1. Current status of agricultural land use

Table 3 shows that agricultural land during this period increased by 4,575.73 ha compared to 2010. Specifically, the area of land planted with dragon fruit in 2010 was 669 ha (accounting for 0.4% of the total agricultural land area). By 2020, it had increased to 4,436 ha (2.57%) (PCBTP, 2023).

Table 3. Situation of agricultural land use in Bac Binh district in the period 2010 - 2020

No.	Land use criteria	Current land use status (ha)				
		2020	2015	Compared with 2015	2010	Compared with 2010
	Total agricultural land area	172,370.79	174,257.15	-1,886.36	167,795.06	4,575.73
1	Rice growing land	16,322.88	12,119.73	4,203.15	10,678.12	5,644.76
2	Other annual crops	29,182.02	38,933.46	-9,751.44	44,352.47	-15,170.45
3	Other annual crops	35,247.27	31,642.22	3,605.05	19,484.95	15,762.32
	Growing dragon fruit	*4,436.00*	*2,500.00*	*1,936.00*	*669.00*	*3,767.00*
4	Protective forest land	47,000.66	47,150.48	-149.82	58,640.82	-11,640.16
5	Production forest land	44,129.47	44,104.74	24.73	34,200.17	9,929.30
6	Aquaculture land	400.88	283.70	117.18	418.92	-18.04
7	Other agricultural land	87.61	22.82	64.79	19.61	68.00

Source: Division of Resourc.es and Environment of Bac Binh district (2022).

3.1.2. Evolution of main crops

The data of Table 4 shows that crop areas tend to increase, particularly in cassava, rice, fruit trees, and vegetables. Notably, the area planted with dragon fruit increased sharply during the period 2015 - 2021, but by 2022, it had suddenly decreased to only 2,933 ha.

Table 4. Developments of main crops in Bac Binh district in the period 2010 - 2022

No	Type land use	Area (ha)				
		2010	2015	2020	2021	2022
1	Rice 2 - 3 crops	26,305	29,793	27,996	28,028	28,058
2	Cassava	6,308	5,162	6,067	6,072	6,076
3	Dragon fruit	669	2,500	4,436	4,549	2,933
4	Beans of all kinds	4,052	4,573	3,972	3,975	3,979
5	Fruit tree (mango, grapefruit, jackfruit...)	1,935	1,874	2,449	2,336	2,340
6	Vegetables	1,827	1,271	1,864	2,664	3,454
7	Peanut	2,514	2,445	1,783	1,785	1,788
8	Cashew tree	1,089	1,089	653	1,453	2,243

Source: Division of Agriculture and Rural Development of Bac Binh district (2022).

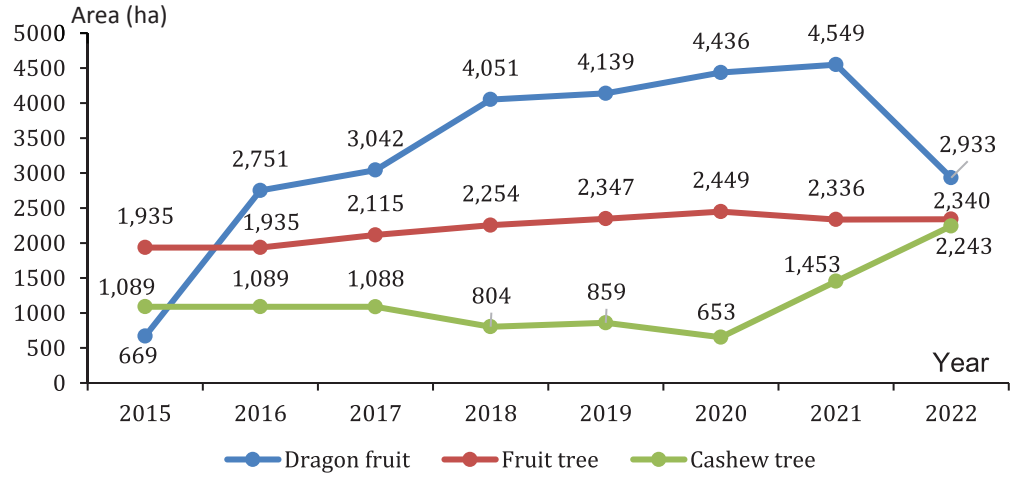

Figure 2. Evolution of perennial crop area in Bac Binh district in the period 2015 - 2022.

The majority of perennial tree areas in the study area are dragon fruit trees, cashew and fruit trees of all kinds (mango, grapefruit, jackfruit...). Figure 2 shows that the area of dragon fruit trees will decrease sharply from 2021, while the area of cashew trees will increase sharply, steadily from 2020 to 2022 while the area of fruit trees is more stable.

3.2. Current status of dragon fruit cultivation

3.2.1. Area, yield and output

The data Table 5 and Figure 3 show that during the period 2015 - 2021, the area planted with dragon fruit increased steadily each year, with a particularly sharp increase of 1,009 ha from 2017 to 2018. However, beginning in 2022, the area of dragon fruit shows signs of a sharp decline, dropping from 4,549 ha to just 2,933 ha. Additionally, productivity has shown a slight and steady increase over the years as growers increasingly adopt new technical processes. Due to the sharp decrease in the cultivated area, dragon fruit production in 2022 was only 61,475 tons, a reduction of 33,644 tons compared to 2021.

Table 5. Area, productivity and output of dragon fruit in the period 2015 - 2022

Year	Area (ha)	Productivity (ton/ha)	Output (tons)
2015	2,500	21.89	54,725
2016	2,751	18.21	50,096
2017	3,042	20.08	61,083
2018	4,051	20.36	82,478
2019	4,139	20.87	86,381
2020	4,436	20.89	92,668
2021	4,549	20.91	95,119
2022	2,933	20.96	61,475

Source: Division of Agriculture and Rural Development of Bac Binh district (2022).

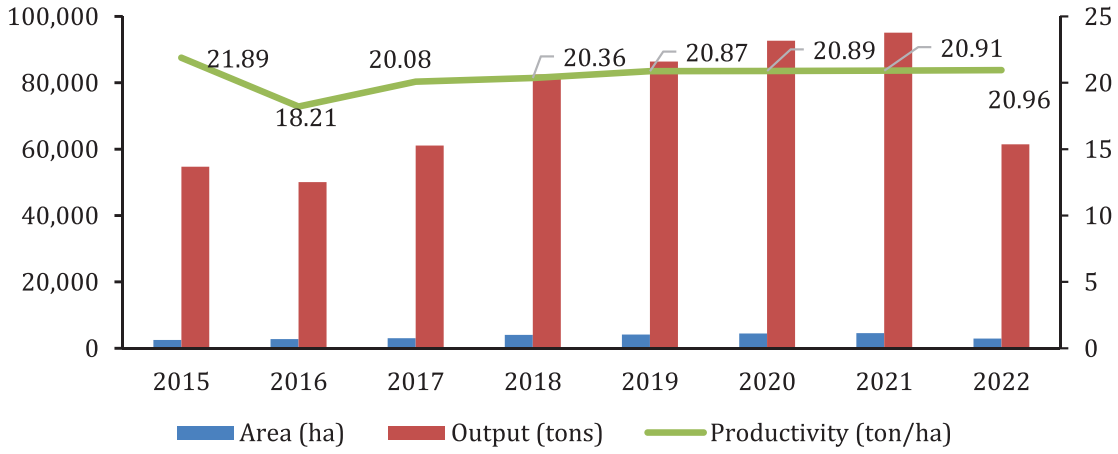

Figure 3. Development of dragon fruit area, productivity, and output in the period 2015 – 2022.

3.2.2. Distribution of dragon fruit

Table 6 shows that by 2020, the area of dragon fruit planted across all communes and towns totaled 4,436 ha, with an annual increase. However, dragon fruit trees are primarily distributed in the following communes and towns: Phan Hiep (478.5 ha), Hong Thai (456.7 ha), Phan Thanh (439.8 ha), Cho Lau Town (425.7 ha), Hai Ninh commune (425 ha), Song Luy commune (413.5 ha).

Table 6. Current distribution status of dragon fruit

No	Administrative unit (commune/town)	Area over the years (ha)				
		2010	2015	2020	2021	2022
1	Cho Lau town	35.5	175.7	425.7	438.7	268.0
2	Luong Son town	20.4	153.1	203.1	203.1	60.0
3	Binh Tan	42.0	162.0	181.0	181.0	86.0
4	Phan Tien	10.0	25.0	25.0	25.0	9.0
5	Song Luy	32.0	259.5	413.5	454.8	180.0
6	Phan Lam	3.0	15.0	55.0	55.0	0.0
7	Phan Son	2.0	9.0	14.0	14.0	0.0
8	Phan Điên	42.3	86.8	219.8	129.8	129.0
9	Phan Thanh	67.9	189.8	439.8	442.8	147.0
10	Phan Hiep	45.8	178.5	478.5	492.6	270.0
11	Phan Ri Thanh	88.0	178.9	278.9	288.9	236.0
12	Phan Hoa	35.0	215.8	265.8	265.8	157.0
13	Binh An	96.0	176.0	226.0	226.0	159.0
14	Song Binh	25.8	146.7	146.7	146.7	53.0
15	Hoa Thang	25.5	82.1	124.1	124.1	207.0
16	Hong Thai	85.1	156.7	456.7	487.8	760.0
17	Hai Ninh	79.5	175.0	425.0	425.0	211.0
18	Hong Phong	5.0	25.0	35.0	35.0	1.0
	Total	669.0	2,403.0	4,436.0	4,549.0	2,933.0

Source: Division of Agriculture and Rural Development of Bac Binh district (2022).

In 2022, the area of land used for dragon fruit cultivation decreased sharply. Table 6 and Figure 4 show that some units, such as Phan Lam and Phan Son, have no cultivated area.

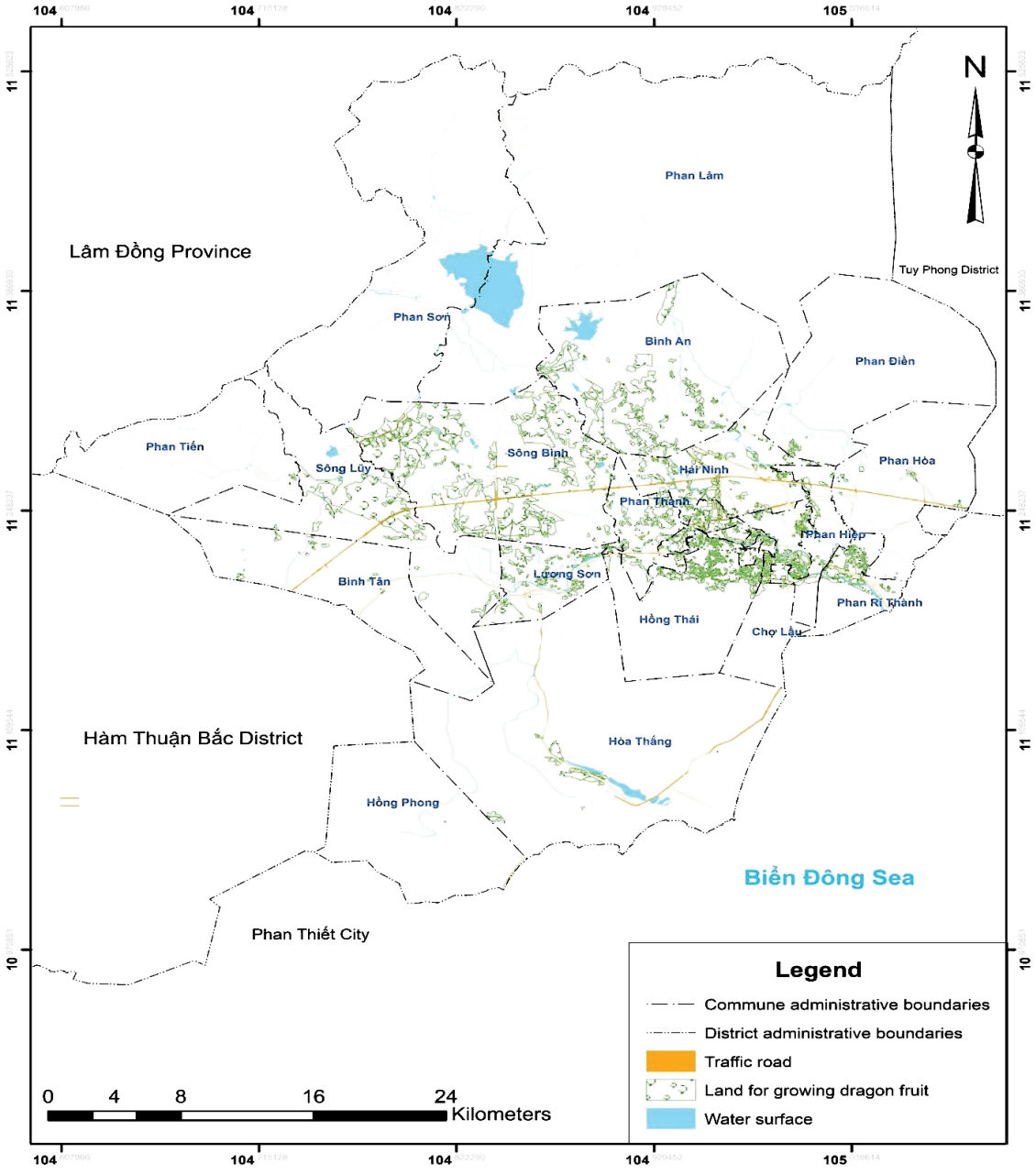

Figure 4. Map of current distribution status of dragon fruit in Bac Binh district in 2022.

3.3. Evaluation of the effectiveness of land use for dragon fruit cultivation

3.3.1. Land adaptation of dragon fruit

Regarding ecological requirements, the most suitable temperature for growing dragon fruit is between 21 and 29°C, with a maximum of no more than 40°C. It is especially suitable for growing in areas with average rainfall and a distinct dry season. Dragon fruit prefers strong light intensity; if it is shaded or the number of hours of light is low, the stems will become weak and flowers will develop slowly (Nguyen, 2022).

Dragon fruit is highly resistant to unfavorable environmental conditions such as drought, but its ability to withstand waterlogging is not high. Dragon fruit can be grown on many different types of soil, from sandy loam to clay loam. However, sandy loam soils with high organic content and good drainage are most suitable for growing dragon fruit. Suitable soil pH ranges from 5.5 to 7.0 (Nguyen, 1997). For the tree to grow well and produce many large fruits, it is necessary to plant dragon fruit in areas with active irrigation, especially during the periods of flower bud development, flowering, and fruiting (Pham et al., 2016; Nguyen, 2022).

Results of assessing natural adaptability according to the method of FAO (1976) show that dragon fruit growing soil in Bac Binh district has a degree of adaptation expressed in the following order: S1 - very adaptable, S2 - adaptable , S3 - less adaptable. Dragon fruit in region S1 has a yield of 24 - 25 tons/ha, S2 was 20 - 21 tons/ha and S3 was 15 - 18 tons/ha. More than 80% of dragon fruit growing land in Bac Binh district has natural adaptation level S2 (Nguyen & Le, 2021).

Assessing sustainable adaptation according to the FAO method (1993, 2007), in addition to natural factors, socio-economic factors also contribute significantly to the level of crop adaptation. For example, dragon fruit in the natural adaptation zone S2 have good yields (20 - 21 tons/ha), but due to high costs (in some places with unfavorable traffic conditions or small-scale production), the proportion of mechanization application is still low. Transportation costs and production costs are high, leading to low economic efficiency (profit (GM) = 2,400 USD/ha, B/C = 1.2). The level of people's acceptance is low, and these factors cause the level of sustainable adaptation to decrease to S3 or even N- no adaptation (Nguyen & Le, 2021).

3.3.2. Analysis of land use efficiency for dragon fruit cultivation

3.3.2.1. Economic efficiency

The results of processing 98 survey forms on the effectiveness of growing dragon in Bac Binh district, considering the cost, revenue, and profit levels, are divided into three levels: high, medium, and low in Table 7.

Table 7. Analysis of economic efficiency of dragon fruit under normal production conditions

No	Category	Unit	Level		
			High	Medium	Short
1	Total cost/ha	USD	5,839.7	5,399.1	4,944.8
1.1	Material costs	USD	2,336.6	2,052.2	1,768.2
1.2	Labor costs	USD	1,920.0	1,920.0	1,920.0
1.3	Other costs	USD	1,583.1	1,416.9	1,256.6
2	Total revenue/ha	USD	11,000	8,652	7,416
2.1	Productivity	(tons/ha)	25	21	18
2.2	Price (average)	USD/kg	0.44	0.41	0.41
3	Economic efficiency/ha				
3.1	Profit	USD	5,160.3	3,747.3	3,460.0
3.2	Aggregate profit	USD	6,816.3	5,667.3	5,300.0
3.3	Revenue/Cost (R/C)		1,88	1,60	1,50
3.4	Profit/Cost (P/C)		1,17	1,05	1,09

In general, the productivity of dragon fruit cultivation in Bac Binh district are relatively stable, and costs are less volatile. Therefore, economic efficiency (profit) mainly depends on the price. According to the results, when the price of dragon fruit is stable at 0.41 - 0.44 USD/kg, growers had profitable, and higher output yield more profit. However, from the end of 2022 until now, the price of dragon fruit has continuously decreased, fluctuating between 0.08 and 0.16 USD/kg. At times, the price fell below 0.08 USD, and traders did not buy it. And currently, the price has increased to between 0.32 - 0.48 USD/kg. In reality, stable dragon fruit production depends greatly on the selling price, particularly the export price.

Additionally, according to the results of calculating the economic efficiency of the dragon fruit production model following VietGAP standards, for every 1 USD of VietGAP-standard production cost, the revenue is 2.26 USD, and the profit is 1.26 USD. The ratio of profit to revenue is 0.56, meaning that for every dollar of revenue, there is 0.56 USD of profit (Tran & Nguyen, 2017).

Table 8. Comparison of economic efficiency of dragon fruit produced normally and according to VietGAP standards

No	Category	Unit	Normal production	Manufactured according to VietGAP standards
1	Total cost /ha	USD	4,944.8 - 5,839.7	10,124
2	Revenue/Cost (R/C)	-	1.50 - 1.88	2.26
3	Profit/Cost (P/C)	-	1.09 - 1.17	1.26

Table 8 shows that the total cost of production according to VietGAP standards is twice as high as normal production costs, but in return, the selling price of products is also higher, so the profit/cost ratio is higher, and the products can be consumed domestically as well as meet more export market demands.

In addition to the economic efficiency analyzed above, using land to grow dragon fruit in Bac Binh district has also created jobs for a large number of agricultural workers. Survey results showed that 16% were less satisfied, and 8% were dissatisfied, with the main reason being the erratic fluctuations in dragon fruit prices, leading to unstable income for growers. As a result, they tend to want to switch to other more stable crops.

3.3.2.2. Social and environmental efficiency

Survey results of 98 dragon fruit growing households showed:

- Growing dragon fruit has created better jobs for farmers (56.67% of households are satisfied and 19.33% of households are very satisfied). However, there are also 16% of households who are less satisfied and 8% of households who are dissatisfied when growing dragon fruit because the selling price is unstable.

- There are 69.7% of surveyed households thought that costs would increase if too much chemical fertilizers and pesticides were used. Therefore, farmers have increasingly tended to choose pest-resistant crop varieties and use organic fertilizers to improve the quality of finished products.

- And in the assessment of sustainable adaptation of dragon fruit trees in Binh Thuan province, Bac Binh has a high level of S1 adaptation, meaning it has little impact on the environment (Nguyen & Le, 2021).

3.4. Solutions to improve land use efficiency for dragon fruit cultivation in Bac Binh district

3.4.1. Factors affecting land use for dragon fruit cultivation

According to the above evaluation results and the survey results of 20 managers related to the research field, it shows that dragon fruit productivity and output in Bac Binh district depends on the following factors:

- Dragon fruit selling price (95%).

- Production scale: dragon fruit growers are spontaneous, unplanned, and ready to change when selling prices decrease (85%).

- The export market is not stable; it still depends on the Chinese market (80%).

- Care techniques: introduction that applies science and technology is not yet popular (75%).

- Domestic consumption enterprises are small-scale and spontaneous (70%).

- Dragon fruit Seedlings (55%).

3.4.2. Proposing solutions to improve land use efficiency for dragon fruit cultivation

Based on an assessment of the current status of dragon fruit cultivation and a survey of dragon fruit growers and experts in agricultural land management and use, this study proposes several specific solutions:

(i) Development of production along the product value chain:

- To increase reliability of product quality.

- Meets export requirements to markets of many countries.

(ii) Solutions to support large-scale business development:

- Increase professional production output.

- Attract businesses with capital, science, technology, and market capacity to lead the value chain efficiently and sustainably.

(iii) Policy solutions:

- Support and create favorable conditions for the development of large-scale dragon fruit processing and consumption enterprises.

- Implement policies to support cooperatives, ensuring output for dragon fruit.

- Create a convenient process for farmers to grow dragon fruit according to GAP standards.

- Attract investment and build large-scale dragon fruit processing factories in industrial zones, helping to consume a large amount of output products during the on-season.

(iv) Human resources solutions:

- Training and equipping farmers with new farming techniques.

- Organize dragon fruit industry seminars and regularly update new technology.

- Attract highly qualified agricultural workers.

4. Conclusions

Bac Binh district had natural conditions, land resources, and climate that are highly favorable for growing dragon fruit. The highly adaptive S1 area used more than 25% of the total area, while the medium and low adaptive areas use only 14.87% and 2.88%, respectively. The potential to

expand the area for this crop in terms of natural adaptation was significant. Research results showed that dragon fruit output in Bac Binh district remained stable, fluctuating between 18.21 and 21.89 tons/ha. Therefore, the quantity of dragon fruit produced mainly depended on the area under cultivation. If the area was large, the quantity would be high, and vice versa. When grown according to VietGAP standards, yield and product quality were higher, but the investment cost of production according to this standard was 1.73 to 2.05 times higher.

The results also indicated that more than 85% of dragon fruit consumption came from foreign markets, mainly exported to China. If dragon fruit from Bac Binh district, and Binh Thuan province in general aims to expand export markets to countries such as Japan, Korea, and Canada, it is essential to improve product quality and ensure food safety according to GAP standards.

Therefore, this study proposed four groups of solutions to improve the efficiency of land use for dragon fruit cultivation: (i) development of production along the product value chain; (ii) solutions to support large-scale business development; (iii) Policy solutions; (iv) Human resources solutions.

Conflict of interest

The authors declare that they have no conflict of interest in this article.

Acknowledgements

The article was made from the research results of the master's thesis in Land Management, Faculty of Land and Real Estate Management, Nong Lam University Ho Chi Minh City in 2022 with the title "Assessment of the current situation and propose solutions to improve the efficiency of land use for dragon fruit cultivation in Bac Binh district, Binh Thuan province" by student Nguyen Van Cang, instructors Nguyen Thi Bich Phuong and Le Ngoc Lam.

References

Nguyen, N. C. (2022). *Assessment of land adaptation to serve the development of dragon fruit trees in Binh Thuan province* (Unpublished master's thesis). Nong Lam University, Ho Chi Minh city, Vietnam.

Nguyen, N. C., & Le, C. D. (2021). Application of the intergrated model of GIS and AHP for evaluating sustainable land-use of dragon fruit in Binh Thuan province. *Vietnam Journal of Earth Sciences* 64(3), 74 - 80.

Nguyen,V. K. (1997). *Dragon fruit*. Ho Chi Minh City, Vietnam: Agricultural publisher.

PCBTP (People's Committee of Binh Thuan province). (2022). Project for sustainable development of dragon fruit until 2030. Retrieved April 22, 2024, from https://skhdt.binhthuan.gov.vn/thong-tin-du-an/phe-duyet-de-an-phat-trien-ben-vung-cay-thanh-long-den-nam-2030-879841.

Pham, C. L., Nguyen, D. L., Le, H. T., Pham, V. H., & Nguyen, K. L. (2016). Application of GIS and analytical hierarchy process in land suitability evaluation for dragon fruit: a case study of Bac Binh district, Binh Thuan province. *GIS 2016 Conference* (186 - 195). Hue, Vietnam: Hue University.

SOB (Statistics Office of Binh Thuan province). (2022). Binh Thuan statistical yearbook 2022. Retrieved April 5, 2023, from http://cucthongke.vn/x-nien-giam-thong-ke.aspx?id=1038.

Sub-NIAPP (Sub-National Institute of Agricultural Planning and Projection). (2020). *Project for developing organic agriculture in Binh Thuan province for the period 2021 – 2030* (research report). Binh Thuan, Vietnam: Sub-NIAPP.

Tran, T. T. H., & Nguyen, N. P. (2017). Economic efficiency of dragon fruit production according to VietGAP standards in Ham Thuan Nam district, Binh Thuan province - Current status and solutions. *Journal of Forestry Science and Technology* 4, 152-161.

Vo, H. T., Nguyen, V. D., Dao, Q. N., Bui, C. K., & Doan, T. P. Y. (2021). *Technical guidance on dragon fruit cultivation to adapt to climate change*. Ha Noi, Vietnam: Agricultural publisher.

Yamane, T. (1967). *Statistics: An introductory analysis* (2nd ed). New York, USA: Harper and Row.

Optimization of soda cooking for cellulose production from sugarcane bagasse

Nhan T. T. Dang[1], Hong K. T. Tang[1]*, & Dien Q. Le[2]

[1]Faculty of Forestry, Nong Lam University, Ho Chi Minh City, Vietnam

[2]School of Chemistry and Life Sciences, Ha Noi University of Science and Technology, Ha Noi, Vietnam

ARTICLE INFO

Research Paper

Received: August 31, 2024
Revised: October 29, 2024
Accepted: October 31, 2024

Keywords

Response surface methodology
Soda pulping
Sugarcane bagasse

***Corresponding author**

Tang Thi Kim Hong
Email:
tangkimhong@hcmuaf.edu.vn

ABSTRACT

Sugarcane bagasse, an agricultural residue, is a fibrous material containing cellulose as its main component, produced in large quantities worldwide. The aim of this work was to investigate the production of unbleached cellulose pulp from sugarcane bagasse using the soda cooking process with sodium hydroxide as the alkaline reagent. The cooking conditions were investigated with dosages of sodium hydroxide from 20% to 25%, temperatures from 150°C to 170°C, and cooking time from 75 to 105 min. The response surface methodology was used to study the effect of pulping variables on observed parameters. The results indicated that the optimal cooking conditions achieved the highest yield of 46.4% w/w and the lowest kappa number of 20.6 at a sodium hydroxide dosage of 23%, a temperature of 155°C, and a cooking time of 93 min. Further analysis of paper produced from the investigated pulp, refined at varying revolutions (0 to 3000 rpm), revealed that optimal strength properties were achieved at a refining level of 31°SR, equivalent to 2500 rpm. At this refining level, handsheets with a basis weight of 85 gsm exhibited a tensile strength of 2 kN/m, a burst strength of 2.7 kgf/cm^2, and a ring crush strength of 6.9 kgf. These findings confirm that the mechanical properties of the refined pulp meet the strength requirements of commercially recycled kraft paper, demonstrating its suitability for similar applications.

Cited as: Dang, N. T. T., Tang, H. K. T., & Le, D. Q. (2024). Optimization of soda cooking for cellulose production from sugarcane bagasse. *The Journal of Agriculture and Development* 23(Special issue 2) 14-24.

1. Introduction

Non-wood plant fibers, such as sugarcane bagasse, represent a promising and sustainable alternative for pulp and paper production. Sugarcane bagasse, a fibrous byproduct of the sugar extraction process, is characterized by a high cellulose content and can effectively substitute wood fibers in pulp production. Cultivated primarily in tropical and subtropical regions, sugarcane production globally amounts to approximately 2 billion tons annually (Okibe et al., 2023). Asia is the predominant producer, contributing nearly 60 million metric tons, with Vietnam producing about 11.5 million metric tons in 2023 (Nguyen, 2024). During the sugar extraction process, approximately 30% of each ton of sugarcane is converted into bagasse (Katakojwala & Mohan, 2022; Narisetty et al., 2022). Comprising fibrous residues dense in polymeric substances, sugarcane bagasse is recognized as a significant source of second-generation lignocellulosic biomass (Konde et al., 2021). As reported by Kumar et al. (2021), sugarcane bagasse contains substantial quantities of cellulose (32 - 45%), hemicellulose (20 - 32%), lignin (17 - 32%), ash (1.0 - 9.0%), and various extractives.

In the pulp and paper industry, wood is traditionally the primary raw material. The extensive consumption of wood, however, poses environmental challenges, including deforestation and associated greenhouse gas emissions. The utilization of alternative agricultural residues, such as rice straw, wheat straw, cotton linters, corn stalks, and notably sugarcane bagasse, can alleviate these environmental impacts. Among these alternatives, sugarcane bagasse is particularly favored for pulp production due to its superior fiber length (El-Sayed et al., 2022).

The growing demand for paper and paper-based packaging in Vietnam has intensified deforestation to meet increasing pulp requirements. Exploring and utilizing alternative raw materials, such as sugarcane bagasse, presents potential environmental benefits, including a reduction in deforestation, and adds economic value to this byproduct. Various chemical pulping methods can be applied to process sugarcane bagasse, including sulfate (kraft), sulfite, soda, and organosolv processes. While sulfate and sulfite processes are widely used, they involve sulfated chemical agents that contribute to environmental pollution through the release of sulfur compounds. Organosolv processes, which use organic solvents as delignifying agents and do not release sulfur compounds, have shown effectiveness only at the pilot scale. Consequently, this study employs the soda pulping process a traditional, sulfur-free method selected to minimize environmental impact. The objective of this study was to evaluate and optimize pulping conditions to produce nanocellulose from sugarcane bagasse for use in food packaging applications.

2. Materials and Methods

2.1. Materials and chemicals

Sugarcane bagasse (SCB) was collected from the An Khe Sugar Mill, Quang Ngai Sugar Joint Stock Company. The raw material underwent a pretreatment procedure that included cutting it into approximately 2 - 3 cm in length, cleaning, air drying, and sorting. For chemical composition analysis, the air-dried material was ground to a particle size of 0.25 to 0.50 mm. Main chemicals used for determining SCB chemical compositions and for cooking SCB were purchased from Sigma-Aldrich. Other chemicals were originally sourced from China.

2.2. Experimental design

The Central Composite Design (CCD) within the framework of Response Surface Methodology (RSM) was employed to assess the effects of three independent variables-X_1: NaOH dosage (% w/w of oven-dry SCB), X_2: cooking temperature (°C), and X_3: cooking time (min)-on the properties of cellulose pulp. The response variables examined were cellulose pulp yield and kappa number. A 17-run CCD experimental design was utilized, incorporating both axial and center points, and was conducted using Minitab (version 21.2). The variable ranges are provided in Table 1, with NaOH dosage varying from 20-25% w/w, cooking temperature from 150 - 170°C, and cooking time from 75 - 105 min. Each independent variable was coded at five levels, as shown in Table 1. The soda cooking conditions generated through RSM with CCD are detailed in Table 2.

Table 1. The range and levels of the variables in soda cooking stage

Factor	Variable	Range and level of coded and actual values				
		-α	-1	0	+1	α
X_1	Dosage of NaOH (%)	18	20	22.5	25	27
X_2	Cooking temperature (°C)	143	150	160	170	177
X_3	Cooking time (mins)	65	75	90	105	115

Table 2. The soda cooking schedules using central composite design

Run	NaOH dosage (%)	Cooking temperature (°C)	Cooking time (min)
1	20	150	75
2	25	150	75
3	20	170	75
4	25	170	75
5	20	150	105
6	25	150	105
7	20	170	105
8	25	170	105
9	18	160	90
10	27	160	90
11	22.5	143	90
12	22.5	177	90
13	22.5	160	65
14	22.5	160	115
15	22.5	160	90
16	22.5	160	90
17	22.5	160	90

2.3. Cellulose production

Soda cooking was conducted in a laboratory rotating digester model Regmed AU/E-20. Soda cooking conditions for each experiment are detailed in Table 2, with a liquor-to-solid ratio of 7:1 (L/kg) for all experiments, using exclusively oven-dry SCB as the solid component. Following cooking, the unbleached cellulose pulp was filtered and washed thoroughly with distilled water.

2.4. Evaluation of chemical composition of SCB, cellulose pulp yield, and kappa number

The solubility and chemical composition of SCB were analyzed following TAPPI standards: TAPPI T 207 om-93 for hot and cold water solubility (TAPPI, 1993), TAPPI T 212 om-93 for 1% NaOH solubility (TAPPI, 1993), TAPPI T 17 wd-70 for cellulose content (TAPPI, 1970), TAPPI T 223 cm-23 for pentosan content (TAPPI, 2023), TAPPI T 222 om-88 for lignin content (TAPPI, 1988), and TAPPI T 211 om-93 for ash content (TAPPI, 1993).

The dry matter content of the washed pulp was determined according to ISO 638 to calculate cellulose pulp yield, kappa number, and for further testing (ISO, 2008). The kappa number was evaluated following the TAPPI T 236 om-13 standard (TAPPI, 2013).

2.5. Cellulose pulp refining and handsheet formation for analysis of cellulose pulp strength properties

The pulp at the optimum conditions of cooking was chosen for refining at different revolutions in PFI mill to study the effect of refining on pulp strength properties. The cooked pulp was refined at the revolutions of 0; 500; 1,000; 1,500; 2,000; 2,500; 3,000 rpm. After refining, the pulp drainability at different refining revolution was determined by measuring the Schopper Riegler degree (°SR). The refined cellulose pulps were made handsheets with a basis weight of 85 gsm were then prepared from the refined pulps using a sheet former. These handsheets were tested to evaluate tensile strength, burst strength, and ring crush strength, following TAPPI standard methods T 494, T 403 (TAPPI, 2022), and T 818 (TAPPI, 2018), respectively.

3. Results and Discussion

3.1. Chemical compositions of SCB

The main chemical components of SCB are presented in Table 3. Compared with the data reported by Kumar et al. (2021), the cellulose and lignin contents are relatively similar. As shown in Table 3, the cellulose content of SCB in this study is only 45.12%, which suggests that the cooked yield obtained is expected to be relatively low. The ash content is approximately 5%, which is significantly higher than that of wood and within the same range as that of non-wood plants (Alonso-Esteban et al., 2022). The presence of silica in SCB ash negatively impacts chemical recovery in the alkaline pulping process; therefore, this chemical component should be assessed when considering the valorization of this agricultural waste in papermaking.

Table 3 shows that SCB is soluble in the used solvents in the following decreasing order: 1% sodium hydroxide > hot water > cold water. This result indicates that SCB exhibits better solubility in alkaline conditions. Consequently, the soda process is selected as the pulping method for this study.

Table 3. Solubility and chemical composition of sugarcane bagasse (expressed as a percentage percent on a dry weight basis)

Solubility and component	Results	
	This study	Kumar et al. (2021)
Hot water solubility	5.01%	
Cold water solubility	4.37%	
1% NaOH solubility	35.65%	
Cellulose	45.12%	32 - 45%
Pentosan	18.7%	20 - 32%
Lignin	24.57%	17 - 32%
Ash	5.49%	1.0 - 9.0%

3.2. Effect of cooking conditions on yield and kappa number of cellulose pulp

The results of cooking are presented in Table 4, including cellulose pulp yield and the kappa number of the pulps. The models to predict each response variable for the samples produced by the soda cooking process were obtained using Minitab 21.2. The final models for all variables are presented below as Equations (1) and (2). These equations are reduced models that include only significant terms, with a significance level or p-value of less than 0.05. The final equations, expressed in terms of the actual factors, are shown below:

$$Y_{\text{Kappa number}} = -104.388 - 0.7888x_1 + 2.1606x_2 - 0.515666667x_3 - 0.00694x_2^2 + 0.002648889\,x_3^2 \quad (1)$$

$$Y_{\text{Yield}}\,(\%) = 89.68 - 1.0632\,x_1 - 0.0977\,x_2 - 0.040133333\,x_3 \quad (2)$$

Table 4. Soda cooking results

Run	NaOH dosage (%)	Cooking temperature (°C)	Cooking time (min)	Cellulose yield (%)	Kappa number
1	20	150	75	49.8	24.5
2	25	150	75	44.2	19.6
3	20	170	75	47.5	22.4
4	25	170	75	43.5	19.3
5	20	150	105	49.5	22.8
6	25	150	105	44.0	19.3
7	20	170	105	47.2	21.8
8	25	170	105	43.0	19.0
9	18	160	90	50.1	25.0
10	27	160	90	40.1	17.5
11	22.5	143	90	49.1	20.2
12	22.5	177	90	44.8	17.5
13	22.5	160	65	48.6	24.0
14	22.5	160	115	44.5	21.0
15	22.5	160	90	46.7	20.9
16	22.5	160	90	46.8	20.9
17	22.5	160	90	46.0	20.9

The models are verified for the adequacy of final equation by investigating values of multiple regressions (R^2), adjusted R^2 and ρ value of regression. In model (1), R^2 and adjusted R^2 are about 97.17% and 93.52%, respectively. In model (2) R^2 and adjusted R^2 are about 95.27% and 89.18%, respectively. The R^2 indicates how well the model explains the variation in the data, whereas the adjusted R^2 indicates how much R^2 overestimates the variance when another predictor is added in the model. The higher the adjusted R^2, the better the goodness of fit.

Figures 1 to 6 and the corresponding data in Table 4 demonstrate that NaOH dosage, cooking temperature, and cooking time significantly affect both cellulose yield and kappa number. The effects of NaOH dosage and temperature on yield are shown in Figure 1 with surface plots (A) and contour plots (B). The results indicate that, at a constant temperature, an increase in NaOH dosage decreases the yield, while an increase in cooking temperature leads to a slight decrease in yield. This occurs because NaOH is used during cooking to remove lignin through reactions that degrade the lignin macromolecules before they can disrupt the cellulose chains.

The effects of NaOH dosage and cooking time on yield are illustrated in Figure 2 with surface plots (A) and contour plots (B). Increasing NaOH dosage up to 24% across a wide range of temperatures (140°C to 175°C) maintains a yield above 45%. However, higher cooking temperatures and longer cooking times decrease the yield (Figure 3). At low temperatures around 145°C and short reaction times around 70 min, the fibers are not completely separated after pulp washing.

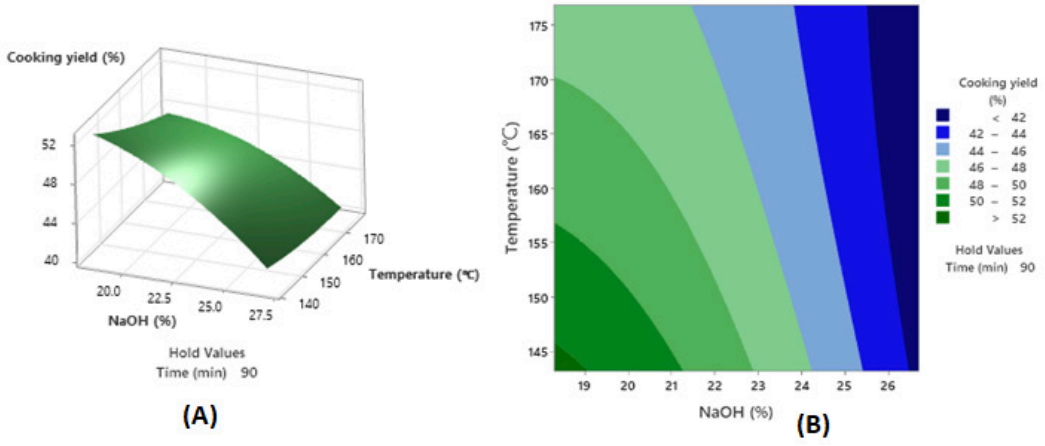

Figure 1. The surface plots (A) and contour plots (B) of cooking yield as function of NaOH dosage and cooking temperature.

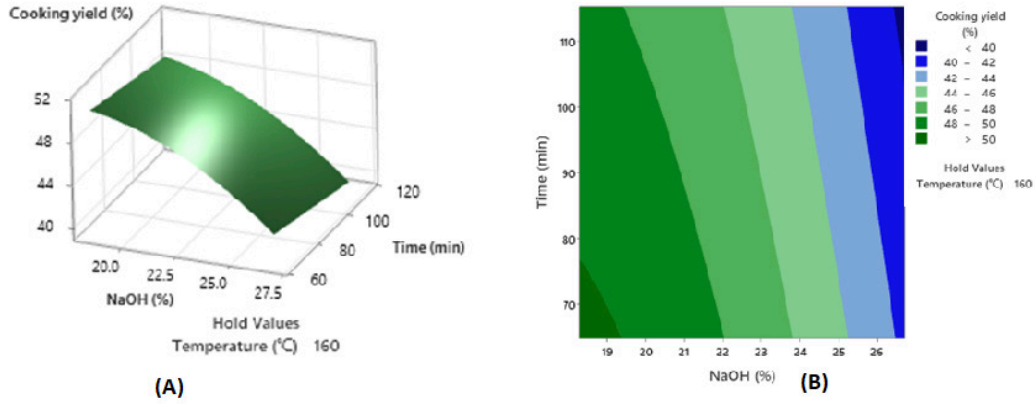

Figure 2. The surface plots (A) and contour plots (B) of cellulose yield as function of NaOH dosage and cooking time.

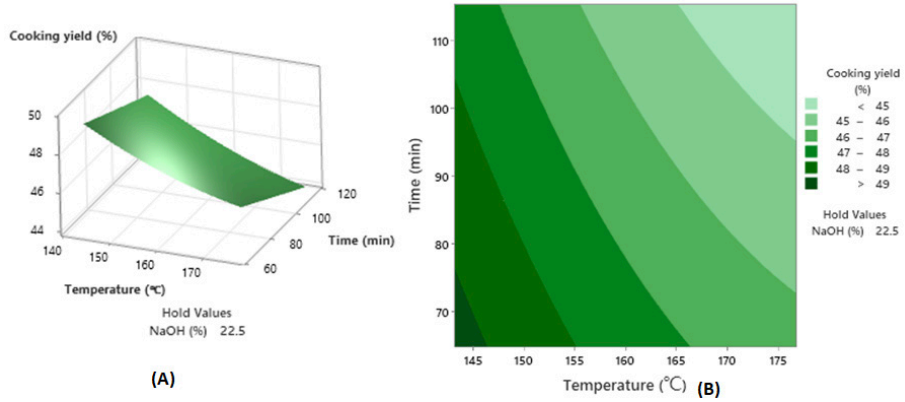

Figure 3. The surface plots (A) and contour plots (B) of cooking yield as function of cooking temperature and pulping time.

For the kappa number, a *P*-value of less than 0.05 indicates that all factors have significant effects on the kappa number, as shown in Figures 4, 5, and 6. Increasing NaOH dosage and cooking temperature reduces the kappa number. As discussed previously, higher NaOH dosage and cooking temperature reduce the lignin content in the cellulose pulp. When NaOH dosage was around 19%, the cooking temperature was below 165°C, and the cooking time was 90 min, the kappa number of the cellulose pulp remained above 24 (Figure 4), and shives were observed after washing under these conditions. Figure 6 shows that cooking at temperatures above 160°C with cooking times ranging from 70 to 120 min results in cellulose pulp with a lower kappa number.

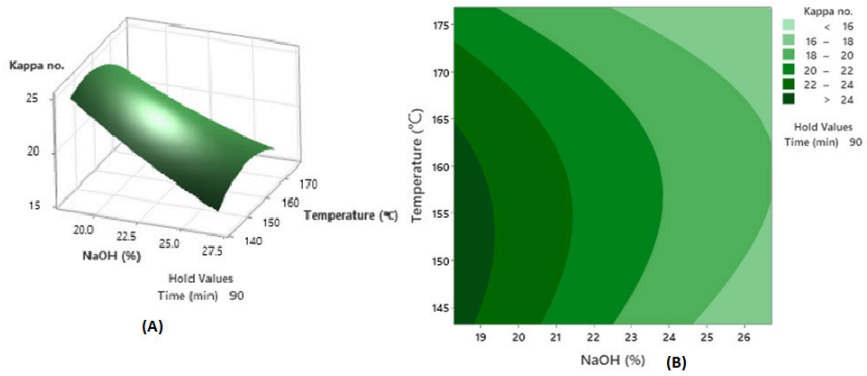

Figure 4. The surface plots (A) and contour plots (B) of kappa number as function of NaOH dosage and cooking temperature.

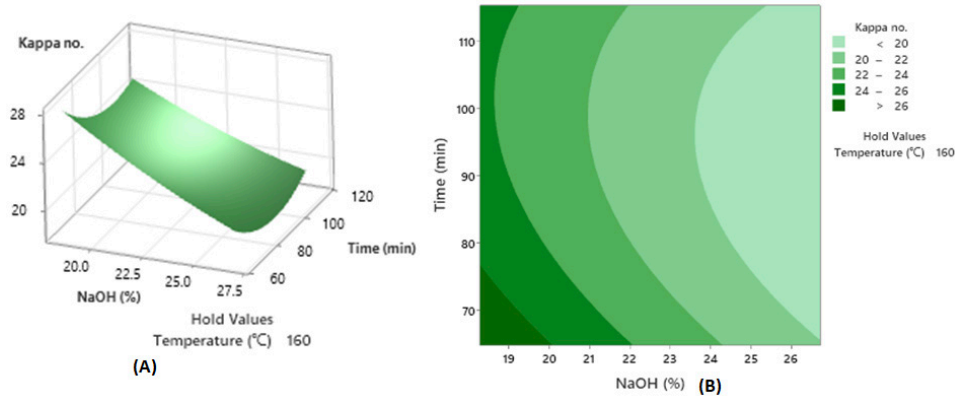

Figure 5. The surface plots (A) and contour plots (B) of kappa number as function of NaOH dosage and cooking time.

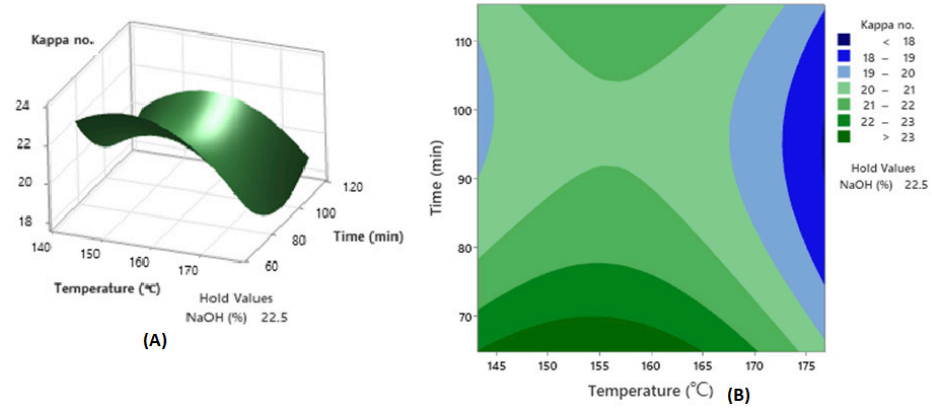

Figure 6. The surface plots (A) and contour plots (B) of kappa number as function of temperature and time of cooking.

As shown in Figure 7, cooking with a NaOH dosage of 23% at 155°C for 93 min was identified as the optimal condition by Minitab 21.2, resulting in the highest yield of 46.4% and the lowest kappa number of 20.6.

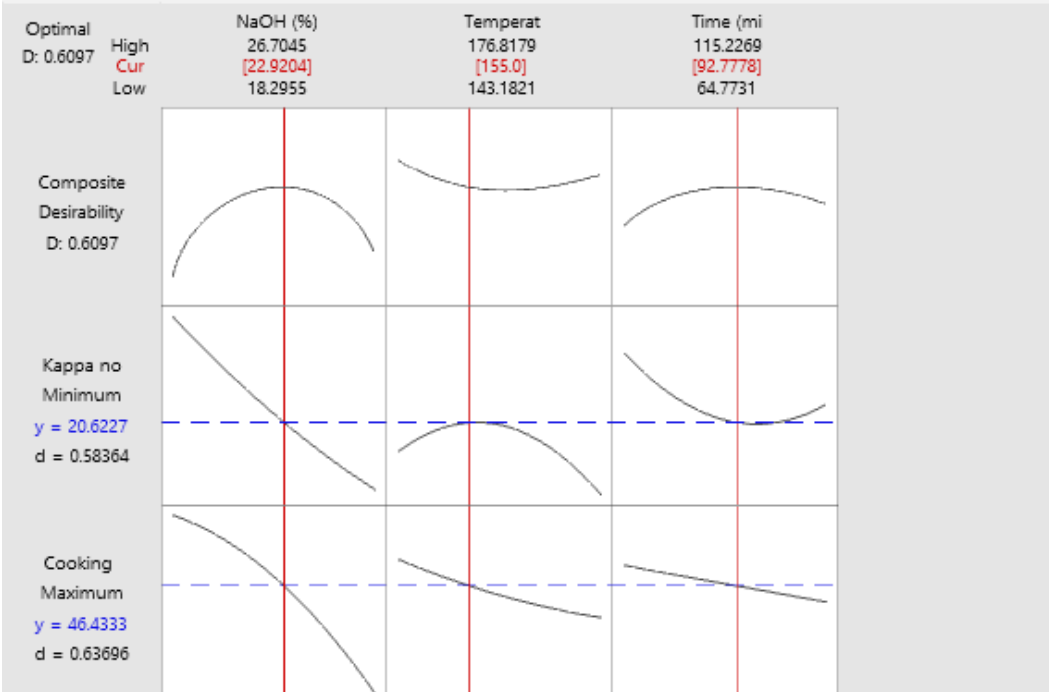

Figure 7. The cross-sectional surface meets the optimum point.

3.3. Effect of cellulose pulp refining on strength properties

The cellulose pulp obtained under optimal conditions was refined using a PFI mill at different revolutions: 0; 500; 1,000; 1,500; 2,000; 2,500 and 3,000 rpm. Cellulose refining is a promising approach to improve pulp quality by altering fiber characteristics (Gharehkhani et al., 2015). During PFI refining, mechanical treatment is primarily caused by the impulses of the beating body bars, which predominantly induce internal fibrillation (Mandlez et al., 2022). The drainability of cellulose at different refining revolutions was assessed by measuring the Schopper-Riegler degree (°SR), and the results are shown in Figure 8. Increasing the refining revolutions resulted in a higher °SR and decreased cellulose drainability. The main reason for this result is the increase in fines produced during refining (Cole et al., 2008).

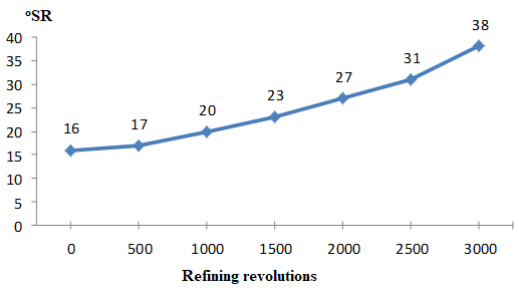

Figure 8. The relation between refining revolutions and °SR.

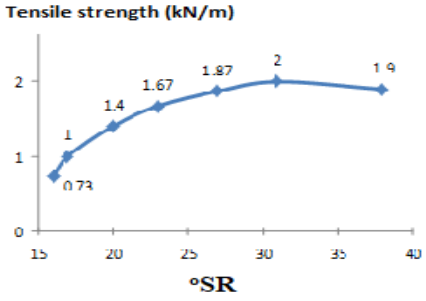

Figure 9. The relation between °SR and tensile strength of unbleached cellulose pulp from sugarcane bagasse.

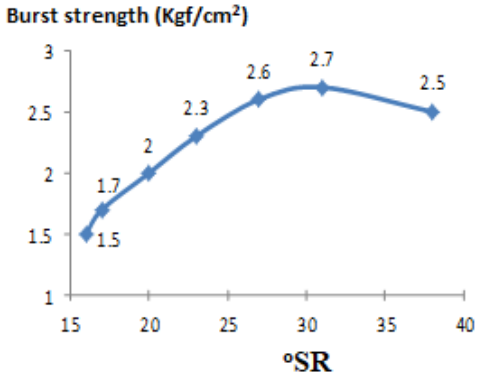

Figure 10. The relation between °SR and burst strength of unbleached cellulose pulp from sugarcane bagasse.

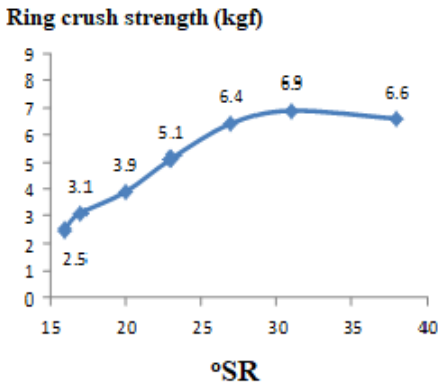

Figure 11. The relation between °SR and ring crush strength of unbleached cellulose pulp from sugarcane bagasse.

The effects of refining on the strength properties of cellulose pulp, including tensile strength, burst strength, and ring crush strength, are illustrated in Figures 9, 10, and 11. The tensile strength of cellulose pulp may be influenced by various interacting factors, such as fiber length, fiber strength, coarseness, and specific bonding strength (Kerekes et al., 2021). Beyond a certain point, the limiting factor for strength is no longer fiber-to-fiber bonding but the strength of the individual fibers. Refining beyond this point begins to decrease strength properties. The results indicate that at a refining level of 31 °SR (corresponding to 2500 rpm), the strength properties of handsheets (basis weight 85 gsm) reached their maximum values, with a tensile strength of 2 kN/m, burst strength of 2.7 kgf/cm², and ring crush strength of 6.9 kgf.

4. Conclusions

The soda cooking process has been successfully applied to produce unbleached cellulose pulp from sugarcane bagasse. Optimal conditions, determined using Minitab 21.2, were found to maximize yield and minimize kappa number: a sodium hydroxide dosage of 23% w/w, a cooking temperature of 155°C, and a cooking time of 93 min. Under these conditions, the cellulose pulp obtained a tensile strength of 2 kN/m, burst strength of 2.7 kgf/cm², and ring crush strength of 6.9 kgf. These properties are comparable to those of cellulose obtained from recycled commercial kraft paper.

Conflict of interest

The authors have no conflict of interest to declare.

Acknowledgements

This research was financially supported by the Nong Lam University, Ho Chi Minh City research funding (the research code: CS-CB23-LN-02).

References

Alonso-Esteban, J. I., Carocho, M., Barros, D., Velho, M. V., Heleno, S., & Barros, L. (2022). Chemical composition and industrial applications of Maritime pine (*Pinus pinaster* Ait.) bark and other non-wood parts. *Reviews in Environmental Science and Bio/Technology* 21(3), 583-633. https://doi.org/10.1007/s11157-022-09624-1.

Cole, C. A., Hubbe, M. A., & Heitmann, J. A. (2008). Water release from fractionated stock suspensions. Part 1 - Effects of the amounts and types of fiber fines. *Tappi Journal* 7(7), 28-32. https://doi.org/10.32964/TJ7.7.28.

El-Sayed, A. M., Hamad, K. H., Eid, Y., Alaa, A., Mohsen, A. R., Hassan, A., Atta, K., Safwat, A. R., Benbella, M., & Tawab, S. A. (2022). Production of paper using chemical pulping process of sugarcane bagasse. *International Journal of Industry and Sustainable Development* 3(1), 57-65. https://doi.org/10.21608/ijisd.2022.145854.1013.

Gharehkhani, S., Sadeghinezhad, E., Kazi, S. N., Yarmand, H., Badarudin, A., Safaei, M. R., & Zubir, M. N. M. (2015). Basic effects of pulp refining on fiber propertie-A review. *Carbohydrate Polymers* 115, 785-803. https://doi.org/10.1016/j.carbpol.2014.08.047.

ISO (International Organization for Standardization). (2008). *ISO 638:2008*. Geneva, Switzerland: International Organization for Standardization.

Katakojwala, R., & Mohan, S. V. (2022). Multi-product biorefinery with sugarcane bagasse: Process development for nanocellulose, lignin and biohydrogen production and lifecycle analysis. *Chemical Engineering Journal* 446, 137233. https://doi.org/10.1016/j.cej.2022.137233.

Kerekes, R. J., Heymer, J. O., & McDonald, J. D. (2021). Refining pulp for tensile strength. *Nordic Pulp and Paper Research Journal* 36(4), 696-706. https://doi.org/10.1515/npprj-2021-0012.

Konde, K. S., Nagarajan, S., Kumar, V., Patil, S. V., & Ranade, V. V. (2021). Sugarcane bagasse based biorefineries in India: potential and challenges. *Sustainable Energy and Fuels* 5(1), 52-78. https://doi.org/10.1039/D0SE01332C.

Kumar, A., Kumar, V., & Singh, B. (2021). Cellulosic and hemicellulosic fractions of sugarcane bagasse: Potential, challenges and future perspective. *International Journal of Biological Macromolecules* 169, 564-582. https://doi.org/10.1016/j.ijbiomac.2020.12.175.

Mandlez, D., Koller, S., Eckhart, R., Kulachenko, A., Bauer, W., & Hirn, U. (2022). Quantifying the contribution of fines production during refining to the resulting paper strength. *Cellulose* 29(16), 8811-8826. https://doi.org/10.1007/s10570-022-04809-x.

Narisetty, V., Okibe, M. C., Amulya, K., Jokodola, E. O., Coulon, F., Tyagi, V. K., Lens, P. N. L., Parameswaran, B., & Kumar, V. (2022). Technological advancements in valorization of second generation (2G) feedstocks for bio-based succinic acid production. *Bioresource Technology* 360, 27513. https://doi.org/10.1016/j.biortech.2022.127513.

Nguyen, M. N. (2024). *Production volume of sugar cane in Vietnam from 2012 to 2023*, Retrieved August 5, 2024, from https://www.statista.com/statistics/671485/production-of-sugar-cane-in-vietnam.

Okibe, M. C., Short, M., Cecelja, F., & Bussemake, M. (2023). Ontology modelling for valorisation of sugarcane bagasse. *Computer Aided Chemical Engineering* 52, 3363-3368. https://doi.org/10.1016/B978-0-443-15274-0.50536-9.

TAPPI (Technical Association of the Pulp & Paper Industry). (2023). *TAPPI T 223 cm-23*. Georgia, USA: Technical Association of The Pulp and Paper Industry.

TAPPI (Technical Association of the Pulp & Paper Industry). (2022). *TAPPI T 403 om-22; TAPPI T 494 om-22*. Georgia, USA: Technical Association of The Pulp and Paper Industry.

TAPPI (Technical Association of the Pulp & Paper Industry). (2018). *TAPPI T 818 cm-18*. Georgia, USA: Technical Association of The Pulp and Paper Industry.

TAPPI (Technical Association of the Pulp & Paper Industry). (2013). *TAPPI T 236 om-13*. Georgia, USA: Technical Association of The Pulp and Paper Industry.

TAPPI (Technical Association of the Pulp & Paper Industry). (1993). *TAPPI T 207 om-93; TAPPI T 211 om-93; TAPPI T 212 om-93*. Georgia, USA: Technical Association of The Pulp and Paper Industry.

TAPPI (Technical Association of the Pulp & Paper Industry). (1988). *TAPPI T 222 om-88*. Georgia, USA: Technical Association of the Pulp and Paper Industry.

TAPPI (Technical Association of the Pulp & Paper Industry). (1970). *TAPPI T 17 wd-70*. Georgia, USA: Technical Association of The Pulp and Paper Industry.

Enhancing agricultural classification models through data augmentation and advanced deep learning techniques

Tien Dang*, & Long D. Phan
Faculty of Information Technology, Nong Lam University, Ho Chi Minh City, Vietnam

ARTICLE INFO

Research Paper

Received: August 31, 2024
Revised: October 10, 2024
Accepted: November 18, 2024

Keywords

Agricultural datasets
Agricultural informatics
CNNs
Data augmentation
ViTs

***Corresponding author**

Dang Minh Tien
Email:
tien.dangminh@hcmuaf.edu.vn

ABSTRACT

In the field of agricultural data analysis, achieving high quality classification modeling remains a significant challenge due to the inherent variability and complexity of agricultural datasets. This study investigated cutting-edge approaches to enhance model performance through data augmentation techniques and the application of advanced deep learning models to artificially enlarge the training dataset, thereby improving model generalizability and robustness. Additionally, the study evaluated the efficacy of state-of-the-art models (i.e., ViT-Ti/16, CaiT-XXS-24, XCiT-T12, Resnet26, ConvNeXt-T) for agricultural data analysis. The experimental results revealed a marked improvement in terms of accuracy and F1-Score when applied data augmentation into the training session. This underscored the potential of these techniques to significantly advance the field of agricultural informatics. Briefly, the findings contributed to the development of more reliable and high performance models for agricultural practices.

Cited as: Dang, T. M., & Phan, L. D. (2024). Enhancing agricultural classification models through data augmentation and advanced deep learning techniques. *The Journal of Agriculture and Development* 23(Special issue 2), 25-32.

1. Introduction

In recent years, the application of information technology in agriculture has attracted significant interest, particularly in the monsoon-influenced climate region such as Vietnam. This interest is driven by the potential of advanced technologies to transform traditional agricultural practices and enhance productivity. Among these technologies, machine learning has emerged as a powerful tool, offering innovative solutions to various agricultural challenges. In information technology, especially in computer vision, models which are designed for image classification, have shown remarkable success in tasks such as crop disease detection, yield prediction, and soil health monitoring. These models can analyze vast amounts of visual data, providing insights that were previously unattainable.

However, one of the critical challenges in applying deep learning to agricultural datasets is the limited availability of labeled data. Therefore, data augmentation has been proposed as a technique that generates new training samples from existing data, has proven to be an effective solution to this problem. By increasing the diversity and size of training datasets, data augmentation enhances the robustness and generalization capabilities of deep learning models. For instance, Vision Transformers (ViT) (Dosovitskiy et al., 2020) have garnered attention for their ability to process and analyze visual data using self-attention mechanisms, capturing long-range dependencies in images. Class-Attention in Image Transformers (CaiT) (Touvron et al., 2021) and Cross-Covariance Image Transformers (XCiT) (El-Nouby et al., 2021) extend the capabilities of ViT by introducing novel architectural modifications that enhance performance and efficiency. Residual Networks (Resnet) (He et al., 2015), renowned for its deep residual learning framework, addresses the vanishing gradient problem, allowing the training of very deep networks. A family of pure ConvNets dubbed ConvNeXt (Liu et al., 2022) was introduced with their hierarchical structure of convolutional layers, remain a cornerstone in the field of image recognition, offering robust feature extraction and classification capabilities.

In this paper, we presents a comprehensive investigation of different deep learning models applied to classification tasks for a specific agricultural dataset, specifically the Vietnamese leaf dataset (Phan & Tran, 2022), with a particular focus on the impact of data augmentation. The models under consideration include ViT, CaiT, ConvNeXt. In the context of agricultural image classification, these models offer unique strengths and limitations. By evaluating their performance, this paper aims to identify the most effective approaches for leveraging data augmentation to improve classification accuracy and robustness.

2. Related Works

The application of artifitial inteligent in agricultural image classification has seen significant advancements, with each model offering unique advantages. In this section, we inform several key models and emphasizes the role of fundamental data augmentation techniques in enhancing classification performance.

2.1. Efficient classification models

Recently, Convolutional Neural Networks have been becoming famous due to it performance relevant to image tasks. For instance, ConvNeXt have established themselves as foundational models in image classification due to their hierarchical structure of convolutional layers. In agriculture, ConvNeXt is widely used for tasks such as soil texture classification, crop yield estimation, and remote sensing analysis, continuing to provide robust feature extraction and classification capabilities (Bhuyan & Singh, 2024). Their widespread use and proven effectiveness make ConvNeXt a staple in agricultural image processing. Moreover, ResNet build on the strengths of CNNs with their deep residual learning framework, which mitigates the vanishing gradient problem and allows for the training of very deep networks. In agricultural contexts, ResNet has demonstrated robust performance in tasks like crop disease detection and fruit sorting by effectively capturing hierarchical features from images. Studies indicate ResNet's reliability and efficacy in various agricultural applications.

Beside, in the past few years, Transformer-based models have been proposed as powerful alternatives to convolutional neural networks. ViT leverages self-attention mechanisms to capture long-range dependencies within images, making them particularly effective in handling complex visual data. Research has demonstrated ViT's ability to differentiate between healthy and diseased crops by analyzing detailed visual features, leading to significant improvements in agricultural image classification tasks. However, ViT has several drawbacks, one of those is the lack of local communication. Therefore, CaiT enhances ViT by introducing class-attention layers, which focus on the Class token information, and XCiT addresses some limitations of ViT by incorporating cross-covariance information between image patches, and it Local Patch Interaction (LPI) was introduced as a module for capturing the local information. This approach enables XCiT to capture fine-grained details in high-resolution images, making it particularly effective for classification tasks.

2.2. Data augmentation

Data augmentation is essential for improving the performance of machine learning models, particularly when working with limited datasets. In computer vision, where obtaining diverse and sufficient training data can be challenging, augmentation techniques address this issue by artificially expanding the training set with various transformations. By increasing both the size and diversity of training data, data augmentation boosts the robustness and generalization capabilities of models, resulting in enhanced performance across a range of tasks. Traditional data augmentation methods include geometric transformations such as rotation, scaling, cropping, and flipping, as well as color jittering and noise addition. These techniques can further enhance model performance by simulating different lighting conditions and image quality degradations, and have been shown to effectively reduce overfitting and improve model robustness across various tasks (Shorten & Khoshgoftaar, 2019). For instance, rotations and translations can help models become invariant to slight changes in object position, while color adjustments can aid in generalizing across different lighting conditions.

In addition to these basic techniques, more sophisticated methods such as MixUp and CutMix have been introduced to further enhance data augmentation. MixUp, proposed by (Zhang et al., 2017), generates new training examples by blending two images and their corresponding labels, creating a smoother decision boundary and improving model robustness. CutMix, introduced by (Yun et al., 2019), goes a step further by cutting and pasting patches from one image onto another, which helps the model focus on different regions and learn more invariant features.

Overall, data augmentation remains a critical component in the development of robust machine learning models, particularly in scenarios with limited data. Its ability to enhance model generalization and reduce overfitting makes it an indispensable tool in modern machine learning pipelines.

3. Experiments

In this section, we demonstrate the effectiveness of several models from the timm librabry such as: ViT, CaiT and XCiT - those models are represent for the transformer-based model, and for the CNNs models, we use Resnet26 and ConvneXt. By applying serveral data augmentation on the Vietnamese leaf dataset which proposed by Phan & Tran (2022), we will evaluate the performance of these data augmentation on different models.

3.1. Dataset

According to (Phan & Tran, 2022) they introduced a new Vietnamese leaf dataset. This dataset comprises of 6800 images for training set and 1707 images for testing. Those leaves are from 15 different food and industrial crops, as well as certain fruit trees. These include corn, sorghum, sweet potato, tapioca, potato, rice, cassava, rubber, coffee, cashew, pepper, rambutan, durian, green beans, and peanuts. However, the authors have eliminated peanuts, mung beans, sago, and rambutan from the dataset after testing due to insufficient sample quantity and poor image quality. Sorghum was also discarded because its leaf shape was too similar to that of corn. To address this issue, we apply several data augmentation and utilze some advanced machine learning models and we decided to use all 15 different type of leaves for our experiments.

3.2. Metrics for classification

Evaluating the performance of classification models involves several key metrics that provide insights into different aspects of the model's capabilities. Assuming that we have a confussion matrix with 4 similarity parameters TP, TN, FP, FN represent for True Positive, True Negative, False Positive, and False Negative, respectively. Here are several metrics that we used:

$$\text{Accuracy} = \frac{\text{TP} + \text{TN}}{\text{TP} + \text{TN} + \text{FP} + \text{FN}}$$

$$\text{Precision} = \frac{\text{TP}}{\text{TP} + \text{FP}}$$

$$\text{Recall} = \frac{\text{TP}}{\text{TP} + \text{FN}}$$

$$\text{F}_1 - \text{score} = \frac{2 \times \text{Precision} \times \text{Recall}}{\text{Precision} + \text{Recall}}$$

In there, the F1-score is the special one due to it balances precision and recall, making it especially useful for classificational tasks. Evaluating models using the F1-score ensures that both FP and FN are considered, leading to a more robust performance.

3.3. Experimental setting

3.3.1. Data augmentation

Our objective is to evaluate the effectiveness of various data augmentation techniques in enhancing the performance of vision models for agricultural image classification. To begin with, we resize the full image to 224 x 224 pixels using bicubic interpolation to normalize the input image. After that, we decided to apply several augmentation methods to enhance the robustness of our models. We utilize Random Horizontal Flip with a probability of 0.5, allowing the model to learn from images that are flipped horizontally, which simulates different viewing angles. Random Rotation is applied to rotate images up to 50 degrees, helping the model become invariant to rotational changes of the input data. Random Erasing (Zhong et al., 2017) with a probability of 0.3 to randomly erase some pixels in the images, obliging the model to focus on the entire context rather than specific features. Additionally, Random Augment (Cubuk et al., 2019) is employed with a probability of 0.5, randomly applying a combination of augmentations to further diversify the training data.

Furthermore, during the training phase, we incorporate Mixup and Cutmix techniques, each with a probability of 0.15. Mixup creates new training samples by blending pairs of images and their corresponding labels, which makes model to be more generalized. On the other hand, Cutmix combines patches from different images, encouraging the model to recognize the label based on fragmented information.

3.3.2. Model and optimizer

We conduct experiments on several tiny variant model based on ViTs and CNNs, all implemented via the timm library. More

precisely like, we explore transformer-based models including ViT-Ti/16, XCiT-T12, and CaiT-XXS-24. For CNN-based models, we use ResNet26 and ConvNeXt-T. For each model, we employ a tailored optimization strategy to ensure optimal performance. For the transformer models, we employ the AdamW optimizer due to its ability to handle sparse gradients and large learning rates. The learning rate is set to with a weight decay of 0.05 to mitigate overfitting. Additionally, we utilize a cosine annealing learning rate scheduler, which gradually reduces the learning rate following a cosine curve, and enhancing the model's convergence during training. Besides, for the CNN-based models, such as ResNet26 and ConvNeXt-T, we also use the AdamW optimizer with similar hyperparameters. However, to further enhance performance, we incorporate several regularization such as Stochastic Depth (Huang et al., 2016) and Label Smoothing (Szegedy et al., 2015), both with a probability of 0.1. Stochastic Depth introduces regularization by randomly skipping layers during training, while Label Smoothing helps to prevent overfitting by softening the target labels.

Table 1. Hyperparameter during training phrase

Training setting	Configuration	
	Transformer-based model	CNN-based model
Input size	224 x 224	
Interpolation	Bicubic	
Optimizer	AdamW	
Learning rate	Base LR = 5×10 − 4 with cosine decay	
Optimizer momentum	β_1, β_2 = 0.9,0.999	
Weight decay	0.05	
Batch size	128	
Total epochs	50	
Warmup epochs	50	
Random Horizontal Flip	0.3	
Random Rotation	50 degrees	
Random Erasing	0.3	
Random Augment	0.5	
Mixup	0.15	
Cutmix	0.15	
Stochastic Depth	-	0.1
Label Smoothing	-	0.1

3.4. Results

In this section, we illustrate our experimental result after training each model for 50 epochs and the setting of hyperparameter is shown in Table 1.

Table 2. Comparison of various model results on Vietnamese leaf dataset

Model	Params (M)	Layers Blocks	Embed-size	Accuracy	F1-score
ViT-Ti/16	5.8	12	192	92.72	92.06
XCiT-T12	6.7	12	192	97.89	97.41
CaiT-XXS-24	12	24 + 2	192	94.42	93.89
Resnet26-t	16	26 blocks {2,2,2,2}	{32, 24, 48, 64}	98.76	98.47
ConvNeXt-T	28.6	18 blocks {3,3,9,3}	{96, 192, 384, 768}	98.47	98.23

As shown in Table 2, all models on our experiments have easily achieved high performance. More precisely like, CNN-based models have surpassed Transformer-based models due to its advancements in local information. To be more specific, Resnet26-t achieved state-of-the-art accuracy and F1-score (98.76 and 98.47, respectively). The second winner is CovNeXt-T with 98.47 in accuracy and 98.23 in F1-score. For transformer models, because of the LPI layer helped collect the local information, XCiT gained a closed-call to Resnet26-t and ConvNeX-T (97.89 for accuracy and 97.47 for F1-score). Finally, although ViT's drawback is that it needs to be trained on a large dataset, it still achieved a high performance with our setting in such a small dataset.

3.5. Ablation study

This section presents the effects of numerous data augmentation and regularization methods. According to Section 3.3.1, the experiment was conducted to write down the performance of each data augmentation by removing one factor at the time, then we make a comparison with the default setting. Also, we employed a few more techniques including Random Crop, Gaussian Blur, Color Jitter, and Random Gray Scale.

Table 3. Comparison of the effects of various data augmentation on various models

Action	Augmentation	Model				
		ViT - T/14	XCiT-T12	CaiT-XXS-24	ResNet26	ConvNeXt -T
	Default	92.72	97.89	94.42	98.76	98.47
Adding	Random Crop	90.39	96.86	93.4	97.63	98.29
	Color Jitter	92.25	97.6	93.97	98.64	98.3
	Random Gray Scale	92.1	97.73	91.67	98.24	97.95
Removing	Random Horizontal Flip	91.97	96.3	92.38	97.68	96.72
	Random Rotation	91.82	97.12	92.95	98.42	97.68
	Random Erasing	90.62	95.32	92.51	98.6	97.96
	Random Augment	92.91	97.82	95.18	99.01	98.62
	Mixup	91.41	95.79	93.65	96.79	98.25
	Cutmix	91.68	95.89	91.67	97.3	98.13
	Stochastic Depth	-	-	-	98.21	96.4
	Label Smoothing	-	-	-	97.6	97.81

As shown in Table 3, although Random Augment was slightly improved the performance of XCiT, we still decided it was the only data augmentation method that restrain the performance of almost all models. Without it, Resnet26-t performance achieved 99.01% in accuracy which surpassed default setting. For that reason, we suggest that Random Augment should not be installed. Random Crop, Color Jitter, and Random Gray Scale was slightly decreased the accuracy of model, therefore, we also removed them out of our setting.

4. Conclusions

In this paper, we aimed to comprehensively evaluate the effectiveness of various data augmentation on different models on the Vietnamese leaf dataset collected by previous researchers We have presented a comprehensive result of both Vision Transformer-based models (ViT-Ti/16, XCiT-T12, CaiT-XXS-24) and Convolutional Neural Networks (ResNet26, ConvNeXt-T) on our setting. Our findings indicate that data augmentation techniques significantly enhance the robustness and generalization capabilities of AI models in agricultural image classification tasks. This improvement contributes to the overall advancement of precision agriculture. Our work underscores the importance of employing diverse data augmentation methods to address the challenges posed by limited agricultural datasets, leading to more resilient and effective agricultural technologies.

Conflict of interest

We hereby declare that this is a scientific research work conducted by our team. The data used in the analysis process has clear origins and has been published in accordance with the regulations. All research results are the product of an honest and objective process of inquiry and analysis. These results have not been published in any other research.

References

Bhuyan, P., & Singh, P. K. (2024). Evaluating deep CNNs and vision transformers for plant leaf disease classification. In Devismes, S., Mandal, P. S., Saradhi, V. V., Prasad, B., Molla, A. R., & Sharma, G. (Eds.), *Proceedings of The 20th International Conference on Distributed Computing and Intelligent Technology ICDCIT 2024, Bhubaneswar, India, January 17-20, 2024* (293-306). Zug, Switzerland: Springer Cham. https://doi.org/10.1007/978-3-031-50583-6_20.

Cubuk, E. D., Zoph, B., Shlens, J., & Le, Q. V. (2020). Randaugment: Practical automated data augmentation with a reduced search space. In Boult, T., Medioni, G., & Zabih, R. (Eds.), *Proceedings of The 2020 IEEE/CVF Conference on Computer Vision and Pattern Recognition Workshops (CVPRW), Seattle, WA, USA, June 14-19* (3008-3017). New Jersey, USA: Institute of Electrical and Electronics Engineers - IEEE. https://doi.org/10.1109/cvprw50498.2020.00359.

Dosovitskiy, A., Beyer, L., Kolesnikov, A., Weissenborn, D., Zhai, X., Unterthiner, T., Dehghani, M., Minderer, M., Heigold, G., Gelly, S., Uszkoreit, J., & Houlsby, N. (2020). An image is worth 16x16 words: Transformers for image recognition at scale. *arXiv* 2010, 11929. https://doi.org/10.48550/arXiv.2010.11929.

El-Nouby, A., Touvron, H., Caron, M., Bojanowski, P., Douze, M., Joulin, A., Laptev, I., Neverova, N., Synnaeve, G., Verbeek, J., & Jegou, H. (2021). Xcit: Cross-covariance image transformers. *arXiv* 2106, 09681v2. https://doi.org/10.48550/arXiv.2106.09681.

He, M. K., Zhang, G. X., Ren, Q. S., & Sun, J. (2015).

Deep residual learning for image recognition. In Tuytelaars, T., Li, F. F., & Bajcsy, R. (Eds.), *Proceedings of The 2016 IEEE Conference on Computer Vision and Pattern Recognition (CVPR), Las Vegas, NV, USA, June 27-30* (770-778). New Jersey, USA: Institute of Electrical and Electronics Engineers - IEEE. https://doi.org/10.1109/cvpr.2016.90.

Huang, G., Sun, Y., Liu, Z., Sedra, D., & Weinberger, K. (2016). Deep networks with stochastic depth. In Leibe, B., Sebe, N., Matas, J., & Welling, M. (Eds.), *Proceedings of Computer Vision - ECCV 2016: 14th European Conference Part IV, Amsterdam, The Netherlands, October 11-14* (646-661). Zug, Switzerland: Springer Cham. https://doi.org/10.1007/978-3-319-46493-0_39.

Liu, Z., Mao, H., Wu, C. Y., Feichtenhofer, C., Darrell, T., & Xie, S. (2022). A convnet for the 2020s. In Chellappa, R., Matas, J., Quan, L., & Shah, M. (Eds.), *Proceedings of The 2022 IEEE/CVF Conference on Computer Vision and Pattern Recognition Workshops New Orleans, Louisiana, June 19-24, 2022* (11976-11986). New Jersey, USA: Institute of Electrical and Electronics Engineers - IEEE. https://doi.org/10.1109/CVPR52688.2022.01167.

Phan, L. D., & Tran, T. S. (2022). Applying convolution neural networks for leaf image recognition with the vietnamese leaf image database. In *Proceedings of The 4th International Conference on Sustainable Agriculture and Environment* (81-94). Ho Chi Minh City, Vietnam: Nong Lam University.

Shorten, C., & Khoshgoftaar, T. M. (2019). A survey on image data augmentation for deep learning. *Journal of Big Data* 6(1), 1-48. https://doi.org/10.1186/s40537-019-0197-0.

Szegedy, C., Vanhoucke, V., Ioffe, S., Shlens, J., & Wojna, Z. (2015). Rethinking the inception architecture for computer vision. In Tuytelaars, T., Li, F. F., & Bajcsy, R. (Eds.), *Proceedings of The 2016 IEEE Conference on Computer Vision and Pattern Recognition (CVPR), Las Vegas, NV, USA, June 27-30* (2818-2826). New Jersey, USA: Institute of Electrical and Electronics Engineers - IEEE. https://doi.org/10.1109/cvpr.2016.308.

Touvron, H., Cord, M., Sablayrolles, A., Synnaeve, G., & Jégou, H. (2021). Going deeper with image transformers. In Berg, T., Clark, J., Matsushita, Y., & Taylor, C. J. (Eds.), *Proceedings of The 2021 IEEE/CVF International Conference on Computer Vision (ICCV), Montreal, QC, Canada, October 11-17* (32-42). New Jersey, USA: Institute of Electrical and Electronics Engineers - IEEE. https://doi.ieeecomputersociety.org/10.1109/ICCV48922.2021.00010.

Yun, S., Han, D., Oh, S. J., Chun, S., Choe, J., & Yoo, Y. (2019). CutMix: Regularization strategy to train strong classifiers with localizable features. In Lee, K. M., Forsyth, D., Pollefeys, M., & Tang, X. (Eds.), *Proceedings of The 2019 IEEE/CVF International Conference on Computer Vision (ICCV), Seoul, South Korea, October 27-November 2,* (6022-6031). New Jersey, USA: Institute of Electrical and Electronics Engineers - IEEE. https://doi.ieeecomputersociety.org/10.1109/ICCV.2019.00612

Zhang, H., Cisse, M., Dauphin, Y. N., & Lopez-Paz, D. (2017). Mixup: Beyond empirical risk minimization. In Bengio, Y., & LeCun, Y. (Eds.), *Proceedings of The 6th International Conference on Learning Representations - ICLR 2018, Vancouver, Canada, April 30-May 3* (1-13). https://doi.org/10.48550/arXiv.1710.09412.

Zhong, Z., Zheng, L., Kang, G., Li, S., & Yang, Y. (2017). Random erasing data augmentation. In *Proceedings of The AAAI Conference on Artificial Intelligence* (13001-13008). https://doi.org/10.1609/aaai.v34i07.7000.

Isolating a group of fungi from soil with the ability to control root-knot nematodes (*Meloidogyne* spp.) damage in vegetables

Van T. Tran[1*], Quyen T. N. Vo[2], Toan Q. Dinh[2], Khanh T. V. Nguyen[1], Linh T. N. Nguyen[3], Thang D. Nguyen[3], & Don D. Le[2]

[1]Research Institute for Biotechnology and Environment, Nong Lam University, Ho Chi Minh City, Vietnam

[2]Faculty of Biological Sciences, Nong Lam University, Ho Chi Minh City, Vietnam

[3]Center of Research and Development - Petro Vietnam Ca Mau Fertilizer JSC, Vietnam

ARTICLE INFO

Research Paper

Received: August 26, 2024
Revised: December 11, 2024
Accepted: December 12, 2024

Keywords

Mariannaea sp.
Meloidogyne spp.
Nematode-trapping fungi
Paecilomyces sp.
Penicillium sp.

***Corresponding author**

Tran Thi Van
Email:
van.tranthi@hcmuaf.edu.vn

ABSTRACT

Vegetable cultivation is essential to Vietnam's agricultural development strategy. *Meloidogyne* spp. has caused a root-knot disease which is dangerous due to decreased plant vitality, yield, and quality. This research aimed to select fungal strains controlling *Meloidogynes* spp., which causes root knots in vegetable plants. As a result, strains of the fungi *Paecilomyces sp.*, *Mariannaea* sp., and *Penicillium* sp. effectively inactivated second-stage juveniles (J2) after 72 h of inoculum. Specifically, *Paecilomyces sp.* was immobilized in 64.5% of the nematodes, *Mariannaea* sp. was 72%, and *Penicillium* sp. was 70%, compared to only 13.5% in the control group without fungal inoculation. In a net house experiment investigating the influence of fungal strains on J2 in Malabar spinach (*Basella alba* L.), the *Mariannae* sp. strain inoculated on plants at a density of 10^7 cfu/mL produced the best results in terms of root length (25.3 cm) and root weight (0.4 g) compared to the control uninoculation (18.5 cm; 0.3 g) and the control with only the nematode (11.2 cm; 0.2 g). Additionally, the *Mariannaea* sp. strain significantly reduced the number of juvenile nematodes per 50 g of soil (15.7 J2) compared to the control (160 J2) in Malabar spinach (*Basella alba* L.) in a net house.

Cited as: Tran, V. T., Vo, Q. T. N., Dinh, T. Q., Nguyen, K. T. V., Nguyen, L. T. N., Nguyen, T. D., & Le, D. D. (2024). Isolating a group of fungi from soil with the ability to control root-knot nematodes (*Meloidogyne* spp.) damage in vegetables. *The Journal of Agriculture and Development* 23(Special issue 2), 33-47.

1. Introduction

Meloidogyne spp. is a root-knot nematode that causes serious damage to many crops in the tropical and subtropical; they have attached roots and reduced vegetable yields (Luc et al., 2005). Due to root-knot nematodes wide host range, controlling these nematodes can be challenging. Pesticides have been used to control nematodes; however, they are toxic to the environment and banned from use (Hutchinson et al., 1999; Nico et al., 2004). Many mechanisms use plant parasitic fungi to control root-knot nematodes. Sharon et al. (2007) reported reduced tomato root damage caused by *Meloidogyne javanica* if tomato pre-planting soil was treated with *Trichoderma harzianum*. Meyer (1999) studied the ability to exhaust egg hatching of *M. incognita* on watermelon of *Verticillium lecanii*. Kerry and Hidalgo-Diaz (2004) developed a management system using *Pochonia chlamydosporia* (*Verticillium chlamydosporium*) to control the root-knot nematode in organic vegetable production. Maehara & Futai (2000) studied the change in the nematode population of the pinewood when applying nine species of fungi isolated from pine trees, in which *Mariannaea elegans* strain was used, however, there was no significant difference in nematode population compared to the control treatment. In Korea, *Mariannaea elegans* was published in 2004 as the anamorph stage of *Cordyceps pruinosa*, an insect pathogenic fungus (Shin *et al.,* 2004). The *Paecilomyces lilacinus* was extensively tested for the biological control of plant parasitic nematodes (Khan et al., 2005). Martez et al. (1996) reported that *P. lilacinus* significantly reduced *M. incognita* in soil and root tomatoes, thereby increasing tomato yield. Sikandar et al. (2020) reported that second-stage juveniles of *M. incognita* increased with increasing fungal concentration and exposure time. The highest mortality of juveniles was recorded at 97.8% in 72 h, respectively, and the highest ovicidal activity was at 100% concentration with 5.2% egg hatching. The study also concluded that *P. chrysogenum* Snef 1216 can be a biocontrol agent against *M. incognita*.

Swe et al. (2011) grouped nematophagous fungi (NF) into group nematode-trapping fungi (NTF), which include: (1) using adhesive or mechanical traps fungi; (2) endoparasitic fungi; (3) egg-parasitic fungi; and (4) toxin-producing fungi (Liu et al., 2009). Nordbring-Hertz et al. (2000) grouped NF into three categories, including nematode-trapping fungi (NTF), endoparasitic, and toxic-compound-producing (NPF). Nematophagous fungi have over 200 species, which are fungi strains that can capture, kill, or parasitize nematodes and use nematodes as an alternative or supplementary source of nutrition. They were classified according to the method of attacking nematodes: nematode-trapping fungi using glue or mechanical traps; endoparasitic fungi using spores; and fungi that parasitize eggs or females with the tips of hyphae and produce toxins and fungal factors that immobilize nematodes before the invasion (Nordbring-Hertz el al., 2006; Hsueha et al., 2013). The egg-parasitic fungi are also one of the potential directions for effective nematode control. The researched strains, including *Paecilomyces* sp., *Pochonia chlamydosporia*, and *Trichoderma viride,* were particularly effective against the root-knot nematodes *Meloidogyne* sp. and *Heterodera* spp. (Moreno-Gavíra et al., 2020; Poveda et al., 2020). Cobb (1917) suggested that NF could be a biological control agent in plant-parasitic nematodes. Linford et al. (1937) used NF for the biological control of nematodes. Currently, both chemical and biological products

are used to control crop-damaging nematodes but are not effective in killing nematodes and cause long-term toxicity to the environment. Meanwhile, biological products used alone, such as Abamectin, Tervigo 20SC, *Bacillus thuringiensis,* and *Trichoderma* supplements, are not as effective in killing nematodes as expected. Therefore, the research aimed to select native nematode-trapping fungi strains that can control root-knot nematodes on vegetable crops.

2. Materials and Methods

2.1. Materials

A total of 35 soil and root of vegetable samples (500 g/sample) were collected in the presence of root-knot nematodes at a depth of about 10 - 20 cm around the root zone of vegetable crops such as carrots, amaranth, spinach, tomatoes, and peppers in Lam Dong province (Da Lat), Ho Chi Minh City (Cu Chi), and Dong Nai (Cam My) for isolating fungi.

Meloidogyne spp. was collected in soil and root Malabar spinach, 10 - 25 cm deep, in Cam My district, Dong Nai province, and identified by morphology according to VS (2020) and Perry et al. (2009). The PDA medium (Himedia) (Potato 200 g, Dextrose 20 g, Agar 20 g), additional 0.1 g/L streptomycin sulfate, and 0.1 g/L penicillin were isolated nematode-trapping fungi.

2.2. Method isolation nematode-trapping fungi

Isolation of the nematode-trapping fungi was performed according to the modified method of Berhanu et al. (2022). Nematodes were collected from soil and roots using a Baermann funnel (Giuma & Cooke, 1971). Weigh 100 g of soil, then put it on a Baermann funnel (mesh diameter of 2 mm) lined with two layers of filter paper. Add sterile water until the water level touches the soil sample. After 24 to 48 h, the nematode suspension was centrifuged at 1.000 rpm for 3 min. The supernatant was then removed, and the pellet was resuspended in 3 mL of distilled water and incubated at room temperature (27°C). After four days, the nematodes were transferred to a 10 mL falcon tube containing 5 mL of sterile distilled water and concentrated (do this step twice). The remaining nematode residue was then transferred to PDA plates (Himedia) supplemented with 0.05 g/L of streptomycin sulfate and 0.05 g/L of penicillin to inhibit bacteria. After 2 - 7 days, the mycelia were checked for fungus growth and purified on PDA. The isolated sample was stored at 4°C in a PDA with glycerin at 15% in the test tube medium.

2.3. Preparation of nematodes and egg material

Nematodes are filtered using the improved Bearman static filtration method. Weigh 100 g of soil and place it on a Baermann sieve (a mesh diameter of 2 mm) lined with two layers of filter paper. Add sterile water until the water level touches the soil sample. The nematodes will move through the filter paper and fall into the tray. Filter for 24 - 48 hours at 28 - 30°C, then examine nematodes under a 10X - 40X stereo microscope.

Nematodes were cultured in an agar medium (1%) after 7 - 10 days, observed under a stereo microscope at 10X magnification, and localized on the agar block with eggs. The agar block containing nematode eggs was cut into a new agar plate (remove the agar block and keep nematode eggs). Besides, root samples with galls suspected to have gall nematodes inside the roots were separated directly on an Olympus stereo microscope to collect adult females and eggs, then cultured on an agar medium and stored in the pots of grown Malabar spinach (Southey, 1986).

2.4. Affected by nematode-trapping fungi to parasitize eggs with *Meloidogyne* spp.

Aspirate 500 µL of fungal spore solution (2 x 10^7 cfu/mL) was cultured in PD (Potato 200 g, dextrose 20 g, water 1000 mL) medium for 5 - 10 days, and then added 1 mL gently spread on a petri dish with 30 nematode eggs. The eggs were placed on 1% water agar plates containing 1% ampicillin (Liang et al., 2020). The experiment was repeated three times for one type of fungus, corresponding to three petri dishes. The control was inoculated with sterile distilled water at 28°C. After 1 - 7 days, the petries were observed under a microscope, stained with methylene blue, and recorded as the percentage of infected eggs until the eggs hatched into juveniles.

2.5. The efficacy of nematode-trapping fungi on second stage junvenlies (J2) (*Meloidogyne* spp.)

The test was in sterile Petri dishes containing 20 µL each of fungal spore suspension at a concentration of 2 x 10^7 spores/mL and 500 µL of nematode suspension containing 50 J2 *Meloidogyne* spp. (Singh & Mathur, 2010). Each treatment was replicated 4 times. The control was sterile distilled water. The effect of fungal spores on nematode activity was recorded after 24 and 72 h. Immobile J2 were transferred to sterile distilled water to check their potential for revival by blue LED light (450 - 490 nm). After 120 sec, nematodes that stopped moving when exposed to blue LED light were considered dead (Rajasekharan et al., 2018). Besides, distinguishing between live and dead J2 was the method by Xiang & Lawrence (2016); nematodes with immobile movement within 2 min exposed to NaOH 1N were considered dead.

2.6. Application of nematode-trapping fungi to *Meloidogyne* spp. on Malabar spinach in a net house

This experiment was performed according to the modified method of Messa et al. (2020), and Naz et al. (2020). Malabar spinach plants were grown in pots measuring 15 - 20 cm, placed 60 cm above the ground, watered daily, and fertilized with NPK (20 - 20 - 15) two days before inoculating nematodes *Meloidogyne* spp. At that time, it had two leaves and was three days older. The inoculum density was adjusted to 1000 eggs and juveniles per 100 cm^3 of soil and incorporated into the soil. The experiment was designed as a completely randomized single factor in a net house. Fungi were cultured in Potato Dextrose Broth medium on a shaker for 5 - 7 days, adjusted spore density to 2 x 10^7 cfu/mL, with the first fungal inoculation occurring ten days after nematode inoculation. Each treatment was replicated 10 times, corresponding to 10 Malarba spinach plants. The treatments were as follows: T0: uninoculated; T1: *Meloidogyne* spp.; T2: *Paecilomyces*. sp.; T3: *Mariannaea* sp.; T4: *Penicillium* sp.; T5: *Meloidogyne* spp. + *Paecilomyces* sp. T6: *Meloidogyne* spp. + *Mariannaea* sp.; T7: *Meloidogyne* spp. + *Penicillium* sp. Measure root length and mass, count the number of galls/root, J2/5g of roots, egg masses/root, and J2/50 g of soil after 40 days of nematode inoculation.

2.7. Data analysis

Data were subjected to analysis of variance (ANOVA) using the SPSS v.22 software and Ducan's test.

3. Results and Discussion

3.1. Isolation nematode-trapping fungi

A total of 12 fungal samples with varying morphology and color colonies were isolated from 35 soil samples collected in vegetable-growing areas in Da Lat (Lam Dong), Cam My (Dong Nai), and Cu Chi (Ho Chi Minh City) and divided into four groups based on morphological characteristics. Group 1 was identified by green fungal colonies, oval spores, and septated spore branches, which occurred in 25% of the samples. Group 2 was determined by purple colonies with elliptical spores growing in chains, flask-shaped, and swollen at the bottom; they grow singly or in clusters of 2 - 4, accounting for 33.3%. Group 3 consisted of purple-red colonies on PDA medium with elliptical to diamond-shaped spores, which grew in phialides chains that were similar vase-shaped and in clusters of 3 - 6 (16.7%). Group 4 were gray or brown colonies on PDA medium, spherical-shaped spores growing in chains, flask-shaped, bulging at the bottom, and gradually getting smaller towards the top (25%).

On PDA, colonies grew slowly, 55 - 60 mm in diameter, after 28 days at 25°C. The colony was round with serrated edges; the mycelium raised above the agar surface, and many dark brown drops appeared. The front of the petri colonies was light orange to brown, and the back was light yellow to orange-brown (Figure 1). The mycelium grows straight, transparent, and without septa. The flasks grow in clusters of 3 - 5 on hyphae and are transparent. The vessel was vase-shaped, bulging at the bottom and gradually getting smaller towards the top, forming a neck shape measuring 4.3 - 15.0 x 2.3 - 2.6 µM. Spores were spherical or subspherical, transparent, and 2.3 - 3.5 x 2.0 - 3.0 µM in size. The morphological characteristics were consistent with those of *Penicillium* sp. (Visagie et al., 2014).

Colonies of fungi in group 2 grew quickly, reaching 75 - 80 mm after 21 days at 25°C. The colony was round with many concentric rings; the color of the colonies changed from white to purple-pink to purple when producing spores, and the mycelium in the center and edges was white. The font of the colony was smooth and covered with a layer of powder. The back was light gray with concentric rings (Figure 2). The mycelium was straight, branched, transparent, and had many septa. The flask grows in clusters of 2 - 4 along the mycelium. The vessels are vase-shaped, short, bulging in the middle, gradually getting smaller towards the tip, measuring 4.1 - 6.7 x 1.6 - 2.2 µM. Spores are spherical, sometimes slightly pointed at both ends and grow in long chains. The chains are often linked to form large, measuring 2.3 - 3.2 x 1.7 - 2.7 µM. The morphological characteristics are consistent with the morphological characteristics of *Paecilomyces lilacinus* (Luangsa-Ard et al., 2011).

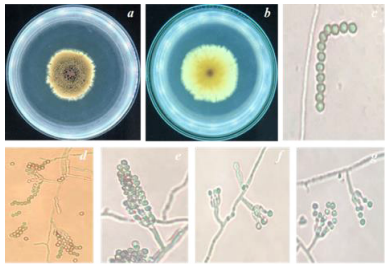

Figure 1. Morphology of *Penicillium* sp. (Group 1). a: front colony on potato dextrose agar (PDA) medium; b: reverse colony on PDA medium; **c**: conidia; d - g: conidia and phialides. Scale bar = 10 µM.

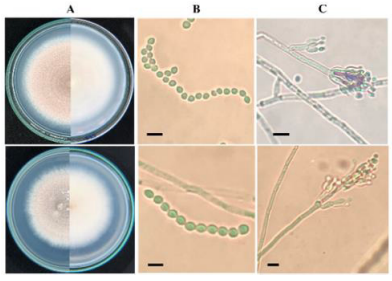

Figure 2. Morphology of *Paecilomyces* sp. (Group 2). A: Colony on potato dextrose agar (PDA) medium, B: Conidia, C: Polyphialides in the aerial mycelium. Scale bar = 10 µM.

The colonies of fungi in group 3 grew quite quickly and reached a diameter of 75 - 80 mm after 14 days at 25°C. The colony was round, divided into many patches with concentric rings; the front of the colony was white; the back surface was dark purple, fading towards the edge; and the mycelium grew close to the agar surface (Figure 3). The hyphae were irregular, complex, and branched, ranging in width from 3 to 7 µM. The flask-shaped body grows from fungal hyphae in clusters of 3 - 6, with dimensions of 9.1 - 25.0 x 1.9 - 3.2 µM. Spores were transparent, elliptical to oblong, swollen in the middle, growing in chains, measuring 4.1 - 8.9 x 2.2 - 3.5 µM. The morphological characteristics were consistent with those of *Mariannaea* sp. (Samson, 1974).

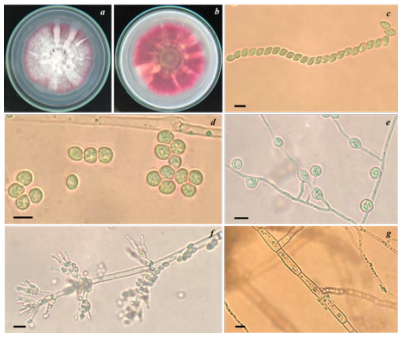

Figure 3. Morphology of *Mariannaea* sp. (group 3). a: Front colony on potato dextrose agar (PDA) medium; b: Reverse colony on PDA medium, c: Conidia, d - e: chlamydospore; f: Polyphialides in the aerial mycelium; g: Mycelium. Scale bar = 10 µM.

In group 4, the colony was round with serrated edges; the upper surface colony was pink with a white line; and the lower surface was yellow-brown. It grew at an average daily rate of 2.19 ± 0.81 mm and reached a diameter of 39 mm after 14 days on PDA (Figure 4). The mycelium was transparent and had no septa. The vessels were 5.32 - 7.64 x 2.03 - 2.72 µM and grew at the top of the mycelium with a dense fan-shaped cluster. Spores were 2.60 - 3.01 x 2.49 - 2.86 µM in size (average 2.80 ± 0.30 x 2.68 ± 0.28 µM, n = 30), spherical. The morphological characteristics were consistent with those of *Aspergillus* sp. (Raper & Fennell, 1965).

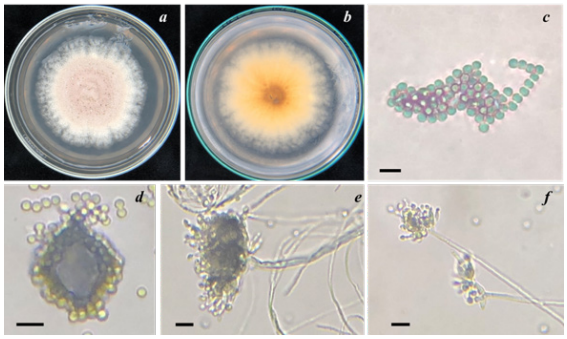

Figure 4. Morphology of *Aspergillus* sp. (group 4); Front colony on potato dextrose agar (PDA) medium; b: Reverse colony on PDA medium, c-d: conidia; e - f: Phialides. Scale bar = 10 µM.

3.2. Parasitism of *Meloidogyne* spp. eggs by nematode-trapping fungi

Table 1. Effect of fungi isolaties on *Meloidogyne* spp. eggs

Treatment	Fugal group	Nematode eggs not hatched after fungal inoculation (%)			
		1 day	3 days	5 days	7 days
LD-CR-7.01	*Mariannaea* sp.	3.00^{ef}	4.33^{cd}	5.67^{f}	9.67^{f}
DN-MT-35.01	*Penicillium* sp.	1.67^{f}	2.67^{d}	3.33^{fg}	5.00^{g}
LD-CC-15.01	*Paecilomyces* sp.	39.33^{a}	53.67^{a}	73.33^{a}	90.67^{a}
LD-OT-11.01	*Mariannaea* sp.	4.33^{e}	7.00^{c}	16.67^{e}	18.33^{e}
CC-CC-8.02	*Paecilomyces* sp.	25.33^{d}	36.67^{b}	49.00^{d}	80.33^{b}
CC-OT-20.01	*Paecilomyces* sp.	29.00^{c}	4.67^{cd}	53.00^{c}	68.33^{d}
LD-RD-6.01	*Penicillium* sp.	0.00^{g}	0.00^{e}	0.00^{g}	0.00^{h}
DN-DL-3.01	*Aspergillus* sp.	0.00^{g}	0.00^{e}	0.00^{g}	0.00^{h}
DN-CC-3.02	*Aspergillus* sp.	0.00^{g}	0.00^{e}	0.00^{g}	0.00^{h}
DN-RC-30.01	*Paecilomyces* sp.	34.33^{b}	50.67^{ab}	68.33^{b}	75.00^{c}
LD-CR-1.01	*Aspergillus* sp.	0.00^{g}	0.00^{e}	0.00^{g}	0.00^{h}
CC-OT-6.03	*Penicillium* sp.	0.00^{g}	0.00^{e}	0.00^{g}	0.00^{h}
Control		0.00^{g}	0.00^{e}	0.00^{g}	0.00^{h}

$^{a-h}$Different letters indicate significant differences within a column at $P < 0.05$.

Four strains of *Paecilomyces* sp. controlled the hatching of nematode eggs, with the percentage of unhatched eggs ranging from 68.33 to 90.67%, of which sample LD-CC-15.01 showed the percentage of eggs not hatching (Table 1), with the highest rate of eggs not hatching being 90.67%. *Mariannaea* sp. (LD-CR-7.01) could control egg hatching, but the rate was low compared to *P. lilacinus*. *Aspergillus* sp. was not able to control nematode egg hatching. According to Hanawi (2016), species in the genus *Paecilomyces*, especially the *P. lilacinus,* were to be able to parasitize *Tylenchulus semipenetrans* eggs. Moreno-Gavíra et al. (2020) and Poveda et al. (2020) recorded that *Paecilomyces* could penetrate eggshells and structural components of juveniles and adult stages in different nematode species through the germination of spores, the branching of mycelium, and the formation of attachments, based on the ability to secrete extracellular enzymes due to destroy the eggshell structure, thereby decreasing the rate of eggs hatching into juveniles. The mycelium was contacted by the host; it penetrated the host through appressorium or secreted enzymes such as cellulase, glucanase, laccase, leucinoxin, lipase, pectinase, protease, chitinase, or xylanase to dissolve the protective layer and protect the outside of the host during infection. Besides, *Paecilomyces* spp. had an active mechanism that controlled the nervous system of nematodes, especially *Meloidogyne* spp., and several other nematode genera such as *Globodera, Rotylenchulus, Heterodera, Xiphinema*, and *Pratylenchus* (Favre-Bonvin et al., 1991). *Paecilomyces lilacinus* decreased *M. incognita* populations in soil and roots and increased tomato yield (Lara et al., 1996). *Paecilomyces lilacinus* has also been reported to infect female nematodes (*Meloidogyne* spp.) and cysts of *Heterodera* spp., and *Globodera* spp. (Jatala, 1986).

3.3. Effect of nematode-trapping fungi on the mobility of J2 *Meloidogyne* spp.

Table 2. Effect of spore suspensions of fungal strains on the mobility of J2 *Meloidogyne* spp.

Treatment	Fugal group	Nematodes (J2) were immobilized at different times (individual)		Percentage of nematodes (J2) immobilized after 72 h (%)
		24 h	72 h	
LD-CR-7.01	*Mariannaea* sp.	$22.3^{bc} \pm 2.2$	$36.0^{ab} \pm 2.9$	72.0
DN-MT-35.01	*Penicillium* sp.	$31.8^{a} \pm 1.3$	$35.0^{ab} \pm 0.82$	70.0
LD-CC-15.01	*Paecilomyces* sp.	$18.3^{cdef} \pm 2.9$	$32.3^{abc} \pm 3.6$	64.6
LD-OT-11.01	*Mariannaea* sp.	$16.0^{fg} \pm 1.15$	$27.3^{cdefg} \pm 1.3$	54.6
CC-CC-8.02	*Paecilomyces* sp.	$20.8^{cd} \pm 1.3$	$28.5^{cdef} \pm 2.1$	57.0
CC-OT-20.01	*Paecilomyces* sp.	$12.0^{hijkl} \pm 1.4$	$30.0^{bcd} \pm 2.8$	60.0
LD-RD-6.01	*Penicillium* sp.	$16.5^{defghi} \pm 2.4$	$26.5^{cdefgh} \pm 3.7$	53.0
DN-DL-3.01	*Aspergillus* sp.	$13.3^{ghijk} \pm 1.5$	$18.0^{jklmn} \pm 1.4$	36.0
DN-CC-3.02	*Aspergillus* sp.	$9.8^{klmn} \pm 2.2$	$18.5^{ijklmn} \pm 2.4$	37.0
DN-RC-30.01	*Paecilomyces* sp.	$18.3^{cdef} \pm 0.5$	$24.3^{defghi} \pm 1.0$	48.6
LD-CR-1.01	*Aspergillus* sp.	$7.0^{mno} \pm 1.6$	$15.3^{lmn} \pm 1.5$	30.6
CC-OT-6.03	*Penicillium* sp.	$4.8^{o} \pm 1.0$	$13.3^{no} \pm 2.8$	26.6
Control		$3.8^{o} \pm 0.5$	$6.8^{p} \pm 1.3$	13.6

$^{a-o}$Different letters indicate significant differences within a column at $P < 0.05$.

The effects of fungal strains on immobile J2 were significantly different ($P < 0.05$) compared to the control treatment after 72 h (Table 2). The results showed that three fungal strains caused the highest inactivation of J2 *Meloidogyne* spp. after 72 h, including *Mariannaea* sp. (LD-CR-7.01) 72%, *Penicillium* sp. (DN-MT-35.01) 70%, and *Paecilomyces* sp. (LD-CC-15.01) 64.6% compared to the control (13.6%). Zarrin et al. (2015) noted that among 13 tested fungi, both *Penicillium* sp. and *Paecilomyces* sp. strains significantly reduced the live larvae of *Trichostrongylidae* after seven days of incubation ($P < 0.01$). The number of larvae (%) was inoculated with the *Penicillium* sp. reduced by 95% and inoculated with the *Paecilomyces* sp. reduced by 91.5% compared to the uninoculated control. The immobile nematodes observed under a microscope (Olympus CX31 RFS) at 20X-40X showed the infection of fungal hyphae into the nematode body (Figure 5) as well as the formation of a sticky trap structure (Figure 6). Studies indicated that *Penicillium* sp. effectively controlled root-knot nematodes such as *P. chrysogenum* (snef1216). Snef1216 could be used as a biological control agent against *M. incognita*, with J2 mortality up to 97.8% after 72 h at 100% concentration (Sikandar et al., 2020). Snef 1216 was also introduced as a biomass enhancer and has potential as a biocontrol agent against *M. incognita* in cucumbers by significantly reducing the density and growth of nematode, reducing fertility rate, interfering with gall formation, and improving seed germination (Sikandar et al., 2019). A compound produced from *P. commune* KACC 45973 was reported for the first time to kill second-stage larvae of *M. incognita, M. hapla*, and *M. arearia*. It also significantly inhibited egg

hatching of *M. incognita* and *M. hapla* after 28 days of treatment with concentrations > 25 µg/mL (Nguyen et al., 2021). *Paecilomyces* spp. was immobilized in J2 of *Meloidogyne* spp. from 28.5% to 60%. Dávila & Hío (2005) noted that *Paecilomyces* sp. can parasitize > 50% of *M. javanica* populations at 72 h under controlled conditions. The mechanism of action of the nematophagus may be that the spores adhere and adhere to the epidermis, mouth, excretory pore, anus, or sensory organs before germination and infection of the nematode. After the production of germ tubes, the nematode cuticle is penetrated and the growth of hyphae occurs, which remain alive until the hyphae reach the vital organs (Devi, 2018). We recorded the image of hyphae growing out of the second-stage juveniles *Meloidogyne* sp. clearly in Figure 5a. In recent years, biological control of nematodes has received attention from researchers in many countries (Larsen, 2002). Current research results demonstrate that some environmentally dispersed saprophytic fungi can effectively reduce the number of second-stage juveniles *Meloidogyne* sp.

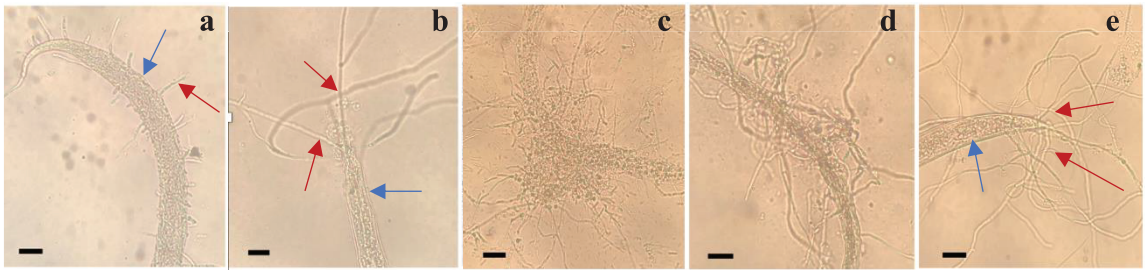

Figure 5. The hypae infecting J2 *Meloidogyne* spp. a, b, c, d: Strains belonging to *Paecilomyces* sp., e: Strains belonging to *Penicillium* sp. Blue arrow: second stage juveniles, red arrow: hypae. Scale bar = 20 µM.

Pramer & Stoll (1959) reported that nematophagous fungi use specialized trapping devices to attack nematodes; they do not produce traps constitutively but rather initiate trap formation in response to their prey. In this study, we noted the characteristics of trap plugs formed in the presence of nematodes; under culture conditions on a PDA medium, the fungus did not form trap structures. Tunlid et al. (1992) reported that sticky traps were triggered by various biotic and abiotic factors, of which direct contact between mycelium and living nematodes was the most important key for nematode-trapping fungi. Nematodes were attracted to fungal traps, and once they touched the trap, they became stuck to the sticky trap. The nematode was paralyzed before the mycelium developed a structure that penetrated the cuticle, allowing the fungus to grow inside the body and eventually completely digest it (Lopez-Llorca et al., 2008). This entire process could take less than 24 h for many nematode-trapping fungi. Li et al. (2000) reported that more than 200 species of fungi belonging to Basidiomycota, Ascomycota, and Zygomycota use sticky trap structures to trap nematodes in soil, indicating that sticky traps are a common type of trap among filamentous fungi. Olivares and Lopez-Llorca (2002) pointed out that the ability to adapt to a variety of environments and the production of extracellular enzymes are two characteristics that make filamentous fungi suitable for use as biocontrol agents.

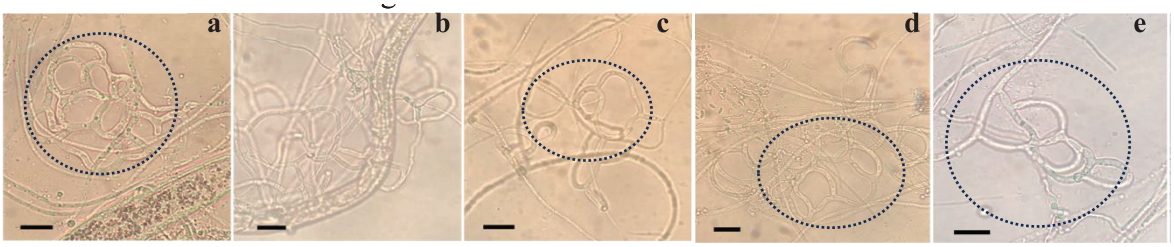

Figure 6. An adhesive network trap structure of five fungi strain. a, b, c, d: *Paecilomyces* sp., e: *Penicillium* sp. Scale bar = 20 µM.

3.4. Application of nematode-trapping fungi to *Meloidogyne* spp. on Malabar spinach in a nethouse

Table 3. Effect of applying nematode-trapping fungi on Malabar spinach in a pot trial with *Meloidogyne* spp.

Treatment	Root length (cm) (± SE)	Root weight (g) (± SE)	Galls/root (± SE) (gall)	Egg masses/ root (egg)	Juveniles J2/50 g soil (± SE)
T0 - control (uninocutaed nematodes)	$18.5^{c} \pm 1.0$	$0.3^{c} \pm 0.15$	0^{e}	0	0^{d}
T1 - control (inoculated nematodes)	$11.2^{e} \pm 1.4$	$0.2^{d} \pm 0$	$6.7^{a} \pm 2.5$	72	$160.0^{a} \pm 9.0$
Paecilomyces sp.	$18.2^{c} \pm 1.6$	$0.3^{c} \pm 0.05$	0^{e}	0	0^{d}
Mariannaea sp.	$20.5^{b} \pm 1.4$	$0.3^{c} \pm 0.1$	0^{e}	0	0^{d}
Penicillium sp.	$26.5^{a} \pm 3.9$	$0.5^{a} \pm 0.1$	0^{e}	0	0^{d}
Meloidogyne spp. + *Paecilomyces sp.*	$14.7^{d} \pm 0.8$	$0.2^{d} \pm 0.05$	$0.3^{d} \pm 0.5$	0	$13.7^{c} \pm 1.5$
Meloidogyne spp. + *Mariannaea* sp.	$25.3^{c} \pm 0.7$	$0.4^{b} \pm 0.05$	$1.7^{c} \pm 0.5$	2	$15.7^{c} \pm 2.5$
Meloidogyne spp. + *Penicillium* sp.	$25.8^{bc} \pm 1.9$	$0.3^{c} \pm 0.05$	$2.0^{b} \pm 1.0$	3	$55.0^{b} \pm 3.0$

$^{a-d}$Different letters indicate significant differences within a column at $P < 0.05$; Inoculated with 1000 Meloidogyne spp. eggs and juveniles per 100 cm^3 soil.

The fungi in the study were isolated from the rhizosphere soil, so it will be monitored for up to 40 days to evaluate the effects of the fungi on plant growth. Table 3 and Figure 7 showed that the root length in the treatments had significant differences after 40 days of injection. The *Penicillium* sp. treatment resulted in longer root lengths than the uninoculated control (26.5 cm compared with 18.5 cm) and the nematode-inoculated control (11.2 cm) on Malabar spinach. Recently, some reports have demonstrated the application of *Penicillium* as a PGPF in crops such as soybean (Bilal et al., 2019), wheat (Elgharably & Nafady, 2021), and corn (Zhao et al., 2021). In addition, several studies have shown the effects of *Penicillium* on plant growth and increased tolerance to salt stress in various plant species. Jin et al. (2022) reported that the phosphate solubilizing strain *P. funiculosum* P1 improved the development of quinoa plants

under salt-stress conditions, with an increase in the antioxidant system by producing organic acids. Miao et al. (2019) showed that *Penicillium brefeldianumon* isolated from melons effectively against *M. incognita*. Gouli et al. (2013) multiplied the biomass of entomopathogenic fungi in the genera *Beauveria, Metarhizium, Mariannaea*, and *Tilachlidium*, which commonly exist in nature as hemisaprophytes in soil and controlling entomopathogenic. In Korea, *Mariannaea elegans* was first published in 2004 as the anamorph stage of *Cordyceps pruinosa*, an insect pathogenic fungus (Shin et al., 2004). Maehara & Futai (2000) studied the change in the nematode population of the pinewood when applying nine species of fungi isolated from pine trees, in which *Mariannaea elegans* strain was tested, however, there was no significant difference in nematode population in the *M. elegans* inoculated treatment compared to the control treatment. Only a few published reports on the control of nematodes by *M. elegans*.

Additionally, the results reported the number of galls/root and the number of juveniles/50 g of soil were both lower than the control, especially the *Paecilomyces* sp. strain treatment, which had the best nematode control effect with 0.3 galls/root compared to the control of 6.7 galls/root. The number of juveniles/50 g of soil was 13.7 J2 compared to the control of 160 J2. Combined *P. lilacinus* and *Monacrosporium lysipagum* reduced 62% of galls and 94% of *M. javanica* juveniles on tomatoes compared to the experiment with no fungi added. Sixty-five percent of *H. avenae* cysts were reduced on barley by combined application of fungi (Khan et al., 2006). As a result, all three native fungal strains (*Penicillium* sp., *Paecilomyces* sp., and *Mariannaea* sp.) affected root and controlled nematode growth on Malabar spinach in the nethouse.

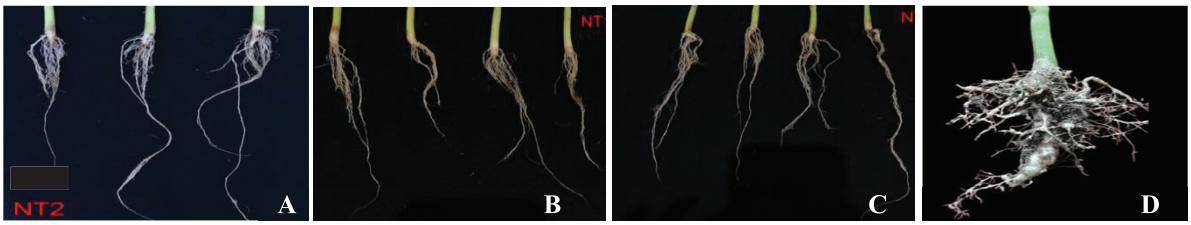

Figure 7. Root length of Malabar spinach at 40 days inoculated nematodes and at 30 days innocuted fungi. A. T0 - control (uninocutaed nematodes), B. T1 - control (inoculated nematodes), C. *Meloidogyne* spp. + *Mariannaea* sp. D. Galls on Malaber spinach root caused by *Meloidogyne* sp. after 60 days in the garden maintaining the nematode source.

4. Conclusions

The study isolated four fungi groups (*Aspergillus* sp., *Paecilomyces* sp., *Mariannaea* sp., and *Penicillium* sp.) from 35 samples collected in soil and roots on carrots, spinach, tomatoes, amaranth, and chilies plants at Lam Dong province (Da Lat city), Ho Chi Minh City (Cu Chi district), and Dong Nai province (Cam My district). *Paecilomyces* sp., *Mariannaea* sp., and *Penicillium* sp. effectively inactivated second-stage juveniles (J2) after 72 h. Specifically, *Paecilomyces* sp. immobilized 64.5% of the nematodes, *Mariannaea* sp. 72%, and *Penicillium* sp. 70%, compared to only 13.5% in the control without inoculation. *Paecilomyces* sp. controlled the hatching of

nematode eggs, with the rate of unhatched eggs ranging from 68.33 to 90.67%. LD-CC 15.01 (*Paecilomyces* sp.) showed the percentage of eggs not hatching to 90.67%. The experiment investigating the influence of fungal strains on J2 in Malabar spinach (*Basella alba* L.) in a net house showed that the *Mariannae* sp. strain inoculated on plants at a density of 10^7 cfu/mL produced the most expected results in terms of root length (25.3 cm) and root weight (0.4 g) compared to the control without fungus inoculation (18.5 cm; 0.3 g) and the control with only the nematode (11.2 cm; 0.2 g). Additionally, the *Mariannaea* sp. significantly reduced the number of juveniles/50 g of soil (13.7 J2) compared to the control (160 J2) in Malabar spinach (*Basella alba* L.) in a net house.

Conflict of interest

The authors have no conflict of interest to declare.

Acknowledgements

We would like to thank the Center of Research and Development - Petro Viet Nam Ca Mau Fertilizer JSC, for partially sponsoring this research.

References

Berhanu, M., Waktole, H., Mamo, G., & Terefe G. (2022). Isolation of nematophagous fungi from soil samples collected from three different agro-ecologies of Ethiopia. *BMC Microbiology* 22, 159-164. https://doi.org/10.1186/s12866-022-02572-4.

Bilal, S., Shahzad, R., Khan, A. L., Al-Harrasi, A., Kim, C. K., & Lee, I. J. (2019). Phytohormones enabled endophytic Penicillium funiculosum LHL06 protects Glycine max L. from synergistic toxicity of heavy metals by hormonal and stress-responsive proteins modulation. *Journal of Hazard Mater* (379), 120824. https://doi.org/10.1016/j.jhazmat.2019.120824.

Cobb, N. A. (1917). A genus of freedom living predatory nematodes: Contributions to a Science of Nematology VI: (With 75 Illustration in the Text). *Soil Science* 3(5), 431-486.

Dávila, L., & Hío, J. C. (2005). Evaluation of activity biocontroller of *Arthrobotrys* sp. and *Paecilomyces* sp. on *Meloidogyne javanica* under in vitro and greenhouse conditions in chrysanthemum (*Drendranthema grandiflora* Andernson). *Agronomia Colombiana* 23(1), 91-101.

Devi, G. (2018). Utilization of nematode destroying fungi for management of plant-parasitic nematodes-a review. *Biosciences Biotechnology Reasearch Asia*. 15(2), 377-396. http://dx.doi.org/10.13005/bbra/2642.

Elgharably, A., & Nafady, N. A. (2021). Inoculation with *Arbuscular mycorrhizae*, Penicillium funiculosum and Fusarium oxysporum enhanced wheat growth and nutrient uptake in the saline soil. *Rhizosphere* 18(1), 100345. https://doi.org/10.1016/j.rhisph.2021.100345.

Favre-Bonvin, J., Ponchet, M., Djian, C., Arpin, N., & Pijarowski, L. (1991). Acetic acid: A selective nematicidal metabolite from culture filtrates of *Paecilomyces lilacinus* (Thom) Samson and *Trichoderma longibrachiatum* Rifai. *Nematologica* 37, 101-112.

Giuma, A. Y., & Cooke, R. C. (1971). Nematotoxin production by *Nematoctonus haptocladus* and N. concurrens. *Transactions of The British Mycological Society* 56(1), 89-IN6.

Gouli, V., Provost, C., Gouli, S., Parker, B. L., & Skinner, M. (2013). Productivity of different species of entomopathogenic fungi based on one type of technology. *International Journal of Agricultural Technology* 9(3), 571-580.

Hsueha, Y. P., Mahantib, P., Schroederb, F. C., & Sternberg, P. W. (2013). Nematode-trapping fungi eavesdrop on nematode pheromones. *Current Biology* 23(1), 83-86.

Hutchinson, C. M., McGiffen, M. E., Ohr, H. D., Sims, J. J., & Becker J. O. (1999). Efficacy of methyl iodide soil fumigation for control of *Meloidogyne incognita*, *Tylenchulus semipenetrans* and *Heterodera schachtii*. *Nematology* 1, 407-414.

Jatala, P. (1986). Biological control of plant-parasitic nematodes. *Annual Review of Phytopathology* 24(1), 453-489.

Jin, X., Xin, Y., Zhang, H., & Cui, J. L. (2022). The microscopic mechanism between endophytic fungi and host plants: from recognition to building stable mutually beneficial relationships. *Microbiology Research* 261, 127056. https://doi.org/10.1016/j.micres.2022.127056.

Khan, A., Williams, K. L., & Nevalainen, H. K. (2006). Control of plant-parasitic nematodes by *Paecilomyces lilacinus* and *Monacrosporium lysipagum* in pot trials. *Biocontrol* 51, 643-658. https://doi.org/10.1007/s10526-005-4241-y.

Lara, J., Acosta, N., Betancourt, C., Vincente, N., & Rodriguez, R. (1996). Biological control of *Meloidogyne incognita* in tomato in Puerto Rico. *Nematropica* 26, 143-152.

Larsen, M. (2002). Biological control in a global perspective–a review with emphasis on Duddingtonia flagrans. In *Biological control of Nematode parasites of small ruminants in Asia.* (1st ed.,19-37). Kualar Lumpur, Malaysia: FAO.

Li, T. F., Zhang, K. Q., & Liu, X. Z. (2000). *Taxonomy of nematophagous fungi*. Beijing, China: Chinese Scientific and Technological Publications.

Liang, Y. J, Ariyawansa, H. A., Becker, J. O., & Yang, J. (2020). The evaluation of egg-parasitic fungi *Paraboeremia taiwanensis* and *Samsoniella* sp. for the biological control of *Meloidogyne enterolobiion* Chinese cabbage. *Microorganisms* 8(6), 828-831. https://doi.org/10.3390/microorganisms8060828.

Linford, M. B., & Oliviera, J. M. (1937). The feeding of hollow-spear nematodes on other nematodes. *Science* 85(2203), 295-297.

Liu, X., Xiang, M., & Che, Y. (2009). The living strategy of nematophagous fungi. *Mycoscience* 50(1), 20-25.

Lopez-Llorca, L. V., Maciá-Vicente, J. G., & Jansson, H. B. (2008). Mode of action and interactions of nematophagous fungi. In Ciancio, A., & Mukerji, K. G. (Eds.). *Integrated management and biocontrol of vegetable and grain crops nematodes* (1st ed., 51-76). Dordrecht, Netherlands: Spinger.

Luangsa-Ard, J., Houbraken, J., van Doorn, T., Hong, S. B., Borman, A. M., Hywel-Jones, N. L., & Samson, R. A. (2011). *Purpureocillium*, a new genus for the medically important *Paecilomyces lilacinus*. *FEMS Microbiology Letters* 321(2), 141-149. https://doi.org/10.1111/j.1574-6968.2011.02322.x.

Luc, M., Sikora, R. A., & Bridge, J. (2005). *Plant-Parasitic nematodes in subtropical and tropical agriculture* (2nd ed.). Oxford, UK: Oxford University Press.

Maehara, N., & Futai, K. (2000). Population changes of the pinewood nematode, Bursaphelenchus xylophilus (Nematoda: Aphelenchoididae), on fungi growing in pine-branch segments. *Applied Entomology and Zoology* 35(3), 413-417.

MARD (Ministry of Agriculture and Rural Development). (2016). Circular No. 07/2016/TT-BNNPTNT dated on May 31, 2016. Prevention and control of terrestrial animal diseases. Retrieved March 14, 2023, from https://thuvienphapluat.vn/van-ban/EN/The-thao-Y-te/Circular-07-2016-TT-BNNPTNT-prevention-of-terrestrial-animal-disease-epidemic/527004/tieng-anh.aspx.

Martez, J. L., Acosta, N., Betancourt, C., Vincente, N., & Rodriguez, R. (1996). Biological control of *Meloidogyne incognita* in tomato in Puerto Rico. *Nematropica* 26(2), 143-152.

Messa, V. R., da Costa, A. C., Kuhn, O. J., & Stroze, C. T. (2020). Nematophagous and endomycorrhizal fungi in the control of Meloidogyne incognita in soybean. *Rhizosphere* 15, 100222. https://doi.org/10.1016/j.rhisph.2020.100222.

Meyer, S. L. (1999). Efficacy of the fungus *Verticillium lecanii* for suppressing root-knot nematode egg numbers on Cantaloupe roots. *HortTechnology* 9, 443-447.

Miao, G. P., Han, J., Zhang, K. G., Wang, S. C., & Wang, C. R. (2019). Protection of melon against Fusarium wilt-root knot nematode complex by endophytic fungi Penicillium brefeldianum HS-1. Symbiosis 77, 83-89. https://doi.org/10.1007/s13199-018-0565-0.

Moreno-Gavíra, A., Huertas, V., Diánez, F., Santos, M., & Sánchez-Montesinos, B. (2020). *Paecilomyces* and its importance in the biological control of agricultural pests and diseases. *Plant Disease*. 9(12), 1-28. https://doi.org/10.3390/plants9121746.

Naz, I., Khan, R. A. A., Masood, T., Baig, A., Siddique, I., & Haq, S. (2021). Biological control of root knot nematode, Meloidogyne incognita, in vitro, greenhouse and field in cucumber. *Biological Control.* 152, 104429. https://doi.org/10.1016/j.biocontrol.2020.104429.

Nguyen, S. D., Trinh, T. H. T., Tran, T. D., Nguyen, T. V., Chuyen, H. V., Ngo, V. A., & Nguyen, A. D. (2021). Combined application of rhizosphere bacteria with endophytic bacteria suppresses root diseases and increases productivity of black pepper (Piper nigrum L.). *Agriculture* 11(1), 15.

Nico, A. I., Jiménez-Dıaz, R. M., & Castillo, P. (2004). Control of root-knot nematodes by composted agro-industrial wastes in potting mixtures. *Crop Protection* 23(7), 581-587.

Nordbring-Hertz, B., Jansson, H. B., & Tunlid, A. (2006). Nematophagous fungi. *Encyclopedia of Life Sciences* 1-11. https://doi.org/10.1038/npg.els.0004293.

Olivares-Bernabeu, C. M., & López-Llorca, L. V. (2002). Fungal egg-parasites of plant-parasitic nematodes from Spanish soils. *Revista Iberoamericana de Micología* 19(2), 104-110.

Perry, R. N., Moens, M., & Starr, J. L. (2009). *Root-knot Nematodes* (Illustrated ed.). California, USA: CAB International.

Poveda, J., Abril-Urias, P., & Escobar, C. (2020). Biological control of plant-parasitic nematodes by filamentous fungi inducers of resistance: *Trichoderma,* mycorrhizal and endophytic fungi. *Frontiers in Microbiology* 11(5), 1-14.

Pramer, D., & Stoll, N. R. (1959). Nemin: A morphogenic substance causing trap formation by predaceous fungi. *Science* 129(3354), 966-967.

Rajasekharan, S. K., Raorane, C. J., & Lee, J. (2018). LED based real-time survival bioassays for nematode research. *Scientific Reports* 8(1), 11531. https://doi.org/10.1038/s41598-018-30016-5.

Raper, K. B., & Fennell, D. I. (1965). *The Genus Aspergillus* (1st ed.). Philadelphia, USA: Williams & Wilkins.

Samson, R. A. (1974). *Paecilomyces and some allied hyphomycetes.* Utrecht, Netherlands: Entraalbureau voor Schimmelcultures.

Sharon, E., Chet, I., Viterbo, A., Bar-Eyal, M., Nagan, H., Samuels, G. J., & Spiegel, Y. (2007). Parasitism of Trichoderma on Meloidogyne javanica and role of the gelatinous matrix. *European Journal of Plant Pathology* 118, 247-258. https://doi.org/10.1007/s10658-007-9140-x.

Shin, J. C., Shrestha, B., Lee, W. H., Park, Y. J., Kim, S. Y., Jeong, G. R., Kim, H. K., Kim T. W., & Sung, J. M. (2004). Distribution and favorable conditions for mycelial growth of Cordyceps pruinosa in Korea. *The Korean Journal of Mycology* 32(2), 79-88. https://doi.org/10.4489/KJM.2004.32.2.079.

Sikandar, A., Zhang, M. Y., Zhu, X. F., Wang, Y. Y., Ahmed, M., Iqbal, M. F., Javeed, A., Xuan,

Y. H., Fan, H. Y., Liu, X. Y., Chen, L. J., & Duan, Y. X. (2019). Effects of Penicillium chrysogenum strain Snef1216 against root-knot nematodes (Meloidogyne incognita) in cucumber (Cucumis sativus L.) under greenhouse conditions. *Applied Ecology and Environmental Research* 17(5), 12451-12464. https://doi.org/10.15666/aeer/1705_1245112464.

Sikandar, A., Zhang, M., Wang, M., Zhu, X., Liu, X., Fan, H., Xuan, Y., Chen, L., & Duan, Y. (2020). In vitro evaluation of Penicillium chrysogenum Snef1216 against Meloidogyne incognita *(root-knot nematode). Scientific Reports* 10(1), 8342. https://doi.org/10.1038/s41598-020-65262-z.

Singh, S., & Mathur, N. (2010). In vitro studies of antagonistic fungi against the root-knot nematode Meloidogyne incognita. *Biocontrol Science and Technology* 20(3), 275-282.

Southey, J. F. (1986). *Laboratory methods for work with plant and soil nematodes* (6th ed.). London, UK: Ministry of Agriculture, Fisheries and Food.

Swe, A., Li, J., Zhang, K. Q., Pointing, S. B., Jeewon, R., & Hyde, K. D. (2011). Nematode-trapping fungi. *Current Research in Environmental and Applied Mycology* 1(1), 1-26.

Tunlid, A., Jansson, H. B., & Nordbring-Hertz, B. (1992). Fungal attachment to nematodes. *Mycological Research* 96(6), 401-412. https://doi.org/10.1016/S0953-7562(09)81082-4.

Visagie, C. M, Houbraken, J., Frisvad, J. C., Hong, S. B., Klaassen, C. H. W., Perrone, G., Seifert, K. A., Varga, J., Yaguchi, T., & Sasmon, R. A. (2014). Identification and nomenclature of the genus *Penicillium*. *Studies in Mycology* 78(1), 343-371. https://doi.org/10.1016/j.simyco.2014.09.001.

VS (Vietnam Standards). (2020). Standard No. TCVN 12194-2-4-2020 dated on December 31, 2020. Procedure for identification of plant parasitic nematodes. Part 2-4: Particular requirements for *Meloidogyne* spp. Retrieved June 15, 2023, from https://tieuchuan.vsqi.gov.vn/tieuchuan/view?sohieu=TCVN+12194-2-4%3A2020.

Xiang, N., & Lawrence, K. S. (2016). Optimization of *In vitro* techniques for distinguishing between live and dead second stage juveniles of *Heterodera glycines* and *Meloidogyne incognita*. *Plos One* 11(5), 0154818. https://doi.org/10.1371/journal.pone.0154818.

Zhao, X., Ni, Y., Zhao, H., Liu, X., He, B., Shi, B., Ma, Q., & Liu, H. (2021). Plant growth-promoting ability and control efficacy of *Penicillium aurantiogriseum* 44M-3 against sesame *Fusarium* wilt disease. *Biocontrol Science and Technology* 31(12), 1314-1329. https://doi.org/10.1080/09583157.2021.1946011.

Evaluation of the control ability of *Phytophthora* sp. to damage on chili plant (*Capsicum annuum* L.) using Arbuscular Mycorrhiza Fungi (AMF) product

Da U. T. Dao[1*], Han T. N. Tran[2], Nghia T. Tran[3], Nghia T. Hoang[2], Nhu N. K. Vu[1], Ha T. T. Tran[1], Ha K. Duong[4], & Hoang P. T. Truong[1]

[1]Research Institute for Biotechnology and Environment, Nong Lam University, Ho Chi Minh City, Vietnam

[2]Faculty of Biological Sciences, Nong Lam University, Ho Chi Minh City, Vietnam

[3]Thanh Thanh Cong Sugarcane Research and Development Company Limited, Tay Ninh, Vietnam

[4]Agriculture Extension Center, HCMC Department of Agriculture and Rural Development, Ho Chi Minh City, Vietnam

ARTICLE INFO

Research Paper

Received: August 31, 2024
Revised: December 23, 2024
Accepted: December 25, 2024

Keywords

Acaulospora
AMF product
Chili
Glomus
Phytophthora

***Corresponding author**

Dao Uyen Tran Da
Email:
duta@hcmuaf.edu.vn

ABSTRACT

The Arbuscular Mycorrhizal Fungi (AMF) form a reciprocal symbiosis with approximately 80% of terrestrial plant species, including various agricultural crops. They provide essential nutrients to host plants, improving drought tolerance, salinity resistance, and disease resistance. This study aimed to evaluate the ability of AMF to control *Phytophthora* disease in chili plants grown in a net house. Eight treatments were applied, including two controls (without AMF), five with AMF supplementation at different formulation ratios (30%, 40%, 50%, 60%, and 70%), and one using a commercially available AMF product. The results showed that AMF enhanced plant growth and development while reducing the negative effects of *Phytophthora* sp. on chili plants. Compared to the control, the 70% AMF treatment exhibited the lowest disease incidence and severity indexes at 17, 24, 31, and 38 days. The corresponding disease index and disease rate during the observation period were 0.8%, 1.2%, 1.8%, and 2.3% for the index, and 4.0%, 5.4%, 8.9%, and 9.9% for the rate, respectively. Furthermore, 24 days after treatment, the 70% AMF treatment demonstrated a 70.1% disease prevention effect.

Cited as: Dao, D. U. T., Tran, H. N. T., Tran N. T., Hoang, N. T., Vu, N. K. N., Tran, H. T. T., Duong, H. K., & Truong, H. P. T. (2024). Evaluation of the control ability *of Phytophthora* sp. to damage on chili plant (*Capsicum annuum* L.) using Arbuscular Mycorrhiza Fungi (AMF) product. *The Journal of Agriculture and Development* 23(Special issue 2), 48-62.

1. Introduction

The area of land devoted to chili cultivation has increased in Vietnam due to the significant economic benefits of the industry. However, climate change has posed challenges to chili farming. Controlling pests and implementing effective cultivation and prevention strategies have become increasingly difficult tasks. Various pests and diseases can damage different parts of the chili plant, but *Phytophthora* spp. disease is among the most destructive.

Every stage of the plant's development is impacted by the disease, and widespread fungal spread can drastically reduce productivity. More importantly, the pathogen can persist in the soil and plant residues, posing a threat to subsequent crops. The disease causes blight in individual plants or groups, especially in water-saturated soil following irrigation or rainfall. Early symptoms include brown necrotic spots on the plant roots and crowns, followed by rapid disease progression and eventual plant death (Ozgonen & Erkilic, 2007).

Approximately 10,000 distinct fungal species are known to cause plant diseases; these fungi are frequently found in soil, air (as spores), and plant lesions (Agrios, 2005). The type of fungus that causes plant root disease varies depending on the host plant's nutrition, and the same is true for The Arbuscular Mycorrhizal Fungi (AMF) colonization in plant roots. Consequently, when AMF and pathogenic fungi are present in the rhizosphere of a host plant's roots, three entities are continuously interacting: the pathogenic fungus, the AMF, and the host plant. When *Phytophthora* sp. and AMF coexist, spatial competition may occur within the root cells, as they occupy different cortical cells of the host plant's roots (Azcón-Aguilar & Barea, 1997).

The trial results also showed that the percentages of healthy roots and shoot weights of mycorrhizal (*Glomus fasciculatus*) sweet orange seedlings inoculated with *Phytophthora parasitica* (20 or 50 chlamydospores per gram of soil) were higher than those of non-mycorrhizal seedlings at either inoculum density, as demonstrated by Davis & Menge (1981). Additionally, a study demonstrated that *Phytophthora* sp. and AMF compete within root cells. It was observed that the growth of *Phytophthora* sp. is restricted by AMF symbiosis, and the pathogen does not infect cells in the presence of AMF or in close proximity to the roots (Akhtar & Siddiqui, 2008).

Symbiosis of AMF in host plants reduces disease inoculation and confines injury locations within the host plant, thereby limiting the spread of the pathogen to other areas. Additional mechanisms by which AMF symbiosis decreases pathogen activity include the formation of wound barriers, clogging of air pores to allow only gas and water vapor to pass through, and improving the host plant's nutritional status to facilitate rapid root recovery after pathogen attack. AMF also act as a physical barrier against pathogens. The extracellular hyphae of AMF cover root tissues, thickening and strengthening them, making it more difficult for pathogens to attack (Akhtar & Siddiqui, 2008).

The AMF forms a reciprocal symbiosis with approximately 80% of terrestrial plant species, including various crops. AMF provide host plants with water and nutrients, primarily nitrogen, phosphorus, potassium, and trace elements, in exchange for photosynthetic products (Smith & Read, 2010). Additionally, AMF enhance drought tolerance, salinity resistance (Augé & Saxton, 2015), and disease resistance (Pozo & Azcón-Aguilar, 2007).

Moreover, AMF can compete with pathogens for space and nutrients both within the roots and in the soil surrounding the rhizosphere. In light of this, the application of biological measures to manage pests and diseases has emerged as an effective alternative to chemical treatments, offering comparable efficacy while being safe for humans and environmentally friendly.

2. Materials and Methods

2.1. Isolation and identification of *Phytophthora* sp. based on morphological characteristics

Collection of soil samples

Chili soil samples were collected in Hoc Mon, Ho Chi Minh City, in March 2022. The symptoms of *Phytophthora* sp. disease on chili plants include brown or black spots on the leaves and stem stubs, as well as rotted roots. Severely infected plants appear black, withered, and dead. Soil samples were collected from the vicinity of symptomatic plants at a depth of 5 to 15 cm. Five soil samples were taken from separate locations in each garden, thoroughly mixed, and combined into a final sample weighing 1,000 g per garden. After collection, the samples were preserved in zip bags labeled with the field name, sampling location, and accompanying code (VS, 1985).

***Isolation and identification of Phytophthora* sp.**

Indirect isolation of *Phytophthora* from soil samples was performed using the rose petal trap method. To begin, 100 g of soil was added to sterile distilled water in a ratio of 1 part soil to 3 parts water. The mixture was gently stirred, allowed to settle for 2 h, and then incubated in the dark at room temperature. Infected rose petals were observed after 1 - 3 days. Re-isolation was performed on water agar (WA) medium (20 g agar; 1,000 mL distilled water).

The samples were sterilized with distilled water twice, washed with 70% ethanol for 30 sec, and rinsed again with distilled water. After sterilization, the samples were cut into small pieces and placed on filter paper to dry for 30 min. The dried samples were cultured on WA medium and incubated at 25°C in dark conditions. After 2 - 3 days on WA medium, the mycelium was transferred to carrot agar (CRA) medium (600 g carrots, 15 g $CaCO_3$, 15 g agar, 1,000 mL distilled water) and incubated at 25°C in dark conditions.

According to Ho (1990), Drenth & Sandall (2001), and Abad et al. (2023), morphological features are the basis for *Phytophthora* sp. identification. Key features include oospores, sporangium size and shape, chlamydospore characteristics, sporangiophore branching, and swollen mycelium.

Preparation of Phytophthora* sp. *solution

Phytophthora sp. was cultured at a concentration of 10^6 CFU/mL in LB medium, and chili plants were evenly watered with the fungal spore solution (50 mL of spore solution per pot) ten days after AMF supplementation.

2.2. Evaluation of AMF bioproducts for controlling *Phytophthora* sp.

Preparation of AMF product

The AMF products were created by mixing the biomass of two genera of AM fungi, *Glomus* sp. and *Acaulospora* sp., at a concentration of 10^2 IP/g (IP - inoculation potential).

Experimental design to evaluate the effect of AMF products on *Phytophthora* sp. diseases on chili plants

The experiment was conducted at the Research Institute for Biotechnology and Environment, Nong Lam University, Ho Chi Minh City, Vietnam. The experimental period

lasted six months, from May 2022 to November 2022. The experiment was carried out in a net house with an area of 50 m^2, where temperatures ranged from 35 - 40°C and humidity levels were between 50% - 65%

The scientific name of chili is *Capsicum frutescens*. Each chili pot contained 4 kg of steamed and sterilized soil and measured 25 cm × 20 cm × 20 cm. NPK fertilizer was applied following the 20 - 20 - 15 formula at a rate of 10 g per pot, with fertilization occurring every 10 days. After the chili plants were incubated in trays for 30 days, they were transplanted into pots, and the AMF product was applied one day later.

Eight randomized complete block design (RCBD) plots with one factor and three replications were used in the experiment. Each plot contained 30 pots of plants, totaling 240 pots. *Phytophthora* sp. was injected into NT1 (positive control) without the use of AMF. The NT2 (negative control) received neither AMF nor *Phytophthora* sp. In addition to being inoculated with *Phytophthora* sp., five plots (NT3, NT4, NT5, NT6, and NT7) were treated with AMF products at concentrations of 30%, 40%, 50%, 60%, and 70%, respectively. Commercial Mycorrhiza products with *Phytophthora* sp. were used in NT8 (Mycorrhiza). The NT8 (Mycorrhiza) was a product of the Institute of Soil and Agrochemistry, Ministry of Agriculture and Rural Development. Following treatment, the experimental monitoring period (days after treatment, DAT) was conducted at 17, 24, 31, and 38 days.

Methods for measuring indicators in experiments

- Plant height (cm): measure from the stem base to the top of the plant.
- Root length (cm): measure from the stem base to the longest root.
- Total number of roots (roots): count all roots emerging from the stem base.
- Root biomass (g): Record the fresh weight of the roots.
- Total number of spores (spore per 100 g soil): Following the method by Brundrett et al. (1996), spores were extracted from the soil using centrifugation in a 50% sucrose solution and moist sieving. Spores were counted under a microscope.
- Symbiotic AMF rate (%): root staining was performed using the method of Phillips & Hayman (1970). Indicators of AMF presence in roots include the branching structure of the mycelium, dusty appearance, and vesicles penetrating the root tissue. The AMF infection rate was calculated using the formula:

  Symbiosis Rate (%) = (Number of root segments containing AMF/Total number of detected root segments) × 100.
- Disease Rate (%): Calculated as

  Disease rate (%) = (Number of diseased roots/Total number of investigated roots) × 100 (VS, 2021).
- Disease Index (%): Calculated using the formula:

  Disease Index (%) = $\sum$ [(N1 × 1) + ... + (Nn × n)]/(N × K) × 100 (VS, 2021), where:
  - *N1* = Number of samples at harm level 1,
  - *Nn* = Number of samples at harm level *n*,
  - *n* = The nth harm level,
  - *N* = Total number of surveyed samples,
  - *K* = The highest harm level in the hierarchy.

Five disease levels, based on Belete et al. (2013), include:

- Grade 0: No decayed roots,
- Grade 1: 1 - 25% decayed roots,
- Grade 2: 26 - 50%,
- Grade 3: 51 - 75%,
- Grade 4: 76 - 100%.

- Control Effectiveness (%) (VS, 2022): Calculated as:

  Control Effectiveness (%) = (1 - Ta/Ca) × 100, where:

  - *Ta* = Disease index of the treatment plot at the time of the record following treatment,
  - *Ca* = Disease index of the control plot at the same time.

2.3. Data analysis

All experimental data evaluating the effect of AMF on chili plants were replicated three times. The data were processed to calculate the mean and standard deviation using Microsoft Excel 2019 software, and the average values were then analyzed using ANOVA with a significance level of 0.5% in SAS 9.1 software.

3. Results

3.1. Isolation and morphological identification of *Phytophthora* sp.

Phytophthora sp. was isolated and identified based on its morphological characteristics. In accordance with Koch's postulates, *Phytophthora* symptoms were reassessed on chili plants grown in net houses. The findings revealed that symptoms began to appear on the chili plants 40 days after inoculation (Figure 1).

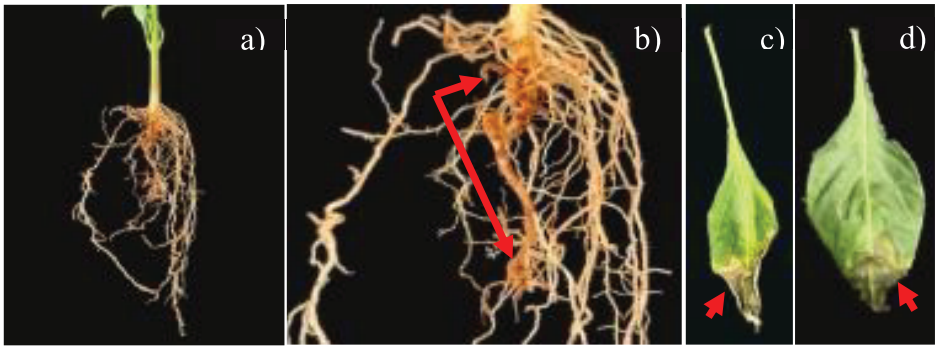

Fiugre 1. The disease symptoms on chili plants 40 days after inoculation.
a-b) symptom on roots; c-d) symptom on leaf.

The pathogen was found to have survived in the soil sample based on the morphology of *Phytophthora* sp. on CRA media and the results of rose trapping (Figure 2, Figure 3). The mycelium of *Phytophthora* sp. consisted of indeterminate, colorless branches; colorless sporangia; and oval, ellipsoid, or ovoid shapes, with lengths ranging from 26 to 37.5 µm and widths between 15.6 and 20 µm. The length-to-width (L/W) ratio ranged from 1.7 to 1.9. The papillate sporangia are well-rounded, measuring 2.8 - 2.2 mm in length and 1.7 - 1.2 mm in width, although they may be absent. The chlamydospore has a thick wall, measuring 1.1 - 1.8 µm, with a diameter of 22 - 27 µm.

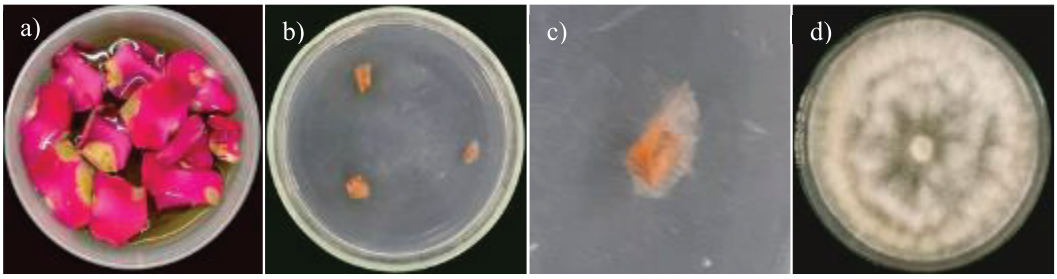

Figure 2. The isolation result of *Phytophthora* sp. by trapping rose. a) Trapping rose after 3 days; b-c), the isolation samples by trapping rose; d) Mycelium of *Phytophthora on* carrot agar (CRA) medium.

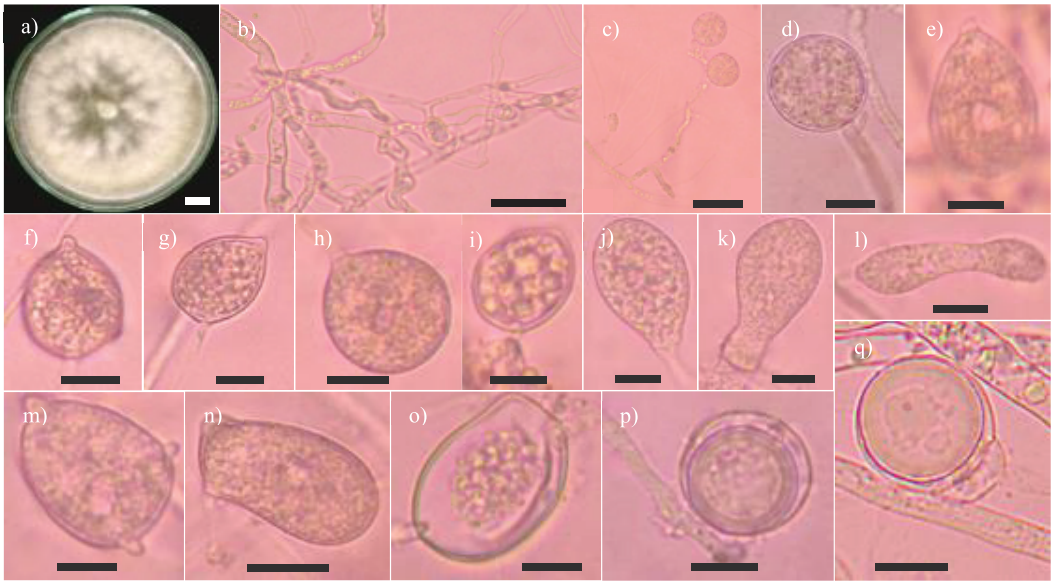

Figure 3. Morphology of P*hytophthora* sp. on carrot agar (CRA). a) colony on medium; b) swelling mycelium; c) Branches carrying pouch spores; d) chlamydospores; e-o) sporangium shape; p-q) oospores; (Bar = 10 µm).

According to Saltos et al. (2022), *P. capsici* causes damage to chili plants by impairing the water-conducting mechanisms of the roots and stems, resulting in light brown discoloration and withering of the leaf tips. Small, black lesions appear on the roots and stem stubs, initially spreading quickly before completely decomposing. The cortical tissue of the stem develops dry, dark brown, or black lesions.

Especially, diseases caused by *P. capsici* can reduce productivity by up to 100% if they develop early in the season and under favorable conditions (Liu et al., 2014). This disease can persist for several years in the absence of a host due to resistant structures known as oospores (Gandariasbeitia et al., 2019). Temperatures between 25 and 28°C and high humidity (> 80%) promote fungal infection and disease propagation, leading to large epidemics (Granke et al., 2011) Humid soils are optimal for the primary inoculum (oospores) to infect susceptible plants (Gandariasbeitia et al., 2019). According to Mchau & Coffey (1995) and Shahnazi et al.

(2012), morphological characteristics form the basis for the identification and classification of many genera, such as *Fusarium* sp. and *Phytophthora* sp.

3.2. Effects of AMF product on the growth and development of chili

The effect of the AMF product on chili plant growth was investigated. Chili plant growth and development data (Figures 4 and 5) demonstrated that the AMF-treated plots outperformed the control plots in all measured parameters, including plant height, root length, number of roots, and biomass. Statistically significant differences were observed between the AMF-treated plots and the control, according to the results of the statistical analysis.

Figure 4A, the plant height target, demonstrated how plant height increased progressively throughout all recording stages. In comparison to the other plots, NT6 (60% AMF) and NT7 (70% AMF) displayed the best results (23.5 cm, 34.1 cm, 46.9 cm, and 62.1 cm) and (23.4 cm, 33.7 cm, 47.1 cm, and 63.0 cm), respectively. The lowest plant height values (18.3 cm, 24.4 cm, 30.2 cm, and 43.8 cm) were found in NT1.

At the follow-up phases, the root length target (Figure 4B) showed that root length results in the AMF-treated plots were better than those in the two control plots. NT6 (60% AMF) and NT7 (70% AMF) produced the best root length results at stages 17 and 24 DAT (26.5 cm, 25.6 cm, and 36.5 cm, 34.5 cm); NT3 (30% AMF) and NT6 (60% AMF) produced the best results at stage 31 DAT (47.4 cm and 46.3 cm); and NT7 (70% AMF) and NT8 (Mycorrhiza) produced the highest root lengths at stage 38 DAT, measuring 55.1 cm and 57.9 cm. Nevertheless, NT1 produced the lowest values (20.1 cm, 30.2 cm, 34.0 cm, and 40.8 cm).

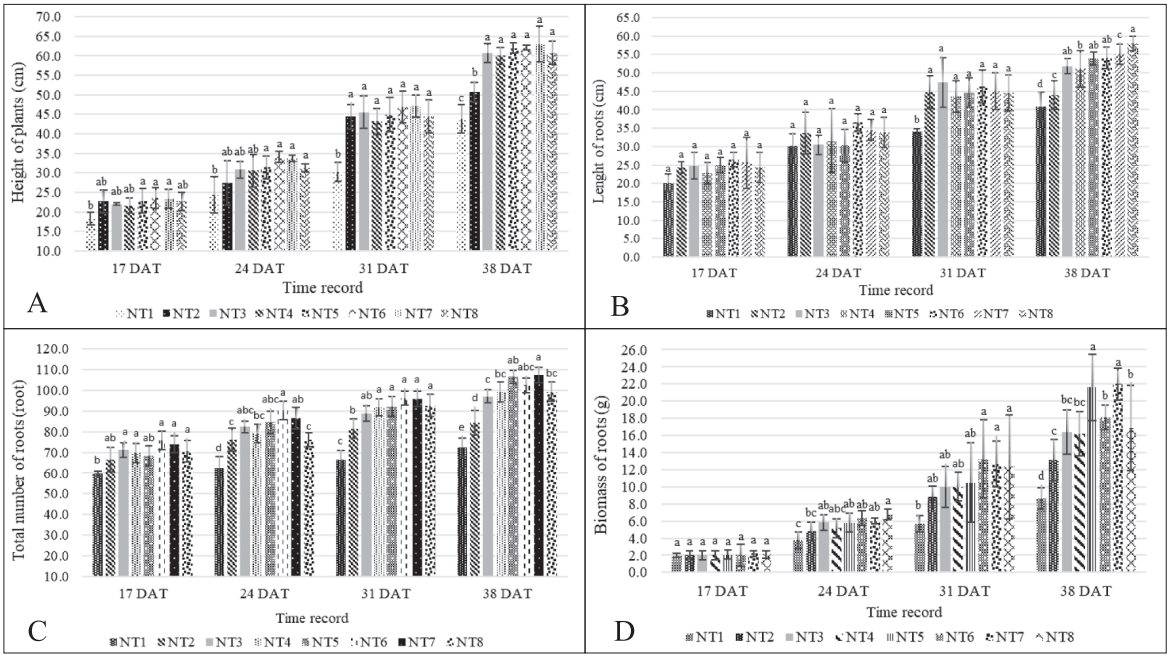

Figure 4. Growth target of chili plants. A: Height of plants; B: Length of roots; C: Total number of roots; D: Biomass of roots.

In Figure 4C, the total number of root targets is displayed. In comparison to the two control plots, the AMF treatment plots displayed a greater total number of roots, with statistically significant differences at the follow-up stages. The highest results were obtained by NT6 (60% AMF) and NT7 (70% AMF) at 17, 24, and 31 DAT (75.5 and 73.8 roots; 90.3 and 86.7 roots; 96.3 and 95.8 roots), while the best results were obtained by NT5 (50% AMF) and NT7 (70% AMF) at 38 DAT (106.5 roots and 107.3 roots). The NT1 achieved the lowest recorded values across all stages (59.8, 62.5, 66.7, and 72.5 roots).

The target for root biomass (Figure 4D) demonstrated that the root biomass in the plots increased steadily over the course of each stage, with the AMF treatment plots outperforming the two control plots at 24, 31, and 38 DAT. Results showed that NT8 (Mycorrhiza) produced the best results at 24 DAT (6.8 g); NT7 (70% AMF) produced the best results at 31 DAT (12.7 g); and NT7 produced the best results at 38 DAT (22.0 g). Furthermore, NT1 produced the lowest root biomass readings (3.8, 5.6, and 8.7 g).

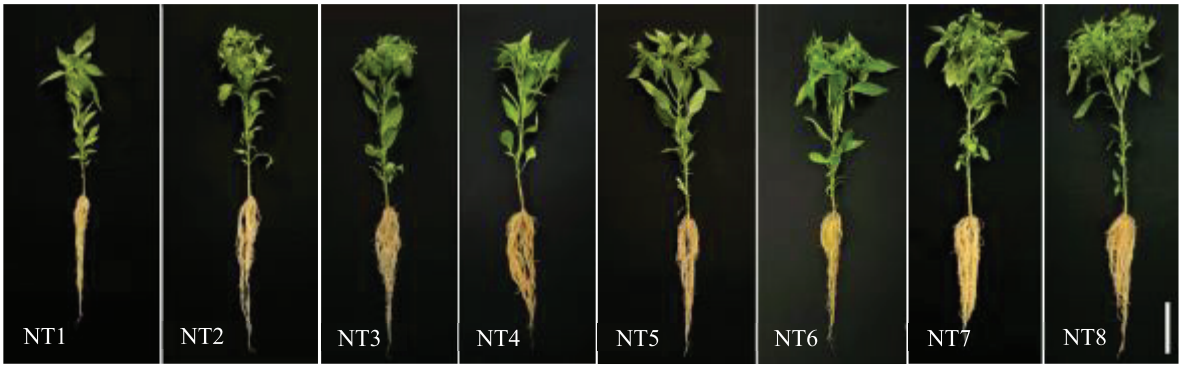

Figure 5. Growth target of chili plants (Bar = 20 cm).

In this experiment, monitoring indicators were collected independently for each plant (destruction indicators), although all plants were subjected to the same experimental conditions (AMF strain, irrigation water, fertilizer, care, etc.). Each plant exhibited different growth patterns, particularly in terms of root development below ground. Additionally, when inoculating AMF into each experimental pot, the symbiosis between the AMF strain and the roots of each plant varies, even though the strain is the same. This variation leads to different levels of root system growth. The experimental data represent the averages for each individual plant, so differences in data collection may arise between plants within the same treatment or between different treatments.

These studies have demonstrated that the addition of AMF products to plant soil influences the growth and development of chili plants, enhancing root biomass and promoting the production of leaves, flowers, fruits, height, plant length, and the number of roots. In the Thai provinces of Ubon Ratchathani and Sisaket, organic chili farms were evaluated for their AMF variety, based on the work of Boonlue et al. (2012). According to the findings, 14 species of AMF were identified, classified into 4 genera: *Acaulospora* sp. (4 species), *Entrophospora* sp. (1 species), *Glomus* sp. (7 species), and *Scutellospora* sp. (2 species). The genus *Glomus* sp. was found to be the most prevalent, followed by *Acaulospora* sp. The total number of AMF spores was consistent across all survey stations.

Additionally, the experimental results demonstrated that, compared to chili plants without AMF treatment, chili plants treated with AMF exhibited higher growth, blooming, and fruiting, as well as increased phosphorus (P) absorption capacity. The results indicated that mycorrhizal inoculation enhances the root absorption area (Anditya et al., 2021). Plant height, branch count, stem diameter, header width, and leaf area index all increased following mycorrhizal inoculation and liquid organic fertilizer treatment. Furthermore, the yield components productivity, fruit weight, fruit length, and fruit number were enhanced. Treatment with 10 g AMF per plant and 15 mL LIF per liter produced the best productivity (11.16 tons/ha), 33% higher than the untreated plants.

3.3. Effect of AMF product on disease rates and disease index on chili roots

The data showed that, during the monitoring period, both the disease index and the disease rate on chili roots were recorded (Table 1). When comparing the AMF-treated plots to the control, statistically significant changes in both the disease rate and disease index were observed. At all recording periods, the disease rate for variety NT7 (70% AMF) was lower than that of NT1 (9.5%, 14.5%, 24.0%, 28.2%) at 4.0%, 5.4%, 8.7%, and 9.9%, respectively. Similarly, the disease index increased gradually at each stage for NT7 (0.8%, 1.2%, 1.8%, and 2.3%) compared to NT1 (1.9%, 3.8%, 5.9%, and 7.1%), with values of 1.1%, 2.6%, 4.1%, and 4.8%, respectively.

The data showed that, during the monitoring period, both the disease index and the disease rate on chili roots were recorded (Table 1). When comparing the AMF-treated plots to the control, statistically significant changes were observed in both the disease rate and disease index. At all recording periods, the disease rate for variety NT7 (70% AMF) was lower than that of NT1, with values of 4.0%, 5.4%, 8.7%, and 9.9% compared to 9.5%, 14.5%, 24.0%, and 28.2%, respectively. Similarly, the disease index increased gradually at each stage for NT7 (0.8%, 1.2%, 1.8%, and 2.3%) compared to NT1 (1.9%, 3.8%, 5.9%, and 7.1%), with values of 1.1%, 2.6%, 4.1%, and 4.8%, respectively.

Table 1. Disease rate and disease index on chili plants (%)

Plots	Disease rate (%)				Disease index (%)			
	17 DAT[1]	24 DAT	31 DAT	38 DAT	17 DAT	24 DAT	31 DAT	38 DAT
NT1 (PC)[2]	9,5^{a}	14,5^{a}	24,0^{a}	28,2^{a}	1,9^{a}	3,8^{a}	5,9^{a}	7,1^{a}
NT2 (NC)[3]	0,0^{c}	0,0^{d}	0,0^{c}	0,0^{c}	0,0^{c}	0,0^{d}	0,0^{c}	0,0^{c}
NT3 (30% AMF)	5,7^{b}	9,3^{b}	11,7^{b}	14,4^{b}	1,1^{b}	1,9^{b}	2,6^{b}	3,2^{b}
NT4 (40% AMF)	5,2^{b}	6,8^{c}	10,6^{b}	14,9^{b}	1,0^{b}	1,4^{bc}	2,6^{b}	3,0^{b}
NT5 (50% AMF)	5,4^{b}	6,0^{c}	10,5^{b}	14,7^{b}	1,1^{b}	1,4^{bc}	2,5^{b}	2,9^{b}
NT6 (60% AMF)	4,4^{b}	6,3^{c}	9,7^{b}	13,0^{b}	0,9^{b}	1,4^{bc}	2,1^{b}	2,6^{b}
NT7 (70% AMF)	4,0^{b}	5,4^{c}	8,7^{b}	9,9^{b}	0,8^{b}	1,2^{c}	1,8^{b}	2,3^{b}
NT8 (Mycorrhiza)	4,7	6,1^{c}	11,7^{b}	12,4^{b}	0,9^{b}	1,6^{bc}	2,3^{b}	3,0^{b}
P	**	**	**	**	**	**	**	**

Note: in the same value group, values with the same accompanying characters are not statistically significant.
[1]DAT: day after treatment.[2] PC: positive control. [3]NC: negative control. AMF: Arbuscular Mycorrhizal Fungi.

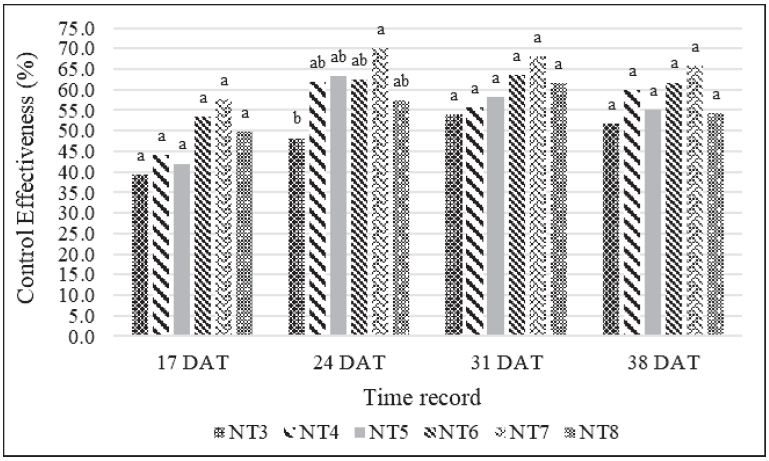

Figure 6. The control effectiveness of *Phytophthora* sp. disease on chili roots.

According to Figure 6, the control efficiency of AMF for *Phytophthora* sp. increased at DAT 17 and 24 but gradually decreased at DAT 31 and 38. Furthermore, the difference in control effect between NT3 (39.4%, 48.2%, 54.0%, 51.7%) and NT7 (57.6%, 70.1%, 68.0%, 65.9%) was 18.2%, 21.9%, 14.0%, and 14.2%, respectively. Thus, NT7 (70% AMF) showed the highest control efficiency, while NT3 (30% AMF) had the lowest at all stages. Specifically, the NT7 plot had the best result for controlling *Phytophthora* sp., with an effect of 70.1% at 24 DAT. Additionally, chili plants in NT1 showed disease symptoms at 38 DAT, whereas the AMF-treated plants exhibited no symptoms at the same time (Figure 7).

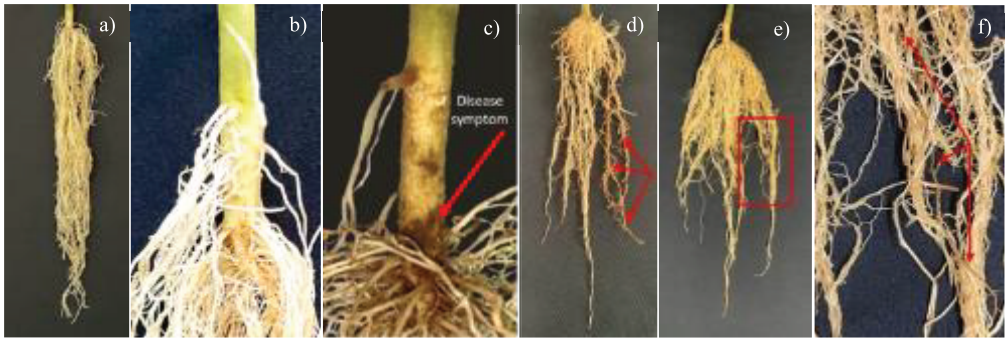

Figure 7. Root system of chili plants. a-b) the root system is not diseased; c-f) *Phytophthora*-disease roots (c,d: roots without Arbuscular Mycorrhizal Fungi (AMF) product; e,f: plant roots with AMF product).

The study by Ozgonen & Erkilic (2007) on chili plants revealed the effect of AMF species (*Glomus mosseae*, *Glomus etunicatum*, *Glomus fasciculatum*, and *Gigaspora margarita*) in controlling Phytophthora blight disease caused by *Phytophthora capsici* under four-week inoculation conditions in greenhouse settings. In these conditions, *G. fasciculatum* significantly boosted yield by 22%. Under pot, greenhouse, and field conditions, *G. mosseae* reduced *P. capsici* disease severity by 91.7%, 43.0%, and 57.2%, respectively. In summary, AM fungi, particularly *G. mosseae*, improved plant growth and reduced Phytophthora blight in chili plants.

AMF-infected roots were 39% and 30%, respectively, substantially fewer than those of plants without AMF, according to a study on tomato plants by Vigo & Hooker (2000) conducted 7 and 16 days after inoculation with the *Phytophthora parasitica* strain. The study also found that AMF had no effect on the spread of the disease or the necrotic regions of infected roots. Plants without AMF exhibited 61% more severe infections 26 days after inoculation with the *Phytophthora parasitica* strain compared to plants with AMF (31%). It was concluded that the effect on the number of infected foci is one mechanism by which AMF achieves biological control of this pathogen in tomatoes.

Watanarojanaporn et al. (2011) report that an experiment was carried out to compare the capacity of two AMF species in suppressing root rot on citrus plants caused by *Phytophthora* sp. Furthermore, by facilitating the plant's increased uptake of nutrients, particularly phosphorus (P), AMF enhanced its ability to protect the root system. The findings of this study were generally consistent with those of other researchers. The results demonstrated that, following 38 days of AMF inoculation in a greenhouse setting, the treatment with AMF products reduced the disease rate by 53%.

3.4. Effect of AMF product on total number of spores and symbiotic rate of AMF in rhizosphere soil and root of chili plants

At every stage, there were more AMF spores overall and a higher rate of symbiosis between the roots and rhizosphere soil of chili plants (Figure 8). All of the plots treated with the AMF product showed a statistically significant difference, with outcomes that increased steadily across all phases. In comparison to the other treatments (Figure 8A), NT 7 (70% AMF) and NT 8 (Mycorrhiza) produced the most AMF spores overall, with no statistically significant difference between the two treatments at any of the recording stages. In contrast, NT 3 (30% AMF) produced the fewest spores per 100 g of soil.

The symbiosis ratio (Figure 8B) revealed that for NT 6 (60% AMF) and NT 7 (70% AMF) at DAT 17, 24, and 31, the symbiosis rate was highest (32.7% and 31.0%; 38.0% and 36.3%; 41.7% and 43.0%). At DAT 38, NT 7 and NT 8 (Mycorrhiza) exhibited the highest rates (52.0% and 55.0%). Regarding the total number of AMF spores, the lowest symbiosis rates (23.3%, 29.0%, 31.0%, and 32.0%) were observed in NT 3 (30% AMF).

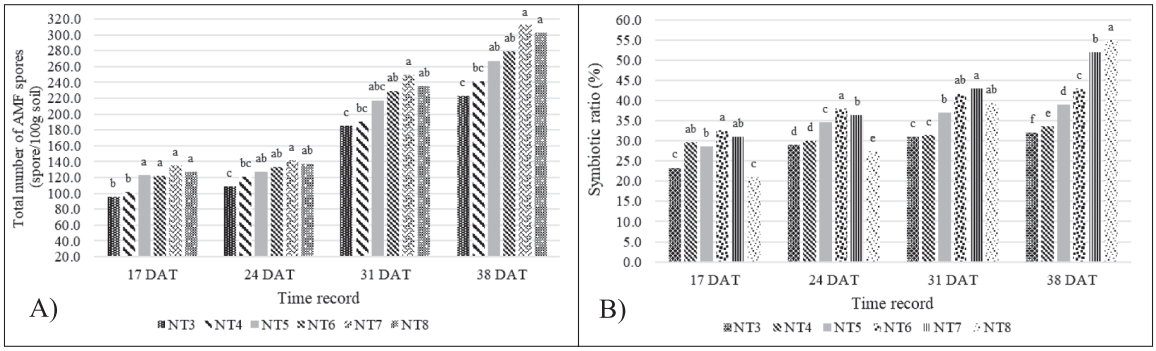

Figure 8. Total number of spores and symbiosis rate of Arbuscular Mycorrhizal Fungi (AMF) in rhizosphere soil and roots of chili plants.

According to Ozgonen & Erkilic's (2007) study on chili plants, four weeks after transplanting, the percentage of pepper roots colonized by AM fungi ranged from 61.3% to 68.1%. The colonization percentages for plants inoculated with *Glomus fasciculatum* and *Glomus mosseae* were 68.1% and 65.7%, respectively. Research has demonstrated that mycorrhizal fungi impact the growth of chili plants, specifically root length and plant height. Additionally, the number of symbiotic mycorrhizal fungal spores, which include various AM fungal strains such as *Acaulospora* sp., *Gigaspora* sp., *Glomus mosseae*, and *Scutellospora* sp., was 51 spores per 50 grams of soil (Aulia et al., 2021).

3.5. Following treatment with AMF products, AMF fungal species were detected in chili roots and rhizosphere soil

According to the identification results, *Glomus* sp. and *Acaulospora* sp. genera were found in the rhizosphere soil of chili plants. As shown by the genus *Glomus* sp. (Figure 9), spores can be found singly or in clusters, with straight spore stalks attached to the mycelium. The spores are spherical or almost spherical, with smooth surfaces, and are pale yellow, orange, brown, or reddish-brown in color. In the genus *Acaulospora* sp. (Figure 10), the spores are oval or spherical and grow singly. The spore wall consists of two to three layers, with one thin outer layer that is colorless. Large oil droplets are visible inside the spores, which have a rough surface with tiny cavities. The spores are pale yellow, yellow-orange, or orange in color.

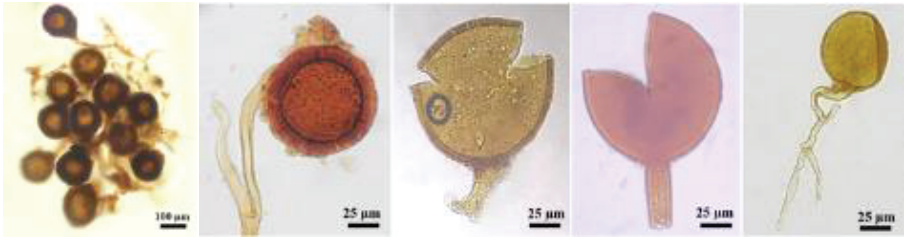

Figure 9. Phenotypes of spores of the genus *Glomus* sp. at the 40X.

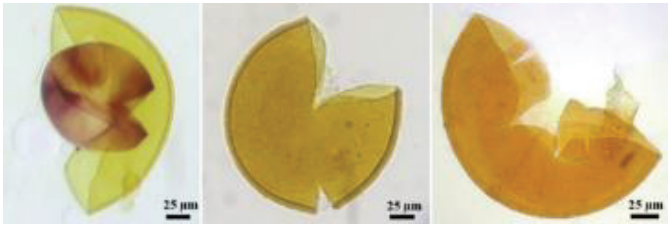

Figure 10. Phenotypes of spores of the genus *Acaulospora* sp. at the 40X.

The symbiotic AMF structures in the tissue of chili roots (Figure 11) showed that mycelium, vesicles, and arbuscular formations (stained with trypan blue) were present in every plot that received AMF treatment. In the intercellular spaces, the mycelium developed along the root cells in two directions (Figure 11c). Trypan blue, a dark dye, was present in the vesicle structures, which were oval in some cases and rectangular in others (Figure 11d). The arbuscular structure, which arises from the branching mycelium, was distributed within the root cells (Figure 11c, d). A ring-coiled filamentous structure was also observed in the root cells, according to the observation results (Figure 11e). The AMF fungi invaded the roots of chili plants, forming endohyphae and arbuscules.

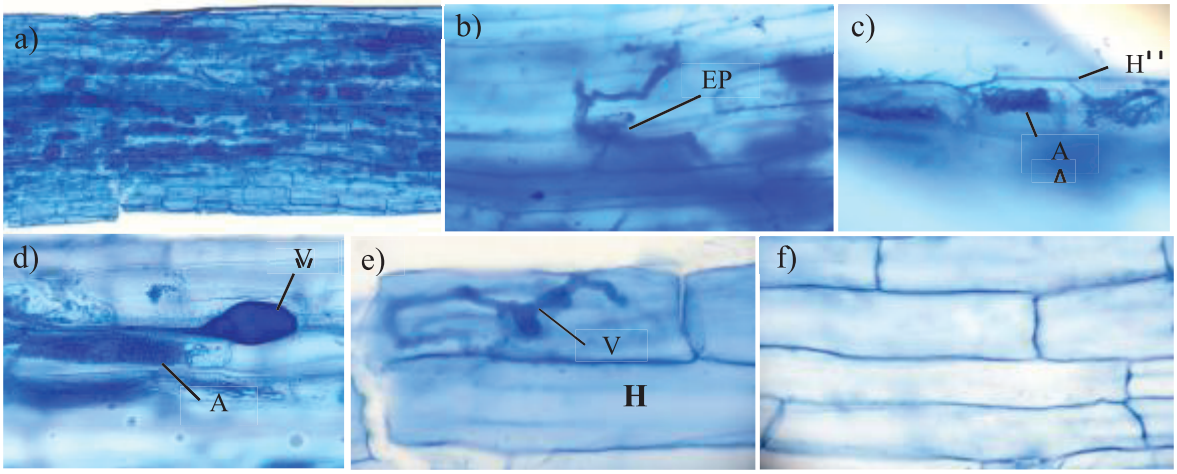

Figure 11. Symbiosis of Arbuscular Mycorrhizal Fungi (AMF) in chili roots and at 10X and 40X. a) AMF is present in roots at 10X; b) The point of infection of AMF; c - e) Symbiotic structure in the roots; f) Root cells do not have symbiosis; A (Arbuscule), H (Hyphae), V (Vesicle).

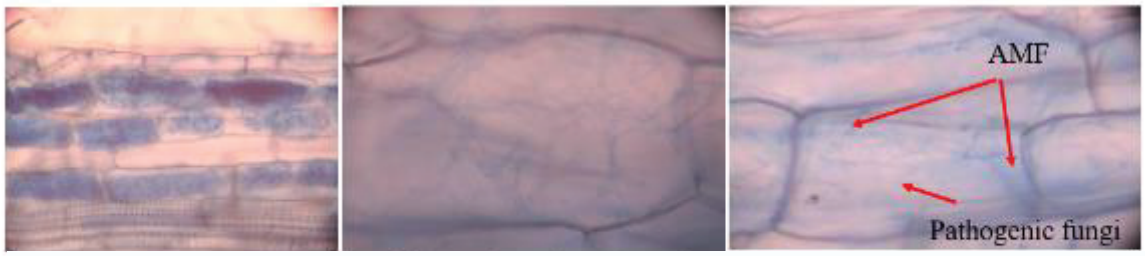

Chili root tissue with a symbiotic AMF | Chili root tissue has a fungal pathogen | Root tissue with parasitic fungal diseases and symbiotic AMF

Figure 12. Characteristics of chili root tissue in the presence of parasitic diseases and symbiotic Arbuscular Mycorrhizal Fungi (AMF).

Within 38 days of AMF product treatment, the source of fungal diseases caused by *Phytophthora* sp. on the roots of the chili plants was isolated (Figure 12). To contain the disease and prevent its spread, AM fungi developed structures that inhibited the growth of *Phytophthora* fungi. By forming wound barriers and obstructing the stomata small openings in the plant that allow only gases and water vapor to pass through AM fungi's invasion of the host plant's cells limits the pathogen's ability to spread. This action localizes the damage to the host plant, thereby reducing the overall spread of the disease.

4. Conclusions

The experiment assessing the efficacy of AMF treatment in controlling *Phytophthora* sp. on chili plants grown in net houses revealed that the AMF-treated plots outperformed the control plots in stimulating plant growth, as evidenced by increases in plant height, root length, root number, and biomass 31 days after treatment. In the AMF-treated plots, where *Phytophthora* sp. was controlled, both the disease rates and disease index were lower than in the untreated plots (positive control). Among the AMF plots, NT7 (70% AMF) yielded the lowest results. However,

by 24 DAT (days after treatment), NT7 (70% AMF) showed the highest control efficiency for *Phytophthora* sp. disease at 70.1%.

Conflict of interest

The authors have no conflict of interest to declare.

Acknowledgements

The authors wish to extend their appreciation to the Science and Technology Department of Ho Chi Minh City for providing the study grant titled "Research on the production of Arbuscular Mycorrhizal Fungi (AMF) to control nematode disease fungi affecting vegetable plants in Ho Chi Minh City." We also extend our appreciation to the Research Institute for Biotechnology and Environment, Nong Lam University, Ho Chi Minh City, Vietnam.

References

Abad, Z. G., Burgess, T. I., Bourret, T., Bensch, K., Cacciola, S. O., Scanu, B., Mathew, R., Kasiborski, B., Srivastava, S., Kageyama, K., Bienapf, J. C., Verkleij, G., Broders, K., Schena, L., & Redford, A. J. (2023). Phytophthora: Taxonomic and phylogenetic revision of the genus. *Studies in Mycology* 106(1), 259-348. https://doi.org/10.3114/sim.2023.106.05.

Agrios, G. N. (2005). *Plant pathology* (5th ed.). Amsterdam, Holland: Elsevier Academic Press.

Akhtar, M. S., & Siddiqui, Z. A. (2008). *Glomus intraradices*, *Pseudomonas alcaligenes*, and *Bacillus pumilus*: Effective agents for the control of root-rot disease complex of chickpea (*Cicer arietinum* L.). *Journal of General Plant Pathology* 74(1), 53-60. http://dx.doi.org/10.1007/s10327-007-0062-4.

Anditya G. R. P., Puji H., & Amalia T. S. (2021). The effect of mycorrhizal inoculation and liquid organic fertilizer on growth and yield of red chili. *E3S Web of Conferences* 306, 01049. https://doi.org/10.1051/e3sconf/202130601049.

Augé, R. M., Toler, H. D., & Saxton, A. M. (2015). Arbuscular mycorrhizal symbiosis alters stomatal conductance of host plants more under drought than under amply watered conditions: A meta-analysis. *Mycorrhiza* 25(1), 13-24. https://doi.org/10.1007/s00572-014-0585-4.

Aulia A. B., Mangunwardoyo, W., Chandra, N. D., Napitupulu, T. P., Idris, I., Kanti, A., Ikhwani, A. Z. N., Sudiana, I. M., & Guswenrivo, I. (2021). Influence of AM fungi inoculation on *Capsicum annuum* L. plant grown in microwave-sterilized media. *E3S Web of Conferences* 306, 01057. https://doi.org/10.1051/e3sconf/202130601057.

Azcón-Aguilar, C., & Barea, J. M. (1997). Arbuscular mycorrhizas and biological control of soil-borne plant pathogens - An overview of the mechanisms involved. *Mycorrhiza* 6, 457-464. https://doi.org/10.1007/s005720050147.

Belete, E., Ayalew, A., & Ahmed, S. (2013). Associations of biophysical factors with faba bean root rot (*Fusarium solani*) epidemics in the northeastern highlands of Ethiopia. *Crop Protection* 52(1-2), 39-46. https://doi.org/10.1016/j.cropro.2013.05.003.

Boonlue, S., Surapat, W., Pukahuta, C., Suwanarit, P., Suwanarit, A., & Morinaga, T. (2012). Diversity and efficiency of arbuscular mycorrhizal fungi in soils from organic chili (*Capsicum frutescens*) farms. *Mycoscience* 53(1), 10-16. https://doi.org/10.1007/s10267-011-0131-6.

Brundrett, M., Bougher, N., Dell, B., Grove, T., & Malajczuk, N. (1996). Working with Glomalean fungi. In Brundrett, M., Bougher, N., Dell, B., Grove, T., & Malajczuk, N. (Eds.). *Working with mycorrhizas in forestry and agriculture* (141-171). Canberra, Australia: Pirie Printers.

Davis, R. M., & Menge, J. A. (1981). *Phytophthora parasitica* inoculation and intensity of vesicular-arbuscular mycorrhizae in citrus. *New Phytologist* 87(4), 705-715. https://doi.org/10.1111/j.1469-8137.1981.tb01705.x.

Drenth, A., Sendall, B., & Australian Centre for International Agricultural Research (ACIAR). (2001). *Practical guide to detection and identification of Phytophthora*. Brisbane, Australia: CRC for Tropical Plant Protection.

Gandariasbeitia, M., Ojinaga, M., Orbegozo, E., Barredo, A. O., Zofío, M. N., Azcue, S. M., &

Larregla, S. (2019). Winter biodisinfestation with Brassica green manure is a promising management strategy for *Phytophthora capsici* control of protected pepper crops in humid temperate climate regions of northern Spain. *Spanish Journal of Agricultural Research* 17(1), e1005. https://doi.org/10.5424/sjar/2019171-13808.

Granke, L. L., Quesada-Ocampo, L. M., & Hausbeck, M. K. (2011). Variation in phenotypic characteristics of *Phytophthora capsici* isolates from a worldwide collection. *Plant Disease* 95, 1080-1088. https://doi.org/10.1094/PDIS-03-11-0190.

Ho, H. H. (1990). Taiwan *Phytophthora*. *Botanical Bulletin Academia Sinica* 31, 89-106.

Liu, W. Y., Kang, J. H., Jeong, H. S., Choi, H. J., Yang, H. B., Kim, K. T., Choi, D., Choi, G. J., Jahn, M., & Kang, B. C. (2014). Combined use of bulked segregant analysis and microarrays reveals SNP markers pinpointing a major QTL for resistance to Phytophthora capsici in pepper. *Theoretical and Applied Genetics* 127(11), 2503-2513. https://doi.org/10.1007/s00122-014-2394-8.

Mchau, G. R., & Coffey, M. D. (1995). Evidence for the existence of two subpopulations in *Phytophthora capsici* and a redescription of the species. *Mycological Research* 99(1), 89-102. https://doi.org/10.1016/S0953-7562(09)80321-3.

Ozgonen, H., & Erkilic, A. (2007). Growth enhancement and Phytophthora blight (*Phytophthora capsici* Leonian) control by arbuscular mycorrhizal fungal inoculation in pepper. *Crop Protection* 26(11), 1682-1688. https://doi.org/10.1016/j.cropro.2007.02.010.

Phillips, J. M., & Hayman, D. S. (1970). Improved procedures for clearing roots and staining parasitic and vesicular-arbuscular mycorrhizal f ungi for rapid assessment of infection. *Transactions of The British Mycological Society* 55(1), 158-161. https://doi.org/10.1016/S0007-1536(70)80110-3.

Pozo, M. J., & Azcón-Aguilar, C. (2007). Unraveling mycorrhiza-induced resistance. *Current Opinion in Plant Biology* 10(4), 393-398. https://doi.org/10.1016/j.pbi.2007.05.004.

Saltos, L. A., Monteros-Altamirano, Á., Reis, A., & Garcés-Fiallos, F. R. (2022). Phytophthora capsici: The diseases it causes and management strategies to produce healthier vegetable crops. *Horticultura Brasileira* 40(1), 5-17. http://dx.doi.org/10.1590/s0102-0536-20220101.

Shahnazi, S., Meon, S., Vadamalai, G., Ahmad, K., & Nejat, N. (2012). Morphological and molecular characterization of *Fusarium* spp. associated with yellowing disease of black pepper (*Piper nigrum* L.) in Malaysia. *Journal of General Plant Pathology* 78(33), 160-169. http://dx.doi.org/10.1007/s10327-012-0379-5.

Smith, S. E, & Read, D. J. (2010). Functioning of Mycorrhizas in broader contexts. In Smith, S. E, & Read, D. J. (Eds.). *Mycorrhizal symbiosis* (3rd ed.). London, UK: Academic Press. https://doi.org/10.1016/B978-0-12-370526-6.X5001-6.

Vigo, C., Norman, J. R., & Hooker, J. E. (2000). Biocontrol of the pathogen *Phytophthora parasitica* by arbuscular mycorrhizal fungi is a consequence of effects on infection loci. *Plant Pathology* 49(4), 509-514. https://doi.org/10.1046/j.1365-3059.2000.00473.x.

VS (Vietnam Standards). (2022). Standard No. TCVN 12561:2022 dated on December 30, 2024. Pesticides - Bio - efficacy field trials. Retrieved May 15, 2023, from https://tieuchuan.vsqi.gov.vn/tieuchuan/view?sohieu=TCVN+12561%3A2022.

VS (Vietnam Standards). (2021). Standard No. TCVN 13268-2:2021 dated on August 6, 2021. Plant protection - Pest surveillance method - Part 2: Vegetable crops. Retrieved May 15, 2023, from https://tieuchuan.vsqi.gov.vn/tieuchuan/view?sohieu=TCVN+13268-2%3A2021.

VS (Vietnam Standards). (1985). Standard No. TCVN 4046-85 dated on September 18, 1985. Soil - Method of sampling. Retrieved May 15, 2023, from https://tieuchuan.vsqi.gov.vn/tieuchuan/view?sohieu=TCVN+4046%3A1985.

Watanarojanaporn, N., Boonkerd, N., Wongkaew, S., Prommanop, P., & Teaumroong, N. (2011). Selection of arbuscular mycorrhizal fungi for citrus growth promotion and *Phytophthora* suppression. *Scientia Horticulturae* 128(4), 423-433. https://doi.org/10.1016/j.scienta.2011.02.007.

Effects of antibacterial peptides in non-antibiotic feeds on the productivity of growing pigs

Phuong T. H. To*, & Dong D. Duong
Department of Animal Nutrition, Nong Lam University, Ho Chi Minh City, Vietnam

ARTICLE INFO

Research Paper

Received: August 12, 2024
Revised: September 12, 2024
Accepted: October 04, 2024

Keywords

Antibacterial peptides
Antibiotics
Growing pigs
Organic compounds

***Corresponding author**

To Thi Hong Phuong
Email:
phuong.tothihong@hcmuaf.edu.vn

ABSTRACT

The objective of this study was to evaluate growth performance of finishing pigs fed diets with two antibiotics or fed with organic-originated supplements. A total of 48 crossbred weaned piglets were randomly assigned into four treatments and the study was conducted in 108 days. Each treatment had 06 replicates and 2 piglets (1 male and 1 female) per replicate. Those organic-originated supplements included phytogenic extracts, organic acid, probiotics or new preparation of anti-bacterial peptides (trade name Halor Tid). The treatment I: pigs were only fed basal diet without antibiotics supplements or other organics feed additives (Negative control). Treatment II: pigs were fed with two antibiotics including colistin 1% and BMD 10% in order to prevent *E. coli* and *Clostridium perfringens* infection (Positive control). Pigs in treatment III were fed with a combination of phytogenic extracts, organic acid and probiotics whereas pigs in treatment IV were fed with a combination of phytogenic extracts, organic acid and anti-bacterial peptides. The results showed that the performance parameters such as body weight gain, feed conversion ratio (FCR) and issues of diarrhea and mortality were the worst in the treatment I; whereas these performance parameters in the treatment III or in treatment IV were better than those in treatment II although this difference was not statistically significant at $P > 0.05$. Besides, the feed cost per kg of live weight of pigs in treatment III and treatment IV was significantly lower than that in treatment I and II.

Cited as: To, P. T. H., & Duong, D. D. (2024). Effects of antibacterial peptides in non-antibiotic feeds on the productivity of growing pigs. *The Journal of Agriculture and Development* 23(Special issue 2), 63-75.

1. Introduction

Pig feed is often composed of plant extracts, organic acids and probiotics, and previously various antibiotics to enhance pig gut health and thereby improve livestock productivity (Pearlin et al., 2020; Rahman et al., 2022). Recently, feed is added preparations holding antimicrobial peptides have been introduced for use in combination with natural preparations to better enhance intestinal health in pigs (Silveira et al., 2021). Wang et al. (2019) showed the role of antimicrobial peptides against the effects of Gram-negative bacteria, Gram-positive bacteria and enhancing the role of the immune system to help animals stay healthy and increase productivity. According to research by Xiao et al. (2015) and Xu et al. (2020), products supplemented with anti-bacterial peptides have the effect of replacing antibiotics in destroying harmful intestinal bacteria and enhancing intestinal health in pigs.

This trial was conducted to evaluate performance of growing pigs as being fed diets which are contain only two kinds of antibiotics or no antibiotics but supplemented of organic materials to enhance gut health status such as combination of phytogenic, organic acid and probiotics or combination of phytogenic, organic acids and a new preparation of anti-bacterial peptides (trade name Halor Tid).

2. Materials and Methods

The trial was conducted from July to November 2023 in Nong Lam University, Ho Chi Minh City. A total of 48 crossbred weaned piglets which bodyweight was about 8.00 ± 0.1 kg/pig, were randomly assigned into four treatments. Each treatment had 06 replicates and there were one male and one female piglets per replicate. Twelve pigs in treatment I served as negative control group, which were fed basal diet with no supplementation of antibiotics or other organics feed additives. Treatment II was positive control, pigs were fed with two antibiotics including Colistin 1% and BMD 10% in order to prevent *E.coli* and *Clostridium perfringens* infection. Pigs in treatment III were fed basal diet like the one of treatment I but supplemented with a combination of phytogenic extracts, organic acid and probiotics as means of enhancing of gut health status; and pigs in treatment IV was fed similar diet of treatment III but the probiotics preparation supplemented was replaced by the anti-bacterial peptides with trade name Halor Tid. The experimental is showed in Table 1.

Table 1. Experimental design

Treatment	Feed + Experimental factors	Replicates	Number of pig
I	Basal feed	6	12
II	Basal feed + Colistin 1% + BMD 10%	6	12
III	Basal feed + Phytogenic + Organic acid + Probiotics	6	12
IV	Basal feed + Phytogenic + Organic acid + Halor Tid	6	12

Colistin 1 % was used at dose 0.5 kg/ton of feed for whole stages; BMD 10% was used at dose 0.3 kg/ton of feed for whole stages; Phytogenic was administered at a dose of 0.5 kg/ton of feed in period 7 – 40 kg and 0.4 kg/ton of feed in period 40 kg - finish; Organic acid was used at a dose of 2 kg/ton of feed in period 7 – 40 kg and 1 kg/ton of feed in period 40 kg - finish; Probiotics were administered at a dose of 1 kg/ton of feed in period 7 – 40 kg and 0.5 kg/ton in period 40 kg – finish; Halor Tid was administered at a dose of 0.5 kg/ton of feed for whole stages.

Feed formulas for experimental treatments at each farming stage are presented in Tables 2, 4 and 6, and calculated nutritional ingredients are presented in Tables 3, 5 and 7.

Table 2. Pig feed formula for the period 7 - 15 kg and period 15 - 25 kg

Ingredient (%)	Period 7 - 15 kg				Period 15 - 25 kg			
	I	II	III	IV	I	II	III	IV
Grain corn	25.00	25.00	25.00	25.00	53.69	53.69	53.09	53.67
Broken rice	11.35	11.25	10.94	11.00	-	-	-	-
Single-cell protein powder	3.00	3.00	3.00	3.00	1.46	1.46	1.45	1.46
Single-cell protein liquid	4.00	4.00	4.00	4.00	3.86	3.86	3.88	3.85
Rice bran I	10.00	10.00	10.00	10.00	4.98	4.98	5.51	5.01
Fermented soy-beans	12.61	12.63	12.67	12.66	2.70	2.70	2.70	2.70
Cassava residue	5.00	5.00	5.00	5.00	5.00	5.00	5.00	5.00
Soybean meal46	10.00	10.00	10.00	10.00	20.00	20.00	20.00	20.00
Meat and bone meal	3.00	3.00	3.00	3.00	-	-	-	-
Lactose	5.00	5.00	5.00	5.00	1.20	1.20	1.20	1.20
Whey	4.00	4.00	4.00	4.00	1.80	1.80	1.80	1.80
Soybean oil	1.49	1.49	1.49	1.49	0.30	0.30	0.32	0.30
Colistin 1%	-	0.05	-	-	-	0.05	-	-
BMD 10%	-	0.03	-	-	-	0.03	-	-
Phytogenics	-	-	0.05	0.05	-	-	0.05	0.05
Organic acid	-	-	0.20	0.20	-	-	0.20	0.20
Probiotics	-	-	0.10	-	-	-	0.10	-
Halor Tid	-	-	-	0.05	-	-	-	0.05
Other Ingredients*	5.55	5.55	5.55	5.55	5.01	4.93	4.70	4.72
Total	100	100	100	100	100	100	100	100

**"Other ingredients" include acid amin, premix, salt, limestone, DCP, enzymes.*

Table 3. Nutrients of feed for the period 7 - 15 kg and period 15 - 25 kg

	Period 7 - 15 kg				Period 15 - 25 kg			
	I	II	III	IV	I	II	III	IV
DM (%)	87.59	87.61	87.64	87,63	86.00	86.00	86.00	86.00
MEg (kcal/kg)	3,236	3,233	3,225	3,226	3,231	3,231	3,230	3,231
CP (%)	21.00	21.00	21.00	21,00	17.95	17.95	17.96	17.95
EE (%)	4.82	4.82	4.82	4,82	3.62	3.62	3.67	3.63
CF (%)	3.54	3.54	3.54	3,54	3.28	3.28	3.33	3.29
Ash (%)	5.18	5.18	5.18	5,19	4.11	4.11	4.14	4.12
Calcium (%)	1.20	1.20	1.20	1,20	0.90	0.87	0.80	0.80
Phosphor total (%)	0.57	0.57	0.57	0,57	0.44	0.44	0.44	0.44
Phosphor available (%)	0.40	0.40	0.40	0,40	0.40	0.40	0.40	0.40
Sodium (%)	0.35	0.35	0.35	0,35	0.17	0.17	0.17	0.17
Chloride (%)	0.53	0.52	0.53	0,53	0.34	0.34	0.34	0.34
dEB	249	249	249	248	200	200	200	200
Lysine SID pig (%)	1.420	1.420	1.420	1,420	1.320	1.320	1.320	1.320
Methionine SID pig (%)	0.606	0.606	0.606	0,606	0.558	0.558	0.558	0.558
Met+Cys, SID pig (%)	0.850	0.850	0.850	0,850	0.790	0.790	0.790	0.790
Threonine SID pig (%)	0.890	0.890	0.890	0,890	0.830	0.830	0.830	0.830
Tryptophan SID pig (%)	0.310	0.310	0.310	0,310	0.290	0.290	0.290	0.290
Valine SID pig (%)	0.970	0.970	0.970	0,970	0.890	0.890	0.890	0.890
Isoleucine SID pig (%)	0.780	0.780	0.780	0,780	0.720	0.720	0.720	0.720

Table 4. Pig feed formula for the period 25 - 40 kg và period 40 - 70 kg

Ingredient (%)	Period 25 - 40 kg				Period 40 - 70 kg			
	I	II	III	IV	I	II	III	IV
Grain corn	54.37	54.37	53.00	53.55	56.40	56.40	56.40	56.37
Single-cell protein powder	0.36	0.36	0.34	0.35	1.35	1.35	1.35	1.35
Single-cell protein liquid	2.81	2.81	2.88	2.84	2.87	2.87	2.87	2.87
Rice bran I	7.32	7.32	8.53	8.05	6.84	6.84	6.85	6.85
Cassava residue	8.00	8.00	8.00	8.00	10.00	10.00	10.00	10.00
Soybean meal46	22.57	22.57	22.54	22.55	17.78	17.78	17.78	17.78
Soybean oil	0.20	0.20	0.24	0.23	0.20	0.20	0.20	0.20
Colistin 1%	-	0.05	-	-	-	0.05	-	-
BMD 10%	-	0.03	-	-	-	0.03	-	-
Phytogenic	-	-	0.05	0.05	-	-	0.04	0.04
Organic acid	-	-	0.20	0.20	-	-	0.10	0.10
Probiotics	-	-	0.10	-	-	-	0.05	-
Halor Tid	-	-	-	0.05	-	-	-	0.05
Other ingredients*	4.40	4.32	4.14	4.15	4.55	4.47	4.36	4.41
Total	100	100	100	100	100	100	100	100

**"Other ingredients" include acid amin, premix, salt, limestone, DCP, enzymes.*

Table 5. Nutrients of feed for the period 25 - 40 kg và period 40 - 70 kg

Treatment	Period 25 - 40 kg				Period 40 - 70 kg			
	I	II	III	IV	I	II	III	IV
DM (%)	86.00	86.00	86.00	86.00	86.00	86.00	86.00	86.00
MEg (kcal/kg)	3,212	3,212	3,210	3,211	3,158	3,158	3,158	3,158
CP (%)	16.82	16.82	16.85	16.84	15.30	15.30	15.30	15.30
EE (%)	3.76	3.76	3.88	3.83	3.71	3.71	3.71	3.71
CF (%)	3.91	3.91	4.02	3.97	3.97	3.97	3.97	3.97
Ash (%)	3.95	3.95	4.02	4.00	3.70	3.70	3.70	3.70
Calcium (%)	0.83	0.80	0.75	0.75	1.03	1.01	0.97	0.99
Phosphor total (%)	0.42	0.42	0.43	0.42	0.38	0.39	0.38	0.38
Phosphor available (%)	0.37	0.37	0.37	0.37	0.35	0.35	0.35	0.35
Sodium (%)	0.17	0.17	0.17	0.17	0.17	0.17	0.17	0.17
Chloride (%)	0.28	0.28	0.28	0.28	0.23	0.23	0.23	0.23
dEB	200	200	200	200	200	200	200	200
Lysine SID pig (%)	1.100	1.100	1.100	1.100	0.940	0.940	0.940	0.940
Methionine SID pig (%)	0.440	0.443	0.443	0.443	0.376	0.376	0.376	0.376
Met+Cys, SID pig (%)	0.670	0.670	0.670	0.670	0.580	0.580	0.580	0.580
Threonine SID pig (%)	0.700	0.700	0.700	0.700	0.610	0.610	0.610	0.610
Tryptophan SID pig (%)	0.220	0.220	0.220	0.220	0.190	0.190	0.190	0.190
Valin SID pig (%)	0.890	0.890	0.890	0.890	0.640	0.640	0.640	0.640
Isoleucine SID pig (%)	0.600	0.600	0.600	0.600	0.520	0.520	0.520	0.520

Table 6. Pig feed formula for the period 70 kg - finish

Ingredient (%)	I	II	III	IV
Grain corn	57.62	57.51	57.36	57.38
Single-cell protein powder	3.00	3.00	3.00	3.00
Single-cell protein liquid	3.20	3.22	3.26	3.24
Cassava residue	15.00	15.00	15.00	15.00
Soybean meal 46	15.30	15.30	15.30	15.30
Soybean oil	0.28	0.28	0.29	0.29
Colistin 1%	-	0.05	-	-
BMD 10%	-	0.03	-	-
Phytogenics	-	-	0.04	0.04
Organic acid	-	-	0.10	0.10
Probiotics	-	-	0.05	-
Halor Tid	-	-	-	0.05
Other ingredients*	5.60	5.60	5.60	5.60
Total	100	100	100	100

** "Other ingredients" include acid amin, premix, salt, limestone, DCP, enzymes.*

Table 7. Nutrients of feed for the period 70 kg - finish

	I	II	III	IV
DM (%)	86.00	86.00	86.00	86.00
MEg (kcal/kg)	3,162.00	3,160.00	3,156.00	3,158.00
CP (%)	14.54	14.53	14.53	14.53
EE (%)	3.09	3.09	3.09	3.09
CF (%)	3.72	3.72	3.71	3.71
Ash (%)	4.31	4.31	4.30	4.30
Calcium (%)	1.20	1.20	1.20	1.20
Phosphor total (%)	0.40	0.40	0.40	0.40
Phosphor available (%)	0.32	0.32	0.32	0.32
Sodium (%)	0.35	0.35	0.35	0.35
Chloride (%)	0.52	0.52	0.52	0.52
dEB (%)	200.00	200.00	200.00	200.00
Lysine SID pig (%)	0.840	0.840	0.840	0.840
Methionine SID pig (%)	0.348	0.349	0.349	0.349
Met+Cys, SID pig (%)	0.530	0.530	0.530	0.530
Threonine SID pig (%)	0.560	0.560	0.560	0.560
Tryptophan SID pig (%)	0.170	0.170	0.170	0.170
Valin SID pig (%)	0.570	0.570	0.570	0.570
Isoleucine SID pig (%)	0.470	0.470	0.470	0.470

Live weight, feed consumption, number of diarrhea days and number of dead/culled of pigs were recorded at beginning and ending of each stage of the trial. The back-fat thickness of every pig was measured at three days before slaughtering by back-fat thickness measuring machine (trade name Renco). At the end of trial, one pig per treatment was slaughted to evaluate carcass on carcass weight percentage and carcass dressing percentage. Finally, make comparisons of economic efficiency of experimental treatment based on the cost of feed and veterinary medicine expense for one kg of pig live weight gained. The data were statistically analyzed by Minitab 17.0 using ANOVA, Tukey test and Chi square test for corresponding parameter. A significant difference was set at $P \leq 0.05$.

3. Results and Discussion

3.1. Growth performance

The average live weight of pigs in all four treatments at the beginning of the experiment was similar. Pigs raised at the 7 - 15 kg stage mostly gained relatively low weight, in which the highest weight was found in treatment II - 13.61 kg/pig, followed by treatment IV - 13.34 kg/pig. During this period, pigs experienced stress due to many factors such as changing the farming environment, joining new herds and changing feed, leading to severe diarrhea and poor feed consumption. Treatment II which supplemented antibiotics in diet reduced diarrhea challenges hence, leading to better growth. At the same time, treatment IV used anti-bacterial peptides combined with phytogenic and organic acids to show the best impact. Replacing antibiotics

with anti-bacterial peptides aimed at improving intestinal health should help pigs have higher weight compared to the other two treatments. The post-weaning period of pigs (7-15 kg) was an extremely sensitive period. Therefore, it is not only the diet be composed of nutrition and high digestible ingredients, but also have supplements that support intestinal health. It would help pigs reduce diarrhea, keep pigs healthy, and better feed intake to achieve high growth, as shown in the results in Table 8.

Table 8. Live weight (LW) (kg/pig ± SD) and average daily weight gain (ADG) (kg/pig per day ± SD) of experimental pigs through stages of feeding

Treatment	I	II	III	IV	*P*
LW 1st day	8.06 ± 1.12	8.02 ± 0.68	8.02 ± 0.54	8.03 ± 0.74	0.999
LW period 7 - 15 kg	13.02 ± 3.04	13.61 ± 5.58	13.10 ± 2.29	13.34 ± 1.37	0.931
LW period 15 - 25 kg	27.91 ± 7.25	30.01 ± 3.76	29.54 ± 3.17	30.47 ± 2.58	0.548
LW period 25 - 40 kg	46.42 ± 13.66	49.57 ± 4.95	48.18 ± 5.53	50.22 ± 4.46	0.670
LW period 40 - 70 kg	64.93 ± 19.96	70.12 ± 5.31	69.22 ± 6.59	70.32 ± 5.41	0.611
LW end day	89.30 ± 28.40	97.61 ± 6.17	96.94 ± 8.25	97.78 ± 6.4	0.478
ADG 7 - 15 kg	0.248 ± 0.16	0.279 ± 0.12	0.254 ± 0.11	0.266 ± 0.06	0.920
ADG 15 - 25 kg	0.647 ± 0.22	0.713 ± 0.07	0.715 ± 0.12	0.745 ± 0.06	0.358
ADG 25 - 40 kg	0.882 ± 0.32	0.931 ± 0.11	0.888 ± 0.15	0.941 ± 0.13	0.837
ADG 40 - 70 kg	0.882 ± 0.32	0.979 ± 0.10	1.002 ± 0.10	0.957 ± 0.08	0.391
ADG 70 kg - finish	1.059 ± 0.47	1.195 ± 0.15	1.205 ± 0.18	1.194 ± 0.13	0.500
ADG whole trial	0.752 ± 0.26	0.830 ± 0.06	0.823 ± 0.08	0.831 ± 0.06	0.467

After a first period, the pigs in treatment II, III and IV showed relatively better weight gain, they continued to grow rapidly and reached an average body weight at slaughter of approximately 97 kg after a 108-day feeding. They also had a pretty good average daily weight gain of about 0.830 kg/pig per day. In contrast pigs in treatment I, the negative control which did not receive means to support intestinal health, reached their final weight and average daily weight gain not good, only 89.30 kg/pig and 0.752 kg/pig per day, respectively.

3.2. Feed efficiency

Table 9. Feed intake and Feed conversion ratio of experimental pigs through stages of feeding

Treatment	I	II	III	IV	*P*
FI[1] 7 - 15 kg	0.403 ± 0.06	0.417 ± 0.04	0.401 ± 0.05	0.407 ± 0.02	0.938
FI 15 - 25 kg	1.213 ± 0.17	1.132 ± 0.10	1.071 ± 0.05	1.147 ± 0.05	0.246
FI 25 - 40 kg	1.797 ± 0.21	1.784 ± 0.15	1.625 ± 0.14	1.682 ± 0.24	0.352
FI 40 - 70 kg	2.561 ± 0.30	2.476 ± 0.14	2.424 ± 0.13	2.366 ± 0.19	0.781
FI 70 kg - finish	3.557 ± 0.43	3.673 ± 0.14	3.587 ± 0.28	3.533 ± 0.34	0.879
FI total trial	1.870 ± 0.13	1.929 ± 0.08	1.853 ± 0.12	1.859 ± 0.13	0.673
FCR[2] 7 - 15 kg	1.83 ± 0.68	1.51 ± 0.16	1.62 ± 0.21	1.55 ± 0.17	0.484
FCR 15 - 25 kg	1.69^{a} ± 0.13	1.59^{ab} ± 0.08	1.51^{b} ± 0.12	1.54^{ab} ± 0.07	0.029
FCR 25 - 40 kg	1.86 ± 0.15	1.92 ± 0.06	1.84 ± 0.09	1.79 ± 0.09	0.220
FCR 40 - 70 kg	2.52 ± 0.16	2.53 ± 0.08	2.43 ± 0.20	2.47 ± 0.18	0.662
FCR 70 kg - finish	3.17 ± 0.52	3.09 ± 0.28	2.98 ± 0.14	2.96 ± 0.13	0.637
FCR total trial	2.49 ± 0.48	2.33 ± 0.08	2.25 ± 0.11	2.24 ± 0.09	0.331

[1]"FI" feed intake (kg/pig per day ± SD), [2]FCR" feed conversion ratio (kg feed/kg gain ± SD). Means in the same row with different superscript letters are significantly different (P < 0.05).

Pigs in good health will eat much to get much more nutrients, to obtain added nutrients, resulting in a rapid increase in body mass. Looking at Table 9, treatment II which supplemented antibiotics in diet had a higher feed intake than treatment I which without added antibiotics; the figures were respectively 1.929 kg/pig per day and 1.870 kg/pig per day. Furthermore, pigs in treatment II had lower diarrhea and good growth, therefore it had a quite good feed conversion ratio (FCR) compared to the FCR of pigs in treatment I (2.33 and 2.49 kg of feed/kg of weight gain, respectively). Although, pigs in treatment III and IV were relatively lower than the diet of pigs in treatment II (1.853 kg/pig per day, 1.859 kg/pig per day and 1.929 kg/pig per day, respectively), but pigs in treatment III and IV still achieved good weight gain as shown in Table 8, leading to a FCR better than pigs in treatment II and of course even better than pigs in treatment I. The reason may be that pigs in treatment III and IV were fed feed which was combined tools to support intestinal health with natural products, while also having the ability to control harmful bacteria, thus minimizing diarrhea and enhance pig health, without causing adverse effects on beneficial bacteria in the pig's intestinal tract like using antibiotics in pig feed in treatment II.

3.3. Health status of experimental pigs

Table 10. Percentage of days of diarrhea in pigs

Stage	Treatment	I	II	III	IV	*P*
7 - 15 kg	Number of pig (pig)	12	12	12	12	
	Number of days of feeding (day)	240	240	240	240	
	Number of days of diarrhea (day)	211	196	217	203	
	Percentage of days of diarrhea (%)	87.92^{ab}	81.67^{b}	90.42^{a}	84.58^{ab}	0.046
15 - 25 kg	Number of pig (pig)	11	12	12	12	
	Number of days of feeding (day)	253	276	276	276	
	Number of days of diarrhea (day)	63	67	54	50	
	Percentage of days of diarrhea (%)	24.28	24.90	19.57	18.12	0.320
Total trial	Number of pig (pig)	12	12	12	12	
	Number of days of feeding (day)	1208	1296	1296	1296	
	Number of days of diarrhea (day)	333	295	310	281	
	Percentage of days of diarrhea (%)	27.57^{a}	22.76^{b}	23.92^{ab}	21.68^{b}	0.044

^{a,b}*Means in the same row with different superscript letters are significantly different (P < 0.05).*

Table 10 showed the percentage of days of diarhea in pigs. In first period of the experiment, pigs in all treatments had a very high rate of diarrhea, especially in treatment I which had not antibiotics or other supplements to protect intestinal health in feed, so pigs had prolonged diarrhea; despite being treated with the same medication as other pigs diarrhea, they still too weak and lost weight, leading to having one pig to be culled at the end of first feeding. Although treatment II used antibiotics to prevent diarrhea in second period, the diarrhea rate was still high and equivalent to treatment I; this may be due to the negative impact of antibiotics on the balance of intestinal microorganisms when used for a long time. In contrast, treatments III and IV after an initial feeding, there was also severe diarrhea, but perhaps the impact to the presence of supplements to protect intestinal health, in the next period it decreased. Treatment IV perhaps helps to use of the anti-bacterial peptides in the feed, it has the effect of inhibiting diarrhea-causing bacteria no less than the effect of antibiotics, without adverse impact on beneficial bacteria in the intestinal tract, so during the entire experimental period, pigs in treatment IV had the lowest rate of diarrhea per day (21.68%) compared to pigs in other treatments. This result is like the study of Duong et al. (2019) in reducing diarrhea in pigs when using products having peptides.

Table 11. Number of pigs alive (pig) and survival ratio (%) of experimental pigs

Period	Treatment I		Treatment II		Treatment III		Treatment IV	
	Number of pig	Survival ratio (%)	Number of pig	Survival ratio (%)	Number of pig	Survival ratio (%)	Number of pig	Survival ratio (%)
7 - 15 kg	12	100	12	100	12	100	12	100
15 - 25 kg	12	91.67	12	100	12	100	12	100
25 kg - finish	11	100	12	100	12	100	12	100
Total trial	12	91.67	12	100	12	100	12	100

Pigs in all three treatments II, III and IV had a survival rate up to 100%, except for treatment I which only reached 91.67% because one pig was eliminated when moving from stage 7 - 15 kg to stage 15 - 25 kg. The pig did not have typical disease symptoms, but it had diarrhea in the first stages, ate less and lost weight suddenly, with no ability to recover, so it must be culled. The detail of figures were presented in Table 11.

Table 12. Carcass traits of finished experimental pigs

Treatment	I	II	III	IV
Live weight (kg)	92.54	93.54	94.48	93.50
Weight of the dressed carcass (kg)	75.70	77.72	80.36	76.36
Percentage of the dressed carcass (%)	81.80	83.09	84.61	81.67
Weight of the carcass (kg)	68.58	66.42	72.64	68.26
Percentage of the carcass (%)	74.11	71.01	76.48	73.01
Back-fat thickness (n = 47), mm	13.33 ± 1.71	14.00 ± 1.39	13.42 ± 2.00	12.61 ± 1.01

At the end of experiment after 108 days of feeding, in each treatment, selected one pig of similar weight to slaughter and evaluate carcass traits. As for back-fat thickness of pigs, it was measured directly on all live pigs 3 days before finishing the experiment. The results in Table 12 did not show much difference between 4 treatments, although pigs in treatment II with feed supplemented of antibiotics had the lowest carcass rate and the highest back-fat thickness compared to pigs in the remaining three treatments, but because the number of slaughtered pigs is only one pig/treatment, it is not enough to analyze the statistical significance of this difference.

3.4. Economic efficiency

Table 13. Compare costs between experimental treatments

	Treatment I	Treatment II	Treatment III	Treatment IV
Feed consumed in stage 1 (kg)	97	100	96	97
Unit price of feed (vnd/kg)	14,162	14,266	14,398	14,516
Feed cost in stage 1 (vnd)	1,373,714	1,426,600	1,382,208	1,408,052
Feed consumed in stage 2 (kg)	299	312	296	316
Unit price of feed (vnd/kg)	11,606	11,715	11,866	11,981
Feed cost in stage 2 (vnd)	3,470,194	3,655,080	3,512,336	3,785,996
Feed consumed in stage 3 (kg)	408	450	410	424
Unit price of feed (vnd/kg)	10,397	10,506	10,659	10,774
Feed cost in stage 3 (vnd)	4,241,976	4,727,700	4,370,190	4,568,176
Feed consumed in stage 4 (kg)	559	624	611	596
Unit price of feed (vnd/kg)	9,825	9,934	9,984	9,995
Feed cost in stage 4 (vnd)	5,492,175	6,198,816	6,100,224	5,957,020
Feed consumed in stage 5 (kg)	890	1014	990	975
Unit price of feed (vnd/kg)	9,497	9,600	9,643	9,752
Feed cost in stage 5 (vnd)	8,452,330	9,734,400	9,546,570	9,508,200
Feed cost all total trial (vnd) (1)	23,030,389	25,742,596	24,911,528	25,227,444
Medicine cost (vnd) (2)	163,480	23,000	41,260	61,790
Total weight gain of experimental pigs (kg) (3)	975	1,075	1,067	1,077
(Feed cost + Medicine cost)/kg weight gain (vnd/kg) (1 + 2)/3	23,789	23,968	23,386	23,481
Compared to treatment I (vnd/kg)	-	+ 179	- 403	- 308
Difference from treatment I (%)	-	+ 0.75	- 1.69	- 1.29
Saved to treatment II (%)	-	-	- 1.68	- 1.28

Price of raw materials used to produce feed as of July 2023.

After 108 days of feeding trial, pigs in treatment I which was fed diet without any supplements to enhance of gut health status expressed worst performance on live weight, daily weight gain (ADG), FCR and especially on problem of diarrhea and survival ratio. Pigs fed diet with combination of phytogenic plus organic acid plus probiotics in treatment III gained body weight and FCR better than pigs which received diet supplemented with antibiotics (treatment II), although this difference is not statistically significant at $P > 0.05$. In another way, the feed cost per kg of live weight of pigs which was showed in Table 13 in treatment III and treatment IV was saved significantly compared to that of pigs in treatment II and of course much better than of pigs in treatment I.

4. Conclusions

From the above results, it shows that using anti-bacterial peptides combined with phytogenic and organic acid helps pigs reduce diarrhea and health, so they will achieve better growth and FCR than only using antibiotics alone, and thereby bring better economic efficiency to farmers.

Conflict of interest

The authors declare no conflict of interest.

Acknowledgements

The authors would like to express our deep gratitude to Anh Duong Khang Ltd. Co. for supporting us with materials and conditions to achieve this study.

References

Duong, K. N., Do, D. T., Dang, A. T. N., Tran, A. T., Tran, K. T. M., Jarchow, A., & Wickern, A. Z. (2019). Investigation of bioactive peptides supplementation in diet for growth performance of weaning-finishing pigs in Vietnam. *Journal of Animal Husbandry Sciences and Technics (JAHST)* 24, 29-33.

Pearlin, B. V., Muthuvel, S., Govidasamy, P., Villavan, M., Alagawany, M., Farag, M. R., Dhama, K., & Gopi, M. (2020). Role of acidifiers in livestock nutrition and health: A review. *Journal of Animal Physiology and Animal Nutrition* 104(2), 558-569. https://doi.org/10.1111/jpn.13282.

Rahman, M. R. T., Fliss, I., & Biron, E. (2022). Insights in the development and uses of alternatives to antibiotic growth promoters in poultry and swine production. *Antibiotics* 11(6), 766. https://doi.org/10.3390/antibiotics11060766.

Silveira, R. F., Roque-Borda, C. A., & Vicente, E. F. (2021). Antimicrobial peptides as a feed additive alternative to animal production, food safety and public health implications: An overview. *Animal Nutrition* 7(3), 896-904. https://doi.org/10.1016/j.aninu.2021.01.004.

Wang, J. J., Dou, J. X., Song, J., Lyu, F. Y., Zhu, X., Xu, L., Li, Z. W., & Shan, S. A. (2019). Antimicrobial peptides: Promising alternatives in the post feeding antibiotic era. *Medicine Research Reviews* 39(3), 831–859. https://doi.org/10.1002/med.21542.

Xiao, H., Shao, Y. F., Wu, M. M., Ren, K. W., Xiong, X., Tan, B., & Yin, L. J. (2015). The application of antimicrobial peptides as growth and health promoters for swine. *Journal of Animal Science and Biotechnology* 6, 19. https://doi.org/10.1186/s40104-015-0018-z.

Xu, B. C., Fu, J., Zhu, L. Y., Li, Z., Wang, Y. Z., & Jin, M. L. (2020). Overall assessment of antimicrobial peptides in piglets: A set of meta-analyses. *Animal* 14(2), 2463-2471. https://doi.org/10.1017/s1751731120001640.

Evaluating the effects of 17 α-Methyltestosterone and nano chitosan on masculinization rate and growth performance in Nile tilapia (*Oreochromis niloticus*) using the immersion method

Tan M. Pham[1], Loi N. Nguyen[1], Minh V. Tran[1], Ha N. Nguyen[2], Tam T. Nguyen[1], & Tu C. P. Nguyen[1]

[1]Faculty of Fisheries, Nong Lam University, Ho Chi Minh City, Vietnam

[2]Research Institute for Biotechnology and Environment, Nong Lam University, Ho Chi Minh City, Vietnam

ARTICLE INFO

Research Paper

Received: August 30, 2024
Revised: October 22, 2024
Accepted: October 30, 2024

Keywords

17 α-Methyltestosterone
Immersion method
Nano chitosan
Oreochromis niloticus
Sex reversal

***Corresponding author**

Nguyen Phuc Cam Tu
Email:
npctu@hcmuaf.edu.vn

ABSTRACT

The study aimed to evaluate the effectiveness of combining 17 α-Methyltestosterone (MT) with nano chitosan on the survival rate, masculinization rate, and growth performance of Nile tilapia (*Oreochromis niloticus*) using the immersion method. A completely randomized design was conducted, with five treatment groups receiving varying concentrations of MT and nano chitosan: chitosan + 1 mg MT/L (1 MC), chitosan + 1.5 mg MT/L (1.5 MC), chitosan + 2 mg MT/L (2 MC), chitosan + 2.5 mg MT/L (2.5 MC), and chitosan + 3 mg MT/L (3 MC). A control group was also included, with each treatment replicated three times. Seven-day-old fry were exposed to the MT solution for 2 h before being transferred to nurseries in hapas within earthen ponds at a stocking density of 1,500 fish/m^2 for a 60-day rearing period. After 2 h of hormone treatment and the 60-day rearing period, the 2.5 MC treatment exhibited the highest survival rate. Male ratios in the MT treatments ranged from 76.67% to 83.33%, significantly higher than in the control group (55.56%) ($P < 0.05$). Specifically, the male ratios in the 2.5 MC and 3 MC treatments were 82.2% and 83.3%, respectively, which were higher than those in the other MT treatments, however,these differences were not statistically significant ($P > 0.05$). While the mean weight and length of fish in the MT treatments were greater than those in the control group, these differences were also not statistically significant ($P > 0.05$). The study further revealed a positive correlation between the average weight of the fish and the hormone concentration. Based on these findings, a dose of 2.5 mg 17 α-MT/L in combination with nano chitosan is recommended for achieving optimal mono-sex male tilapia production.

Cited as: Pham, T. M., Nguyen, L. N., Tran, M. V., Nguyen, H. N., Nguyen, T. T., & Nguyen, T. C. P. (2024). Evaluating the effects of 17 α-Methyltestosterone and nano chitosan on masculinization rate and growth performance in Nile tilapia (*Oreochromis niloticus*) using the immersion method. *The Journal of Agriculture and Development* 23(Special issue 2), 76-84.

1. Introduction

Sex reversal in fish is a critical area of study with significant implications for aquaculture, fish farming, and conservation. This phenomenon, where an individual fish changes its sex from male to female or vice versa, occurs naturally in various species and can be influenced by environmental factors, social cues, and hormonal treatments (Piferrer, 2001b; Devlin & Nagahama, 2002). Globally, species such as groupers, wrasses, and clownfish are well-known for their sex-changing capabilities (Sadovy & Liu, 2008). In many countries, sex reversal is particularly relevant for species like the Asian sea bass (*Lates calcarifer*) and tilapia (*Oreochromis* spp.), which are vital to the local aquaculture industry (Mair et al., 1997). The ability to control sex differentiation through hormonal treatments has opened new avenues for optimizing fish production and maintaining ecological balance (Pandian & Sheela, 1995b).

Manipulating the sex of fish populations is essential for several reasons. In hatchery production, achieving a desired sex ratio can enhance reproductive efficiency and yield. For example, in species where one sex grows faster or reaches market size more quickly, producing monosex populations can significantly improve economic returns (Beardmore et al., 2001). In fish farming, controlling the sex ratio can prevent unwanted breeding, reduce competition for resources, and promote uniform growth (Mair et al., 1997). Additionally, in conservation, sex reversal can help restore endangered populations by ensuring a balanced sex ratio, which is crucial for successful breeding programs (Wedekind, 2002).

Tilapia farming plays a vital role in global aquaculture, providing a significant source of affordable protein and contributing to food security, especially in developing countries (FAO, 2020). In Vietnam, tilapia is a key species in freshwater aquaculture, supporting rural livelihoods and export markets due to its adaptability and high growth potential. The cultivation of mono-sex male tilapia is particularly important, as males grow faster and more efficiently than females, leading to higher productivity and profitability in aquaculture systems (El-Sayed, 2006). Controlling the sex ratio not only enhances growth performance but also minimizes issues associated with uncontrolled breeding and competition for resources (Beardmore et al., 2001).

Various methods have been developed to induce sex reversal in fish, including environmental manipulation, genetic techniques, and hormonal treatments. Hormonal treatments are the most widely used approach due to their effectiveness and relative ease of application (Pandian & Sheela, 1995b). Common hormones include androgens like 17 α-methyltestosterone (MT), which induce masculinization, and estrogens like estradiol, which promote feminization (Guerrero III, 1975). These hormones can be administered through feed, injections, or immersion baths, depending on the species and desired outcome (Piferrer, 2001b). Each method of sex reversal has its advantages and disadvantages: i) Environmental manipulation using techniques such as temperature changes are non-invasive and sustainable but can be less precise and effective; ii) Genetic techniques offer long-term solutions and high specificity but involve complex and costly procedures; iii) Hormonal treatments are cost-effective, easy to implement, and provide rapid results (Pandian & Sheela, 1995b). However, methods like hormone feeding can lead to inconsistent dosages, lengthy processing times, and high production costs (Piferrer, 2001b).

The hormone immersion method offers several advantages over the feeding method for fish sex reversal. It ensures uniform hormone uptake, especially during the early developmental stages, leading to more consistent and effective sex reversal outcomes (Piferrer, 2001a). This method also reduces the risk of environmental contamination from uneaten hormone-treated feed and minimizes labor costs associated with hormone-enriched diets (Pandian & Sheela, 1995a). Moreover, immersion treatment allows for precise control over hormone exposure time, improving the efficiency of the process (Beardmore et al., 2001).

The MT is a widely used androgen for inducing masculinization in fish. It is particularly effective in species where males are preferred for their growth rates, market value, or reproductive characteristics (Guerrero III, 1975). The dosage and method of administration vary depending on the species and desired sex ratio. Typically, MT is administered through feed during the early developmental stages when gonadal differentiation is most responsive (Piferrer, 2001b).

Nano chitosan, derived from chitosan, is a biopolymer known for its biocompatibility, biodegradability, and non-toxicity (Rinaudo, 2006). When combined with hormones, nano chitosan can enhance the effectiveness of sex reversal treatments (Rather et al., 2013). The nanoscale size increases the surface area and improves the delivery and absorption of hormones in fish (Kumar et al., 2004). Studies have shown that the combination of nano chitosan with hormones like MT can lead to more consistent and efficient sex reversal results (Zhao et al., 2013).

Given the potential advantages of combining MT with nano chitosan, there is a need to evaluate the effects of this combination on the masculinization rate and growth performance in Nile tilapia (*Oreochromis niloticus*) using the immersion method. This research aims to assess the efficacy and practicality of this approach, providing insights that could enhance fish production techniques and support sustainable aquaculture practices.

2. Materials and Methods

2.1. Broodstock development

The broodstock, weighing between 200 to 250 g, were sourced from the Aquatic and Crop Breeding Center, Saigon Agriculture Corporation, Vietnam. For spawning, the broodstock were paired in six mating hapas (12 m x 5 m x 1.5 m) at a ratio of 3 females to 1 male per square meter in earthen ponds (30 m x 50 m x 2 m). They were fed with a commercial floating pelleted feed containing approximately 30% crude protein, twice daily at 3% of their body weight.

2.2. Fry collection

After 15 days of pairing, fry were collected every seven days. Collection was done using a soft net early in the morning to minimize stress and mortality. The collected fry were acclimated in three composite tanks (1 m^3/tank) for one day, during which weak and dead fry were removed and the remaining fry were sorted by mesh size.

2.3. Preparation of hormone treated solutions

MT Solution: The 17 α-methyltestosterone hormone was obtained from Argent, Philippines. A stock solution was prepared by dissolving 400 mg of MT in 1 liter of 96% ethanol to achieve a nominal concentration of 400 mg/L.

MT + chitosan treatment solution (MC): Nano chitosan used in the present study was obtained from the Institute of Biotechnology and Environmental Research, Nong Lam University, Vietnam. To prepare the solution, 0.2 g of chitosan were dissolved in 10 mL of acetic acid and maintained at room temperature for 3 h. Subsequently, 40 mL of double-distilled water was added, and the mixture was stirred at 1500 rpm for 20 min using a magnetic stirrer. The pH of the solution was adjusted to 3.8 using NaOH (2 N), and distilled water was added to make a total volume of 100 mL. This solution was stirred at 1500 rpm for 20 min and then allowed to settle overnight at 4°C. For conjugation with MT, 20 mg of MT was dissolved in 2 mL of ethanol (96%) and added dropwise to the 100 mL chitosan solution while stirring continuously at 1500 rpm for 25 min. The resulting chitosan + MT (CS + MT) solution was stored at 4°C for later use.

2.4. Experimental design

The experiment was conducted in 5-liter glass tanks containing 3 liters of water, using a completely randomized design. The experiment included five MC concentrations of 1.0, 1.5, 2.0, 2.5 and 3 mg/L and a control group containing MT-free water. Each treatment was repeated three times. Following a one-day acclimatization in continuously aerated composite tanks, 750 tilapia fries were randomly stocked into the glass aquaria according to the MC concentrations and control conditions. Fish were exposed to the MT solution for two hours, after which the fry were transferred to nurseries in hapas (1 m x 1 m x 1 m) suspended in earthen ponds at a density of 1.500 fish/m^2 for 60 days. During this period, the fish were fed commercial floating pellets with varying crude protein levels: 40% (size 0.6 mm) from days 1 to 15, at a feeding rate of 10% of body weight, administered four times daily; 40% (size 0.6 - 1.5 mm) from days 16 to 30, at a feeding rate of 7% of body weight, administered three times daily; and 35% (size 2.0 mm) from days 31 to 60, at a feeding rate of 5% of body weight, administered twice daily.

2.5. Sex reversal

At the end of the experiment, 30 fish were randomly collected from each experimental replicate to determine their sex. Gonadal morphology was examined and recorded. Sex determination was carried out using the standard aceto-carmine gonad squashing technique as described by Guerrero III & Shelton (1974).

2.6. Growth performance

Every 30 days, 30 fish were randomly collected from each experimental replicate to measure mean growth (average weight and total length) and were then released back into the experimental hapas. Survival rates were recorded two hours after immersion in the MT solutions and at the end of the 60-day growth experiment.

2.7. Statistical analysis

Data were statistically analyzed using SPSS version 16.0. One-way ANOVA was performed, and Duncan's multiple range test (DMRT) was employed to determine significant differences between means at the 5% level of significance.

3. Results

3.1. Water quality parameters

The water quality parameters monitored throughout the experiment remained within the optimal range for Nile Tilapia, ensuring that external factors did not influence the outcomes of the treatments. The temperature ranged between

29.0 - 32.0°C, dissolved oxygen (DO) levels varied from 5.4 - 6.6 mg/L, pH levels were maintained between 6.4 - 7.4, and ammonia (NH_3) levels were kept below 0.25 mg/L (Table 1). These conditions are consistent with the standard environmental requirements for the species, confirming that the experiment's outcomes are likely attributable to the treatment effects rather than environmental stressors (Boyd, 1990).

Table 1. Water quality parameter during the experiment

Temperature (°C)	Dissolved oxygen (mg/L)	pH	NH_3 (mg/L)
29.0 - 32.0	5.4 - 6.6	6.4 - 7.4	< 0.25

3.2. Fish survival and sex ratio

The survival rates and sex ratios of the fish treated with various concentrations of MT and nano chitosan are summarized in Table 2. The survival rate at the day 60 did not significantly differ across treatments, indicating that the treatments were not toxic or detrimental to the overall health of the fish. However, the percentage of males varied significantly among the different treatment groups. The control group exhibited a male percentage of 55.56%, which aligns with the natural sex ratio expected in Nile Tilapia populations (Yamazaki, 1983). In contrast, the groups treated with combination of MT and nano chitosan showed a significant increase in male percentage, with the highest masculinization rate observed in the 3 MC group (83.33%). This trend indicates that the combination of MT and nano chitosan effectively enhances the masculinization process in Nile Tilapia, particularly at higher concentrations.

Table 2. Fish survival and mean percent of male of each combination of 17 α-Methyltestosterone and nano chitosan (MC) treatment groups and control group

Treatment	Number of analyzed fish (individual)	Survival rate after 2 h (%)	Survival rate at day 60 (%)	Male (%)	Female (%)
Control	90	100	87.78 ± 0.1	55.56 ± 5.1^a	44.44 ± 5.1
1 MC	90	100	89.04 ± 0.4	76.67 ± 10.0^b	23.33 ± 10.0
1.5 MC	90	100	85.96 ± 0.8	77.78 ± 8.4^b	22.22 ± 8.4
2 MC	90	100	85.71 ± 1.3	77.78 ± 1.9^b	22.22 ± 1.9
2.5 MC	90	100	93.00 ± 4.5	82.22 ± 3.3^b	17.78 ± 3.3
3 MC	90	100	86.60 ± 3.8	83.33 ± 3.8^b	16.67 ± 3.8

Values (mean of data for triplicate groups) with different superscripts in the same column are significantly different (one-way ANOVA and Tukey test, P < 0.05).

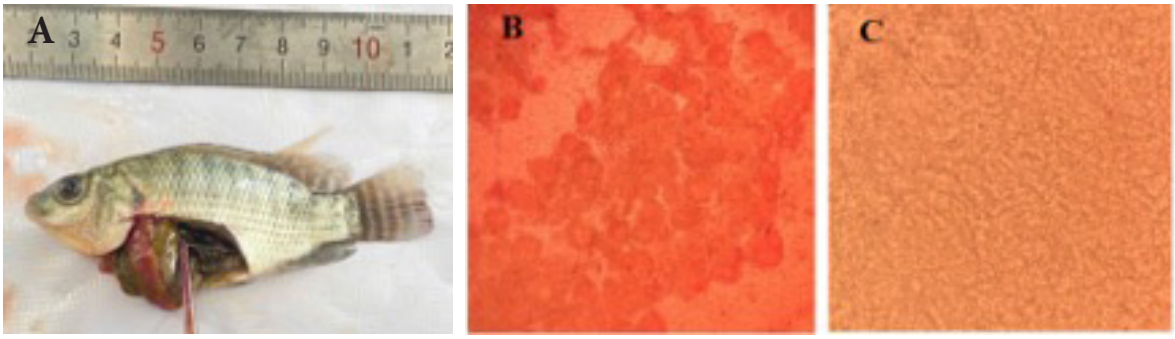

Figure 1. The observed gonad of male and female tilapia after 60 days of 17 α-Methyltestosterone treatment. (A) Gonad removal (B) Eggs, and (C) Testis under light microscope.

3.3. Growth performance

The growth performance of the experimental fish over the 60-day period is detailed in Table 3. All groups, including the control, displayed significant growth, with final weights ranging from 6.63 g in the 3 MC group to 5.17 g in the control group. The highest weight gain (WG) was observed in the 3 MC group (6.62 g), which also had the highest specific growth rate (SGR) at 10.53% per day. These results suggest that the combination of MT and nano chitosan not only promotes masculinization but also enhances growth performance, particularly at higher concentrations. This finding is consistent with previous studies indicating that MT can boost growth in fish by promoting feed efficiency and protein synthesis (Johnstone, 1985).

Table 3. The growth performance of experiment fish in 60 days after being exposed in different combinations of 17 α-Methyltestosterone and nano chitosan (MC) concentrations

Treatment	Initial weight (g)	Final weight (g)	Weight gain (g)	Specific growth rate (%/day)
Control	0.01 ± 0.0	5.17 ± 0.16	5.16 ± 0.16	10.73 ± 0.05
1 MC	0.01 ± 0.0	5.34 ± 0.43	5.33 ± 0.43	10.17 ± 0.14
1.5 MC	0.01 ± 0.0	5.40 ± 0.19	5.38 ± 0.19	10.20 ± 0.06
2 MC	0.01 ± 0.0	5.88 ± 0.48	5.87 ± 0.48	10.34 ± 0.14
2.5 MC	0.01 ± 0.0	5.21 ± 0.24	5.20 ± 0.24	10.14 ± 0.07
3 MC	0.01 ± 0.0	6.63 ± 0.37	6.62 ± 0.37	10.53 ± 0.11

Values (mean ± standard deviation of data for triplicate groups).

4. Discussion

Maintaining optimal water quality is crucial for the success of aquaculture operations. The parameters recorded in this study were within the optimal range for Nile tilapia, supporting the physiological processes necessary for growth and masculinization (El-Sayed, 2006). The stability of these parameters highlights the importance of proper management practices in experimental settings to minimize stress and potential confounding factors. Proper water quality management ensures that environmental conditions such as temperature, pH, dissolved oxygen, and ammonia levels are conducive to

the health and growth of the fish (Boyd, 1990). This is essential as suboptimal water conditions can lead to stress, reduced immune function, and lower survival rates (Kubitza, 2004). Therefore, maintaining stable optimal water quality parameters throughout the experiment was a critical factor in the success of this study.

The combination of MT and nano chitosan significantly influenced the sex ratio of Nile tilapia. Higher MT concentrations (2.5 MC and 3 MC) resulted in a significant increase in the male ratio, demonstrating the effectiveness of this method in achieving the desired sex ratio for commercial purposes (Pandian & Sheela, 1995b). This finding is consistent with previous studies that have demonstrated the effectiveness of MT in inducing masculinization in fish species (Piferrer, 2001b). The high survival rates across all treatment groups indicate that the immersion method of hormone application combined with nano chitosan is a safe and effective approach for masculinization (Johnston et al., 2009). This hormone method minimizes stress and potential injuries, concerns often associated with other methods such as oral or injectable hormones (Hunter & Donaldson, 1983). Furthermore, nano chitosan has been shown to enhance the efficacy of hormone treatments by facilitating better absorption and sustained release of the hormone within the fish (Sánchez et al., 2012; Abd El-Naby et al., 2019; Wu et al., 2020). This synergistic effect likely contributed to the high masculinization rates observed in the study.

The enhanced growth performance observed in the treatment groups, particularly in the 3 MT group, aligns with previous findings that anabolic steroids can promote growth by enhancing protein synthesis and feed conversion efficiency (Sundararaj & Vasal, 1976; Guerrero III & Guerrero, 1988; Pandian & Sheela, 1995b). The use of MT in aquaculture has been associated with improved growth rates due to its anabolic effects, enhancing muscle development and overall body mass (MacIntosh & Little, 1995; Pandian & Sheela, 1995b; Zohar & Mylonas, 2001). Nano Chitosan may enhance growth performance by improving nutrient absorption and immune response (Sánchez et al., 2012; Manaf et al., 2020) . Chitosan has been reported to have various beneficial effects on fish health, including enhanced gut health, better nutrient uptake, and improved resistance to diseases (Gopalakannan & Arul, 2006). These properties make nano chitosan a valuable additive in feed and treatment protocols for aquaculture. The results of this study demonstrate the potential of combined MT and nano chitosan therapies in optimizing growth performance and production efficiency in Nile tilapia aquaculture. The significant improvements in growth performance observed suggest that this combination can be effectively used to enhance the productivity and profitability of tilapia farming operations (El-Sayed, 2006).

The findings from this study have important implications for aquaculture practices. The use of MT and nano chitosan can be integrated into existing farming protocols to improve both the growth rates and the desired sex ratios of Nile tilapia populations (Little et al., 2003). This can lead to more efficient production cycles and higher economic returns for fish farmers. Moreover, the safety and efficacy of the hormone immersion method provide a viable alternative to more invasive techniques, potentially reducing labor costs and improving animal welfare (Guerrero III & Guerrero, 1988). The integration of nano chitosan also offers additional benefits such as enhanced disease resistance and better overall

health of the fish, contributing to sustainable aquaculture practices (Sánchez et al., 2012).

5. Conclusions

The combination of 17 α-Methyltestosterone and nano chitosan significantly improved the male sex ratio and survival rates of Tilapia. Their combination enhanced growth performance and optimizing production efficiency of Tilapia. Thus, applying this method into existing aquaculture protocols can increase productivity and profitability in Tilapia farming. A dose of 2.5 mg 17 α-MT/L in combination with nano chitosan is recommended for achieving optimal mono-sex male tilapia production.

Conflict of interest

The authors declare no conflict of interest.

References

Abd El-Naby, F. S., Naiel, M. A. E., Al-Sagheer, A. A., & Negm, S. S. (2019). Dietary chitosan nanoparticles enhance the growth, production performance, and immunity in *Oreochromis niloticus*. *Aquaculture* 501, 82-89. https://doi.org/10.1016/j.aquaculture.2018.11.014.

Beardmore, J. A., Mair, G. C., & Lewis, R. I. (2001). Monosex male production in finfish as exemplified by tilapia: applications, problems, and prospects. *Aquaculture* 197(2001), 283-301. https://doi.org/10.1016/B978-0-444-50913-0.50015-1.

Boyd, C. E. (1990). *Water quality in ponds for aquaculture*. Alabama, USA: Alabama Agricultural Experiment Station, Auburn University.

Devlin, R. H., & Nagahama, Y. (2002). Sex determination and sex differentiation in fish: an overview of genetic, physiological, and environmental influences. *Aquaculture* 208(3-4), 191-364. https://doi.org/10.1016/S0044-8486(02)00057-1.

El-Sayed, A. F. M. (2006). *Tilapia culture*. Iowa, USA: CAB International.

FAO (Food and Agriculture Organization of the United Nations). (2020). *The state of world fisheries and aquaculture 2020*. Rome, Italy: Food and Agriculture Organization of the United Nations.

Gopalakannan, A., & Arul, V. (2006). Immunomodulatory effects of dietary intake of chitin, chitosan and levamisole on the immune system of *Cyprinus carpio* and control of *Aeromonas hydrophila* infection in ponds. *Aquaculture* 255(1-4), 179-187. https://doi.org/10.1016/j.aquaculture.2006.01.012.

Guerrero III, R. D., & Guerrero, L. A. (1988). Feasibility of commercial production of sex-reversed Tilapia in the Philippines. *In ICLARM Conference Proceedings (Philippines)* 10(2), 4-6.

Guerrero III, R. D. (1975). Use of androgens for the production of all-male Tilapia aurea (Steindachner). *Transactions of The American Fisheries Society* 104(2), 342-348.

Guerrero III, R. D., & Shelton, W. L. (1974). An aceto-carmine squash method for sexing juvenile fishes. *The Progressive Fish-Culturist* 36(1), 56-56.

Hunter, G. A., & Donaldson, E. M. (1983). 5 Hormonal sex control and its application to fish culture. *Fish Physiology* 9B, 223-303. https://doi.org/10.1016/S1546-5098(08)60305-2.

Johnston, I. A., Fernandez, D. A., Calvo, J., Vieira, V. L., North, A. W., Abercromby, M., & Garland, T. (2009). Reduction in muscle fibre number during the metamorphic transformation of a flatfish. *Journal of Fish Biology* 74(3), 720-732.

Johnstone, R. (1985). The role of 17 α-Methyltestosterone in growth and sexual differentiation in fish. *Journal of Fish Biology* 27(6), 745-758.

Kubitza, F. (2004). Water quality and management for fish ponds. *Aqua Cultura* 39(1), 40-45.

Kumar, M. N. V. R., Muzzarelli, R. A. A., Muzzarelli,

C., Sashiwa, H., & Domb, A. J. (2004). Chitosan chemistry and pharmaceutical perspectives. *Chemical Reviews* 104(12), 6017-6084. https://doi.org/10.1021/cr030441b.

Little, D. C., Bhujel, R. C., & Pham, T. A. (2003). Advanced nursing of mixed-sex and mono-sex tilapia (*Oreochromis niloticus*) fry, and its impact on subsequent growth in fertilized ponds. *Aquaculture* 221(1), 265-276. https://doi.org/10.1016/S0044-8486(03)00008-5.

MacIntosh, D. J., & Little, D. C. (1995). Nile tilapia (*Oreochromis niloticus*) fry production in irrigated rice-fields using hormone-treated supplementary feed: The effects of varying treatment period and feed quality. *Aquaculture* 132(1-2), 265-274.

Mair, G. C., Abucay, J. S., Skibinski, D. O. F., Abella, T. A., & Beardmore, J. A. (1997). Genetic manipulation of sex ratio for the large-scale production of all-male tilapia *Oreochromis niloticus*. *Canadian Journal of Fisheries and Aquatic Sciences* 54(2), 396-404. https://doi.org/10.1139/f96-282.

Manaf, M., Soliman, M. A., & El-Mohamady, R. S. (2020). Nano chitosan as a potential dietary supplement to improve growth performance and immunity in fish. *Aquaculture International* 28(2), 721-733.

Pandian, T. J., & Sheela, S. G. (1995a). Hormonal induction of sex reversal in fish. *Aquaculture* 138(1-4), 1-22. https://doi.org/10.1016/0044-8486(95)01075-0.

Pandian, T. J., & Sheela, S. G. (1995b). Hormonal induction of sex reversal in fish. *Aquaculture* 138(1-4), 1-22. https://doi.org/10.1016/0044-8486(95)01075-0.

Piferrer, F. (2001a). Endocrine sex control strategies for the feminization of teleost fish. *Aquaculture,* 197(1-4), 229-281.

Piferrer, F. (2001b). Endocrine sex control strategies for the feminization of teleost fish. *Aquaculture* 197(1-4), 229-281.

Rather, M. A., Sharma, R., Gupta, S., Ferosekhan, S., Ramya, V. L., & Jadhao, S. B. (2013). Chitosan-Nanoconjugated Hormone Nanoparticles for Sustained Surge of Gonadotropins and Enhanced Reproductive Output in Female Fish. *Plos One* 8(2), e57094. https://doi.org/10.1371/journal.pone.0057094.

Rinaudo, M. (2006). Chitin and chitosan: Properties and applications. *Progress in Polymer Science* 31(7), 603-632.

Sadovy, Y., & Liu, M. (2008). Functional hermaphroditism in teleosts. *Fish and Fisheries* 9(1), 1-43. https://doi.org/10.1111/j.1467-2979.2007.00266.x.

Sánchez, A., Vázquez, A., & Domínguez, F. (2012). Chitosan: An update on its effect on immunity and applications for vaccine adjuvant and delivery systems. *Marine Drugs* 10(6), 106-116.

Sundararaj, B. I., & Vasal, S. (1976). Steroid-induced sterility in fish. *Indian Journal of Experimental Biology* (14), 488-494.

Wedekind, C. (2002). Manipulating sex ratios for conservation: Short-term risks and long-term benefits. *Animal Conservation Forum* 5(1), 13-20. https://doi.org/10.1017/S1367943002001026.

Wu, Y., Rashidpour, A., Almajano, M. P., & Metón, I. (2020). Chitosan-Based Drug Delivery System: Applications in Fish Biotechnology. *Polymers* 12(5), 1177. https://doi.org/10.3390/polym12051177.

Yamazaki, F. (1983). Sex control and manipulation in fish. *Aquaculture* 33(1-4), 329-354. https://doi.org/10.1016/0044-8486(83)90413-1.

Zhao, X., Li, J., Zhu, C., Sun, L., Wang, Z., & Zhou, Y. (2013). Enhancement of fish growth performance using chitosan nanoparticles. *Fish and Shellfish Immunology* 35(3), 901-906.

Zohar, Y., & Mylonas, C. C. (2001). Endocrine manipulations of spawning in cultured fish: From hormones to genes. *Aquaculture* 197(1-4), 99-136. https://doi.org/10.1016/B978-0-444-50913-0.50009-6.

Current situation of beef cattle production on household farms in some districts of Lam Dong province

Hai T. Nguyen[1*], Lanh V. Nguyen[1], Van T. Nguyen[1], Anh N. T. Dang[1], Nhan M. T. Nguyen[1], & Thinh P. Pham[2]

[1]Department of Animal Production, Nong Lam University, Ho Chi Minh City, Vietnam

[2]Department of Animal Nutrition, Nong Lam University, Ho Chi Minh City, Vietnam

ARTICLE INFO

Research Paper

Received: August 31, 2024
Revised: October 16, 2024
Accepted: November 04, 2024

Keywords

ADG
Beef cattle
Breeds
Husbandry methods
Husbandry scale

***Corresponding author**

Nguyen Thanh Hai
Email:
hai.nguyenthanh@hcmuaf.edu.vn

ABSTRACT

The objective of this study was to assess the current situation of beef cattle production in households in some districts of Lam Dong province. Ninety household beef cattle farms (HBCFs) were chosen from Cat Tien, Don Duong and Duc Trong districts (10 households/commune and 3 communes/district) to perform the survey using pre-printed questionnaires and direct interviews on a cross-section study model and the Participatory Rural Appraisal method. Results showed that beef cattle husbandry householders have an extensive experience in beef farming with 36.7% having 11 - 15 years of experience ($P < 0.01$), although their educational levels were low, with 31.1% at the primary level ($P < 0.01$). There were 7.3 cattle/household in the total number of herd and and a beef cattle group of 4.7 cattle. Most households operated a husbandry scale from 1 - 5 cattle/household comprising 60.00% of the total herd ($P < 0.01$) and 69.32% of the beef cattle group ($P < 0.01$). High-yielding breeds dominated the current beef production systems in HBCFs, in which BBB cross-breeds accounted for 57.95% and 76.84% of households and total cattle, respectively; Charolais cross-breed accounted for 25.00 and 12.6%, respectively ($P < 0.01$). There was a high level (92.22%) of husbandry and management method as tied stall form ($P < 0.01$). Additionally, 76,14% of HBCFs applied fattening procedure for beef cattle before selling to abattoirs ($P < 0.01$), but artificial insemination application in HBCFs was just 48.86% ($P = 0.763$). The average daily gain of the beef herd for whole husbandry and fattening periods reached 580.3 and 696.4 g/day, respectively. Briefly, these results suggest that there are some limitations in beef cattle production on household farms for developing sustainably high-yielding beef cattle farming in Lam Dong. Therefore, there should be more application of scientific advancements to improve the present situation.

Cited as: Nguyen, H. T., Nguyen, L. V., Nguyen, V. T., Dang, A. N. T., Nguyen, N. M. T., & Pham, T. P. (2024). Current situation of beef cattle production on household farms in some districts of Lam Dong province. *The Journal of Agriculture and Development* 23(Special issue 2), 85-97.

1. Introduction

In Vietnam, beef cattle industry is developing strongly with a gradual decrease in the number of small-scale cattle farms for an increase in the intensive large scale, and the preference of raising high-yielding beef breeds (BBB, Charolais, DroughtMaster, etc) (Pham et al., 2018; Duong et al., 2019; Nguyen & Do, 2020) to get high economic efficiency. Small-scale production with 1 - 2 cattle/household has gradually changed to about 5 - 20 cattle/household (Nguyen et al., 2021a). In 2023, beef cattle industry developed steadily and increased by 2.4% of the nationwide total live beef output (Thuy, 2023). However, in the first 6 months of 2024, the number of beef cattle showed a downward trend could be due to the impact of the market economy, pandemic, increased feed cost, and low beef-product price (Hoang, 2024; La, 2024).

Lam Dong (LD) is one of the provinces with a developed beef cattle industry in Vietnam, applying the program of hybridizing cattle and upgrading high-yielding cross-breeds, thus having a central role in the overall development of national beef cattle industry. It possesses several advantages in natural conditions, grassland, feed ingredients, a variety of good beef cattle breeds and a favorable climate (Ngo et al., 2022) for developing the high yielding cross-bred beef breeds. However, a recent survey mentioned that beef cattle production was mainly focused on the small scale with various cross-breeds (Nguyen et al., 2021b). Therefore, evaluating the current situation of beef cattle production and identifying the reasons for limitation of the actual development potential of the high-yielding cross-bred cattle industry is essential.

Although there have been recent investigations evaluating the status of beef cattle production at both farm and household scales in many provinces of Vietnam, such as Dak Lak (Pham et al., 2021a; Ngo et al., 2022), Quang Binh (Hoang et al., 2009), Quang Ngai (Le et al., 2021), Tay Ninh (Pham et al., 2021b), Thua Thien Hue (Pham et al., 2022), Tien Giang (Nguyen et al., 2021c), Tra Vinh (Pham et al., 2021c), or Ho Chi Minh City (Pham et al., 2021d), no survey has yet been conducted in LD. Therefore, determining the current situation of beef cattle production in LD is necessary to find feasible technical solutions to improve the productivity, quality of beef cattle and beef production efficiency in LD sustainable development.

2. Materials and Methods

2.1. Location

This survey was carried out directly at household beef cattle farms (HBCFs) in 3 districts of Lam Dong (LD) from 06/2024 to 09/2024. The LD is in the south of the Central Highlands of Vietnam, which possesses good natural conditions, including large land, fertile soil, mild weather, and a favorable climate year-round.

2.2. Approach

Using retrospective data: From previous reports of the Department of Livestock, Veterinary and Fisheries of Lam Dong province on beef cattle production in three districts of LD to estimate the number of HBCFs (sample size).

Collecting raw data through direct interviews with pre-printed questionnaires at HBCFs as cross-

section study model by using the Participatory Rural Appraisal method in three districts.

2.3. Sampling method and survey implementation at HBCFs

The direct interviews were conducted at HBCFs using pre-printed questionnaires through sampling method of hierarchical nested sampling design with 3 levels (level 1 includes some districts in LD, level 2 includes some wards/communes in each district, and level 3 includes some households in each ward/commune). Specifically, a total of 90 HBCFs (N = 90) were randomly surveyed in 3 districts of LD (Cat Tien, CT; Duc Trong, DT; Don Duong, DD) with 3 wards/communes for each district and 10 HBCFs for each ward/commune. In fact, the CT, DT and DD are three typical districts in the beef cattle farming sector of the LD province. Therefore, these three districts and 3 wards (for each district) and 10 households (randomly for each ward) were chosen as the hierarchical sampling to ensure representativeness of the current status of beef cattle production in the LD province.

2.4. Survey measurements and parameters

General information of HBCFs: Experience and education level.

Important indicators associated with beef cattle production activities: Husbandry method, husbandry goal, origin of cattle of HBCFs, main income source of HBCFs, selling method of beef cattle, fattening application before selling for beef and culling breeding female cattle (BFC), and labor sources at HBCFs.

Parameters related to the beef cattle herd on farms: Herd scale, structure, and beef cattle breeds.

Indicators related to the growth and development of beef cattle: Live weight (LW), average daily gain (ADG, g/day) of beef cattle throughout the whole beef cattle production stage (WBPS) and fattening stage (FS).

Parameters associated with the breeding female cattle (BFC) group: Breeds and some critical indicators associated with artificial insemination (AI) (awareness, application, level and implementer).

2.5. Statistical analysis

Data from survey as cross-section study model were analysed by using Minitab 16.2. Quantitative values (Mean ± SD) were compared using ANOVA followed by Tukey test while qualitative values (%) were compared using $\chi 2$ test with significant differences at $P < 0.05$.

3. Results and Discussion

3.1. General information on HBCFs

The majority of experience distribution in beef cattle production among households in LD was in the range of 11 - 15 years (36.7%) and > 20 years (27.8%) with the minority in the range of < 1 year and 1 - 5 years (2.2% and 3.3%, respectively) ($P < 0.01$; Figure 1). Cattle production experience is a crucial factor in determining economic efficiency in agricultural production in general and livestock production in particular (Tran & Do, 2021). Therefore, LD is considered as a region with a long history of beef cattle production, and HBCFs have accumulated beef cattle experience in many years of practice.

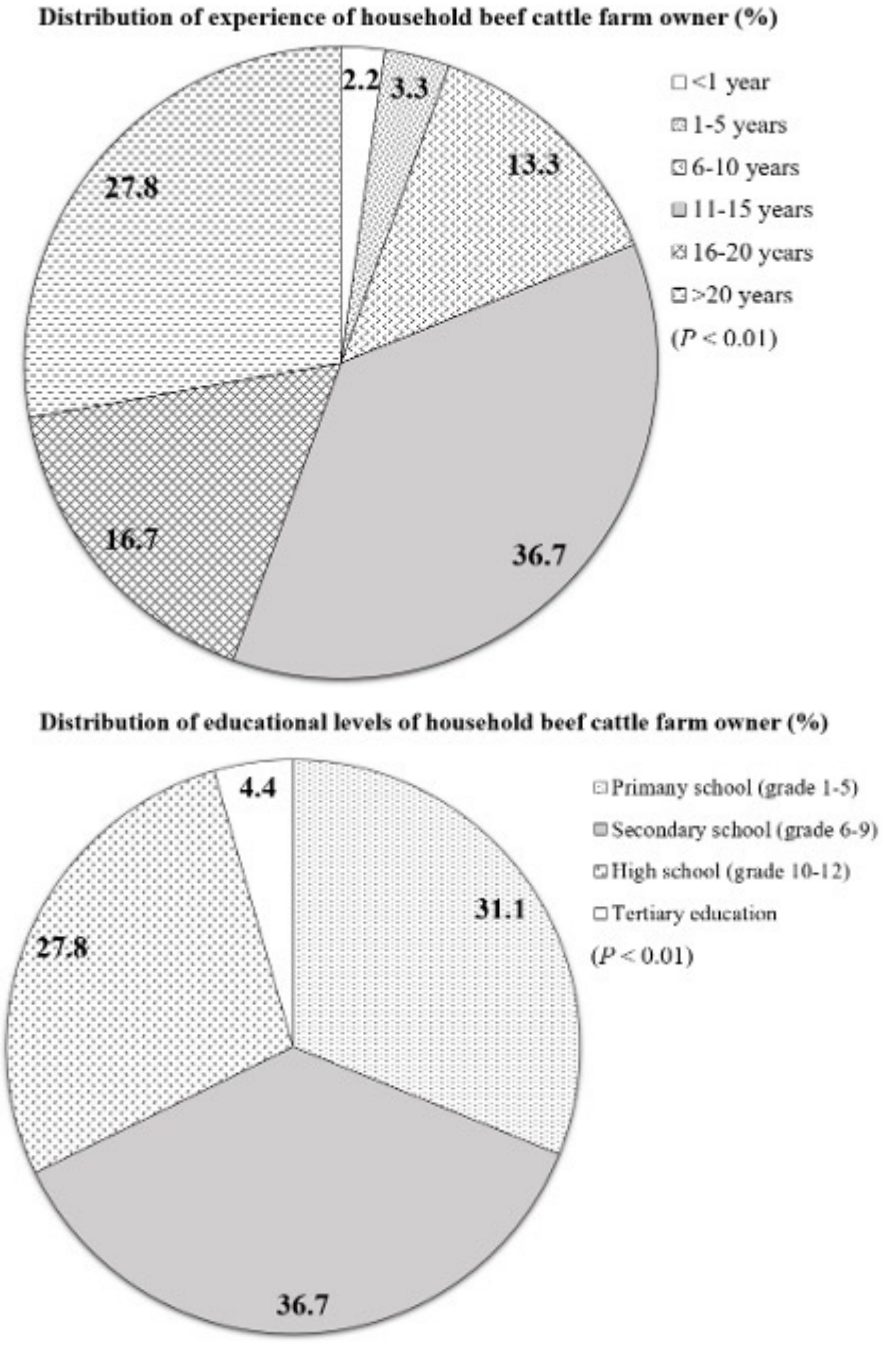

Figure 1. Experience and education level of household beef cattle farm owners (N = 90).

Furthermore, HBCFs owners in LD with tertiary education (college/university level) just accounted for 4.4%, significantly lower ($P < 0.01$) than those of secondary (36.7%), primary (31.1%) and high school level (27.8%). Therefore, improving education levels and participating in training workshops or practical field trips are necessary to effectively access, understand and apply scientific and technological models in livestock production (Kim, 2024).

3.2. Some important parameters related to beef cattle production activities

Table 1. Indicators associated with beef cattle production activities

Parameters	Classifications	Quantity	%	*P*
Beef cattle husbandry method (N = 90)	Full confinement	83	92.22[a]	< 0.001
	Semi-grazing	7	7.78[b]	
Beef cattle husbandry goal (N = 90)	Only beef cattle husbandry	2	2.22[b]	< 0.001
	Combination of beef cattle & BFC	86	95.56[a]	
	Only breeding female cattle (BFC) husbandry	2	2.22[b]	
Source of current beef cattle (N = 88)	Buying from outside for raising and fattening	2	2.27[c]	< 0.001
	Calves born from farm dams	34	38.64[b]	
	From both sources	52	59.09[a]	
Main income source (N = 90)	Beef cattle	16	17.78[b]	< 0.001
	BFC	74	82.22[a]	
Selling beef cattle (N = 88)	Through estimating live weight/appearance	88	100.00[a]	< 0.001
	Through estimating age	0	0.00[b]	
	Through weighing LW with market price	0	0.00[b]	
Fattening beef cattle before selling (N = 88)	Fattening application	67	76.14[a]	< 0.001
	No fattening	21	23.86[b]	
Fattening the culling breeding cattle (N = 88)	Fattening before selling	75	85.23[a]	< 0.001
	Selling immediately	13	14.77[b]	
Labor source for farming (N = 90)	Family labor	83	92.22[a]	< 0.001
	Outsource	1	1.11[b]	
	Both	6	6.67[b]	

[a-c] *Values within each parameter with different superscript letters differ (P < 0.01).*

Percentage of beef cattle husbandry method as the complete confinement (92.22%) was significantly higher than that of semi-grazing method (7.78%) ($P < 0.001$; Table 1). Previous surveys also indicated that confined farming and feeding at barn was predominant, and a common trend in beef cattle production in Dak Lak (95%) (Ngo et al., 2022) and Tra Vinh (86.67%) (Pham et al., 2019).

The proportion of combined husbandry of beef cattle and BFC was very popular (95.56%) and significantly higher than those of two other husbandry goals (only beef cattle, only BFC) ($P < 0.001$). The reason could be that this model produces high-yielding cross-bred calves with rapid growth suited for meat production (Lam, 2020) and enhance economic efficiency in beef cattle production (Thuy, 2020). The buying/importation of calves/cattle for raising/fattening occupied 2.27%, significantly lower than the source of beef cattle raised from calves born from farm dams (38.64%) and a combination of both methods (59.09%) ($P < 0.001$).

The percentage of HBCFs selling beef cattle through estimating the live weight/appearance of cattle was 100% ($P < 0.001$). Most HBCFs applied the fattening procedure for beef cattle and culling BFC before selling for slaughter (76.14% and 85.23%, respectively) ($P < 0.001$). The labor force in HBCFs was mainly from the family members (92.22%), and significantly higher ($P < 0.001$) than those of two other sources.

3.3. Parameters related to the beef cattle herd on farms

3.3.1. Herd scale and structure

The currently average total herd was 7.3 cattle/household, with the highest number in DD (9.1 cattle/household), followed by CT (7.9) and the lowest in DT (4.9) ($P < 0.05$; Table 2). The current herd size in LD was lower than that of the results in Dak Lak (8.06 cattle/household) (Pham et al., 2021a) and Ho Chi Minh City (11.19) (Pham et al., 2021d), but higher than that in Quang Ngai (4.8) (Le et al., 2021).

There was the majority of beef cattle (4.7 beef cattle/household at 57.4% of the total herd) in the general herd structure, with the highest proportion in DD (7.5 cattle/household at 78.4%) ($P < 0.05$; Table 2). The number of the BFC was significantly higher in CT (2.8 cattle/household at 43.4%) and DT (1.8 cattle/household at 35.4%) than that in DD ($P < 0.05$). The number of calves was highest in CT with an average of 1.0 calve/household ($P = 0.267$) and accounted for 17.7% of herd ($P < 0.05$). Currently, DD is promoting the development in agricultural sectors, especially livestock, leading to an annual increase in cattle herds and supporting farmers with more access to scientific advancements and quality breeds (Van, 2024). Meanwhile, CT is the area with its tradition of raising the BFC to supply calves to northern districts of Central Highland, so there was higher number of BFC and calves than those of DD and DT.

There currently was a vast percentage of beef cattle production scale by total herd and by beef cattle group of HBCFs in the range of 1 - 5 (60.00% and 69.32%, respectively) or 6 - 10 cattle/household (17.78% and 15.91%, respectively) compared with other scale groups ($P < 0.01$; Figure 2). It has been reported that beef cattle production in Central Highland was mostly small-scale with an average of 2.9 cattle/household, while large-scale farms only accounted for 32.94% with 9.19 cattle/household (Nguyen et al., 2021b). In LD, there has been a gradual change of scale from 1 - 2 to 5 - 20 cattle/household (Nguyen et al., 2021a) to achieve intensive cattle production with medium and large-scale in future.

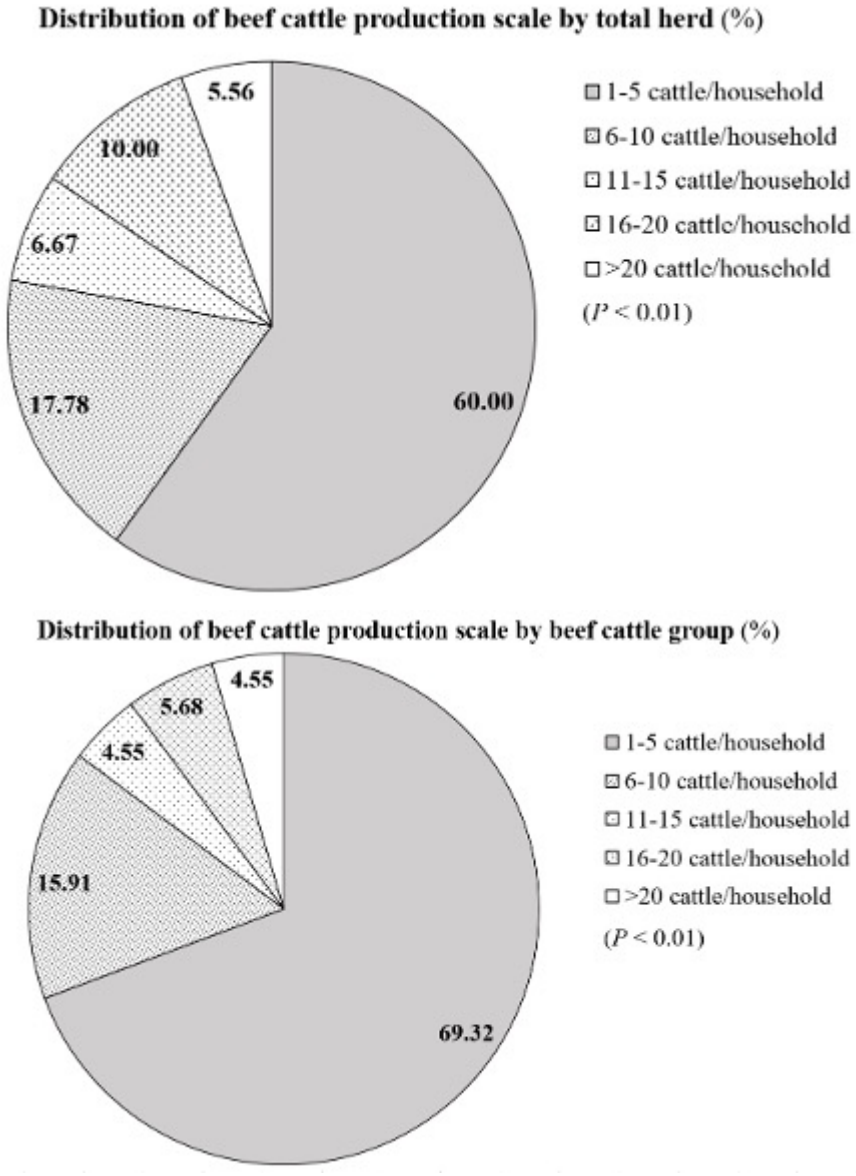

Figure 2. Beef cattle scale by total herd and by beef cattle group (N = 90).

Table 2. Structure of average cattle herd

Districts/ Parameters	N (households)	Average of total herd (cow/ household)	Beef cattle		Breeding female dams		Calves	
			Quantity (cow/ household)	%	Quantity (cow/ household)	%	Quantity (cow/ household)	%
Cat Tien	30	$7.9^{ab} \pm 6.1$	$4.1^{ab} \pm 5.6$	$38.8^{b} \pm 38.5$	$2.8^{a} \pm 2.4$	$43.4^{a} \pm 26.8$	1.0 ± 1.4	$17.7^{a} \pm 19.1$
Don Duong	30	$9.1^{a} \pm 8.6$	$7.5^{a} \pm 8.4$	$78.4^{a} \pm 38.4$	$1.1^{b} \pm 2.1$	$15.8^{b} \pm 28.8$	0.5 ± 0.9	$5.8^{b} \pm 12.6$
Du Trong	30	$4.9^{b} \pm 4.5$	$2.4^{b} \pm 2.3$	$55.4^{ab} \pm 41.7$	$1.8^{ab} \pm 2.3$	$35.4^{a} \pm 35.8$	0.7 ± 1.5	$9.2^{ab} \pm 13.8$
Average	90	7.3 ± 6.8	4.7 ± 6.3	57.6 ± 42.4	1.9 ± 2.3	31.6 ± 32.5	0.7 ± 1.3	10.9 ± 16.0
P		0.042	0.005	0.001	0.018	0.003	0.267	0.011

$^{a-b}$Values within column with different superscript letters differ ($P < 0.05$).

Table 3. Common beef cattle breeds

Districts/Breeds	BBB cross-breed		Charolais cross-breed		Sind cross-breed		Other breeds	
	% households	% cattle	% households	% cattle	% households	% cattle	% households	% cattle
Cat Tien (N = 28)	53.57	69.29^{b}	28.57	21.26^{a}	10.70	7.87^{ab}	7.14	1.57
Don duong (N = 30)	70.00	91.94^{a}	20.00	2.69^{b}	3.33	4.30^{b}	6.67	1.08
Duc Trong (N = 30)	50.00	49.25^{c}	26.67	23.88^{a}	16.70	20.90^{a}	6.67	5.97
Average (N = 88)	57.95	76.84	25	12.6	10.2	8.42	6.82	2.11
P	0.248	< 0.001	0.728	< 0.001	0.230	< 0.001	0.997	0.096

$^{a-b}$Values within column with different superscript letters differ ($P < 0.001$).

Table 4. Parameters associated with live weight (LW) and average daily gain (ADG) during the whole beef cattle production stage (WBPS) and fattening stage (FS)

Districts/Indicators	Starting age WBPS (month)	Starting LW of WBPS (kg)	Starting age of FS (month)	Starting LW of FS (kg)	Ending age of FS (month)	Ending LW of FS (kg)	ADG during WBPS (g/day)	ADG during FS (g/day)
Cat Tien (N = 28)	$8.0^{a} \pm 0.8$	139.3 ± 8.3	17.3 ± 0.5	301.8 ± 41.4	$22.8^{a} \pm 1.1$	413.0 ± 33.0	570.8 ± 124.0	685.0 ± 202.4
Don Duong (N = 30)	$7.7^{ab} \pm 0.4$	136.7 ± 3.8	17.5 ± 0.4	308.3 ± 34.9	$22.3^{b} \pm 0.6$	413.2 ± 29.6	573.5 ± 112.1	741.0 ± 192.6
Duc Trong (N = 30)	$7.6^{b} \pm 0.3$	136.3 ± 3.5	17.4 ± 0.3	311.7 ± 40.9	$22.7^{ab} \pm 0.5$	418.5 ± 39.9	595.9 ± 152.1	662.3 ± 119.1
Average (N = 88)	7.8 ± 0.6	137.4 ± 5.6	17.4 ± 0.4	307.4 ± 38.9	22.6 ± 0.8	414.9 ± 45.2	580.3 ± 129.6	696.4 ± 175.9
P	0.021	0.092	0.439	0.623	0.017	0.785	0.721	0.206

$^{a\text{-}b}$*Values within column with different superscript letters differ (P < 0.05).*

Table 5. Common beef female cattle breeds

Districts/Breeds	Sind cross-breed		Brahman cross-breed		Charolais cross-breed		Local Yellow cattle	
	% households	% cattle	% households	% cattle	% households	% cattle	% households	% cattle
Cat Tien (N = 28)	76.67	80.77^{a}	6.67	3.85^{b}	3.33	1.28	13.33	14.10
Don Duong (N = 30)	72.41	58.54^{b}	13.79	24.39^{a}	10.34	9.76	3.45	7.32
Duc Trong (N = 30)	58.62	56.14^{b}	24.14	22.81^{a}	10.34	8.77	6.90	12.28
Average (N = 88)	69.32	67.61	14.77	14.77	7.95	5.68	7.95	11.93
P	0.109	< 0.01	0.194	0.001	0.768	0.220	0.790	0.194

$^{a\text{-}b}$*Values within column with different superscript letters differ (P < 0.01).*

3.3.2. Breeds and genders

The BBB and Charolais cross-bred cattle are currently the two preferred breeds for raising. Percentage of BBB cross-bred cattle was 57.95% of households and 76.84% of the total herd, while the percentage of Charolais cross-breed was 25.00% of households and 12.60% of the herd (Table 3). In contrast, Sind cross-breed was only 10.2% of households and 8.42% of the herd. The proportion of BBB cross-breed was the highest in DD (91.94%), followed by CT (69.29%) and lowest in DT (49.25%) ($P < 0.001$). However, the proportion of Charolais cross-breed was the highest in DT (23.88%), followed by CT (21.26%), and lowest in DD (2.69%) ($P < 0.001$). A previous survey by Ngo et al. (2022) in Dak Lak showed that cross-breed occupied only 55.66% compared to 43.34% of local yellow cattle. In Ho Chi Minh City, cross-bred beef cattle accounted for 95.46% of the total herd, including 5.38% from BBB cross-breed, 6.47% from Charolais cross-breed and 77.15% from Zebu cross-breed (Pham et al., 2021a). Nguyen et al. (2021b) reported that the Central Highlands has a diversity of crossbred cattle with the popular breed from Sind and Brahman cross-breed. However, the current results confirmed that high-yielding beef breeds have been increasingly favored by HBCFs in LD due to their economic efficiency, productivity and good adaptation to local area.

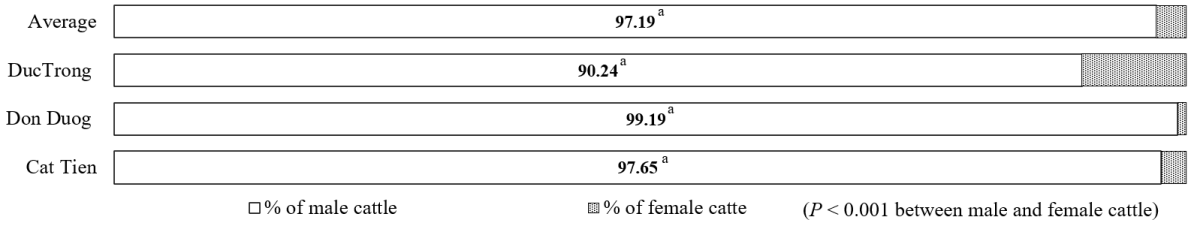

Figure 3. Gender distribution of beef cattle herd (%).

Male cattle seemed to be prioritizedly selected for animal husbandry of meat production (97.19%, from 90.24% - 99.19%) and was significantly higher than that of female cattle ($P < 0.001$; Figure 3). This difference could be due to faster growth, higher maximum LW at maturity and greater carcass yield in male cattle at the same age (Le, 2013), contributing to higher economic efficiency in beef industry.

The results from the survey and calculations in Table 4 revealed that ADG of beef cattle throughout WBPS and FS reached 580.3 g/day and 696.4 g/day, respectively. Moreover, it also indicated similar results in ADG of beef cattle throughout the WBPS and FS among three districts ($P > 0.05$). These results were similar to the previous findings of high-yielding cattle breeds raised in Ben Tre (Duong et al., 2019); however, it was lower than those of high-yielding cross-breeds raised in Ho Chi Minh City (Nguyen & Do, 2020).

3.4. Parameters related to the BFC

Sind cross-breed cattle were the most common breed of BFC in all three districts (69.32% of households and 67.61% of the total cattle) (Table 5). Specifically, the percentages of Sind cross-breed were highest in CT (76.67% of households and 80.77% of cattle), followed by DD (72.41 and 58.54%, respectively), and lowest in DT (58.62 and 56.14%, respectively) ($P < 0.01$; Table 5). Brahman cross-breed were mainly raised in DD and DT (24.39 and 22.81% of cattle, respectively), and lowest in CT (3.85%)

(P = 0.001). Sind or Brahman cross-bred female cattle were primarily chosen as the breeding females mainly due to their good adaptability to Vietnam's severe climate, good resilience, low disease incidence, relatively high meat yield and high reproductive efficiency (Bang, 2021). Therefore, this contributes to the creation of next generations of high-yielding cross-bred beef cattle to supply qualified calves (good adaptability and growth) for local farmers and to reduce the importation from other regions.

The majority of HBCFs were aware of AI methods (61.11%) (P < 0.001; Table 6), while the AI application on their farms was still limited (only 48.86%) (P = 0.763). At HBCFs using AI, it was primarily applied to cattle from the second parity (60.47%), significantly higher than that of all female cattle (16.28%) (P < 0.001). Moreover, AI manipulation in HBCFs was mostly done by outside hired technicians (74.42%) (P < 0.001), and most HBCFs owners using AI cared for the breeds of bull semen before implementing AI (86.04% of households) (P < 0.001). The current application of AI reached a relatively good conception rate with 81.13% at the frequency of services per conception in a range of 1 - 2 times (P < 0.001). The average cost per AI was 303,125 VND, and it took about 1.7 time of AI for pregnancy. This result was similar to the finding in Tra Vinh on BFC but higher than that of female heifers (Pham et al., 2021c), as well as significantly higher than in Ho Chi Minh City (Pham et al., 2021d).

Table 6. Other parameters associated with the breeding female cattle

Qualitative indicators	Classifications	Quantity	%	*P*
Knowing of artificial insemination (AI) (N = 90)	Know	55	61.11[a]	0.003
	Unknow	35	38.89[b]	
AI application in their beef farm (N = 88)	Apply	43	48.86	0.763
	Not apply	45	51.14	
Levels of AI application (N = 43)	All female cattle	7	16.28[b]	< 0.001
	Only cattle from 2nd parity	26	60.47[a]	
	Only cattle from 3rd parity	10	23.26[b]	
Who doing AI in farm (N = 43)	Outsource	32	74.42[a]	< 0.001
	Farm's worker	11	25.58[b]	
Pay attention to the breeds of semen when doing AI (N = 44)	Attention	37	86.04[a]	< 0.001
	Not attention	6	13.95[b]	
Frequency of service per conception (N = 43)	1-2 times	35	81.39[a]	< 0.001
	2-3 times	7	16.27[b]	
	3-4 times	1	2.33[c]	
Quantitative indicators		Mean ± SD	Min - max	
Cost for one services of AI (VND, N = 32)		303,125 ± 42,001	250,000 - 400,000	
Number of services per conception (time, N = 43)		1.70 ± 0.42	1.00 - 4.00	

[a-c]*Values within each parameter with different superscript letters differ (P < 0.01).*

4. Conclusions

The LD is a region with a long history of beef cattle production and HBCFs owners have many-year experience in, but the educational level is still relatively low. The most common husbandry method currently applied in HBCFs is complete confinement. The combined production of beef cattle and BFC is also the most popular. The labor force HBCFs mainly comes from family members, and the HBCFs apply the fattening procedure for both the beef and culling BFC rather than selling immediately. On average, there are 7.3 cattle/household in total herd and 4.7 cattle/household in beef cattle group. Most of the scale distribution of HBCFs is still small scale. The ADG throughout the WBPS and FS has only reached the modest level. Therefore, further investigations are urgently required to assess the other aspects (house conditions, cattle health, feed and daily diets) of HBCFs. In summary, these findings suggest that there are limitations of HBCFs for developing sustainably high-yielding beef cattle production in LD and there should be more applied new techniques to overcome the current situation.

Conflict of interest

No competing interest declared.

Acknowledgements

Authors are grateful to Nong Lam University for providing scientific research grant for Nguyen Thanh Hai (project ID No. CS-GV24-CNTY-01).

References

Bang, G. (2021). *Sind crossbred cattle and rearing methods*. Retrieved January 15, 2021, from https://niengiamnongnghiep.vn/hiep-hoa-chu-trong-phat-trien-dan-bo-lai-sind.html#google_vignette.

Duong, N. K., Nguyen, Q. T., & Nguyen, T. H. (2019). Growth performance of beef crossbred calves in Ben Tre province. *Journal of Animal Science and Technology* 98, 33-40.

Hoang, K. G. (2024). Recent developments in beef and goat meat production and future development directions. In *Proceedings of The Conference on Effective and Sustainable Beef and Goat Meat Production (ILDEX Vietnam 2024)* (1-3). Ho Chi Minh City, Vietnam.

Hoang, M. Q., Le, D. P., & Nguyen, X. B. (2009). Current status and solutions for beef cattle farming in households with technological advancements in Quang Trach, Quang Binh. *Journal of Science, University of Hue* 52, 117-126.

Kim, Y. (2024). *Effectiveness of some livestock models in ethnic minority areas in Di Linh*. Retrieved July 29, 2024, from https://khuyennong.lamdong.gov.vn/thong-tin-nong-nghiep/chan-nuoi/3141-hi%E1%BB%87u-qu%E1%BA%A3-m%E1%BB%99t-s%E1%BB%91-m%C3%B4-h%C3%ACnh-ch%C4%83n-nu%C3%B4i-v%C3%B9ng-%C4%91%E1%BB%93ng-b%C3%A0o-d%C3%A2n-t%E1%BB%99c-thi%E1%BB%83u-s%E1%BB%91-t%E1%BA%A1i-di-linh.

La, V. T. (2024). Recent developments in beef and goat meat production and future development directions. In *Proceedings of The Conference on Effective and Sustainable Beef and Goat Meat Production (*3-29). Ho Chi Minh City, Vietnam.

Le, D. T., Le, V. N., Van, N. P., Tran, T. N., Hoang, H. T., Le, T. T. H., Tran, N. L., Duong, T. H., Vo, T. M. T., Le, T. H., & Dinh, V. D. (2021). Crossbred cattle production scale, herd structure and raising method of farmers in Quang Ngai province. In *Proceedings* of *National Conference on Animal Science and Veterinary Medicine* (608-613). Hue city, Vietnam: Hue University Publisher. Retrieved April 8, 2023, from https://csdlkhoahoc.hueuni.edu.vn/data/2023/5/74-NL5-avs23_QUY_MO_CO_CAU_DAN_BO_TAI_QUANG_NGAI.pdf.

Le, T. V. (2013). *Intensive beef cattle farming techniques in units*. Retrieved July 14, 2024, from https://web.archive.org/web/20131203172536/

http://www.qdnd.vn/qdndsite/vi-VN/61/43/319/324/324/256410/Default.aspx.

Ngo, T. K. C., Tran, Q. H., Mai, T. X., Bui, T. N. L., Le D. N., & Pham, T. H. (2022). Current status of beef livestock at households in Dak Lak province. *Journal of Animal Husbandry Sciences and Technics* 285, 61-68.

Nguyen, T. H., & Do, H. Di., (2020). Growth performance and disease resistancy of some groups of high-yielding beef calves in Ho Chi Minh City. *Journal of Animal Husbandry Sciences and Technics* 257, 80-86.

Nguyen, T. T., Pham, V. Q., Nguyen, V. T., Hoang, T. N., Bui, N. H., & Giang, V. S. (2021c). Current situation herbivorous livestock in Tien Giang. *Journal of Animal Science and Technology* 129, 38-48.

Nguyen, V. D., Nguyen, D. D, Nguyen, T. P., Nguyen, D. T., & Vu, D. T. (2021b). *Characteristics, productivity and efficiency of beef cattle farming in the central highlands.* Retrieved July 16, 2021, from https://nhachannuoi.vn/dac-diem-nang-suat-va-hieu-qua-chan-nuoi-bo-thit-vung-tay-nguyen/

Nguyen, V. L., Dinh, D. T., Tat, T. H., Nguyen, T. H., & Ngo, H. P. (2021a). Effects of ration formulation using the local agricultural by-products and the heating method on growth performance and heath of BBB crossbred beef cattle. *Journal of Animal Husbandry Sciences and Technics* 267, 41-47.

Pham, V. G., Giang, H. H., Nguyen, C. T., & Su, T. L. (2022). An assessment of actual situation of beef cattle production in Thua Thien Hue province. *Journal of Animal Science and Technology* 133, 69-79.

Pham, V. Q., Hoang, T. N., Nguyen, T. T., Nguyen, V. T., Giang, V. S., Bui, N. H., Le, V. B., Nguyen, M. T., & Pham, V. T. (2021d). Current situation of beef cattle production and beef cattle breeds in Tay Ninh province. *Journal of Animal Husbandry Sciences and Technics* 266, 34-39.

Pham, V. Q., Nguyen, T. T., Hoang, T. N., Nguyen., V. T., Giang, V., S., Bui, N.H., Nguyen, T. T, Nguyen, T. N. A', Ho, N. T., & Phuong, K. H. (2021b). Current Status of beef cattle farming and beef breed structure in Tay Ninh province. *Journal of Animal Husbandry Sciences and Technics* 271, 30-38.

Pham, V. Q., Nguyen, V. T., Giang, V. S, Hoang, A. D., Nguyen, M. C., H, T. N., Tran, Q. H., Nguyen, D. D., & Le N. T. (2021a). Current situation of beef cattle production in Dak Lak province. *Journal of Animal Husbandry Sciences and Technics* 269, 20-27.

Pham, V. Q., Nguyen, V. T., Giang, V. S., Hoang, T. N., Bui, N. H, Nguyen, T. T., Huynh, V. T., Nguyen, T. N. H, Tran, V. N., & Thach, T. H. (2021c). *Situation of beef crossbred on production and reproduction in Tra Vinh province*. Retrieved July 18, 2022, from https://hoichannuoi.vn/hien-trang-ve-chan-nuoi-va-sinh-san-cua-dan-bo-lai-huong-thit-tai-tinh-tra-vinh.html.

Pham, V. Q., Tran, T. C., Le, T. M. H., Giang, V. S., & Bui, N. H. (2018). Current situation of beef cattle production and beef cattle breeds in Tay Ninh province. *Journal of Animal Science and Technology* 86, 19-33.

Thuy, K. (2023). *Development of beef cattle farming in vietnam*. Retrieved December 14, 2023, from https://nguoichannuoi.vn/phat-trien-chan-nuoi-bo-thit-o-viet-nam/#:~:text=Theo%20%C4%91%C3%A1nh%20gi%C3%A1%20c%E1%BB%A7a%20B%E1%BB%99,n%E1%BB%81n%20kinh%20t%E1%BA%BF%20ph%C3%A1t%20tri%E1%BB%83n.

Thuy, L. (2020). *Good income from combining breeding and fattening cattle*. Retrieved July 14, 2023, from https://www.baosoctrang.org.vn/nong-nghiep/thu-nhap-tot-nho-nuoi-bo-sinh-san-ket-hop-bo-vo-beo-40117.html.

Tran, H. N., & Do, M. H. (2021). Assessment of changing to technical eficiency in the dairy farmers in Don Duong district, LD. *Journal of Forestry Science and Technology* 5, 166-174.

Van, V. (2024). *Restructuring agricultural production in Don Duong*. Retrieved February 02, 2024, from https://baolamdong.vn/kinh-te/202402/co-cau-lai-san-xuat-nong-nghiep-o-don-duong-3e328be/.

Biochemical composition of the mud crab *Scylla paramamosain* (Estampador, 1949) fatted under the recirculating water system

Quy M. Ong[1], Tu P. C. Nguyen[1*], Ha N. Nguyen [2,3], Minh V. Tran[1], & Thy T. T. Ho[1]

[1]Faculty of Fisheries, Nong Lam University, Ho Chi Minh City, Vietnam

[2]Research Institute for Biotechnology and Environment, Nong Lam University, Ho Chi Minh City, Vietnam

[3]Faculty of Biological Sciences, Nong Lam University, Ho Chi Minh City, Vietnam

ARTICLE INFO

Research Paper

Received: August 31, 2024
Revised: November 21, 2024
Accepted: November 22, 2024

Keywords

Biochemical compositions
Gender
Molting stage
Mud crab
Scylla paramamosain

***Corresponding author**

Nguyen Phuc Cam Tu
Email:
npctu@hcmuaf.edu.vn

ABSTRACT

The meat yield, biochemical compositions of muscles, and hepatopancreas of mud crab (*Scylla paramamosain*) fatted under a recirculating water system were compared concerning molting stages, gender, and kinds of fresh feed. In the postmolt stage, the juvenile crabs (100 - 200 g of body weight) were reared into the recirculating water system and fed with two kinds of fresh feed (bivalvia and tilapia meat). As the crab developed from the postmolt stage going to the intermolt and end at the premolt stage, it was harvested and analyzed for its biochemical components. The results showed that meat yield from the legs-claw muscle of male crabs was higher ($P < 0.05$) than that of females, and hepatopancreas of crabs in the premolt stage was also accumulated higher ($P < 0.05$) than that of crabs in the intermolt stage. In terms of molting stages, the moisture content of muscles and hepatopancreas of crabs in the premolt stage was lower ($P < 0.05$) than that of crabs in the intermolt stage. The Fe content of hepatopancreas was the same result too ($P < 0.05$). Conversely, other biochemical components such as protein and lipid contents of legs-claw and hepatopancreas, Mg content of body and legs-claw muscles, and K content of legs-claw and hepatopancreas of crab in the premolt stage were higher ($P < 0.05$) than those of crabs in the intermolt stage. For the gender aspects, lipid contents of body muscle and hepatopancreas, P content of the legs-claw and hepatopancreas, and K content of the legs-claw muscle were higher ($P < 0.05$) in females than in males. In comparison, the ash content of body muscle and the Fe content of hepatopancreas of male crabs were higher ($P < 0.05$) than those of females. Regarding feed, crabs fed by bivalvia meat accumulated ash in body muscle, Ca, Mg, and P contents in hepatopancreas higher than those of crabs feeding tilapia meat. The results illuminate the possibilities for both consumers and processors to correctly select the molting stages and gender to cater specifically to their requirements.

Cited as: Ong, Q. M., Nguyen, T. P. C., Nguyen, H. N., Tran, M. V., & Ho, T. T. T. (2024). Biochemical composition of the mud crab *Scylla paramamosain* (Estampador, 1949) fatted under the recirculating water system. *The Journal of Agriculture and Development* 23(Special issue 2), 98-109.

1. Introduction

The mud crab *Scylla* sp. is considered as one of the most popular and expensive seafood in Asian Countries, especially in South East Asian Countries (Parvathi & Padmavathi, 2020). In Vietnam, *Scylla paramamosain* is an important species cultured in the southern coast (Le Vay et al., 2001; Lindner, 2005). Recently, crabs have increased rapidly in demand due to their unique flavor and rich nutrition. Crab meat and hepatopancreas are not only rich in protein but also in minerals that are important for human body maintenance and development (Hosseini et al., 2014).

In nature, the crab growth has to undergo through the molting process. The molt cycle was divided into 4 major stages namely: the molt stage, postmolt stage, intermolt stage and premolt stage (Drach, 1939). The newly molt cycle starts from the molt stage, goes to postmolt, intermolt and end at the premolt stage. During the molting process, nutrients and minerals obtained from food and seawater are accumulated continuously to create muscle, hepatopancreas and their shell. Hence, their biochemical components vary complicatedly among period stages. In addition, meat yield and proximate composition of mud crabs were found differently in regards to different species, sizes, sexes, body parts, molt stage, season and capturing location (Parvathi & Padmavathi, 2020; Wang et al., 2021; Islam et al., 2022). The variation of the meat yield and biochemical composition would be affected by flavor and delicacy of consumers as well as the quality and value of products.

There were many studies reported on meat yield and biochemical composition of mud crabs, however, studies about the nutritional status of mud crab of *Scylla paramamosain* species concerning gender, molt stages and feed sources is limited. Thus, the primary objectives of the study were to quantify the meat and hepatopancreatic yield, and biochemical composition of fattening crabs relative to gender, molt stages and feed sources.

2. Materials and Methods

2.1. Source of mud crabs

Eighty juvenile male and female mud crabs (weight of 150 ± 50 g/crab) were collected from the extensive shrimp farm in the Ca Mau province, Vietnam (8°46'00"N; 105°01'40"E). These crabs were exactly selected in the postmolt stage following the description of Freeman & Perry (1985) and Drach (1939). All the crabs were transported quickly to Experimental farm for Aquaculture in Nong Lam University, Ho Chi Minh City, where the crabs were acclimated for three days before stocking into the Recirculating Water System (RWS) such as Figure 1. Plastic tubes of the RWS were divided into five private chambers with length x diameter (25 cm x 110 cm) by the bulkhead. Each crab was stocked individually in each chamber and arranged for genders and kinds of feeds. In Part A, twenty male crabs stocked in lines 1, 2, 3 and 4, and twenty female crabs stocked in lines 5, 6, 7 and 8 would be fed by tilapia meat. Similarly, the other male and female crabs were stocked in Part B and fed bivalvia meat. So, a 2 × 2 factorial experimental design with four various combinations of male or female crabs (gender factor) fed one of two kinds of feed (feed factor) was tested.

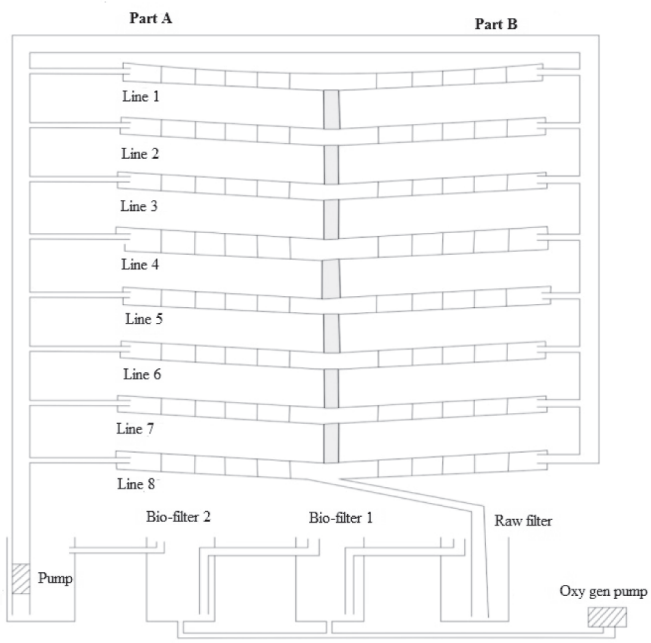

Figure 1. Diagram of the recirculating water system.

These crabs were fattened from the postmolt stage going to the intermolt stage and the end of the premolt stage. When these crabs developed into the intermolt stage, twenty-four crabs (including 6 males and 6 females fed tilapia meat and 6 males and 6 females fed bivalvia meat) were taken out, put individually crab in each plastic bag with the label and preserved in a freezer at -18 ± 2°C in the Research Institute Biotechnology and Environment for further dissection. The others would continue to rear until development into the premolt stage. When they developed into the premolt stage, they were also taken out of the RWS and preserved in the freezer at -18 ± 2°C for sample analysis. Checking and selecting the intermolt and premolt stages of crabs was based on the description of Freeman & Perry (1985) and Drach (1939).

2.2. Chemical analyses of the tissue from mud crab

At the laboratory, crabs were washed carefully with cool water. Whole-body weight of each crab was measured, and then body muscle, legs-claw muscle, and hepatopancreas were thoroughly separated by using a clean stainless steel scalpel blade. Meat and hepatopancreas removal were weighed and kept in a polyethylene bag, and immediately stored in a freezer at -18 ± 2°C for further biochemical composition analysis.

Three kinds of tissues: body muscle, legs-claw muscle, and hepatopancreas of male and female crabs from the intermolt and the premolt stages were subjected to the analyses of moisture, protein, lipid, fiber and ash contents according to TCVN 3700-90 (VS, 1990), TCVN 3705-90 (VS, 1990), TCVN 3703:2009 (VS, 2009), TCVN 4329:2007 (VS, 2007), and TCVN 5105:2009 (VS, 2009). Whereas minerals of these tissues were also determined by EDTA titrations (calcium-Ca, magnesium-Mg), photometric (phosphorous-P, iron-Fe) and flame photometric (potassium-K, sodium-Na) methods according to TCVN 12598:2018 (VS, 2018), TCVN 9516:2012 (VS, 2012), TCVN 8119:2009 (VS, 2009), and 9132:2011 (VS, 2011).

2.3. Statistical analysis

The data were checked for normality and homogeneity of variance. Data was subjected to three-way ANOVA and mean comparison was carried out using Tukey's test. A P-value < 0.05 was regarded as a statistically significant difference. A few indicators appeared interactions (interaction among two or three factors) but it was not much, so interactions among these factors would be ignored in the current study. All statistical analyses were conducted using the IBM SPSS Statistics for Windows, Version 22.0 (Armonk, NY: IBM Corp). All data were expressed as the mean ± standard deviation (SD).

3. Results

3.1. Meat yield of crab with regard to gender, molting stage and kinds of fresh feed

Meat yield (% of total body weight) from body muscle, legs-claw muscle, and hepatopancreas of fattening male and female mud crabs in the RWS is shown in Table 1. As for the body parts, meat yield from legs-claw muscle was the highest (15.22% - 20.67%) followed by body muscle (15.43% - 16.78%) and hepatopancreas (6.94% - 10.97%) (Table 1). Both fresh feeds (tilapia and bivalvia meat) used to fatten crabs were not affected ($P > 0.05$) by to meat yield of any body parts of the crab. Meat yield of the body and legs-claw muscle was also not significantly different between the intermolt and the premolt stage, whereas meat yield of the legs-claw muscle depended on gender ($P < 0.05$). The legs-claw muscles of male crabs had a high value compared to female crabs.

Gender and fresh feed used to fatten crabs did not influence ($P > 0.05$) hepatopancreas yield, however, the molting stage affected ($P < 0.05$) this yield. The Hepatopancreas yield of crabs in the premolt stage was higher than that of crabs in the intermolt stage.

Table 1. Meat yield (% of total body weight) from body muscle, legs-claw muscle, and hepatopancreas of male and female mud crabs

Tissue	Molting stages	Male Crab		Female Crab	
		Tilapia meat	Bivalvia meat	Tilapia meat	Bivalvia meat
Body muscle	Intermolt	15.43 ± 2.38	15.86 ± 1.43	15.73 ± 1.68	15.73 ± 1.68
	Premolt	16.72 ± 1.80	15.74 ± 2.04	15.56 ± 2.30	16.78 ± 1.58
Legs-claw muscle	Intermolt	[1]19.85 ± 1.26	[1]21.20 ± 2.26	[2]19.01 ± 2.31	[2]15.22 ± 1.91
	Premolt	[1]20.67 ± 1.65	[1]20.27 ± 2.03	[2]18.75 ± 2.03	[2]18.03 ± 1.93
Hepatopancreas	Intermolt[A]	7.01 ± 1.05	7.22 ± 1.44	8.60 ± 1.82	6.94 ± 1.32
	Premolt[B]	10.97 ± 3.28	7.92 ± 1.60	10.28 ± 2.79	10.32 ± 1.28

Significant differences were found between the intermolt and the premolt stages with different superscript capital letters ($P < 0.05$) in the molting stage column for each tissue.

Significant differences were also found between male and female for each tissue with different superscript numbers ($P < 0.05$) in the same row.

Significant differences were also found between crabs fed tilapia meat and those fed bivalvia meat for each tissue with different superscript letters ($P < 0.05$) in the same row.

No superscript (capital letters, letters and numbers) in the same row or column in the same section shows no significant difference ($P > 0.05$).

3.2. Biochemical composition

The biochemical composition of the body muscle of a fattening mud crab in the intermolt and the premolt stages is shown in Table 2. Protein, fiber, Ca, Fe, P, K and Na content of body muscle crab in the intermolt and the premolt stage was not significantly different ($P > 0.05$), regardless of gender and kinds of fresh feed. Conversely, the moisture and Mg content of crab in the intermolt and the premolt stage was significantly different ($P < 0.05$), regardless of gender and fresh feed. The moisture content of the crab in the intermolt stage was higher than that of the crab in the premolt stage, while the Mg content of the crab in the intermolt was lower than that of the crab in the premolt stage. Additionally, the lipid and ash content of body female and male crabs were significantly different ($P < 0.05$), regardless of the molting stage. The lipid content of female crabs was higher than that of male crabs, whereas the ash content of female crabs was lower than that of male crabs. Furthermore, the ash content of crab fed by tilapia meat was lower ($P < 0.05$) than that fed bivalvia meat, irrespective of gender and molting stage.

Table 2. Biochemical composition of body muscle of fattening mud crab between the intermolt and the premolt stages (% of wet weight)

Biochemical composition	Molting stages	Male Crab		Female Crab	
		Tilapia meat	Bivalvia meat	Tilapia meat	Bivalvia meat
Moisture (%)	Intermolt^{A}	81.69 ± 0.84	82.45 ± 1.72	81.10 ± 1.42	82.50 ± 1.42
	Premolt^{B}	79.89 ± 0.67	80.65 ± 0.06	78.85 ± 2.35	77.92 ± 2.55
Crude Protein	Intermolt	12.72 ± 1.34	12.10 ± 0.94	13.76 ± 1.34	12.50 ± 0.97
(%)	Premolt	14.40 ± 4.09	11.03 ± 0.89	14.86 ± 1.53	14.90 ± 1.36
Lipid (%)	Intermolt	^{1}8.09 ± 0.34	^{1}7.37 ± 1.76	^{2}8.74 ± 1.14	^{2}8.16 ± 1.11
	Premolt	^{1}7.37 ± 1.85	^{1}7.65 ± 0.80	^{2}9.10 ± 0.16	^{2}9.24 ± 0.31
Crude Fiber	Intermolt	0.59 ± 0.18	0.48 ± 0.17	0.61 ± 0.42	0.89 ± 0.08
(%)	Premolt	0.55 ± 0.07	0.73 ± 0.34	0.58 ± 0.27	0.66 ± 0.32
Ash (%)	Intermolt	^{1}2.27 ± 0.04^{a}	^{1}2.49 ± 0.24^{b}	^{2}2.15 ± 0.23^{a}	^{2}2.24 ± 0.09^{b}
	Premolt	^{1}2.18 ± 0.24^{a}	^{1}2.44 ± 0.13^{b}	^{2}1.90 ± 0.37^{a}	^{2}2.11 ± 0.13^{b}
Ca (mg/100g)	Intermolt	161.54 ± 18.99	212.16 ± 38.16	131.25 ± 27.26	156.26 ± 35.45
	Premolt	147.13 ± 32.12	138.80 ± 10.00	145.47 ± 13.79	155.70 ± 38.39
Mg (mg/100g)	Intermolt^{A}	32.92 ± 7.90	29.89 ± 5.42	39.41 ± 9.38	36.22 ± 12.39
	Premolt^{B}	40.80 ± 3.60	47.67 ± 5.31	37.26 ± 3.65	45.15 ± 8.61
Fe (mg/100g)	Intermolt	9.72 ± 0.99	8.83 ± 1.30	9.41 ± 1.06	9.18 ± 1.56
	Premolt	8.60 ± 1.43	9.78 ± 0.52	8.28 ± 1.89	7.86 ± 2.49
P (mg/100g)	Intermolt	126.12 ± 7.60	121.42 ± 23.40	183.85 ± 73.30	123.20 ± 8.76
	Premolt	207.63 ± 64.74	160.30 ± 49.98	125.17 ± 12.52	125.35 ± 34.74
K (mg/100g)	Intermolt	181.37 ± 7.98	176.22 ± 31.39	191.27 ± 22.53	158.79 ± 21.65
	Premolt	193.45 ± 49.31	157.23 ± 10.38	220.60 ± 43.90	204.23 ± 34.52
Na (mg/100g)	Intermolt	540.81 ± 34.69	513.63 ± 32.66	489.26 ± 30.32	548.96 ± 22.00
	Premolt	482.76 ± 80.73	584.91 ± 37.88	454.61 ± 73.83	472.84 ± 67.16

Significant differences were found between the intermolt and the premolt stages with different superscript capital letters ($P < 0.05$) in the molting stage column for each tissue.

Significant differences were also found between male and female for each tissue with different superscript numbers ($P < 0.05$) in the same row.

Significant differences were also found between crabs fed tilapia meat and those fed bivalvia meat for each tissue with different superscript letters ($P < 0.05$) in the same row.

No superscript (capital letters, letters and numbers) in the same row or column in the same section shows no significant difference ($P > 0.05$).

The biochemical composition of the legs-claw muscle of fattening mud crab in the intermolt and the premolt stages is shown in Table 3. Similarly, the Fiber, ash, Ca, Fe and Na content of the legs-claw muscle of crab in the intermolt and the premolt stage was not significantly different ($P > 0.05$), regardless of gender and kinds of fresh feed. Meanwhile, moisture, lipid and Mg content of the legs-claw muscle of crab in the intermolt and the premolt stage were different ($P < 0.05$), regardless of gender and fresh feed. The moisture content of the legs-claw of crab in the intermolt stage was higher ($P < 0.05$) than that of crab in the premolt stage, while lipid and Mg content of crab in the intermolt was lower ($P < 0.05$) than those of crab in the premolt stage. In addition, protein and K content of crab totally depended ($P < 0.05$) on molting stage and gender, regardless of fresh feed. Protein and K content of female crabs or crabs in the premolt stage were higher than those of male crabs or crabs in the intermolt stage. Moreover, the phosphor content of the legs-claw of female crabs was higher than that of male crabs, regardless of molting stage and fresh feed.

Table 3. Biochemical composition of the legs-claw muscle of fattening mud crab between the intermolt and the premolt stages (% of wet weight)

Biochemical composition	Molting stages	Male Crab		Female Crab	
		Tilapia meat	Bivalvia meat	Tilapia meat	Bivalvia meat
Moisture (%)	Intermolt^{A}	82.36 ± 0.39	82.32 ± 2.03	80.41 ± 1.54	81.82 ± 2.12
	Premolt^{B}	78.51 ± 2.20	80.62 ± 0.19	78.93 ± 1.70	76.98 ± 2.70
Crude Protein (%)	Intermolt^{A}	^{1}12.44 ± 0.67	^{1}12.21 ± 1.90	^{2}14.71 ± 1.04	^{2}13.42 ± 1.78
	Premolt^{B}	^{1}15.61 ± 2.34	^{1}11.72 ± 0.62	^{2}15.57 ± 1.30	^{2}15.88 ± 1.67
Lipid (%)	Intermolt^{A}	5.66 ± 1.87	4.93 ± 1.18	4.71 ± 0.45	4.60 ± 1.30
	Premolt^{B}	7.93 ± 1.01	7.48 ± 0.16	8.93 ± 1.43	8.94 ± 0.41
Crude Fiber (%)	Intermolt	0.79 ± 0.24	0.66 ± 0.09	0.27 ± 0.09	1.81 ± 0.79
	Premolt	0.82 ± 0.23	0.48 ± 0.19	0.82 ± 0.24	0.77 ± 0.13
Ash (%)	Intermolt	2.15 ± 0.05	2.29 ± 0.46	2.33 ± 0.34	2.28 ± 0.64
	Premolt	2.20 ± 0.32	2.55 ± 0.09	2.37 ± 0.02	2.26 ± 0.20
Ca (mg/100g)	Intermolt	161.94 ± 43.34	188.37 ± 69.74	167.04 ± 6.73	164.62 ± 29.35
	Premolt	207.50 ± 8.69	152.33 ± 26.63	186.10 ± 16.07	201.65 ± 47.49
Mg (mg/100g)	Intermolt^{A}	30.63 ± 8.73	63.86 ± 23.56	46.16 ± 8.02	58.29 ± 5.59
	Premolt^{B}	69.51 ± 19.57	70.13 ± 3.04	68.21 ± 16.77	50.42 ± 14.61
Fe (mg/100g)	Intermolt	9.21 ± 0.35	9.85 ± 0.96	8.37 ± 1.67	8.39 ± 1.60
	Premolt	8.22 ± 2.39	7.71 ± 1.26	9.79 ± 1.68	7.59 ± 0.93
P (mg/100g)	Intermolt	^{1}102.10 ± 6.71	^{1}102.62 ± 11.75	^{2}128.37 ± 14.10	^{2}115.20 ± 23.25
	Premolt	^{1}122.63 ± 33.11	^{1}96.96 ± 13.14	^{2}150.52 ± 39.13	^{2}122.36 ± 2.72
K (mg/100g)	Intermolt^{A}	^{1}165.85 ± 13.51	^{1}178.55 ± 17.36	^{2}199.72 ± 10.04	^{2}175.28 ± 21.54
	Premolt^{B}	^{1}203.89 ± 15.86	^{1}175.82 ± 17.22	^{2}196.23 ± 13.81	^{2}212.94 ± 19.16
Na (mg/100g)	Intermolt	514.05 ± 24.14	521.65 ± 85.98	539.36 ± 112.58	524.41 ± 79.34
	Premolt	493.42 ± 62.02	579.21 ± 22.28	506.18 ± 43.65	512.68 ± 86.87

Significant differences were found between the intermolt and the premolt stages with different superscript capital letters ($P < 0.05$) in the molting stage column for each tissue.

Significant differences were also found between male and female for each tissue with different superscript numbers ($P < 0.05$) in the same row.

Significant differences were also found between crabs fed tilapia meat and those fed bivalvia meat for each tissue with different superscript letters ($P < 0.05$) in the same row.

No superscript (capital letters, letters and numbers) in the same row or column in the same section shows no significant difference ($P > 0.05$).

The biochemical composition of the hepatopancreas of fattening mud crab in the intermolt and the premolt stages is shown in Table 4. Fiber, ash and Na content of hepatopancreas of crab in the intermolt and the premolt stage was not significantly different ($P > 0.05$), regardless of gender and kinds of fresh feed. On contrary, the moisture, protein and K content of hepatopancreas of crab in the intermolt and the premolt stage were different ($P < 0.05$), regardless of gender and fresh feed. The moisture content of crab in the intermolt stage was higher than that of crab in the premolt stage, while the protein and K content of crab in the intermolt was lower than those of crab in the premolt stage. Moreover, lipid and Fe content of hepatopancreas depended on ($P < 0.05$) gender and molting stage, regardless of fresh feed. The hepatopancreatic lipid and K content of crab in the intermolt stage were lower than those of crab in the premolt stage. Similarly, the hepatopancreatic lipid and K content of male crabs were lower than those of female crabs. In addition, regardless of gender and molting stage, the Ca and Mg content of the hepatopancreas of crabs were affected ($P < 0.05$) by fattening fresh feed. Crab fed bivalvia meat accumulated high amounts of Ca and Mg in the hepatopancreas as comparing with crab fed tilapia meat.

Table 4. Biochemical composition of the hepatopancreas of fattening mud crab between the intermolt and the premolt stages (% of wet weight)

Biochemical composition	Molting stages	Male Crab		Female Crab	
		Tilapia meat	Bivalvia meat	Tilapia meat	Bivalvia meat
Moisture (%)	Intermolt^{A}	81.81 ± 2.37	80.50 ± 6.03	77.20 ± 2.99	82.24 ± 4.72
	Premolt^{B}	76.08 ± 7.25	80.55 ± 0.43	72.66 ± 4.29	72.66 ± 1.98
Crude Protein (%)	Intermolt^{A}	6.81 ± 2.39	7.71 ± 1.39	8.61 ± 0.88	7.36 ± 1.75
	Premolt^{B}	10.31 ± 2.32	8.07 ± 0.26	11.36 ± 2.98	13.49 ± 4.87
Lipid (%)	Intermolt^{A}	^{1}7.41 ± 1.31	^{1}4.20 ± 1.90	^{2}6.25 ± 1.11	^{2}7.56 ± 1.81
	Premolt^{B}	^{1}6.69 ± 0.72	^{1}7.25 ± 1.46	^{2}8.93 ± 0.45	^{2}8.65 ± 1.54
Crude Fiber (%)	Intermolt	1.06 ± 0.29	0.54 ± 0.14	0.55 ± 0.47	1.12 ± 0.27
	Premolt	2.04 ± 0.90	0.86 ± 0.30	1.06 ± 0.67	0.50 ± 0.16
Ash (%)	Intermolt	2.82 ± 0.42	3.85 ± 0.87	3.19 ± 0.29	3.40 ± 0.96
	Premolt	3.23 ± 0.48	2.97 ± 0.48	3.18 ± 1.17	2.98 ± 1.17
Ca (mg/100g)	Intermolt	287.98 ± 57.50^{a}	406.85 ± 41.17^{b}	358.89 ± 33.85^{a}	425.48 ± 65.41^{b}
	Premolt	276.54 ± 61.64^{a}	309.64 ± 83.99^{b}	276.47 ± 82.14^{a}	414.16 ± 65.27^{b}
Mg (mg/100g)	Intermolt	39.87 ± 3.59^{a}	144.95 ± 43.86^{b}	75.15 ± 24.92^{a}	83.81 ± 45.21^{b}
	Premolt	83.21 ± 6.27^{a}	90.97 ± 17.81^{b}	66.77 ± 12.89^{a}	171.64 ± 14.73^{b}
Fe (mg/100g)	Intermolt^{A}	^{1}12.54 ± 0.33	^{1}14.70 ± 1.58	^{2}13.98 ± 1.63	^{2}12.05 ± 1.43
	Premolt^{B}	^{1}12.35 ± 0.35	^{1}11.92 ± 1.11	^{2}10.16 ± 2.28	^{2}10.62 ± 1.01
P (mg/100g)	Intermolt	^{1}142.62 ± 55.87^{a}	^{1}213.44 ± 16.45^{b}	^{2}226.91 ± 42.14^{a}	^{2}229.98 ± 38.74^{b}
	Premolt	^{1}160.52 ± 31.74^{a}	^{1}148.07 ± 50.18^{b}	^{2}152.17 ± 35.06^{a}	^{2}344.85 ± 47.56^{b}
K (mg/100g)	Intermolt^{A}	114.60 ± 11.96	133.39 ± 25.10	117.97 ± 16.88	109.96 ± 21.71
	Premolt^{B}	153.29 ± 8.64	128.42 ± 3.28	173.66 ± 56.95	163.37 ± 18.98
Na (mg/100g)	Intermolt	573.63 ± 3.04	585.35 ± 74.15	577.06 ± 54.59	606.93 ± 55.68
	Premolt	580.91 ± 116.27	629.97 ± 6.32	511.27 ± 89.86	488.53 ± 53.80

Significant differences were found between the intermolt and the premolt stages with different superscript capital letters ($P < 0.05$) in the molting stage column for each tissue.

Significant differences were also found between male and female for each tissue with different superscript numbers ($P < 0.05$) in the same row.

Significant differences were also found between crabs fed tilapia meat and those fed bivalvia meat for each tissue with different superscript letters ($P < 0.05$) in the same row.

No superscript (capital letters, letters and numbers) in the same row or column in the same section shows no significant difference ($P > 0.05$).

4. Discussion

The results of this study are consistent with the results of Sreelakshmi et al. (2016), legs-claw muscle of male crabs was higher than that of female crabs in both species of *S. serrata* and *S. tranquabarica*. However, this study result showed slightly higher value of meat yield than the finding of Sreelakshmi et al. (2016) with 16.8% of male and 11.43% of female crab of *S. serrata*, and 13.4% of male and 11.4% of female crab of *S. tranquebarica*. This variation might be linked to different species, feed, seasonal capture and environmental live. Moreover, the current study also found that the hepatopancreatic yield of crab accumulated in the premolt stage was higher than in the intermolt stage. It could be a result of fully accumulating nutrition and energy to readily prepare the molting for the next molt cycle.

The biochemical composition of crabs varies significantly with regard to gender, crab sources (Sarower et al., 2013), size and season (Bharathi et al., 2018), species (Parvathi & Padmavathi, 2020), body parts (Sreelakshmi et al., 2016) and feed sources (Olakiya & Kotiya, 2022). Moisture content is the major component of proximate composition (Islam et al., 2022). In the present study, the moisture content varied from 77.92% to 82.50% in body muscle, from 76.98% to 82.36% in legs-claw muscle and from 72.66% - 82.24% in the hepatopancreas of fattening crabs. This finding is consistent with early report that showed 75.30% - 81.30% in fattening crab and 76.90% - 78.20% in natural crab of *S. serrata* (Sarower et al., 2013), 78.51% - 83.85% in *S. serrata* and 78.60% - 82.40% in *S. tranquebarica* (Sreelakshmi et al., 2016), 78.20% - 79.50% in blue swimmer crab of *Portunus pelagicus* (Wu et al., 2010), 82.10% in snow crab of *Chionoecetes opilio* (Mizuta et al., 2001). The present study showed that the moisture content of all body parts and hepatopancreas of crab in the intermolt stage was higher than that in the premolt stage. It is in agreement with the results of Benjakul & Suthipan (2008) who reported a higher moisture content of body meat of soft shell (postmolt stage) compared to that of hard shell (intermolt stage) mud crab *S. serrata*. Similar results have been reported by Mizuta et al. (2001) in snow crab *Chionecetes opilio*. During the molt cycle, crab's growth is an increase in the dry weight of the body when tissue water is replaced by a protein inside its new shell (Havens & McConaugha, 1990).

For the protein content, the current study presented that protein content of body parts and hepatopancreas were 11.03% - 15.88% and 6.81% - 13.49%, respectively. More or less similar to the current result provided by previous studies, which ranged from 10.27% to 16.42% in *S. serrata* and from 11.19% to 17.63% in *S. tranquebarica* (Sreelakshmi et al., 2016) and from 18.02% to 22.14% in *S. olivacea* (Parvathi & Padmavathi, 2020). Furthermore, the current result found that the legs-claw protein content of female crabs was higher than that of male crabs. This observation is in agreement with that of Sreelakshmi et al. (2016) and Sarower et al. (2013) in *S. serrata*. In addition, the legs-claw and hepatopancreatic protein content of crab in the premolt stage was higher than that of crab in the intermolt stage, however, this information is limited in other such studies.

For the lipid content, this parameter presented significantly at both the molting stage and gender. Especially, the lipid content of female crabs in whole body parts was definitely higher than that of male crabs. It is in agreement with the results of Sarower et al. (2013), Sreelakshmi et al. (2016) and Islam et al. (2022). The lipid

content of crabs varied from 0.53% to 1.54% in *S. serrata* and 0.65% to 1.37% in *S. tranquebarica* (Sreelakshmi et al., 2016), from 5.3% to 6.9% in *S. serrata* (Bharathi et al., 2018) and 4.4% to 6.9% in the same species (Islam et al., 2022). It is a slightly lower value of lipid content than the present result. Variations in the lipid content of crabs might be due to sampling season, location, sexes and size (Sarower et al., 2013; Bharathi et al., 2018). Moreover, the lipid content of crab in the premolt stage was higher than that of crab in the intermolt stage. This finding was supported by Sudhakar et al. (2008) who reported that the lipid content of hard shell (intermolt stage) crab (*Portunus sanguinolentus*) was higher than that of soft shell (postmolt stage) crab.

In the present study, the ash content was only significantly different in body muscle. The ash content of male crabs was higher than that of female crabs. Similarly, the ash content of crabs fed bivalvia meat was higher than that of crabs fed tilapia meat. This result was supported by Islam et al. (2022) who showed the ash content of fattening male was higher than female. However, limited study supported for effect of diet on ash content. The ash content shown by a previous study was 4.2% - 4.9% (Islam et al., 2022) and 2.02% - 7.65% (Sarower et al., 2013) in fattening crab of *S. serrata*, 1.2% - 2.34% in natural crab of *S. serrata* (Zafar et al., 2004), 1.80% - 2.51% in natural crab of *S. serrata* and 1.60% - 2.63% in natural crab of *S. tranquebarica* (Sreelakshmi et al., 2016). Varied value might be linked to crab size, species to species, location and capturing season.

Macroelements and microelements are essential elements for several metabolic activities and biochemical processes as well as for human body development and maintenance (Barrento et al., 2009; Hosseini et al., 2014). In the present study, five macroelements (Na, K, Mg, Ca, and P) and one microelement (Fe) were determined in crab tissue and hepatopancreas. In there, three macroelements such as Ca, Mg and P content of hepatopancreas of crabs were affected by input feed source. These element contents in the crabs fed bivalvia meat were over the crabs fed tilapia meat. This may be because bivalvia meat contains appreciable amounts of mineral elements such as Ca, $CaCO_3$, Mg, K and P (Elegbede et al., 2023). Furthermore, the Mg content in all muscle parts and K content in both legs-claw muscle and hepatopancreas of crab in the premolt stage accumulated to be higher than those of crab in the intermolt stage. It limited study on the intermolt and the premolt stage of crabs to support for this result. Only one report by Sudhakar et al. (2009) stated the total contribution of minerals including calcium, sodium, potassium, zinc and magnesium in hard shell crab (*P. sanguinolentus*) over when compared to soft shell crab.

Another element such as Fe content showed a high level in the male crabs compared to the female crabs and the Fe of crab in the intermolt stage was higher than that of crab in the premolt stage. According to Benjakul & Sutthipan (2008) who showed the Fe content in the intermolt stage nearly doubled when compared to that in the postmolt stage. However, no study reported the Fe content of crab in the premolt stage.

Crab meat is rich in essential macroelements and microelements. Wang et al, (2021) showed that the Ca, Mg, Fe, P, K and Na in edible tissue of crab (*S. paramamosain*) were 47.8 - 59.9 mg/100 g, 25.2 - 35.5 mg/100 g, 1.6 - 3.0 mg/100 g, 191 - 226 mg/100 g, 277 - 358 mg/100 g and 138 - 310 mg/100 g, respectively, and in hepatopancreas were 111 - 341 mg/100 g, 33.3 - 74.6 mg/100 g,

3.9 - 11.2 mg/100 g, 327 - 679 mg/100 g, 240 - 517 mg/100 g and 211 - 492 mg/100 g, respectively. According to Benjakul & Sutthipan (2008), the Ca, Mg and Fe content of hard shell crab (*S. serrata*) legs were 69.9 mg/100 g, 40.6 mg/100 g and 1.3 mg/100 g, respectively, and crab claw was 64.4 mg/100 g, 41.8 mg/100 g and 1.0 mg/100 g, respectively. Similar reports were given by Islam et al. (2022) who showed that the Ca, Mg, Fe and P were 903 - 1199 mg/100 g, 22.6 - 29.5 mg/100 g, 12.6 - 14.2 mg/100 g and 46.5 - 56.9 mg/100 g, respectively, in fattening crab of *S. serrata*. The finding of minerals of tissue muscle and hepatopancreas in the present study is more or less similar to the results provided by Wang et al, (2021), Benjakul & Sutthipan (2008) and Islam et al. (2022) may be linked to different source, sexes, parts of body and molt stage.

5. Conclusions

This study shows that there exists a significant difference in the meat yield and biochemical compositions of mud crabs relative to the molting stage, gender and fattening fresh feed. Female crabs in the premolt stage had a higher value of meat and nutrition than male crabs in the intermolt stage. The crabs fattened by bivalvia meat accumulated a higher level of mineral content than crabs fattened by tilapia meat. This information supports the valuable knowledge to consumers who have more choices of select good crab sources in the market. Further studies are required to analyse on the amino acid profile to give full knowledge to consumers.

Conflict of interest

The authors have no conflict of interest to declare.

Acknowledgements

This research was financially supported by the Nong Lam University Ho Chi Minh City research funding (the research code: CS-CB23-TS-02).

References

Barrento, S., Marques, A., Teixeira, B., Anacleto, P., Carvalho, M. L., Vaz-Pires, P., & Nunes, M. L. (2009). Macro and trace elements in two populations of brown crab *Cancer pagurus*: ecological and human health implications. *Journal of Food Composition and Analysis* 22(1), 65-71. http://dx.doi.org/10.1016/j.jfca.2008.07.010.

Benjakul, S., & Sutthipan, N. (2008). Comparative study on chemical composition, thermal properties and microstructure between the muscle of hard shell and soft shell mud crabs. *Food Chemistry* 112(3), 627-633. https://doi:10.1016/j.foodchem.2008.06.019.

Bharathi, V. T., Chakravarty, M. S., & Ganesh, P. (2018). Biochemical composition of the of mud crab *Scylla serrata* (Forskal) of Coringa mangroves, Andhra Pradesh, India. *International Journal of Advanced Science and Research* 3(1), 11-15.

Drach, P. (1939). Mue et cycle d'intermue chez les Crustaces Decapodes. *Annales De L Insitut Oceanocraphique* 19, 103-391.

Elegbede, I., Lawal-Are, A., Favour, O., Jolaosho, T., & Goussanou, A. (2023). Chemical compositions of bivalves shells: *Anadara senilis*, *Crassostrea gasar*, and *Mytilus edulis* and their potential for a sustainable circular economy. *SN Applied Sciences* 5(1), 44. https://doi.org/10.1007/s42452-022-05267-7.

Freeman, J. A., & Perry, H. M. (1985). The crustacean molt cycle and hormonal regulation: its importance in soft shell blue crab production. In Perry, H. M., & Malone, R. F. (Eds.). *Proceedings of National Symposium on The Soft-*

Shelled Blue Crab Fisheries (20-30). Mississippi, USA: National Oceanic and Atmospheric Administration - NOAA.

Havens, K. J., & McConaugha, J. R. (1990). Molting in the mature female blue crab, "*Callinectes sapidus*" Rathbun. *Bulletin of Marine Science* 46, 37-47.

Hosseini, H., Mahmoudzadeh, M., Rezaei, M., Mahmoudzadeh, L., Khaksar, R., Khosroshahi, N. K., & Babakhani, A. (2014). Effect of different cooking methods on minerals, vitamins and nutritional quality indices of kutum roach (*Rutilus frisii kutum*). *Food Chemistry* 148C(3-5), 86-91. https://doi.org/10.1016/j.foodchem.2013.10.012.

Islam, T., Saha, D., Bhowmik, S., Nordin, N., Islam, S., Nur, A. A. U., & Begum, M. (2022). Nutritional properties of wild and fattening mud crab (*Scylla serrata*) in the south-eastern district of Bangladesh. *Heliyon* 8(6), e09696. https://doi.org/10.1016/j.heliyon.2022.e09696.

Le Vay, L., Vu, U. N., & Jones, D. A. (2001). Seasonal abundance and recruitment in an estuarine population of mud crabs, *Scylla paramamosain*, in the Mekong Delta, Vietnam. *Hydrobiologia* 449, 231-239. https://doi.org/10.1023/A:1017511002066.

Lindner, B. (2005). *Impacts of mud crab hatchery technology in Vietnam* (Impact Assessment Series Report No. 36). Canberra, Australia: Australian Centre for International Agricultural Research - ACIAR.

Mizuta, S., Kobayashi, Y., & Yoshinaka, R. (2001). Chemical and histological characterization of raw muscle from soft and hard crabs of snow crab *Chionoecetes opilio*. *Journal of Food Science* 66(2), 238-241. https://doi.org/10.1111/j.1365-2621.2001.tb11324.x.

Olakiya, V. V., & Kotiya A. S. (2022). Effect of different dietary protein level on growth of mud crab *Scylla serrata* (Forsskal, 1755) reared in bamboo baskets in brackish water pond in Saurashtra of Gujarat state. *Biological Forum - An International Journal* 14(4), 88-100.

Parvathi, D., & Padmavathi, P. (2020). Proximate composition of mud crabs *Scylla serrata* and *Scylla olivacea* from the coast of Visakhapatnam, Andhra Pradesh, India. *Bulletin of Environment, Pharmacology and Life Science* 10(1), 22-24.

Sarower, M. G., Bilkis, S., Rauf, M. A., Khanom, M., & Islam, M. S. (2013). Comparative biochemical composition of natural and fattened mud crab *Scylla serrata*. *Journal of Scientific Research* 5(3), 545-553. http://dx.doi.org/10.3329/jsr.v5i3.14082.

Sreelakshmi, K. R., Manjusha, L., Vartak, V. R., & Venkateshwarlu, G. (2016). Variation in proximate composition and fatty acid profiles of mud crab meat with regard to sex and body parts. *Indian Journal of Fisheries* 63(2), 147-150. https://doi:10.21077/ijf.2016.63.2.34511-23.

Sudhakar, M., Manivannan, K., & Soundrapandian, P. (2009). Nutritive value of hard and soft shell crabs of *Portunus sanguinolentus* (Herbst). *International Journal of Animal and Veterinary Advances* 1(2), 44-48.

VS (Vietnam Standards). (2018). Standard No. TCVN 12598:2018 dated on December 28, 2018. Fertilizers - Determination of total calcium and magnesium content by volumetric method. Retrieved on June 16, 2023, from https://tieuchuan.vsqi.gov.vn/tieuchuan/view?sohieu=TCVN+12598%3A2018.

VS (Vietnam Standards). (2012). Standard No. TCVN 9516:2012 dated on December 27, 2012. Foodstuffs - Determination of phosphorus content - Spectrophotometric method. Retrieved on June 16, 2023, from https://tieuchuan.vsqi.gov.vn/tieuchuan/view?sohieu=TCVN+9516%3A2012.

VS (Vietnam Standards). (2011). Standard No. TCVN 9132:2011 dated on December 30, 2011. Animal feeding stuffs - Determination of potassium and sodium contents - Methods using flame

- Emission spectrometry. Retrieved on May 20, 2023, from https://tieuchuan.vsqi.gov.vn/tieuchuan/view?sohieu=TCVN+9132%3A2011.

VS (Vietnam Standards). (2009). Standard No. TCVN 3703:2009 dated on December 31, 2009. Fish and fishery products - Determination of fat content. Retrieved on May 20, 2023, from https://tieuchuan.vsqi.gov.vn/tieuchuan/view?sohieu=TCVN+3703%3A2009.

VS (Vietnam Standards). (2009). Standard No. TCVN 5105:2009 dated on December 31, 2009. Fish and fishery products - Determination of ash content. Retrieved on May 20, 2023, from https://tieuchuan.vsqi.gov.vn/tieuchuan/view?sohieu=TCVN+5105%3A2009.

VS (Vietnam Standards). (2009). Standard No. TCVN 8119:2009 dated on October 28, 2009. Fruits, vegetables and derived products - Determination of iron content - 1,10-phenanthroline photometric method. Retrieved on May 20, 2023, from https://tieuchuan.vsqi.gov.vn/tieuchuan/view?sohieu=TCVN+8119%3A2009.

VS (Vietnam Standards). (2007). Standard No. TCVN 4329:2007 dated on May 08, 2007. Animal feeding stuffs - Determination of crude fibre content - Method with intermediate filtration. Retrieved on April 18, 2023, from https://tieuchuan.vsqi.gov.vn/tieuchuan/view?sohieu=TCVN+4329%3A2007.

VS (Vietnam Standards). (1990). Standard No. TCVN 3700:1990 dated on November 30, 1990. Aquatic products - Method for the determination of moisture content. Retrieved on April 18, 2023, from https://tieuchuan.vsqi.gov.vn/tieuchuan/view?sohieu=TCVN+3700%3A1990.

VS (Vietnam Standards). (1990). Standard No. TCVN 3705:1990 dated on November 30, 1990. Aquatic products - Method for determination of total nitrogen and protein contents. Retrieved on April 18, 2023, from https://tieuchuan.vsqi.gov.vn/tieuchuan/view?sohieu=TCVN+3705%3A1990.

Wang, F. T., He, J., Jiang, S. T., Lin, L., & Lu, J. F. (2021). Comparison of nutritional quality and nutrient compositions of three edible tissues from different sourced cultured female mud crabs (*Scylla paramamosain*). *Journal of Food Composition and Analysis* 104, 104163. https://doi.org/10.1016/j.jfca.2021.104163.

Wu, X. G., Zhou, B., Cheng, Y. X., Zeng, C. S., Wang, C. L., & Feng, L. (2010). Comparison of gender differences in biochemical composition and nutritional value of various edible parts of the blue swimmer crab. *Journal of Food Composition and Analysis* 23(2), 154-159. https://doi:10.1016/j.jfca.2009.08.007.

Zafar, M., Siddiqui, M. Z. H., & Hoque, M. A. (2004). Biochemical Composition in *Scylla serrata* (Forskal) of Chakaria Sundarbanarea, Bangladesh. *Pakistan Journal of Biological Sciences* 7(12), 2182-2186. https://doi.org/10.3923/pjbs.2004.2182.2186.

Construction of multiplex RT-PCR to determine the expression of ZO-1, Claudin-1, and Occludin genes in pig's intestine

Nhu T. Q. Nguyen[1], Tram T. Q. Le[1], Nguyen V. Dang[1], Mi M. T. Nguyen[1], Trang T. Dong[2], Thieu Q. Nguyen[2], & Phat X. Dinh[1*]

[1]Faculty of Biological Sciences, Nong Lam University, Ho Chi Minh City, Vietnam

[2]Faculty of Animal Science and Veterinary Medicine, Nong Lam University, Ho Chi Minh City, Vietnam

ARTICLE INFO

Research Paper

Received: August 31, 2024
Revised: November 18, 2024
Accepted: November 20, 2024

Keywords

Claudin-1
mRT-PCR
Occludin
pig
ZO-1

***Corresponding author**

Dinh Xuan Phat
Email:
dinhxuanphat@hcmuaf.edu.vn

ABSTRACT

Tight junction (TJ) proteins play a critical function in forming a strong intestinal barrier that protects against ingested pathogens and harmful agents. This study aimed to utilize multiplex RT-PCR (mRT-PCR) to assess the expression of ZO-1, Claudin-1, and Occludin genes at mRNA level in the intestines of pigs using specific primer pairs yielding amplicons of 167 bp, 500 bp, and 235 bp, respectively. The mRT-PCR protocol was optimized for annealing temperature and primer concentrations, including primer specificity, and determining the limit of detection. Subsequently, the optimized mRT-PCR was applied to detect these genes in 48 pig intestinal samples, including duodenum, jejunum and ileum. The mRT-PCR demonstrated specificity for these genes with the annealing temperature at 58°C. The primer pair ratio for ZO-1, Claudin-1, and Occludin was 0.4 µM:0.4 µM:0.4 µM (2:2:2). The detection rate for ZO-1, Claudin-1, and Occludin genes were 83.33% (40/48), 29.17% (14/48) and 4.17% (2/48) respectively. Intriguingly, one sample tested positive for all three mRNA, while negative results were observed in 12.5% of the samples. In conclusion, in the present study, the mRT-PCR was successfully established to detect ZO-1, Claudin-1, and Occludin expression in pig intestinal tissues.

Cited as: Nguyen, N. T. Q., Le, T. T. Q., Dang, N. V., Nguyen, M. M. T., Dong, T. T., Nguyen, T. Q., & Dinh, P. X. (2024). Construction of multiplex RT-PCR to determine the expression of ZO-1, Claudin-1, and Occludin genes in pig's intestine. *The Journal of Agriculture and Development* 23(Special issue 2), 110 -118.

1. Introduction

The intestinal mucosa is crucial for protecting the intestinal epithelium by preventing toxic substances and pathogens from entering the body. It consists of three layers: the mucosal epithelium, connective tissue, and muscle. The mucosa regulates nutrient intake, absorbs molecules, and maintains mucus thickness while eliminating toxins. However, when the intestinal barrier is compromised, it can lead to bacterial translocation, increased disease susceptibility, and impaired nutrient absorption, which negatively impacts pigs' health and the pig's industry (Wijtten et al., 2011).

The ZO-1 gene encoded the ZO-1 protein, a peripheral membrane protein with a mass of 210 to 225 kDa that is a scaffolding protein that links transmembrane proteins such as claudin and occludin to the cytoskeleton, playing a crucial role in strengthening junctions and maintaining intestinal barrier integrity (González-Mariscal et al., 2000). ZO-1 was vital for the structural integrity of the intestinal epithelium. Changes in ZO-1 activity can weaken tight junctions, leading to increased intestinal permeability, known as "leakage" which can result in conditions like enteritis (Sheth et al., 2000). The Occludin gene encodes the occludin protein, which is essential for tight junctions in epithelial and endothelial cells, with a molecular weight of 60 - 65 kDa (Otani & Furuse, 2020). Occludin consists of two extracellular and two intracellular (transmembrane) domains that regulate tight junction stability (González-Mariscal et al., 2000). Occludin directly interacts with the zonula occludin proteins ZO-1, ZO-2, and ZO-3, which are vital for the stability of the junction complex. The first half of occludin binds to ZO-1, helping maintain epithelial cell polarity necessary for optimal intestinal function and nutrient transport. Occludin indirectly interacts with the actin cytoskeleton and junctional adhesion molecule (JAM) via the ZO protein (Sheth et al., 2000). Claudin-1 gene was discovered in 1998 by Mikio Furuse and Shoichiro Tsukita in Japan through a cDNA library screening aimed at identifying unknown tight junction (TJ) components (Furuse et al., 1998). Claudin-1 is a transmembrane protein weighing 20 - 27 kDa, featuring four transmembrane domains and creating an "electrostatic filter" that regulates the movement of ions and enhances intercellular adhesion, crucial for the barrier function of skin and epithelial tissues (Anderson & Van Itallie, 2009). Although claudins share structural similarities with occludin, they lack sequence homology (Shin et al., 2006).

In this study, an mRT-PCR was constructed to detect the expression at mRNA level of these genes in intestinal samples. This process involves two reactions: reverse transcription of the target mRNA molecules into cDNAs, followed by PCR to amplify the cDNAs. In this study, an mRT-PCR was constructed to detect the expression of ZO-1, Claudin-1, and Occludin gene at mRNA level from pig intestine samples to support for the further diagnostic conditions.

2. Materials and Methods

2.1. Primers for multiplex RT-PCR

Primer pair detecting ZO-1, Occludin and Claudin-1 (167 bp, 235 bp, and 500 bp, respectively) were obtained from published documents with minor modification and shown in Table 1. The primers were checked by Primer3Plus and NCBI Blast Primer tools and synthesized by IDT (Integrated DNA Technologies).

Table 1. Primers were used in this study

Gene	Sequence 5' - 3'	Length	Amplicons	References
ZO-1	F: GGATGGTCACACCGTG	16	167 bp	(Liu et al., 2017)
	R: GGAGGATGCTGTTGTCTC	18		
Claudin-1	F: AAGATTTACTCCTACGCTGGT	21	500 bp	(Zhang et al., 2018)
	R: CTTGGTGTTGGGTAAGATG	19		
Occludin	F: ACGAGCTGGAGGAAGACTGGATC	17	235 bp	(Luo et al., 2017)
	R: TGAGCCGTACATAGATCCAGAAGC	23		

2.2. Field samples and control samples

Forty-eight pig's intestinal samples, comprising 16 duodenum, 16 jejunum colon, and 16 ileum samples, were obtained from pig farms in Dong Nai and Binh Duong Provinces. The KT-Biotech Accutive pDNA/RNA Prep Kit was used to extract mRNA according to manufacturer's recommendation, then mRNA was kept at -20°C for further use.

Positive control was selected by choosing the field samples positive for all three mRNAs of ZO-1, Claudin-1 and Occludin by mRT-PCR and confirmed by sequencing method. Our positive control showed sequence identities up to 99.40%, 95.61%, and 100%, respectively when compared to Accession number AJ318101.1, NM_001161635.1, and NM_001163647.2.

2.3. Two-step mRT-PCR

cDNA was synthesized by RevertAid First Strand cDNA Synthesis Kit (#K1622, Thermo Scientific) and kept at -20°C for later uses.

Each mRT-PCR reaction contained 12.5 µL of DreamTaq Green PCR Master Mix (Cat# K1081, Thermo Scientific), primer mix with an initial concentration of 20 µM, cDNA of 3 µL and DEPC (Cat# K1081, Thermo Scientific) - treated water added to a total volume of 25 µL. The thermal cycling was pre-denaturation at 95°C for 5 min followed by 35 cycles of denaturation at 95°C for 30 sec, annealing temperature 95°C for 30 sec, extension at 72°C for 40 sec and final extension at 72°C for 7 min. Next, amplification products were analyzed by electrophoresis on a 1.2% (w/v) agarose gel in 0.5X Tris-Acetate-EDTA (TAE) buffer (Cat#B49, ThermoFisher) containing Midori Green Advance DNA dye (Cat#MG04, Nippon Genetics). 1Kb plus DNA labeling (Cat#10787018, Invitrogen) was added to each DNA gel to indicate PCR product size and analyzed by UV transillumination.

2.4. Optimization of the primer concentration for the mRT-PCR assay

In order to optimize primer concentration of mRT-PCR, different primer concentrations for the three genes were tested, including ZO-1:Claudin-1:Occludin at 1:1:1 (0.2 µM:0.2 µM:0.2 µM); 1:2:1 (0.2 µM:0.4 µM:0.2 µM); 1:2:2 (0.2 µM:0.4 µM:0.4 µM); 2:2:2 (0.4 µM:0.4 µM:0.4 µM), 2:3:2 (0.4 µM:0.6 µM:0.4 µM), 2:4:2 (0.4 µM:0.8 µM:0.4 µM). Amplification results analyzed on agarose gel figured out the optimal concentration.

2.5. Evaluation of the specificity of the mRT-PCR assay

The specificity of primers used in the study were first checked through reliable information sites such as NCBI-BLAST and Insilico tool. Furthermore, the specificity of the primers was experimented with DNA extracted from unrelated microorganism such as *Salmonella, E. coli, Clostridium perfringens, Staphylococcus* spp., and ASF virus.

2.6. Determination of the detection limit of the mRT- PCR assay

Pure PCR products of each gene were recovered from low-melting agarose gel using the TopPURE ® Tissue Viral Extraction kit and the DNA concentration of each gene was adjusted to 1 ng/µL by diluting with TE buffer (1X). Subsequently, of the mixed samples was diluted in a 10-fold series from 1 ng/µL to 10^{-9} ng/µL. The lowest concentration produced visual band on an agarose gel would be considered as the limit of detection (LOD) of the mRT-PCR assay.

2.7. Application of the established mRT-PCR assay on field samples

The optimized mRT-PCR was applied on 48 intestine samples. The detection rate for each gene expression was determined to calculate the applicability of the assay.

3. Results

3.1. Optimal conditions of two-step mRT-PCR

To make sure the primer pairs function well, single RT-PCR was conducted at temperatures ranging from 56°C to 62°C for the ZO-1, Claudin-1, and Occludin genes, which have target sizes of 167 bp, 500 bp, and 235 bp, respectively. Electrophoresis demonstrated that the primers successfully amplified the expected mRNA at all tested temperatures: 56°C, 58°C, 60°C, and 62°C (Figure 1A-C). Among these, 58°C yielded the best amplification for all three genes and thus this temperature was used in mRT-PCR (Figure 1D). Later on, 58°C was selected as the optimized annealing temperature for the mRT-PCR assay.

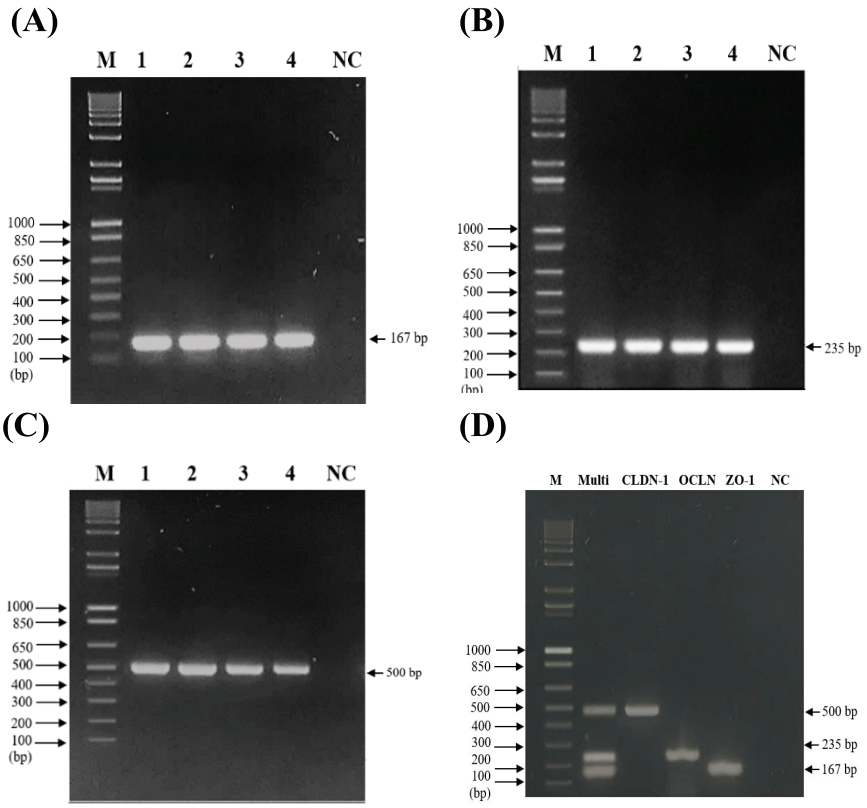

Figure 1. Results of investigation of optimal annealing temperature. A. The sRT-PCR detected ZO-1 gene (167 bp); B. The sRT-PCR detected Occludin (235 bp); C. The sRT-PCR detected Claudin-1 (500 bp); D. The mRT-PCR detection ZO-1, Claudin-1, and Occludin genes at 58°C. Lane M: DNA ladder 1 Kb plus; Lane 1: 56°C, Lane 2: 58°C, Lane 3: 60°C, and Lane 4: 62°C. Lane NC: negative control with nuclease-free water.

Next, the primer concentration of mRT-PCR was optimized. Figure 2 showed that the amplification effectiveness varies significantly when primers concentrations changed. The concentration ratio of 2:2:2 (0.4 µM:0.4 µM: 0.4 µM) in lane 4 produced equal and bright bands and was chosen as the concentration for subsequent reactions.

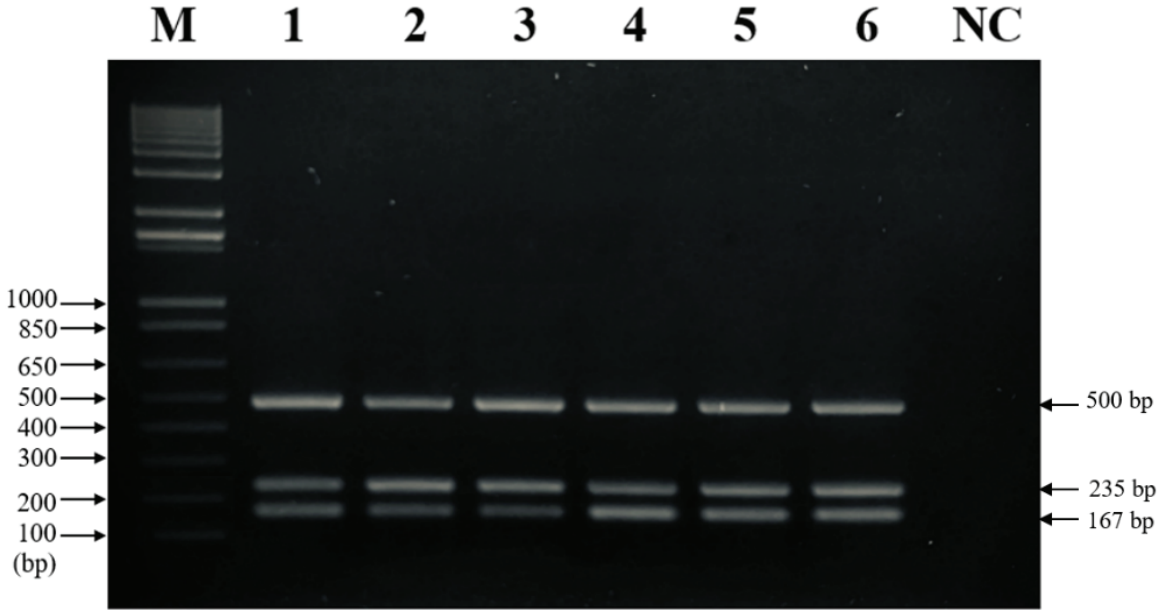

Figure 2. Electrophoresis results of optimizing of the primer concentration ratio of Claudin-1 (500 bp), Occludin (235 bp) and ZO-1 (167 bp). Lane M: 1 Kb Plus DNA marker, Lane 1: 1:1:1 (0.2 µM:0.2 µM:0.2 µM), Lane 2: 1:2:1 (0.2 µM:0.4 µM:0.2 µM), Lane 3: 1:2:2 (0.2 µM:0.4 µM:0.4 µM), Lane 4: 2:2:2 (0.4 µM:0.4 µM:0.4 µM), Lane 5: 2:3:2 (0.4 µM:0.6 µM:0.4 µM), Lane 6: 2:4:2 (0.4 µM:0.8 µM:0.4 µM); Lane NC: negative control with nuclease-free water.

3.2. Specificity and limit of detection of two-step mRT-PCR

To confirm the ability of accurate amplification of the primers in mRT-PCR, different DNA/RNA from unrelated bacteria and virus that are commonly found in environment and potentially contaminate the samples were used, including *Salmonella*, *E. coli*, *Clostridium*, *Staphylococcus* spp., African Swine Fever (ASF) virus. DNA from ducks and chickens were also added to the check list. Figure 3 confirmed that the positive control mRT-PCR reaction produced the expected bands at the correct sizes, while there was no amplification occurring for the unrelated DNA/RNA template (Figure 3). This result demonstrated that the mRT-PCR specifically detected ZO-1, Claudin-1, and Occludin mRNA and the primer pairs did not bind nonspecifically onto some common microorganism investigated.

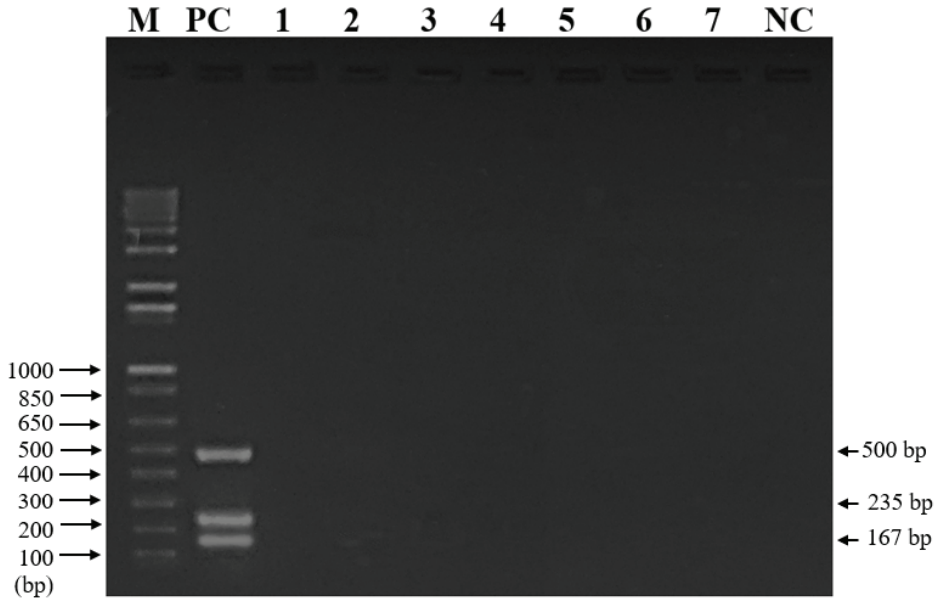

Figure 3. Electrophoresis results of testing the specificity of the mRT-PCR. Lane M: Ladder 1 Kb plus DNA, Lane PC: Positive control, Lane 1: *Salmonella*; Lane 2: *E. coli*, Lane 3: *Clostridium*; Lane 4: *Staphylococcus spp*, Lane 5: Chicken intestines; Lane 6: duck intestines, Lane 7: ASF; Lane NC: negative control with nuclease-free water.

To examine the detection limit of the mRT-PCR, the assay was investigated using template at various concentration, up to 10^{-9} ng/ µL. Figure 4 illustrated that the mRT-PCR could detect all the three target mRNA simultaneously in lane 6, corresponding to the concentration of 10^{-4} ng/ µL. The experiment was reproducible in triplicate which indicating that the detection limit of the mRT-PCR was 10^{-4} ng/ µL per reaction for each target mRNA.

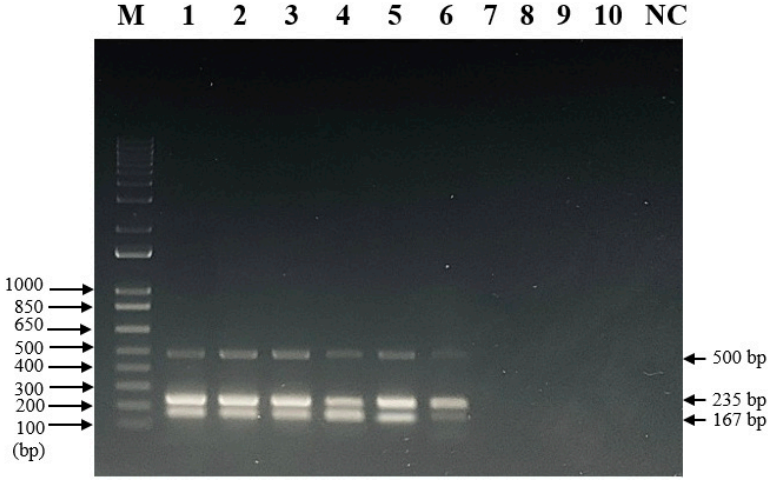

Figure 4. Determining the detection limit of mRT- PCR. Lane M: Ladder 1 Kb plus DNA, Lane 1: 1 ng/µL, Lane 2: 10^{-1} ng/µL, Lane 3: 10^{-2} ng/µL, Lane 4: 10^{-3} ng/µL, Lane 5: 10^{-4} ng/µL, Lane 6: 10^{-5} ng/µL, Lane 7: 10^{-6} ng/µL, Lane 8: 10^{-7} ng/µL, Lane 9: 10^{-8} ng/µL, Lane 10: 10^{-9} ng/µL, Lane NC: negative control with nuclease-free water.

3.3. Application of the optimized mRT-PCR assay to pigs intestinal samples

The optimized mRT-PCR was used to investigate 48 pig intestine samples (16 duodenum, 16 colons, and 16 ileum samples) collected pig farms in Dong Nai and Binh Duong Provinces to determine the expression of ZO-1, Claudin-1, and Occludin genes. Results showed that the positive rate of ZO-1 mRNA in the duodenum was 81.25% (13/16), jejunum was 75% (12/16) and ileum was 93.75% (15/16). For Occludin, its mRNA was detected in 12.5% (2/16) of ileum but not detected in duodenum and jejunum (0/16). For Claudin-1, its mRNA was found in 25% (4/16) of the duodenum, in 43.75% (7/16) of jejunum and 18.75% (3/16) of ileum. The positive rates of each mRNA in the total number of samples were 83.33% (40/48), 4.17% (2/48) and 29.17% (14/48), respectively for ZO-1, Occludin and Claudin-1. Table 2 shows that the positive rate of the ZO-1 gene was higher than that of Claudin-1 and Occludin genes in all three locations: duodenum, jejunum, and ileum. Furthermore, there was one sample positive for all three genes, accounting for 2.08% and the negative rate for all three genes was 12.5% (6/48). Therefore, the mRT-PCR reaction could be used to determine the presence of these genes in field samples (Figure 5).

Table 2. Detection rate of the three gene expression

Sample type	Number of samples	ZO-1 mRNA n (%)	Claudin-1 mRNA n (%)	Occludin mRNA n (%)
Duodenum	16	13 (81.25)	4 (25)	0 (0.00)
Jejunum	16	12 (75)	7 (43.75)	0 (0.00)
Ileum	16	15 (93.75)	3 (18.75)	2 (12.5)
Total	48	40 (83.33)	14 (29.17)	2 (4.17)

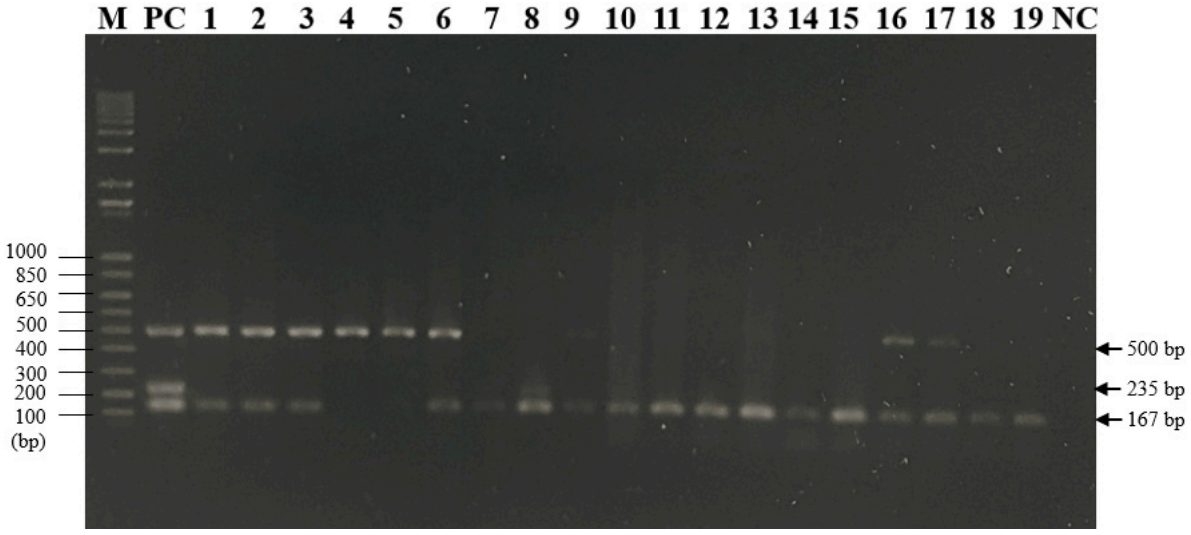

Figure 5. Detection of ZO-1, Claudin-1, and Occludin mRNA in intestinal samples. Lane 1-16: T1.1TT - T2.2TT; Lane 17 - 19: T2.2KT - T2.3TT; M: Ladder 1kb plus DNA, PC: Positive control, Lane NC: negative control with nuclease-free water.

3.4. Sequencing analysis

To evaluate the accuracy of the primer's pairs, the amplified product was sequenced. The sequencing results were analyzed on the BioEdit 7.2 and NCBI blast.

The amplicon of ZO-1 gene (sample T2.4HT) was 167 nucleotides and shared 99.40% similarity to the reference sequence AJ318101.1. Similarly, 500 nucleotides of Claudin-1 shared 95.61% identity with the reference sequence NM_001161635.1. Lastly, PCR product of Occludin gene showed 100% similarity at nucleotide level to the reference sequence NM_001163647.2.

4. Discussion

Tight Junction (TJ) family members like ZO-1, Claudin-1, and Occludin are vital in maintaining the intestinal barrier's integrity and protecting the body against pathogen invasion. Determining the expression of these gene can help evaluate the strength of the intestinal mucosa in different nutritional conditions or stress situation in animals.

In this study, we effectively established a Multiplex RT-PCR technique for simultaneously detecting the expression of ZO-1, Claudin-1, and Occludin genes in pig's intestinal tissue. The ZO-1 gene had the highest detection rate (83.33%), followed by the Claudin-1 and Occludin genes at 29.17% and 4.17%, respectively. In contrast, Dong et al. (2019) demonstrated that normally Occludin was expressed more than ZO-1, but when the pigs were fed with ZnO in the diet, the expression of ZO-1 was upregulated compared to Occludin. It indicated that the detectivity of these genes is dependent on the host's physiological conditions and the nutritional status. Unfortunately, in our study, due to lacking of the information about the nutritional condition, it was unable to figure out why ZO-1 was the most expressed in the samples.

In addition, the expression of these genes also depends on the location in the intestine. For example, the highest detection rate of the ZO-1 mRNA was in ileum (93.75%), while Occludin mRNA was barely detected in the duodenum and ileum. Other research revealed that Occludin level in pig intestinal cells was particularly susceptible to downregulation during stress conditions (Wu et al., 2020). These findings further highlight the expression of these three genes depends on various factors such as nutrition, stress, environmental conditions as well as physiological status of the animals.

5. Conclusions

The multiplex RT-PCR reaction was successfully optimized to determine the expression of ZO-1, Claudin-1 and Occludin at mRNA level in pig intestine. Optimal primer concentration ratio was 2:2:2 (0.4 µM:0.4 µM:0.4 µM). mRT-PCR functions well at annealing temperature of 58°C, and its detection limit was 10^{-4} ng/µL. The sequencing results of PCR amplification products for the ZO-1, Claudin-1 and Occludin genes confirmed the accuracy and reliability of the mRT-PCR for application in the field samples.

Conflict of interest

The authors have no conflict of interest related to this publication.

Acknowledgements

The author would like to express their deep gratitude to Nong Lam University, Ho Chi Minh City, Vietnam for funding this study.

References

Anderson, J. M., & Van Itallie, C. M. (2009). Physiology and function of the tight junction. *Cold Spring Harbor Perspectives in Biology* 1(2), a002584.

Dong, Y. X., Xu, Q. Q., Wang, C., Zou, T. X., & Lu, J. J. (2019). Supplemental-coated zinc oxide relieves diarrhoea by decreasing intestinal permeability in weanling pigs. *Journal of Applied Animal Research* 47(1), 362-368. https://doi.org/10.1080/09712119.2019.1645673.

Furuse, M., Fujita, K., Hiiragi, T., Fujimoto, K., & Tsukita, S. (1998). Claudin-1 and-2: Novel integral membrane proteins localizing at tight junctions with no sequence similarity to occludin. *The Journal of Cell Biology* 141(7), 1539. https://doi.org/10.1083%2Fjcb.141.7.1539.

González-Mariscal, L., Betanzos, A., & Ávila-Flores, A. (2000). MAGUK proteins: Structure and role in the tight junction. *Seminars in Cell and Developmental Biology* 11(4), 315-324. https://doi.org/10.1006/scdb.2000.0178.

Liu, H. W., Mi, M. S., Ruan, Z., Li, J., Shu, G. X., Yao, K., Jiang, M., & Deng, Y. Z. (2017). Dietary tryptophan enhanced the expression of tight junction protein ZO-1 in intestine. *Journal of Food Science* 82(2), 562-567. https://doi.org/10.1111/1750-3841.13603.

Luo, L. X., Guo, J. L., Zhang, J., Xu, F. Y., Gu, H. W., Feng, L., & Wang, Y. (2017). Tight junction protein occludin is a porcine epidemic diarrhea virus entry factor. *Journal of Virology* 91(10), e00202-17. https://doi.org/10.1128/jvi.00202-17.

Otani, T., & Furuse, M. (2020). Tight junction structure and function revisited. *Trends in Cell Biology* 30(10), 805-817. https://doi.org/10.1016/j.tcb.2020.08.004.

Sheth, B., Fontaine, J. J., Ponza, E., McCallum, A., Page, A., Citi, S., Louvard, D., Zahraoui, A., & Fleming, T. P. (2000). Differentiation of the epithelial apical junctional complex during mouse preimplantation development: A role for rab13 in the early maturation of the tight junction. *Mechanisms of Development* 97(1-2), 93-104. https://doi.org/10.1016/S0925-4773(00)00416-0.

Shin, K., Fogg, V. C., & Margolis, B. (2006). Tight junctions and cell polarity. *Annual Review of Cell and Developmental Biology* 22(1), 207-235. https://doi.org/10.1146/annurev.cellbio.22.010305.104219.

Wijtten, P. J. A., van der Meulen, J., & Verstegen, M. W. A. (2011). Intestinal barrier function and absorption in pigs after weaning: A review. *British Journal of Nutrition* 105(7), 967-981. https://doi.org/10.1017/S0007114510005660.

Wu, T. J., He, M. C., Bu, J., Luo, Y., Yang, Y. S., Ye, Y. C., Yu, L. S., He, S. B., Yin, L. Y., & Yang, P. X. (2020). Betaine attenuates LPS-induced downregulation of Occludin and Claudin-1 and restores intestinal barrier function. *BMC Veterinary Research* 16(1), 75. https://doi.org/10.1186/s12917-020-02298-3.

Zhang, X. M., Huang, Y., Zhang, K., Qu, L. H., Cong, X., Su, J. Z., Wu, L. L., Yu, G. Y., & Zhang, Y. (2018). Expression patterns of tight junction proteins in porcine major salivary glands: A comparison study with human and murine glands. *Journal of Anatomy* 233(2), 167-176. https://doi.org/10.1111/joa.12833.

Detection of tomato mosaic virus infecting tomato using realtime RT-PCR

Quyen N. D. Cao[1], Toan Q. Truong[2], & Biet V. Huynh[1,2*]

[1]Faculty of Biological Sciences, Nong Lam University, Ho Chi Minh City, Vietnam

[2]Research Institute for Biotechnology and Environment, Nong Lam University, Ho Chi Minh City, Vietnam

ARTICLE INFO

Research Paper

Received: August 31, 2024
Revised: November 02, 2024
Accepted: November 22, 2024

Keywords

Escherichia coli JM109
Realtime RT-PCR
RNA virus
Tomato mosaic virus

***Corresponding author**

Huynh Van Biet
Email: hvbiet@hcmuaf.edu.vn

ABSTRACT

Tomato mosaic virus (ToMV) is known as one of the most common and devastating tomato viruses worldwide. It causes mosaic disease, which significantly impacts the productivity and quality of tomatoes in Vietnam. Early and accurate detection of ToMV in tomatoes is essential for effective disease control. This study developed a detection and quantification procedure for ToMV based on realtime RT-PCR. In this study, a positive control carrying ToMV's target gene segment was amplified to a size of 595 bp, then cloned into pJET1.2 vector and transformed into *Escherichia coli* JM109. A realtime RT-PCR procedure was established using designed primers to amplify a 182 bp gene segment of the RdRP-ORF2 gene region. A calibration curve was created with the equation y = -3.777x + 41.973, resulting in a correlation coefficient (R^2) of 0.9939, which was used to quantify the ToMV virus. Additionally, the procedure quantified test samples with viral loads ranging from 1.7 x 10^4 to 9.5 x 10^6 copies/µL

Cited as: Cao, Q. N. D., Truong, T. Q., & Huynh, B. V. (2024). Detection of tomato mosaic virus infecting tomato using realtime RT-PCR. *The Journal of Agriculture and Development* 23(Special issue 2), 119-130.

1. Introduction

According to data from the Food and Agriculture Organization (FAO, 2022) approximately 189 million tons of tomatoes were produced worldwide in 2021. In Vietnam, tomatoes have been cultivated for over 100 years, with significant growth in various regions across the country. In 2011, the tomato cultivation area reached 23,083 ha, with an average yield of 25.55 tons per ha, resulting in a total output of 589.83 thousand tons. However, tomato diseases pose major challenges to production in Vietnam and globally. Tomato viral diseases, in particular, cause substantial damage to plants, leading to symptoms such as curled leaves, deformed flowers, leaf drop, and small, malformed fruits with poor quality. The tomato mosaic virus (ToMV) and tomato mottle mosaic virus (ToMMV) are among the most prevalent and significant viruses affecting tomato plants (Hanssen et al., 2010). The ToMV is found in tomato-growing regions worldwide and damages most commercial tomato varieties in the field,

with potential yield reductions of up to 25%. It is notable for its high survival rate outside plant cells and in dead tissues (Lanter et al., 1982). The virus's capacity for rapid spread complicates early disease detection and exacerbates the impact on crop productivity and quality. Currently, there is no effective treatment for ToMV, and management relies on controlling the source of infection and developing resistant varieties (Dhaliwal et al., 2019). Rapid and accurate diagnosis of ToMV is crucial for effective disease surveillance and management strategies to minimize damage to tomato crops. Various diagnostic methods are available, including symptom observation, electron microscopy, ELISA, RT-PCR, and realtime RT-PCR. While symptom-based diagnosis is quick and generally accurate, it can lead to confusion, particularly when distinguishing between diseases with similar external symptoms caused by different pathogens. Microscopic diagnosis is commonly used for viruses that form characteristic intracellular inclusions (Varma & Singh, 2020). However, viruses in host cells may exist in amorphous crystalline forms, making them difficult to observe. The ELISA is a straightforward and user-friendly method but often has low sensitivity and can be time-consuming (Hu et al., 1993). Reverse transcription (RT)-PCR has been widely employed to diagnose many plant diseases; while conventional PCR can detect plant pathogens, the advent of realtime PCR has enhanced the ability to identify and quantify them (Varma & Singh, 2020). Realtime RT-PCR demonstrates significantly higher specificity and sensitivity compared to traditional ELISA or RT-PCR methods (Kogovsek et al., 2008; Bertolini et al., 2010).

In this study, the realtime RT-PCR method was employed to develop an assay for the early and accurate diagnosis of ToMV disease in tomatoes. This approach aimed to support the management of viral diseases in tomato crops and facilitate research on the development of virus-resistant tomato varieties in Vietnam.

2. Materials and Methods

2.1. Materials

Tomato leaf samples suspected of being infected with the ToMV virus were collected from tomato gardens in Duc Trong district, Lam Dong province, Vietnam. The positive control for ToMV was provided by the Research Institute for Biotechnology and Environment at Nong Lam University in Ho Chi Minh City. The *E. coli* JM109 bacterial strain was used for gene cloning.

2.2. Methods

2.2.1. Sample collection method

Sampling methods were carried out in accordance with TCVN 9016:2011 (VS, 2011). Tomato leaf samples were collected diagonally to ensure inclusion of leaves exhibiting symptoms of ToMV disease, such as curled leaves, deformed flowers, and small, malformed fruits, in Duc Trong district, Lam Dong province, Vietnam.

2.2.2. Extracting viral RNA

Total RNA was extracted from 50 mg of leaf sample using the EZ-10 Spin Column Plant RNA Miniprep Kit (Biobasic), following the manufacturer's protocol. A volume of 1 µL of the extracted total RNA was used to determine the concentration (ng/µL) and assess RNA purity using a spectrophotometer (Biodrop, UK).

2.2.3. Synthesis of cDNA

cDNA was synthesized from RNA according to the manufacturer's protocol of the SensiFAST™

cDNA Synthesis Kit. The incubation steps were carried out using a thermal cycler (GeneAmp® PCR System 9700). The thermal cycling conditions for the reaction included denaturation at 25°C for 10 min, reverse transcription at 42°C for 15 min, incubation at 48°C for 15 min, and final denaturation at 85°C for 5 min.

2.2.4. PCR amplification of the target gene of ToMV

The 595 bp gene fragment was amplified using the primer pair ToMV-F (5'-AAGATGTCAAACCAACTTA-3') and ToMV-R(5'-GAAACATCCAACTCAAGTACG-3') (Sui et al., 2017). The reaction was conducted in a total volume of 50 µL, comprising 25 µL of MyTaq Mix (2X), 20 µL of nuclease-free water, 1 µL (20 µM) of each forward and reverse primer, and 3 µL of the DNA sample. The thermal cycling conditions included 1 cycle at 95°C for 5 min; followed by 35 cycles of 95°C for 30 sec, 60°C for 30 sec, and 72°C for 40 sec; and a final extension at 72°C for 7 min. The amplification products were analyzed by electrophoresis on a 1.5% agarose gel for 30 min at 100 V.

The amplified gene segment was sent for sequencing to Nam Khoa Trading and Service Company Limited in Ho Chi Minh City. The sequencing results will be compared with virus sequences available in the NCBI GenBank database to assess their similarity and confirm the presence of the ToMV virus.

2.2.5. Creating a bacterial strain carrying the target gene segment of the ToMV virus

The target gene fragment, after amplification by PCR, was inserted into the pJET1.2 vector following the manufacturer's protocol of the CloneJET Cloning Kit (Thermo). The resulting vector was transformed into *E. coli* JM109 bacteria using the heat shock transformation method. The transformed *E. coli* JM109 cell solution was spread on a petri dish containing LB medium supplemented with 50 mg/L ampicillin and cultured overnight at 37°C. Colonies that grew on the antibiotic medium were then checked by colony PCR using the primers pJET1.2-F (5'-CGACTCACTATAGGGAGAGCGGC-3') and pJET1.2-R (5'-AAGAACATCGATTTTCCATGGCAG-3').

2.2.6. Extraction and purification of recombinant plasmid

Colonies containing the recombinant vector were grown in 5 mL of LB medium (supplemented with ampicillin) at 37°C for 16 h. Plasmid DNA was extracted and purified following the manufacturer's protocol of the TopPURE® Plasmid DNA Extraction Kit (ABT, Vietnam). The purity and concentration (ng/µL) of the plasmid DNA samples were determined using a spectrophotometer (BioDrop, UK). The presence of the target gene on the plasmid was confirmed by PCR using the primer pair p-JET1.2 F/R. The amplified product was analyzed by electrophoresis on a 1.5% agarose gel for 30 min at 100 V. Plasmid DNA samples were subsequently sequenced at Nam Khoa Trading and Service Company Limited (Ho Chi Minh City). The sequencing results were compared with the pre-cloning sequence and with virus sequences published on GenBank (NCBI).

2.2.7. Designing specific primer pairs for virus detection using realtime RT-PCR method

Primers used for realtime RT-PCR to detect ToMV virus were designed using Primer3 software to amplify a 182 bp gene segment. The forward primer was ToMVDQ-F (5-ACCAGAGTTGTCCGGAGTAG-3'), and the reverse was ToMVDQ-R (5-CGGCCAACTGACCAATTGTG-3').

The sequence of primers was checked for the non-specific binding in NCBI Primer Blast tool. This primer pair had a high specificity to only pair with ToMV (Figure 1).

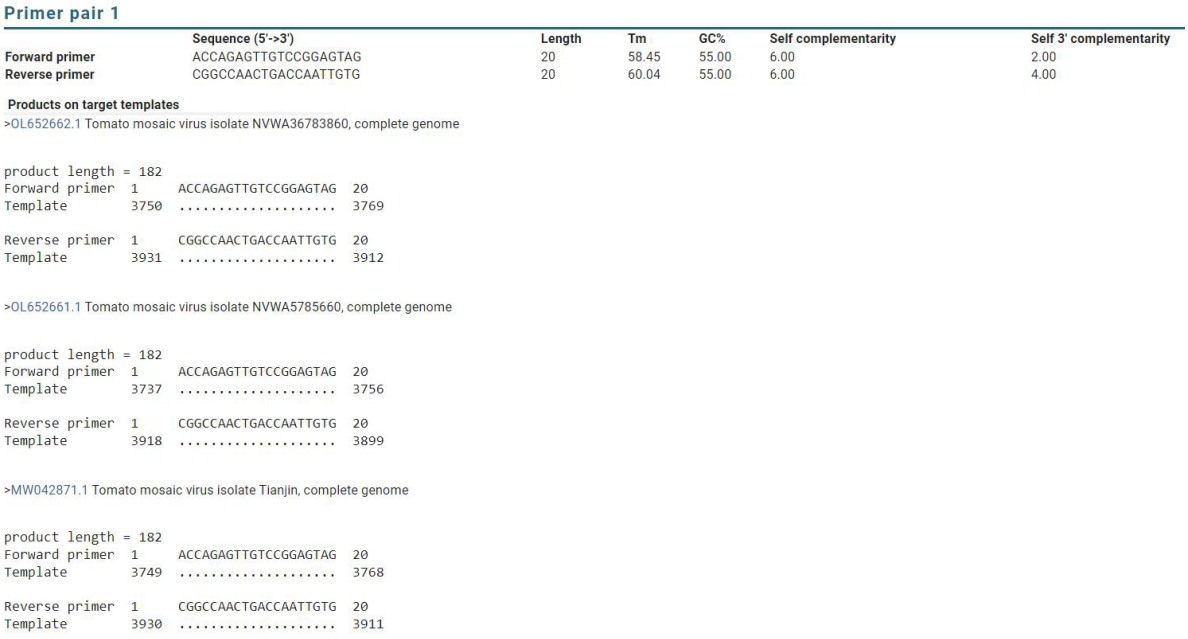

Primer pair 1

	Sequence (5'->3')	Length	Tm	GC%	Self complementarity	Self 3' complementarity
Forward primer	ACCAGAGTTGTCCGGAGTAG	20	58.45	55.00	6.00	2.00
Reverse primer	CGGCCAACTGACCAATTGTG	20	60.04	55.00	6.00	4.00

Products on target templates

>OL652662.1 Tomato mosaic virus isolate NVWA36783860, complete genome

```
product length = 182
Forward primer  1     ACCAGAGTTGTCCGGAGTAG  20
Template        3750  ....................  3769

Reverse primer  1     CGGCCAACTGACCAATTGTG  20
Template        3931  ....................  3912
```

>OL652661.1 Tomato mosaic virus isolate NVWA5785660, complete genome

```
product length = 182
Forward primer  1     ACCAGAGTTGTCCGGAGTAG  20
Template        3737  ....................  3756

Reverse primer  1     CGGCCAACTGACCAATTGTG  20
Template        3918  ....................  3899
```

>MW042871.1 Tomato mosaic virus isolate Tianjin, complete genome

```
product length = 182
Forward primer  1     ACCAGAGTTGTCCGGAGTAG  20
Template        3749  ....................  3768

Reverse primer  1     CGGCCAACTGACCAATTGTG  20
Template        3930  ....................  3911
```

Figure 1. The result of the primer was compared to the target sequences by using Primer Blast tool on NCBI Genbank.

2.2.8. Setting up realtime RT-PCR reaction

The realtime RT-PCR reaction was performed with standard samples on an Applied Biosystems® 7500 Realtime PCR machine, following the manufacturer's protocol for the SensiFAST™ SYBR® Lo-ROX Kit. The reaction components included 10 µL of 2x SensiFAST SYBR® Lo-ROX Mix (2X), 0.8 µL (10 µM) of each forward and reverse primer, 2 µL of DNA sample, and 6.4 µL of nuclease-free water. The thermal cycling conditions consisted of 1 cycle at 95°C for 2 min, followed by 40 cycles of 95°C for 5 sec, 60°C for 10 sec, and 72°C for 35 sec.

2.2.9. Generation of a standard curve

The number of copies of plasmid DNA was calculated according to the formula (Staroscik, 2004):

$$\text{Number of copies} = \frac{6{,}022 \times 10^{23} \times C}{650 \times 10^{9} \times L}$$

In there:

C: mass of plasmid sample (ng)

L: plasmid length (bp)

The plasmid DNA sample was diluted with nuclease-free water. Ten-fold serial dilutions from 10^7 to 10^3 copies of the recombinant plasmid were prepared using nuclease-free water and used as templates. Realtime PCR reactions were performed on standard samples with concentrations ranging from 10^7 to 10^3 copies/µL. The standard curve was constructed based on the threshold cycle (Ct) values and the corresponding log values (number of copies) of the standard samples. The equation of the standard curve is given by:

$$Y = aX + b$$

Where Y represents the Ct value, X represents the log of the copy number, a is the slope, and b is the y-intercept.

2.2.10. Evaluation of the specificity of the RT-PCR

The cDNA of other Tobamovirus including TMV (Tobacco mosaic virus), ToMMV (Tomato mottle mosaic virus), and ToBRFV (Tomato brown rugose fruit virus) were tested with ToMV primer to verify the specificity of the RT-PCR assay.

2.2.11. Diagnosis of ToMV in field samples using the newly established realtime RT-PCR process

The realtime RT-PCR procedure was employed to detect and quantify the infection levels in field samples. Following the reaction, the copy number of ToMV in the infected samples was determined by substituting the threshold cycle values into the standard curve equation for each gene.

3. Results and Discussion

3.1. Amplifying the target gene segment of the virus

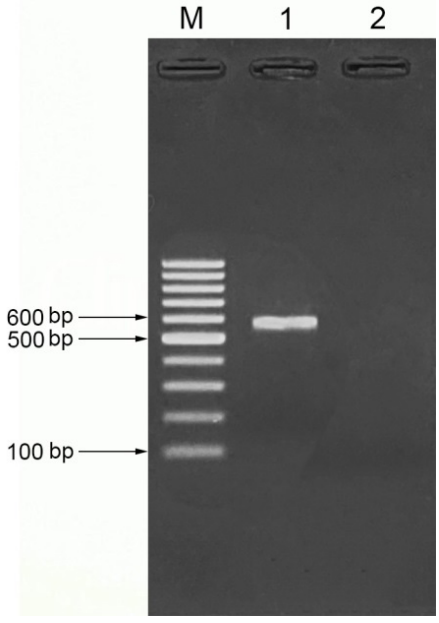

Figure 2. Electrophoresis results of PCR product of target gene segment of Tomato mosaic virus (ToMV) with primer pair ToMV-F/ToMV-R. DNA ladder (M), positive control (well 1), negative control (well 2).

The PCR reaction yielded a DNA band at nearly 600 bp, indicating successful amplification of the expected 595 bp gene segment of ToMV (well 1, Figure 2). This result confirms that the PCR reaction effectively amplified a gene segment of the anticipated size. To verify that the amplified sequences correspond to viral gene sequences, the DNA segment obtained from the amplification reaction was sequenced.

Comparison of the sequence with entries in NCBI GenBank revealed that the amplified gene segment shares 98.99% similarity with the published gene sequence MH393623.1 (Bae et al., 2019). This confirms that the PCR reaction developed in this study successfully amplified the correct gene segment of the ToMV virus.

3.2. Create clones and check the sequence of the amplified gene segment

Figure 3. Colony of *E. coli* bacteria after being transformed with a vector carrying the tomato mosaic virus (ToMV) gene.

The successfully cloned product resulted in white colonies on LB medium supplemented with 50 mg/L ampicillin (Figure 3). This outcome indicates that the target gene segment was inserted into the pJET1.2 vector, and the transformation process into *E. coli* was successful. The transformed bacterial strains are able to grow and form colonies on ampicillin-containing media because the pJET1.2 vector carries an ampicillin resistance gene. Additionally, the negative selection gene eco47IR helps eliminate strains containing self-ligated vectors.

To confirm the presence of the correct target gene, the colonies were tested by PCR using the primer pair pJET1.2. Theoretically, the expected amplification product size was approximately 713 bp. The results showed a DNA band of about 713 bp, positioned near the 700 bp marker, consistent with expectations (Figure 4). Therefore, it can be initially confirmed that the vector containing the target gene segment has been successfully transformed into the bacteria.

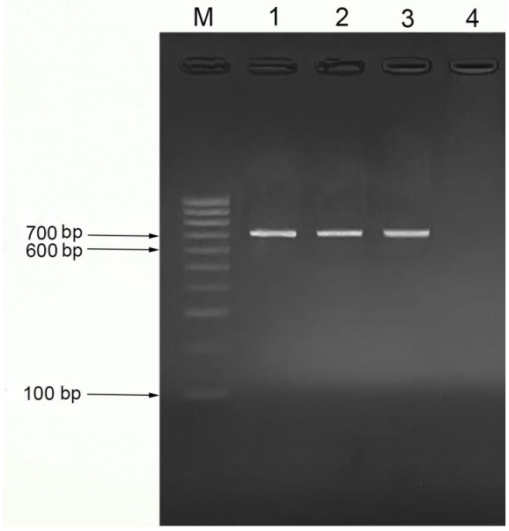

Figure 4. Electrophoresis results of PCR products of suspected colonies with primer pair PJET1.2. DNA ladder (M), Colony sample (wells 1-3), negative control (well 4).

3.3. Extraction and purification of recombinant plasmid DNA

The results of electrophoresis of the extracted and purified total plasmid DNA revealed a DNA band at 3687 bp, corresponding to the combined length of the vector and the target gene (Figure 5). This indicates that the plasmid sample was successfully inserted into the bacteria.

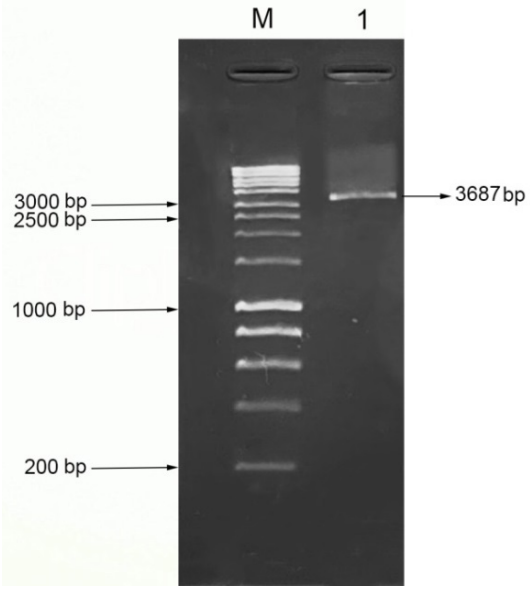

Figure 5. Electrophoresis results of total plasmid DNA of purified plasmid sample. DNA ladder (M), purified plasmid DNA sample (well 1).

The electrophoresis results of PCR products from the purified plasmid samples, using the primer pair PJET 1.2, showed a DNA band of approximately 713 bp, which is close to the expected size of 700 bp (Figure 6). However, to confirm the accuracy of this result, sequencing of the target gene segment inserted into the plasmid is necessary.

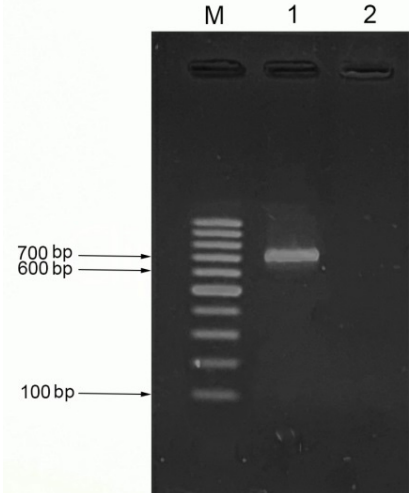

Figure 6. Electrophoresis results of PCR products of purified plasmid DNA samples with primer pair PJET1.2. DNA ladder (M), plasmid sample (well 1), negative control (well 2).

The comparison of the obtained sequence with NCBI GenBank revealed that the sequence of the amplified gene segment was 100% identical to the original gene segment before it was inserted into the plasmid. Additionally, it showed 98.99% similarity to the ToMV virus gene sequence with accession number MH393623.1 (Bae et al., 2019). This confirms that the gene segment inserted into the plasmid is indeed the ToMV viral gene segment and can be effectively used to detect the presence of the virus in tomato samples.

3.4. Generation of a standard curve

Table 1. Ct values of the realtime RT-PCR amplification reaction for the plasmid samples

Sample (copies/µL)	Log of copies number	Threshold cycle (Ct) (Mean ± SD)	Coefficient of Variation (%)
10^7	7	15.37 ± 0.28	1.79
10^6	6	19.27 ± 0.29	1.49
10^5	5	23.32 ± 0.34	1.44
10^4	4	27.15 ± 0.31	1.15
10^3	3	30.32 ± 0.74	2.42
(-)	0	_	_

_: Not detected; (-): Negative control.

Plasmid DNA samples with concentrations of 10^7, 10^6, 10^5, 10^4, and 10^3 copies were successfully amplified, as shown by the amplification chart (Figure 8) and the melting curve (Figure 9). The threshold cycle values (Ct) were obtained after performing the realtime RT-PCR reaction with samples at different concentrations, each repeated three times (Table 1). The standard curve equation is expressed as y = -3.777x + 41.973 with a correlation coefficient of R^2 = 0.9939 (Figure 7). The slope of the standard curve was 3.777 deducing the efficiency of the Realtime PCR reaction was 84%. The reaction efficiency was low but still acceptable with a value greater than 80%.

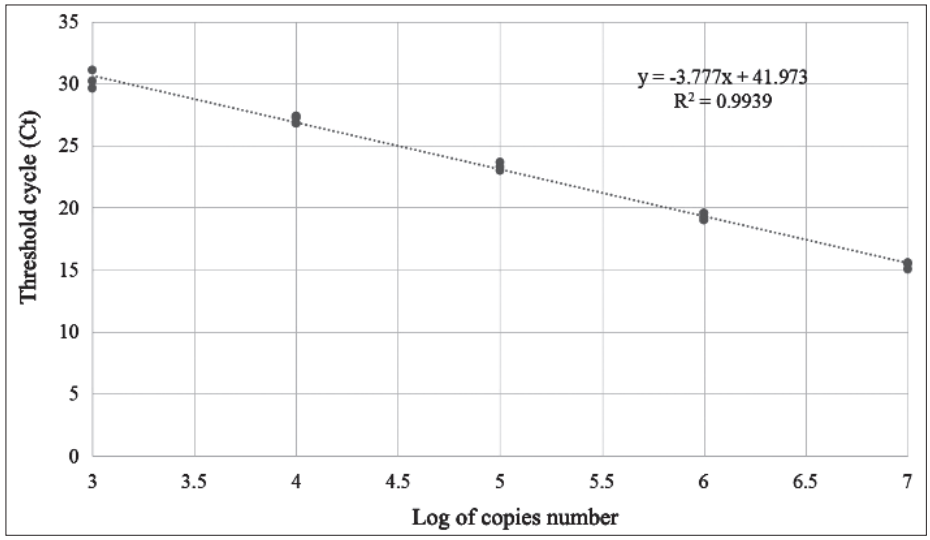

Figure 7. Standard curve generated from the plasmid containing the target gene.

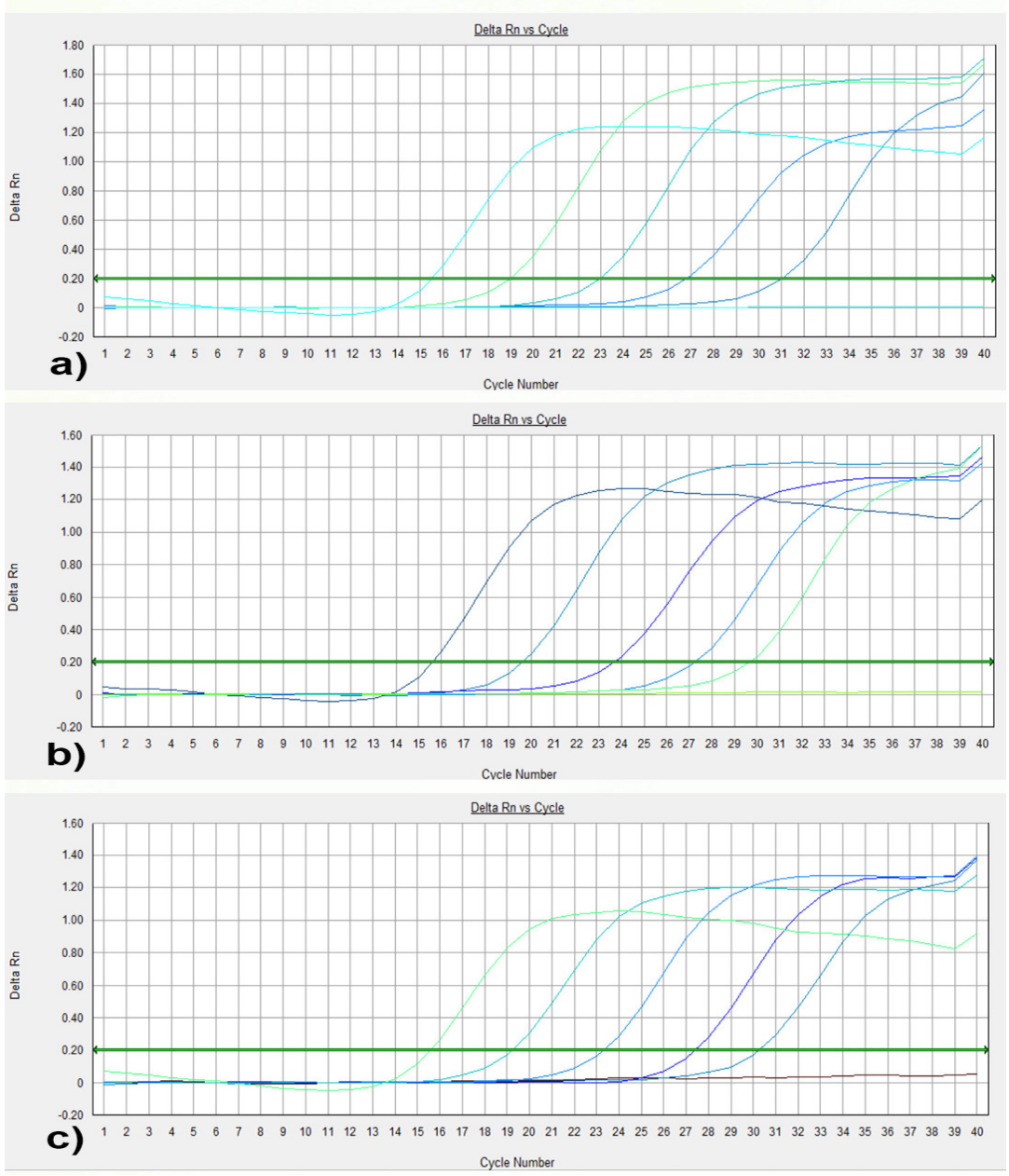

Figure 8. Gene segment amplification chart of tomato mosaic virus based on fluorescence signal. Fluorescence signal (Y vertical axis), threshold cycle (Ct) (X horizontal axis). first replication (a); second replication (b); third replication (c).

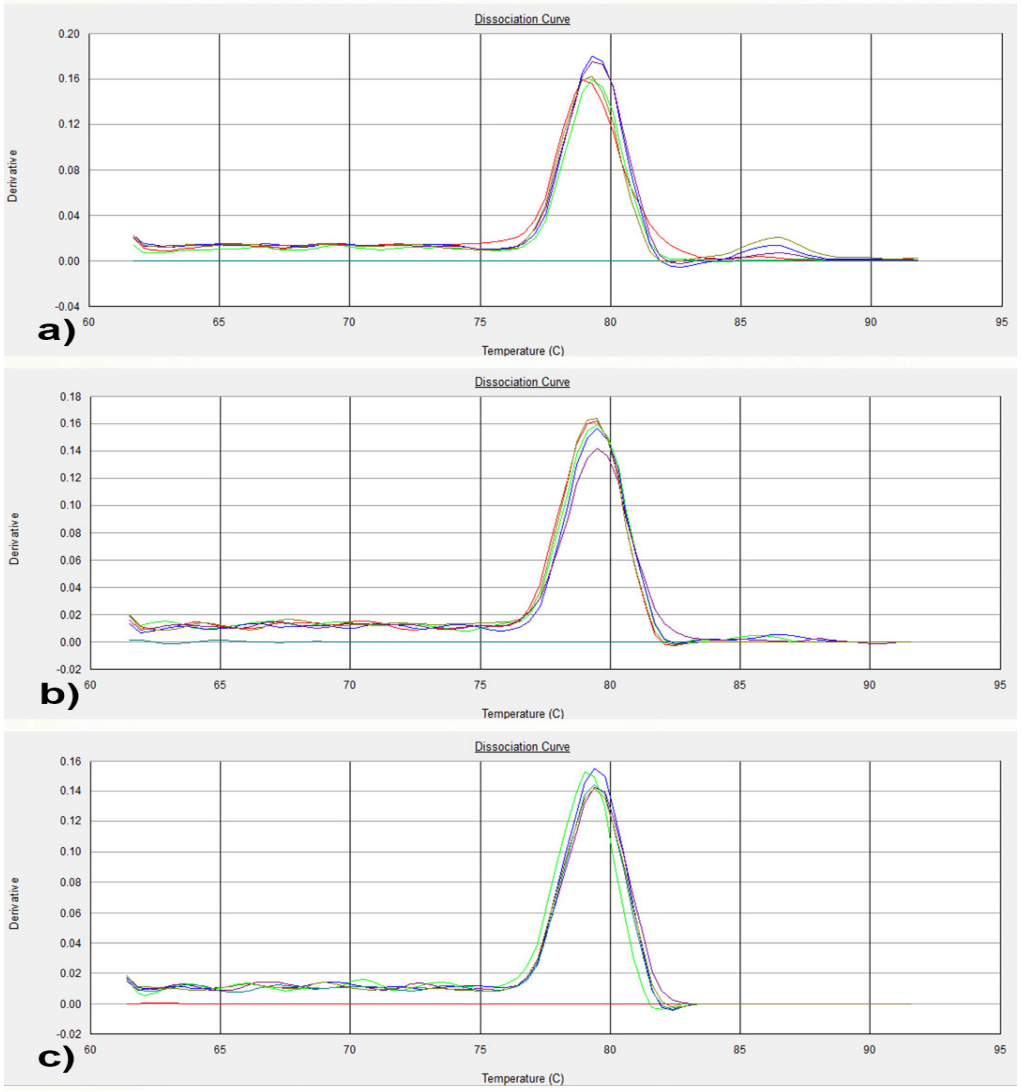

Figure 9. Melting temperature analysis chart of tomato mosaic virus gene segments. first replication (a); second replication (b); third replication (c).

3.5. Evaluation of the specificity of the realtime RT-PCR

Table 2. The results for the specificity evaluation of the realtime RT-PCR

	Threshold cycle (Ct)	Quantitative value (number of copies/ µL)	Qualitative
ToMV	16.40	5.9×10^6	+
ToMMV	_	_	-
TMV	_	_	-
ToBRFV	_	_	-

ToMV: Tomato mosaic virus; ToMMV: Tomato mottle mosaic virus; TMV: Tobacco mosaic virus; ToBRFV: Tomato brown rugose fruit virus. "+": positive , "-": negative, _ : not detected.

The result in Table 2 showed that the RT-PCR assay did not detect the virulence gene in the cDNA of TMV, ToMMV, and ToBRFV. This result suggested that the primer was specified with ToMV.

3.6. Diagnosis of ToMV on field samples with realtime RT-PCR procedure

Table 3. Tomato leaf samples were diagnosed using realtime RT-PCR and PCR methods

Sample symbol	Realtime RT-PCR method			PCR method
	Threshold cycle (Ct)	Quantitative value (number of copies/µL)	Qualitative	Qualitative
1.1	15.61	9.5×10^6	+	+
1.2	_	_	-	-
1.3	23.85	6.3×10^4	+	+
1.4	20.04	6.3×10^5	+	+
1.5	20.15	5×10^5	+	+
1.6	23.12	9.7×10^4	+	+
1.7	_	_	-	-
1.8	_	_	-	-
1.9	25.89	1.7×10^4	+	+
(+)	15.54	9.7×10^6	+	+
(-)	_	_	-	-

+: positive; -: negative; (-): negative control; (+): positive control ; _ : not detected; 1.1-1.9: Field samples 1-9.

The developed Realtime RT-PCR process detected 6 positive samples out of a total of 9 field samples. Additionally, the method quantified the field samples, with concentrations ranging from 1.7×10^4 to 9.5×10^6 copies/µL (Table 3).

The qualitative results showed 100% concordance between the realtime RT-PCR method and the RT-PCR method, which was explained by the fact that the field sampling process collected samples with symptoms of ToMV disease, so the positive samples had a high enough virus concentration to reach the detection threshold of both methods. In addition, the realtime RT-PCR method successfully quantified the ToMV virus concentration in tomato leaf samples. The realtime RT-PCR method also shows its superiority in terms of time savings compared to the RT-PCR method due to the omission of the PCR product electrophoresis step. This is important in detecting diseases early on tomatoes, thereby providing treatment and prevention measures to avoid disease outbreaks in order to reduce costs and improve crop productivity and quality for farmers.

4. Conclusions

A process for diagnosing the ToMV virus, which causes disease in tomato plants, has been established using the realtime RT-PCR method. This procedure successfully detects and quantifies the presence of the ToMV virus in tomato leaf samples, with virus amounts ranging from 1.7×10^4 to 9.5×10^6 copies/µL.

Conflict of interest

The authors declare that there are no conflict of interest to disclose related to this manuscript.

Acknowledgements

The authors send their sincere thanks to the Research Institute for Biotechnology and Environment, Ho Chi Minh City Nong Lam University for providing actual funding to carry out this research and to the farmers at the collection site. sample assisted in completing this study.

References

Bae, M., Jo, Y., Choi, H., Tran, P. T., & Kim, K. H. (2019). First report of tomato mosaic virus isolated from tomato and pepper in Vietnam. *Journal of Plant Pathology* 101(1), 181-181. http://doi.org/10.1007/s42161-018-0127-6.

Bertolini, E., Garcia, J., Yuste, A., & Olmos, A. (2010). High prevalence of viruses in table grape from Spain detected by Real-time RT-PCR. *European Journal of Plant Pathology* 128(3), 283-287. http://doi.org/10.1007/s10658-010-9663-4.

Dhaliwal, M. S., Jindal, S. K., Abhishek S., & Prasanna H. C. (2019). Tomato yellow leaf curl virus disease of tomato and its management through resistance breeding: A review. *The Journal of Horticultural Science and Biotechnology* 95(4), 425-444. https://doi.org/10.1080/14620316.2019.1691060.

FAO (Food and Agriculture Organization of the United Nations). (2022). Agricultural production statistics 2000-2021. *FAOSTAT Analytical Brief Series* 60. https://doi.org/10.4060/cc3751en.

Hanssen, I. M., Lapidot, M., & Thomma, B. P. H. J. (2010). Emerging viral diseas of tomato crop. *Molecular Plant-Microbe Interactions* 23(5), 539-548. https://doi.org/10.1094/mpmi-23-5-0539.

Hu, J. S., Ferreira S., Wang, M., & Xu, M. Q. (1993). Detection of cymbidium mosaic virus, odontoglossum ringspot virus, tomato spotted wilt virus, and potyviruses infecting orchids in Hawaii. *Plant Disease* 77(5), 464-468. https://doi.org/10.1094/PD-77-0464.

Kogovsek, P., Gow, L., Pompe-Novak, M., Gruden, K., Foster, G. D., Boonham, N., & Ravnikar, M., (2008). Single-step RT Real-time PCR for sensitive detection and discrimination of Potato virus Y isolates. *Journal of Virological Methods* 149(1), 1-11. https://doi.org/10.1016/j.jviromet.2008.01.025.

Lanter, J. M., McGuire, J. M., & Goode, M. J. (1982). Persistence of *Tomato mosaic virus* in tomato debris and soil under field conditions. *Plant Disease* 66, 552-555. https://doi.org/10.1094/pd-66-552.

Staroscik, A. (2004). *Calculator for determining the number of copies of a template*. Retrieved March 12, 2023, from http://cels.uri.edu/gsc/cndna.html.

Sui, X. L., Zheng, Y., Li, R. G., Padmanabhan, C., Tian, T. Y., Groth-Helms, D., Keinath, A. P., Fei, Z. J., Wu, Z. J., & Ling, K. S. (2017). Molecular and biological characterization of tomato mottle mosaic virus and development of RT-PCR detection. *Plant Disease* 101(5), 704-711. https://doi.org/10.1094/pdis-10-16-1504-re.

Varma, A., & Singh, M. K. (2020). Diagnosis of plant virus diseases. In Awasthi, L. P. (Ed.). *Applied plant virgology*. Massachusetts, USA: Academic Press. http://doi.org/10.1016/B978-0-12-818654-1.00006-2.

VS (Vietnam Standards). (2011). Satndard No. TCVN 9016:2011 dated on December 30, 2011. Fresh vegetables - Sampling method on the field. Retrieved March 24, 2023, from https://tieuchuan.vsqi.gov.vn/tieuchuan/view?sohieu=TCVN+9016%3A2011.

Applying Google Earth Engine for geospatial analysis of land use/land cover change in Can Gio district, Ho Chi Minh City, Vietnam

Son H. Pham[1], Thy N. Nguyen[1], Nhi Y. Huynh[1*], & Pamela McElwee[2]

[1]Faculty of Land and Real Estate Management, Nong Lam University, Ho Chi Minh City, Vietnam

[2]Department of Human Ecology, Rutgers School of Environmental and Biological Sciences, New Jersey, USA

ARTICLE INFO

Research Paper

Received: September 10, 2024
Revised: November 21, 2024
Accepted: November 22, 2024

Keywords

Can Gio district
Google Earth Engine (GEE)
Landsat
Land use/land cover change

***Corresponding author**

Huynh Yen Nhi
Email:
nhi.huynhyen@hcmuaf.edu.vn

ABSTRACT

As a gateway of Ho Chi Minh City to the sea, Can Gio district plays an important role in economy, society, defense, environment and international integration with a famous Can Gio biosphere reserve forest area. In the coming time, Can Gio district will have many large national projects. The development of Can Gio will also be associated with tasks and solutions to protect the biosphere. Therefore, monitoring land use/land cover (LULC) changes contributes to support sustainable Can Gio planning. In this study, multi-temporal Landsat satellite image data was used to extract land use information by Google Earth Engine (GEE). At the same time, the Geographic Information System (GIS) method was also used to process data layers and calculate LULC changes in 1990, 2000, 2010 and 2024. Research results showed that, from 1990 to 2024, the bare land or wasteland in Can Gio has been effectively converted. That had increased the area of land types such as: forest, residental- contructional and aquacultural land. Because of the forest restoration and forest protection policies of Government, local officials, youth volunteers and residents, the area of mangrove forest had been increased in Can Gio (1.8 times with 15,441 ha). Besides, the increase of population and economic development led increasing residental and constructional land areas (4.2 times with 875 ha). Study results also showed that GEE geospatial processing service is a useful solution for LULC analysis on a large scale such as Can Gio district. It contributes to quickly and effectively support the supervision of local authority in master planning, land use planning… where comprehensive and sustainable development is needed.

Cited as: Pham, S. H., Nguyen, T. N., Huynh, N. Y., & McElwee, P. (2024). Applying Google Earth Engine for geospatial analysis of land use/land cover change in Can Gio district, Ho Chi Minh City, Vietnam. *The Journal of Agriculture and Development* 23(Special issue 2), 131-142.

1. Introduction

Land cover is one of the important factors affecting the conditions and functions of ecosystems (Lunetta et al., 2022). In particular, land cover fluctuations show the interaction between human activities on the ecological environment (Nguyen et al., 2014). Detecting land cover fluctuations quickly will help support making reasonable decisions for land resource use and management (Mallupattu & Reddy, 2013). Currently, Can Gio has an opportunity for outstanding development when there are two national projects which are being implemented: Sea reclamation tourist urban area and international container transshipment port. Therefore, to ensure the development in accordance with the land use planning of Can Gio district, it is necessary to monitor closely and regularly land use management.

The application of Remote Sensing (RS) and Geographic Information System (GIS) in managing land use changes is convenient for observing on a large scale (Congalton et al., 1998). In Can Gio, there have also been many studies applying radar and optical satellite images, which mainly focus on mangrove management (Pham et al., 2019; Singh et al., 2021). However, the creation of land use/land cover (LULC) maps for a large area over a long period of time requires a large data source (Wan et al., 2015). Thanks to significant advances in satellite image processing and storage technology, the Google Earth Engine (GEE) platform is a powerful solution for multi-temporal mapping (Shelestov et al., 2017). Therefore, some recent studies have applied GEE to create LULC maps, instead of using RS image processing software as before. In this study, multi-temporal Landsat satellite image data is used to create a map of LULC in Can Gio district for the period 1990 - 2024 based on the GEE platform. At the same time, spatial analysis methods are also used to overlay maps and calculate the changing area of land types. From there, the study conducted an assessment of developments and changes in land use types in Can Gio district in the period of 1990 - 2024. The research results are expected to contribute for providing a scientific and practical basis to assess the situation and trends of LULC changes in the case study by the application of GEE. From there, the desired result is to encourage local agencies to increase the application of RS technology and GIS in monitoring and managing the implementation of land use planning.

2. Materials and Methods

2.1. Study area

Can Gio, a coastal district, locates in the southeast of Ho Chi Minh City with the area occupying about 1/3 of the total area of Ho Chi Minh City and its geographic coordinates is from 106°46'12" to 107°00'50" East longitude and from 10°22'14" to 10°40'00" North latitude (Figure 1).

Can Gio is the gateway of Ho Chi Minh City to the East Sea with international maritime routes in the East Sea, the project of Can Gio international container transshipment port is considered to have many advantages to attract international commodities from countries in the region (Pham et al., 2022). In addition, the government has also approved the expansion of the Can Gio sea reclamation tourist urban area project, which aims to develop infrastructure for marine economic sectors and marine urban space (Nguyen, 2019). Major projects are planned currently and will start constructing in 2025. This will help awaken the potential of Can Gio district, creating a motivation for the city to develop strongly in the coming period. Besides,

the benefits of economic development, many aquaculture, rice, and vegetable farming areas were abandoned when large project planning information was disseminated in the study area. These mean that it is necessary to monitor quickly the LULC fluctuation process, which contributes to supporting the comprehensive and sustainable planning of Can Gio.

2.2. Dataset

To extract LULC information, this study collected the Landsat surface reflectance dataset with a spatial resolution of 30 m. This data is hosted by the United States Geological Survey (USGS) and available in the GEE cloud database. The images in 1990, 2000 and 2010 are from the Landsat 5 thematic mapper (TM) sensor. In 2024, the images are from Landsat 9 operational land imager (OLI) sensor. In addition, the Can Gio district Land Use Status Quo Map dataset was also collected to serve as a reference for identifying objects on satellite images. Statistics and analysis reports on land use history in Can Gio were also collected, which supported the assessment of LULC change processes in the locality. Details of the data used in this study are described in Table 1.

Table 1. The table describes detailed information about the used data

Datasets	Year	Spatial resolution	Data source
LANDSAT/LT05/C01/T1_SR	1990, 2000, 2010	30 m	USGS
LANDSAT/LC09/C01/T1_SR	2024	30 m	USGS
Can Gio District Land Use Status Quo Map	2010, 2014, 2020	1/25.000	The Can Gio District Department of Natural Resources and Environment
Field GPS data	March 2024		Authors
Google Earth data	April 2024		Google
Statistics on Area of Land Types	2023		People's Committee of Can Gio District

USGS: United States Geological Survey.

The sample size in this study was determined by the binomial distribution according to the formula to $N = Z^2(p)(q)/E^2$ (Van Genderen & Lock, 1977), where $Z = 2$, p is the expected percentage accuracy, $q = 100 - p$ and E is the allowable error. Therefore, if the expected result of the post-classification accuracy (p) is 85% with the allowable error (E) of 5%, then the number of evaluation samples is 204 samples. In this study, a sample dataset of 212 points was collected to aid in image interpretation and evaluate the accuracy of the classification results for the year 2024. Because the study area has a dense river system and mangrove forests covering 50% of the area, there is an uneven spatial distribution of the samples surveyed by GPS. That also leads to this study, the Judgmental Sampling sampling method is applied to the GPS survey points, while the GE survey points are applied according to the Simple Random (Mu et al., 2015). Of these, land cover information of 52 points was collected from GPS field surveys by the authors in March 2024, and land cover information of 160 points was collected from high-resolution satellite imagery of Google Earth in April 2024. The locations of the evaluation points are identified as shown in Figure 1.

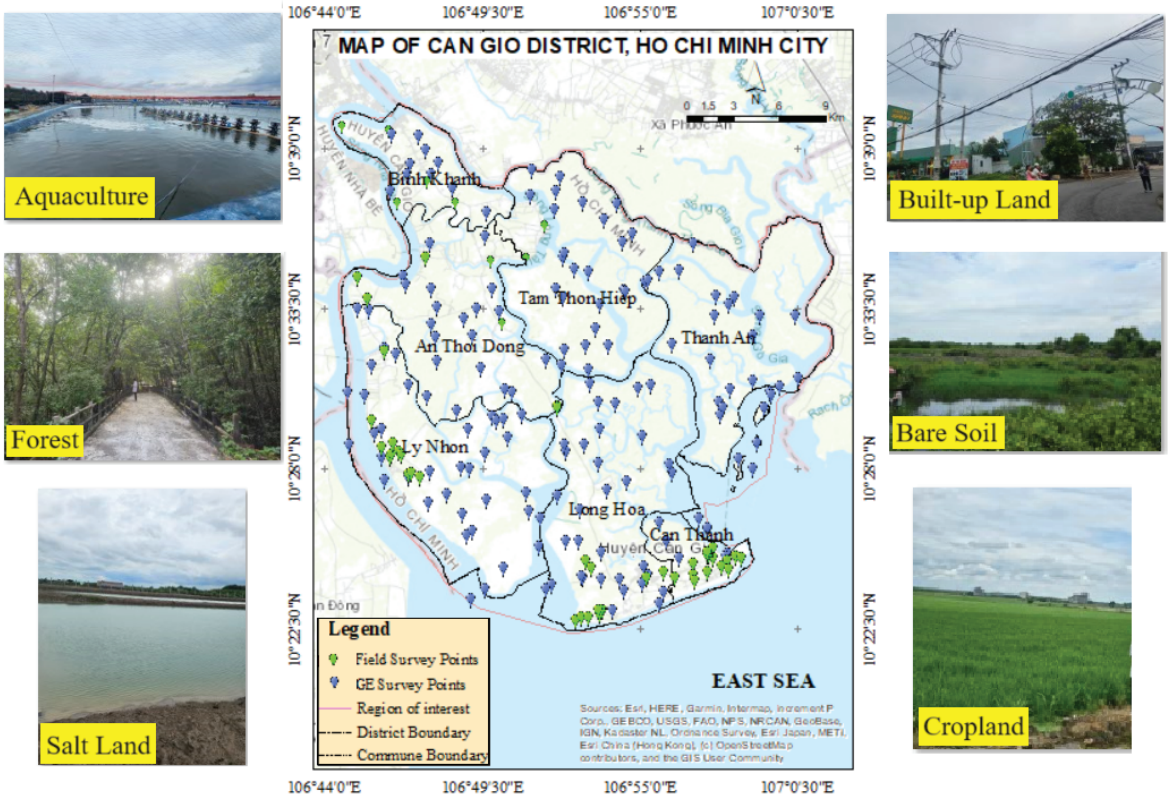

Figure 1. Map of the study area and location of evaluation samples.

3. Methods

In this study, to extract LULC information, the data processing steps were performed including image preprocessing, preprocessing, creating training sets, classification, data export, post-classification processing, accuracy assessment, and result statistics. The above operations were performed on the GEE platform, ArcGIS software, and Excel. The flowchart (Figure 2) shows the methodology applied in this study to achieve the objectives.

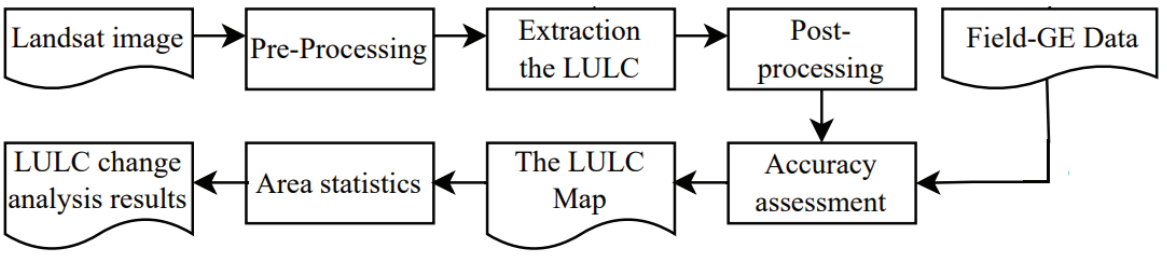

Figure 2. Flowchart of the methodology. LULC: Land use/land cover.

3.1. Pre-processing

This study used Landsat surface reflectance datasets to extract land cover information over time. These data were atmospherically corrected using the Landsat Ecosystem Disturbance Adaptive Processing System (LEDAPS) for Landsat 5 and the Landsat 8 Surface Reflectance Code (LaSRC) for Landsat 8. To minimize the influence of elements such as clouds and shadows, the cloud filtering function "QA_PIXEL" was applied to remove these unwanted components. The GEE cloud computing platform allows users to create composite images from individual images in the collection "ee.ImageCollection". Therefore, the "filterDate" function was used to create a composite image for the dry season (January to March) for all study periods. With filtered collection, a composite is created using the median reducer "ee.Reducer.median()". Reducers are the GEE way to aggregate data over time, space, bands, arrays, and other data structures. Furthermore, the "clip()" function is then used to clip the composite into the study area. To display the image of the preprocessing results, the "Map.addLayer" function is used with the visParams argument.

3.2. Extraction of the LULC

3.2.1. Determination of LULC classification system

In this study, LULC was divided into eight classes as follows: Forest, Cropland, Aquaculture, Salt Land, Built-up Land, Bare Soil and Water, which were based on the characteristics of the study area and the resolution of satellite image data. The detailed description of the Land use/ Land cover classes is shown in Table 2.

Table 2. Land use/land cover system

LULC	Description
Forest (F)	Including natural forests and planted forests.
Cropland (C)	Including perennial crop land, annual crop land and rice land.
Aquaculture (A)	Used specifically for the purpose of aquaculture in brackish, saltwater and freshwater.
Salt Land (SL)	Land for salt production.
Built-up Land (BL)	Built-up or under-construction land area.
Bare Soil (BS)	Uncultivated or abandoned land.
Water (W)	Water surface of canals, rivers, streams.

LULC: Land use/land cover.

3.2.2. Creating training samples

The training data is a FeatureCollection with a property storing the class label and properties storing predictor variables. A set of polygon training samples for 4 years was selected directly on the GEE platform, which were selected based on the classifier's experience and Can Gio District Land Use Status Quo Map. The detailed number of training samples is shown in Table 3.

Table 3. The detailed number of training samples

LULC	No. of Polygons			
	1990	2000	2010	2024
Forest (F)	152	171	132	144
Cropland (C)	59	42	46	65
Aquaculture (A)	154	157	189	238
Salt Land (SL)	77	103	163	94
Built-up Land (BL)	7	13	27	76
Bare Soil (BS)	44	36	24	35
Water (W)	88	95	132	104
Total	581	617	713	756

LULC: Land use/land cover.

3.2.3. Classification and post-classification of LULC

Google Earth Engine (GEE) provides users with a variety of supervised classification algorithms, such as Support Vector Machine (SVM), Classification And Regression Tree (CART) and Random Forest (RF), Naïve Bayes (NB). Among the popular supervised machine learning algorithms, the RF algorithm has been proven effective in resisting noise and outliers (Pelletier et al., 2016). At the same time, this algorithm is more effective for mapping in wetlands or mangrove forests (Berhane et al., 2018; Amani et al., 2019; Ghorbanian et al., 2021). For that reason, it is used in this study to create the LULC map of Can Gio. The Random Forests is a Machine Learning-based method, which was proposed by Breiman in 2001 (Breiman, 2001). The Random Forests classifier is an ensemble classifier that produces multiple decision trees, using a randomly selected subset of training samples and variables. In GEE, the Random Forest algorithm can be defined using the function "ee.Classifier.smileRandomForest". The training samples data variable is specified as the training data in the features argument, which is fed into the processing pipeline via the "classifier.train() function".

The image classification results are exported to vector format for post-classification processing, which is done using the "classified. reduceToVectors" function. Then, the data layers are processed to redistribute objects between layers and generalize objects through GIS methods. Finally, overlay and statistical techniques are used to count areas, analyze changes and create LULC maps in Can Gio district over time.

3.3. Accuracy assessment

To assess the reliability of the LULC 2024 results, the study used an evaluation dataset of 212 points, which were collected in 2024. Of these, 52 points were from GPS field data sources and 160 points were from GE high-resolution satellite imagery sources (Figure 1). After the error matrix was established, the Kappa coefficient and overall accuracy were used to evaluate the agreement between the evaluation data and the classification results (Cohen, 1960). In addition, statistical data on land area in Can Gio district in 2023 were also collected to assess the difference between classification results and actual data.

4. Results and Discussion

4.1. LULC information extraction results

Figure 3 showed the LULC classification results from Landsat satellite images in Can Gio district in the years 1990, 2000, 2010 and 2024.

The classification results were evaluated for accuracy by comparing with the evaluation sample set at time 2024, which was shown in Table 4. The results of the accuracy assessment of 2024 LULC had an overall accuracy and Kappa coefficient of 87% and 0.84, respectively. Thus, the LULC extraction results in Can Gio district had a fairly high level of reliability, which was performed by using the Random Forests algorithm through the supervised classification method on the GEE platform. The evaluation results showed that misclassification mainly occurs in the land types: Aquaculture, Salt Land and Bare Soil, which have similar spectral reflectance properties. The reasons were explained as follows: 1/ Aquaculture land and salt land are cultivated alternately by farmers; 2/ Land serving aquaculture and salt production is not economically efficient, so farmers leave it fallow for a long time, becoming flooded bare land.

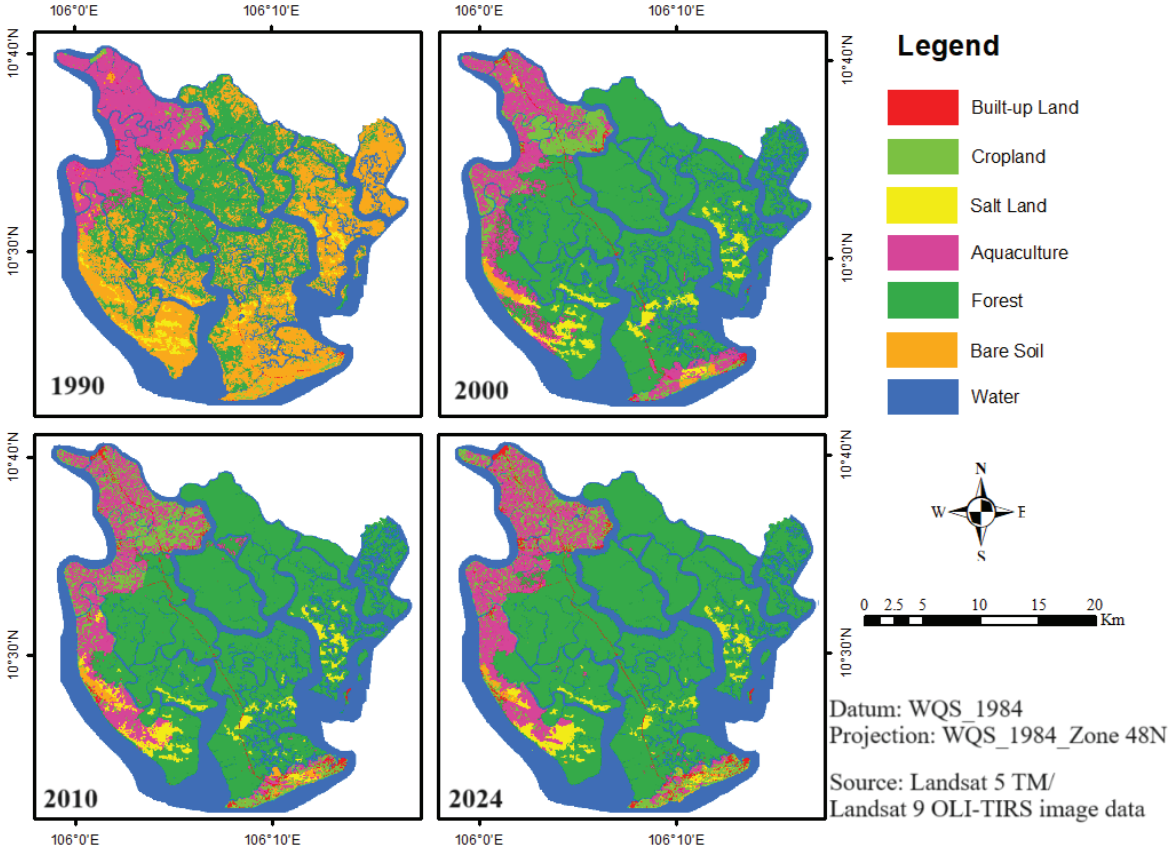

Figure 3. LULC of Can Gio district. LULC: Land use/land cover.

Table 4. Classification result error evaluation matrix

Classified data	Evaluation Data							
	F	C	A	SL	BL	BS	W	Total
F	53	2				1		56
C		19			2	1		22
A	4		34	1		1	2	42
SL	1		2	25	1			29
BL		1		1	17	1		20
BS		2				13	1	16
W	2		2				23	27
Total	60	24	38	27	20	17	26	212

Table 5. Percent accuracy of classification results compared to statistics

LU LC	2024 Classification (ha)	2023 Statistics (ha) (*)	Difference (%)
F	34631	34349	0.8
C	4789	4115	16.4
A	6281	6100	3.0
SL	1866	2245	16.9
BL	1149	1696	32.3
BS	445	1029	56.8
W	21343	20906	2.1

LULC: Land use/Land cover.

(*) PC HCMC (2024).

Comparing the difference between the 2024 classification results and 2023 published statistical data (Table 5) shows that: Forest, Water and Aquaculture have the lowest difference, corresponding to 0.8% (281 ha), 2.1% (437 ha) and 3.0% (181 ha). In contrast, Bare Soil and Built-up Land have the highest difference, corresponding to 56.8% (584 ha) and 32.3% (547 ha). This high difference is explained by the difference in the definition of land types in this study with published statistical data on Current Land Use Status in 2023: 1/ In this study, Bare Soil is defined as land that is in a state of abandonment. Meanwhile, according to published statistics in Can Gio, Bare Soil is unused land on the coast or around islands. 2/ Built-up Land in this study is defined as areas of land that have been built or are under construction. According to published statistics in Can Gio, areas that are already in the construction planning area are also considered as Built-up Land.

4.2. LULC fluctuation analysis results

From the LULC classification results from Landsat satellite images, the study analyzed LULC fluctuations in Can Gio district from 1990 to 2024. The calculated data on LULC area results in 1990, 2000, 2010 and 2024 were shown in the Figure 4 and Table 6.

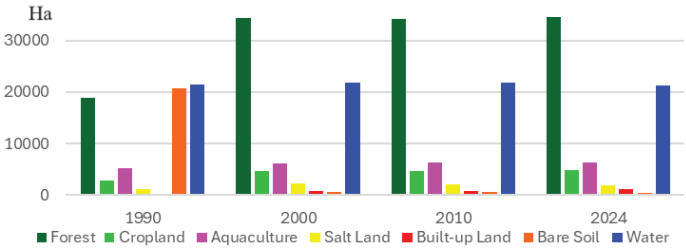

Figure 4. Graph of LULC changes in the period of 1990 - 2024.

Table 6. Statistics results of LULC area

LULC	Area (ha)			
	1990	2000	2010	2024
F	18909	34391	34277	34631
C	2836	4621	4717	4789
A	5284	6209	6254	6281
SL	1088	2174	2149	1866
BL	274	692	823	1149
BS	20719	550	536	445
W	21394	21867	21748	21343

LULC: Land use/Land cover.

An, Long Hoa and part of Ly Nhon. And since 2000 to present, the mangrove forest area has been protected and maintained stably, despite the pressure of the rapid urbanization process in Ho Chi Minh City. The restoration of Can Gio Mangrove Forest contributed greatly to the process of socio-economic development, national defense and security and environmental protection. At the same time, this activity helped people who are contracted to protect the forest to improve their lives and increase their income.

The analysis of LULC fluctuations also showed that the area of Built-up Land in Can Gio district has a tendency to increase continuously. The Bare Soil (Wetlands) converted to urban land occur in scattered riverine or coastal areas. In 1990, Built-up Land occupied a very small area of 274 ha. The urban population was sparsely concentrated, mainly in coastal areas. It can be seen that the concentrated residential areas of the district have been formed since the 1980s such as: Binh Khanh ferry area, An Thoi Dong ferry and Can Thanh. In the following period, there was a rapid increase in the area in densely populated areas since Duyen Hai district changed its name to Can Gio district in 1991. In the 2000s, in addition to the three existing residential areas, new residential areas began to appear such as: Long Tau riverside, Dong Hoa wharf, 30/4 coastal tourism services and Thanh An island commune. In particular, when Can Thanh town was established in 2003, which played the role of a heart of Can Gio district, it helped the rapid expansion of urban areas in coastal areas. The government began to focus on urban management and development. Transport infrastructure (bridges, roads, ferry terminals, ferry terminals, etc.), electricity, clean water, residential housing, irrigation systems, schools, hospitals, and rural markets were invested in and built (PCHCMC, 2021).

The analysis results of LULC change at 1990 and 2024 show: the land types with the most fluctuating areas were Forest, Bare Soil and Built-up Land. Of which, the Bare Soil area decreased significantly, from 20,719 ha to 445 ha (equivalent to a decrease of 29% to 1%). In contrast, there was a clear increase in Forest cover from 18,909 ha to 34,631 ha (equivalent to an increase from 27% to 49%). In addition, the Built-up Land area also increased from 274 ha to 1,149 ha (equivalent to an increase from 0.39% to 2%). From 1990 to 2024, the remaining LULC types also fluctuated but at a negligible rate.

More specific analysis showed that, in the period 1990 - 2000, there was a significant increase in the area of mangrove forests (increased by 15,482 ha, equivalent to 1.8 times). Before that, from 1961 to 1971, Can Gio forest was heavily sprayed with reclamation chemicals due to the war. Almost all the trees of the mangrove forest here were destroyed. In 1978, the Ho Chi Minh City government launched a campaign to replant Can Gio forest (Le et al., 2021). In 2000, the United Nations Educational, Scientific and Cultural Organization (UNESCO) recognized this as the first Biosphere Reserve in Vietnam, belonging to the world biosphere reserve system (Nam, 2014). This achievement was thanks to the forest restoration policies of the Government, local officials, Youth Volunteers and residents, who helped the mangrove forest in Can Gio regenerate. This result was also considered a miracle because in the early 1970s, American ecologists estimated that "It will take about 100 years to restore the Can Gio mangrove ecosystem" (VAN, 2012). Thanks to the above achievements, a large area of Bare Soil land has been converted to Forest throughout Can Gio district, specifically in communes covered with forests such as: Tam Hiep, An Thoi Dong, Thanh

All of these changes created the premise for the economic development of the district in the next period. By 2010, the Urban Planning had ensured the aesthetic architecture of rural areas and formed an eco-tourism area. The locality had also basically completed the concreting of rural roads. Environmental management had positive changes, creating favorable conditions for urban development and new rural construction. Some new residential areas were systematically formed, such as along Rung Sac road in Binh Khanh commune, the center of Ly Nhon commune, residential areas along Duyen Hai and Luong Van Nho roads. At the same time, planned residential areas were also formed, such as Phuoc Loc residential area and Tac Suat residential area near Can Gio - Vung Tau ferry terminal. In addition, information about important projects licensed for implementation in Long Hoa commune and Can Thanh town which made the status of the complicated land use conversion (Nguyen, 2021). By 2024, the Built-up Land area increased rapidly (1,149 ha) due to trends of population growth and migration from other areas. Previously established residential areas will continue to expand. Shops, factories and houses will be built along old roads and upgraded roads such as Ly Nhon and Duyen Hai. At the same time, some residential areas will also appear in some areas along large bridges such as Vam Sat bridge, An Nghia bridge and Soai Rap river. Local authorities developed various solutions to improve and develop the urban area. In the coming time, the Government's main goal is to develop Can Gio district following the direction of a marine ecological urban area associated with the implementation of the Smart Urban Project so that the quality life of the local people is improved more and more.

5. Conclusions

The study extracted successfully LULC information from Landsat satellite images in Can Gio district in the years of 1990, 2000, 2010 and 2024 on the GEE platform. The results of the accuracy assessment of the classification results in 2024 showed that the overall accuracy and Kappa coefficient were 87% and 0.84, respectively. Besides, the results of comparing the differences with the published statistics in 2024 show that: Forest, Water and Aquaculture land have the lowest differences; Bare Soil and Built-up Land have the highest differences. The failure to assess the accuracy of the classification results in the years 1990, 2000, and 2010 is a limitation of this study.

The results of the land cover change analysis showed that the Bare Soil area decreased by 20,274 ha from 1990 to 2024. In contrast, Forest increased by 15,441 ha, which was achieved thanks to effective forest restoration efforts after the War in Can Gio. The study also showed that the Urban Land area in Can Gio district increased steadily over the years, this is suitable with development trend of the case study area.

Currently, many large projects are about to be implemented such as: Can Gio sea reclamation tourist urban area, Can Gio international container transhipment port and Can Gio Bridge, which will contribute to economic growth and LULC changes.

The above results showed that monitoring LULC changes through GEE Cloud Computing Platform allowed users to effectively exploit the search and processing features of RS data, which was done quickly and accurately. The study also showed that Landsat satellite images are a suitable data source to assess LULC changes

over long periods of time and over large areas. From there, it showed that RE and GIS are useful in supporting land management for local government, especially in coastal areas where are affected by climate change and urbanization.

Conflict of interest

All authors declare that they have no conflict of interest.

Acknowledgements

This work was financially sponsored by HCMC. Nong Lam University through the scientific project No. CS-CB23-QLDD-03.

References

Amani, M., Brisco, B., Afshar, M., Mirmazloumi, S. M., Mahdavi, S., Mirzadeh, S. M. J., Huang, W., & Granger, J. (2019). A generalized supervised classification scheme to produce provincial wetland inventory maps: An application of Google Earth Engine for big geo data processing. *Big Earth Data* 3(4), 378-394. https://doi.org/10.1080/20964471.2019.1690404.

Berhane, T. M., Lane, C. R., Wu, S. Q., Autrey, B. C., Anenkhonov, O. A., Chepinoga, V. V, & Liu, X. H. (2018). Decision-tree, rule-based, and random forest classification of high-resolution multispectral imagery for wetland mapping and inventory. *Remote Sensing* 10(4), 580. https://doi.org/10.3390/rs10040580.

Breiman, L. (2001). Random forests. *Machine Learning* 45, 5-32. https://doi.org/10.1023/A:1010933404324.

Cohen, J. (1960). A coefficient of agreement for nominal scales. *Educational and Psychological Measurement* 20(1), 37-46. https://doi.org/10.1177/001316446002000104.

Congalton, R. G., Balogh, M., Bell, C., Green, K., Milliken, J. A., & Ottman, R. (1998). Mapping and monitoring agricultural crops and other land cover in the Lower Colorado River Basin. *Photogrammetric Engineering and Remote Sensing* 64(11), 1107-1114.

Ghorbanian, A., Zaghian, S., Asiyabi, R. M., Amani, M., Mohammadzadeh, A., & Jamali, S. (2021). Mangrove ecosystem mapping using Sentinel-1 and Sentinel-2 satellite images and random forest algorithm in Google Earth Engine. *Remote Sensing* 13(13), 2565. https://doi.org/10.3390/rs13132565.

Le, T. X., Phan, D. T. A., Tran, H. T. M., Nguyen, M. C., & Nguyen, H. T. T. (2021). Mangrove forests policy implementation: Case studies of Ngoc Hien and Can Gio mangrove forests in the Southern Vietnam. *Preprints* 2021, 2021010175. https://doi.org/Preprints. 2021010175.

Lunetta, R. S., Knight, J. F., Ediriwickrema, J., Lyon, J. G., & Worthy, L. D. (2022). Land-cover change detection using multi-temporal MODIS NDVI data. In Lyon, J. G., & Lyon, L. (Eds.). *Geospatial information handbook for water resources and watershed management - Volume II*. Florida, USA: CRC Press. https://doi.org/10.1201/9781003175025.

Mallupattu, P. K., & Reddy, J. R. S. (2013). Analysis of land use/land cover changes using remote sensing data and GIS at an Urban Area, Tirupati, India. *The Scientific World Journal* 2013(1), 268623. https://doi.org/10.1155/2013/268623.

Mu, X. H., Hu, M. G., Song, W. J., Ruan, G. Y., Ge, Y., Wang, J. F., Huang, S., & Yan, G. J. (2015). Evaluation of sampling methods for validation of remotely sensed fractional vegetation cover. *Remote Sensing* 7(12), 16164-16182. https://doi.org/10.3390/rs71215817.

Nam, V. N., Sinh, L. V., Miyagi, T., Baba, S., & Chan, H. T. (2014). An overview of Can Gio district and mangrove biosphere reserve. *Vietnam Mangrove Ecosystems Technical Reports 6*, 1-7.

Nguyen, H. T. T., Pham, T. V., & Nguyen, T. K. (2014). Assessing land use and land cover change: A

case of Tien Yen District, Quang Ninh Province from 2000 to 2010. *Journal of Science and Development* 1(12), 43-51.

Nguyen, T. N. (2019). *Three issues in Can Gio urban tourism project*. Retieved March 10, 2023, from https://ir.vnulib.edu.vn/bitstream/VNUHCM/7654/1/N.T.%20NGUYEN%20%282019%29%20Ba%20v%E1%BA%A5n%20%C4%91%E1%BB%81%20trong%20d%E1%BB%B1%20%C3%A1n%20%C4%91%C3%B4%20th%E1%BB%8B%20du%20l%E1%BB%8Bch%20C%E1%BA%A7n%20Gi%E1%BB%9D.pdf.

Nguyen, T. S. (2021). Strict control requirement for environmental problems of sea encroachment projects. *Journal of Human Geography Research* 33(2), 11-19.

PCHCMC (Ho Chi Minh City People's Committee). (2024). Decision No. 1081/QD-UBND dated on April 3, 2024. Ho Chi Minh City People's Committee on approving the land use plan of Can Gio district in 2024. Retrieved May 16, 2024, from https://thuvienphapluat.vn/van-ban/Bo-may-hanh-chinh/Quyet-dinh-1081-QD-UBND-2024-cong-bo-thu-tuc-hanh-chinh-the-duc-the-thao-nganh-Van-hoa-Dong-Nai-610242.aspx.

PCHCMC (Ho Chi Minh City People's Committee). (2021). *History of revolutionary struggle, construction and development of the Party Committee and People of Can Gio district*. Ho Chi Minh City, Vietnam: Ho Chi Minh City General Publishing House.

Pelletier, C., Valero, S., Inglada, J., Champion, N., & Dedieu, G. (2016). Assessing the robustness of Random Forests to map land cover with high resolution satellite image time series over large areas. *Remote Sensing of Environment* 187, 156-168. https://doi.org/10.1016/j.rse.2016.10.010.

Pham, L. T. H., Vo, T. Q., Dang, T. D., & Nguyen, U. T. N. (2019). Monitoring mangrove association changes in the Can Gio biosphere reserve and implications for management. *Remote Sensing Applications: Society and Environment* 13, 298-305. https://doi.org/10.1016/j.rsase.2018.11.009.

Pham, T. H., Ngo, T. V., Pham, T. T., Bui, T. T., & Nguyen, G. T. L. (2022). *The contribution of mangroves in supporting the reduction of emissions and pollution from port activities* (Report No. 230). Bogor, Indonesia: Center for International Forestry Research - CIFOR. https://doi.org/10.17528/cifor/008487.

Shelestov, A., Lavreniuk, M., Kussul, N., Novikov, A., & Skakun, S. (2017). Exploring Google Earth Engine platform for big data processing: Classification of multi-temporal satellite imagery for crop mapping. *Frontiers in Earth Science* 5, 232994. https://doi.org/10.3389/feart.2017.00017.

Singh, S., Nguyen, L. V., & Truong, B. T. H. (2021). Monitoring mangrove forest reclamation using geospatial tools in Can Gio mangrove biosphere reserve, Viet Nam. *International Journal of Ecology and Environmental Sciences* 39(3), 147-157.

VAN (Vietnam Agriculture Newspaper). (2012). Can Gio miracle. Retrieved April 1, 2024, from https://nongnghiep.vn/ky-tich-can-gio-d99724.html.

Van Genderen, J. L., & Lock, B. F. (1977). Testing land-use map accuracy. *Photogrammetric Engineering and Remote Sensing* 43(9), 1135-1137.

Wan, B., Guo, H. Q., Fang, F., Su, J. Y., & Wang, R. (2015). Mapping US urban extents from MODIS data using one-class classification method. *Remote Sensing* 7(8), 10143-10163. https://doi.org/10.3390/rs70810143.

Emissions of gases during bio-conversion of agro-waste by black soldier fly larvae

Ha N. Nguyen[1,2], Thuy T. T. Thai[1], Vu K. Luong[2], & Tu P. C. Nguyen[3*]

[1]Research Institute for Biotechnology and Environment, Nong Lam University, Ho Chi Minh City, Vietnam

[2]Faculty of Biological Sciences, Nong Lam University, Ho Chi Minh City, Vietnam

[3]Faculty of Fisheries, Nong Lam University, Ho Chi Minh City, Vietnam

ARTICLE INFO

Research Paper

Received: August 31, 2024
Revised: December 09, 2024
Accepted: December 12, 2024

Keywords

Ammonia
Black soldier fly
Carbon dioxide
Hermitia illucens
Hydrogen sulfide

***Corresponding author**

Nguyen Phuc Cam Tu
Email:
npctu@hcmuaf.edu.vn

ABSTRACT

This laboratory-scale study was designed to investigate the emissions of carbon dioxide (CO_2), ammonia (NH_3), and hydrogen sulfide (H_2S) gases during the bio-conversion of agro-waste by black soldier fly larvae (BSFL) for 14 days. The study included three experimental treatments: a control group without waste and BSFL (T0, lab background), treatment 1 containing waste with BSFL (T1), and treatment 2 containing only waste (without BSFL, T2). Process efficiency was measured by waste reduction and bio-conversion rate. Gas emissions from the process were collected using the static chamber method and determined using the gas absorption method. The results in the treatment T1 showed a notable BSFL survival rate of 99.7%, indicating a favorable condition for BSFL growth. The waste reduction rate in the T1 treatment (74.3%) was approximately two times higher than that of T2 (38.7%), indicating the ability of BSFL to decompose organic wastes efficiently. The pH and moisture content of the waste were monitored throughout the 14-day trial for both T1 and T2, and similar trends were observed. Compared to T0, gas emissions from T1 and T2 were higher. Furthermore, the CO_2 and H_2S emissions in T1 were higher than those in T2, while NH_3 levels released in T2 were relatively higher than in T1. The preliminary results presented here could be the basis of future studies on gas emission via BSFL treatment of agro-waste.

Cited as: Nguyen, H. N., Thai, T. T. T., Luong, V. K., & Nguyen, T. P. C. (2024). Emissions of gases during bio-conversion of agro-waste by black soldier fly larvae. *The Journal of Agriculture and Development* 23(Special issue 2), 143-154.

1. Introduction

In 2022, agricultural production in Vietnam generated a large amount of organic waste, about 159 million tons, of which crop residues account for 56.6%, livestock by-products 39%, aquatic production 0.6%, and forestry 3.8% (Nguyen & Cao, 2024). Composting has become an adaptable method for converting agricultural wastes or by-products into organic fertilizer. However, the composting process also releases greenhouse gas (GHG), such as carbon dioxide (CO_2), methane (CH_4), and nitrous oxide (N_2O), sulfur compounds (such as hydrogen sulfide, H_2S), and ammonia (NH_3). According to Barrington et al. (2002), the organic carbon (C) loss rates during composting were 13.6% - 51.3%, with almost all the C (70%) being emitted into the air as CH_4 and CO_2. Moreover, about 9.6% - 74% of the initial total nitrogen level is lost through composting, primarily by NH_3 volatilization (Barrington et al., 2002; Jiang et al., 2013; Yang et al., 2015). The volatilization of C- and N-containing gases into the atmosphere not only decreases the quality of the final organic fertilizers but also causes secondary atmospheric pollution (Yang et al., 2015). While H_2S was the most abundant compound, with 39.0 - 43.0% of the total five volatile sulfur compounds generated during the composting of municipal solid waste (Zhang et al., 2013).

For implementing circular economy principles, insect-based bioconversion using black soldier fly larvae (*Hermetia illucens*) (BSFL) is one of the sustainable approaches to managing organic waste (Wang & Shelomi, 2017; Huis, 2020). These larvae can decompose a wide range of organic waste and convert it into high-quality biomass for livestock and aquaculture. Industrial-scale BSF farm requires less land area and water than livestock, resulting in a lower water footprint (Wang & Shelomi, 2017; Huis, 2020; Coudron et al., 2024). Besides, it generates fewer GHG, H_2S, and lower NH_3 emissions than any conventional pasture (Wang & Shelomi, 2017; Michishita et al., 2023).

Since 2022, BSF has been allowed to be raised in Vietnam according to the Decree No. 46/2022/ND-CP (GV, 2022). Although there are various advantages to BSFL production, its environmental impact, such as CO_2, H_2S, and NH_3 emissions, has recently become a critical consideration. When the industry of manufacturing BSF grows, information on direct CO_2, H_2S, and NH_3 releases from BSFL bioconversion is required. To date, the Vietnamese literature needs more data on the CO_2, H_2S, and NH_3 emitted during composting agro-waste by BSFL. Therefore, this study aimed to compare CO_2, H_2S, and NH_3 emissions from composting with and without BSFL and the effects of inoculation with BSFL on the efficiency and rate of agro-waste treatment.

2. Materials and Methods

2.1. Materials

The experiment was conducted at the Research Institute for Biotechnology and Environmental (RIBE), Nong Lam University, Ho Chi Minh City. The BSF larvae used for the trial were taken from the BSF Research Facility of CJ Korea, RIBE. This study used an agro-waste mixture of brewery waste, coconut meal, soy pulp, and water as the substrate for the BSFL throughout the trial according to our rearing protocol (RIBE, 2017). After egg hatching, the BSFLs were fed this mixture for seven days. Seven-day-old larvae (DOL) with an average weight of 13.8 mg were used for the trial.

2.2. Experimental design and methods

In this study, three experimental treatments, including a control group without the addition of waste mixture and BSFL (T0, lab background), treatment 1 containing waste mixture with BSFL (T1, BSFL composting), and treatment 2 containing only waste mixture (T2, without BSFL), were tested in triplicate for 14 days. The control treatment was used to check that no background studied gases were present at the location of the gas measurement.

Based on preliminary trials, 1,000 BSFLs were inoculated into the composting tray with a feeding rate of 500 mg wet weight/larva per day. The larvae were fed on days 1, 2, 4, 7, and 10 of the treatment T1 and T2 by adding 500 g of new substrate to each tray without mixing. The larvae were reared at 28°C, 90% relative humidity, under natural light conditions, which were chosen to mimic the larvae's natural habitat (RIBE, 2017). To ensure optimal larval development, the density, feeding rate and frequency, and environmental conditions were used according to our rearing protocol (RIBE, 2017).

A photo of a composting tray and its associated equipment is shown in Figure 1. The laboratory-scale composting experiment was done in a plastic composting tray (61 × 42 × 15 cm) mounted with an airtight transparent acrylic lid, with a total volume of 53.2 L, for 14 days.

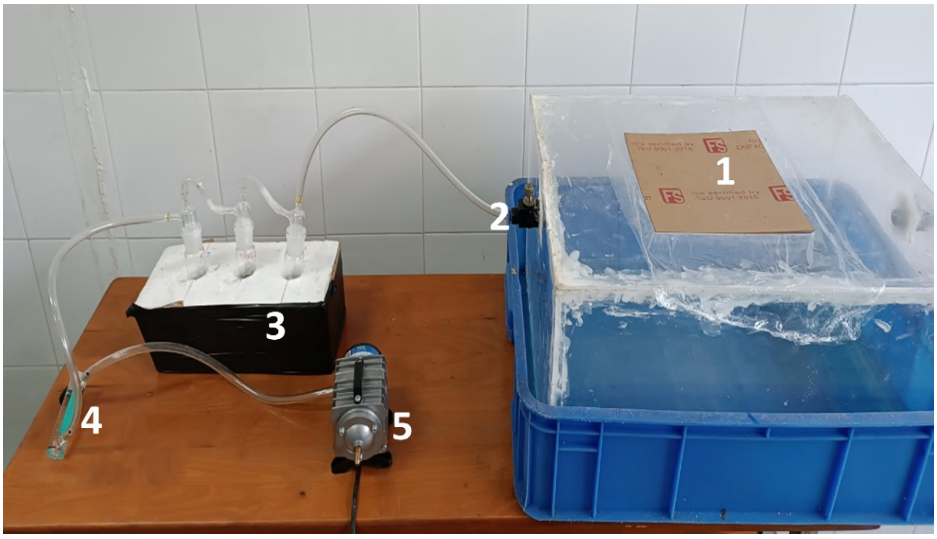

Figure 1. Diagram of a laboratory-scale composting system for measurement of gaseous emissions. (1) Composting tray with acrylic lid, (2) air valve, (3) three consecutive impingers, (4) rotameter, (5) air pump.

2.3. Bioconversion efficiency

Substrate samples were taken from the initial agro-waste mixture and leftover frass at the end of the bioconversion. The number of larvae per tray was determined by manually separating them from their substrate and counting them. After that, the total weight of larvae (*g*, wet weight (ww) and survival rate (%) were recorded per tray. To measure the dry weight (dw), substrates and BSFL were dried at 105°C for 24 h.

In addition, the humidity and pH of the substrate were measured daily using a handheld Humidity - pH meter (Model DM-15, Takemura, Japan) in treatments T1 and T2 after measuring

gas emission. To evaluate the efficiency of agro-waste treatment and larval rearing in the experiment, the waste reduction rate and bioconversion rate were also estimated with the following equations (Arabzadeh et al., 2022):

$$\text{The waste reduction rate (\%)} = \frac{M-m}{M} \times 100 \quad (1)$$

$$\text{The bioconversion rate (\%)} = \frac{(B_{end}-B_{ini})}{(N-n)} \times 100 \quad (2)$$

where: M and m are the weight (in g of ww) of substrate added in the tray for 14 days and residues at the end of the experiment, respectively; B_{end} and B_{ini}, are the larval biomass (in g of dw) determined at the end and at the beginning of the experiment, respectively, and N and n are the weight (in g of dw) of substrate added in the tray for 14 days and residues at the end of the experiment, respectively.

2.4. Measurements of gas emissions

During composting, the gas evaporated from the tray was collected daily via a ten mm-silicone tube into three consecutive glass impingers with a fritted nozzle. The gas flow rate was maintained at 0.5 L/min for 10 min using an air pump and a rotameter. The first impinger contained 30 mL of 0.02 N sulfuric acid to absorb NH_3 (VS, 1995). The further impinger was filled with 30 mL of $HgCl_2$/KCl solution (WHO, 1981), and the last one was filled with 30 mL $Ba(OH)_2$/$BaCl_2$ solution (MOH, 1989) to absorb H_2S and CO_2, respectively. Three impingers were submerged in an ice bath, and sun exposure was avoided during the experiments.

The air samples containing NH_3, H_2S, and CO_2 were analyzed daily. During BSFL composting, the released NH_3, H_2S, and CO_2 were determined by the indophenol method (VS, 1995), the methylene blue method (WHO, 1981), and the absorption method using barium saccharate (MOH, 1989), respectively.

Daily emissions of a substance based on the concentration measurements in the units of milligrams per cubic meter were calculated using the following equation:

$$\text{Gas emission (mg/m}^3\text{)} = \frac{(A-B) \text{ x } V \text{ x } 24}{1000 \text{ x } T} \quad (3)$$

where: A and B are concentrations of the collected gas sample and the lab background air sample (T0) (mg/m^3), respectively, V is the volume of the acrylic lid (L) (V = 53.2 L), 24 is time of the day, 1000 is the conversion factor for converting m^3 to liters, and T is gas accumulation time (hours) (T = 20.5 h).

2.5. Statistical analysis

Data were analyzed by one-way analysis of variance (ANOVA). Tukey's honestly significant difference test (Tukey's HSD) was used to test the significant differences among treatment means. The statistical analyses' significance was accepted at $\alpha \leq 0.05$ level. All statistical analyses were conducted using the IBM SPSS Statistics for Windows, Version 22 (Armonk, NY: IBM Corp). All data were expressed as the mean ± standard deviation (SD).

3. Results and Discussion

3.1. Composting efficiency

Table 1 shows the bioconversion performance. In this study, 1,000 7-DOLs decomposed a 2,500 g waste mixture for 14 days, resulting in a final weight of residues of 0.643 ± 0.01 kg ww, while the treatment without BSFL just reduced substrate to 1.53 ± 0.03 kg ww. The average waste reduction rates in the treatments T1 and T2 were 74.3% and 38.7%, respectively. The waste reduction rate in the T1 treatment was approximately two

times higher than that of T2, implicating that the BSFL effectively bio-converted agro-waste into biomass, and the treatment efficiency using BSFL was better than typical composting.

Mean larval weight increased from 13.79 ± 0.48 g ww (2.84 ± 0.28 g dw) to 136.86 ± 4.08 g ww (43.9 ± 1.3 g dw) with a larval mass gain over time of 895 ± 94% for a trial of 14 days (Table 1). The average bioconversion rate of T1 is 14.33 ± 0.56% (Table 1). The survival rate was 99.7 ± 0.10%, indicating that the substrate used in this study was suitable.

Our results agree with the other published results regarding waste reduction, bioconversion, and larval survival rates during agro-waste valorization with BSFL. The BSFL can be reared on various organic wastes, including human and livestock fecal, vegetable, and kitchen wastes. It is well-known that the bio-waste to larvae conversion ratio could vary according to feeding rates, differences in substrate characteristics, and larval densities. In previous studies, the substrate reduction rate of organic wastes ranged between 13.2 and 84.8% (Giannetto et al., 2020; Ebeneezar et al., 2021; Arabzadeh et al., 2022), showing the ability of BSFL to convert organic wastes efficiently. While the biomass conversion ratios were 0.2 - 15.2% (Lalander et al., 2019), 8 - 10% (Giannetto et al., 2020), and 6.80% (Ebeneezar et al., 2021). In the present study, the survival rate in BSFL was found to be similar to or higher than those reported in the previous studies (Oonincx et al., 2015; Lalander et al., 2019; Arabzadeh et al., 2022). It has been stated that the diet properties less affect the survival rate in BSFL (Oonincx et al., 2015; Arabzadeh et al., 2022).

Table 1. Effects of composting with or without BSFL on bioconversion efficiency

Parameters	T1		T2	
	Before	After	Before	After
Waste (kg, ww)	2.5	0.643 ± 0.01	2.5	1.53 ± 0.03
Waste (kg, dw)	0.473	0.188 ± 0.003		
Waste reduction (%)	74.3 ± 0.46		38.7 ± 2.31	
Larvae weight (g, ww)	13.79 ± 0.48	136.86 ± 4.08	-	
Larvae weight (g, dw)	2.84 ± 0.28	43.9 ± 1.3	-s	
Bioconversion rate (%)	14.33 ± 0.56		-	
Number of larvae	1,000	997 ± 3.6	-	
Survival rate (%)	99.7 ± 0.10		-	

3.2. Effects of pH and humidity on gas emissions

The pH and moisture content of the compost substrate were monitored throughout the 14-day composting process for both T1 and T2. The initial pH values were similar between the treatments, starting around 8.0 for T1 and T2 (Figure 2). Throughout the composting process, T1 exhibited a slight increase in pH during the first few days, reaching approximately 8.3 by Day 4. This was followed by a relatively stable period where pH values fluctuated minimally, maintaining a range between 7.8 and 8.3 for the remainder of the process. T2, on the other hand, demonstrated a more gradual and consistent decrease in pH, reaching a value of about 7.5 by the end of the experiment. This decline suggests ongoing microbial activity and organic matter

degradation. The pH is a critical factor affecting gaseous emissions and the activity of BSFL and bacteria. The outcomes of this study support the conclusions drawn by Ma et al. (2018) and Meneguz et al. (2018), suggesting that BSFL can change the pH of the substrate to 8.5 - 9.2. Additionally, there is a negative correlation between pH and CO_2 emissions, while a positive correlation exists between pH and NH_3 emissions (Pang et al., 2020a).

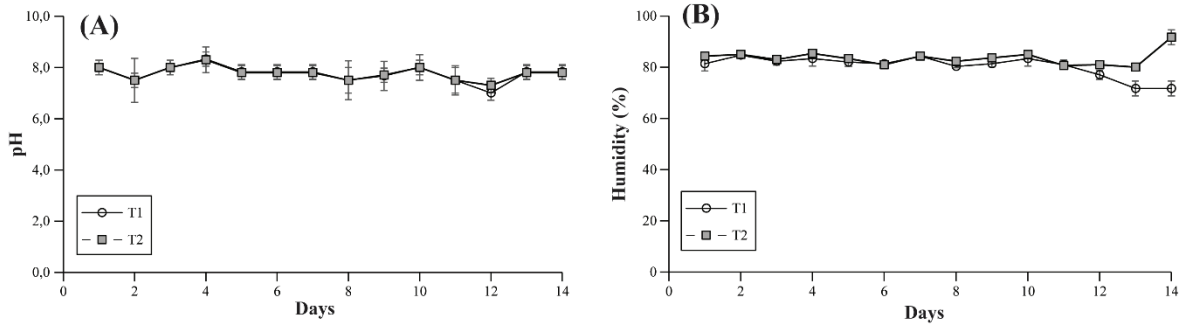

Figure 2. Effects of composting with or without black soldier fly larvae on pH (A) and humidity (B). Error bars represent the standard error of the mean, $n = 3$.

While treatments T1 and T2 maintained relatively high moisture levels, around 80 - 85%. Throughout the composting process, T1 showed a steady moisture content, with only slight fluctuations, mainly remaining stable at around 80% for the first 11 days but eventually dropping to around 72% by the end of the 14 days. On the other hand, T2 experienced a slight decrease in moisture content over time. However, a significant increase in moisture content was observed on Day 14 in T2, rising sharply to approximately 92%.

The high level of moisture (80 - 85%), as in this study, led to abnormal and improper growth of BSFL. Chen et al. (2019) conducted a quantification of GHG and NH_3 emissions from BSFL raised on pig manure under varying moisture conditions. With the increase in water levels from 45% to 75%, the NH_3 emissions increased for the first six days. The treatment at 75% water level showed the second-lowest level of NH_3 releases. Conversely, the NH_3 emissions from the treatments 85% exhibited a gradual increase during the initial six days, followed by a sharp rise in the subsequent two days (Chen et al., 2019). Meanwhile, it was reported that all treatments of moisture content inoculating BSFL reduced total CO_2 emissions compared to conventional composting, except the 75% treatment during the eight-days (Chen et al., 2019).

3.3. Gas emission during composting

Figure 3 shows the emission pattern of NH_3, H_2S, and CO_2 with composting time in three treatments.

3.3.1. The NH_3 emissions

As presented in Figure 3A, the NH_3 gas produced in the control group, T1 and T2 ranged from 128 - 736 mg/m^3, 414 - 2268 mg/m^3, and 414 - 2541 mg/m^3, respectively. The results showed apparent differences between treatments in NH_3 emission levels during 14 days of monitoring. In the T0, NH_3 concentrations remained low throughout the experimental period, indicating that under our laboratory

conditions, NH_3 emissions are minimal. In both composting treatments, NH_3 emissions showed similar trends and were significantly higher than those in T0 ($P < 0.05$). In the first seven days, the NH_3 volatilization rose, then decreased rapidly in the following days and slowly increased until the end of the trial. In general, NH_3 levels released in T2 were relatively higher than in T1. Ammonia emission increased sharply with the substrate added on days 2, 4, 7, and 10, caused by the rapid decomposition of the organic nitrogen compound, and on the 4th and 7th days, the NH_3 production reached its peak. Our research results show that BSFL composting and waste without BSFL significantly increase NH_3 emissions compared to lab background conditions. Additionally, using BSFL in the composting process does not substantially reduce NH_3 emissions compared to composting without BSFL.

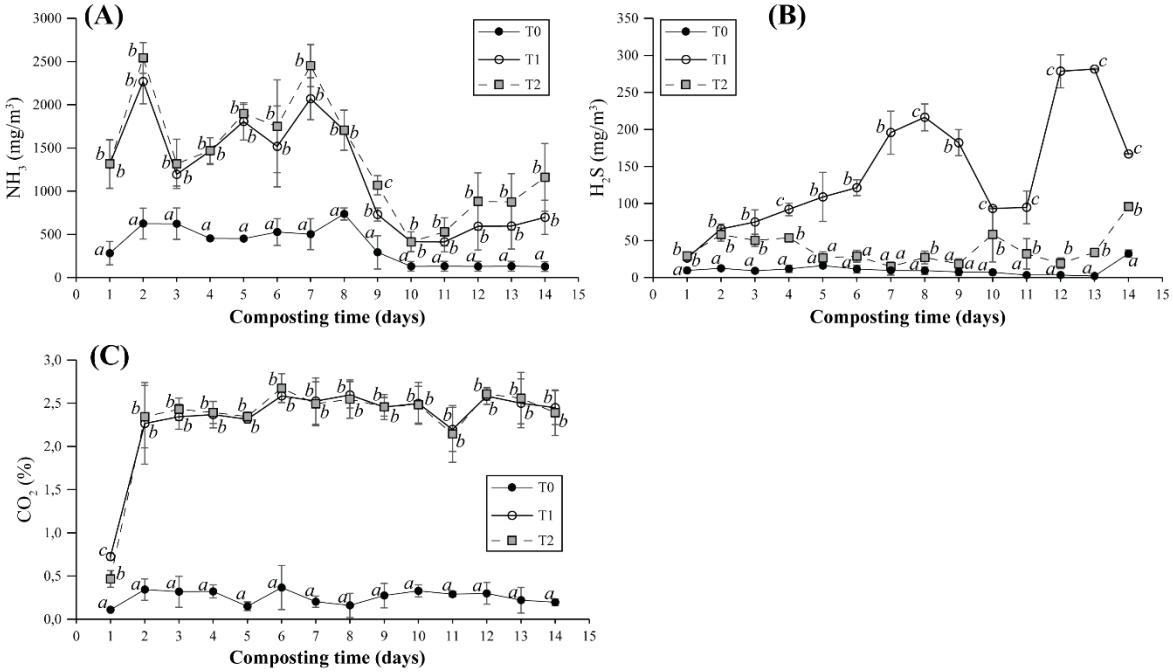

Figure 3. Changes of concentrations of NH_3 (A), H_2S (B), and CO_2 (C) among treatments measured via the static chamber during 14-day composting of agro-waste. Error bars are mean ± SD (n = 3). Different letters above the error bars indicate significant differences at the 0.05 level (ANOVA and Tukey's HSD).

High levels of NH_3 emissions during composting could negatively affect the environment, as NH_3 is a gas that has the potential to pollute the atmosphere and contribute to the formation of acid rain. Lindberg et al. (2022) reported that NH_3 emission in conventional composting was 100-fold higher than in BSFL composting. However, other studies and BSFL mass-production producers have reported high levels of NH_3 emissions in BSFL composting, in the range of 30 - 40% of the input nitrogen (Lalander et al., 2019; Yang, 2019; Lopes et al., 2020).

Nitrogen losses via NH_3 emissions from BSFL composting are one of the critical environmental problems resulting from larval production and affect the quality of the final product as organic fertilizer. Many factors, such as water content,

pH, temperatures, and other physicochemical factors, influence ammonia volatilization (Koerkamp, 1994). As discussed above, the high moisture content enables the absorption of NH_3, which hinders microbial activity and NH_3 emission (Guo et al., 2012; Chen et al., 2019). Furthermore, to avoid NH_3 emission, the equilibrium between NH_4^+ and NH_3 should be maintained by keeping an acidic pH and temperatures below 20°C (Koerkamp, 1994). The higher NH_3 emissions obtained in this study might be due to higher pH, as Chen et al. (2019) indicated.

3.3.2. The H_2S emissions

Figure 3B exhibits the H_2S concentration recorded during the composting trial. The results showed apparent differences between treatments in H_2S emission levels. In the control group (T0), H_2S concentration was kept very low and unchanging throughout the trial time, with values ranging from 2 to 32 mg/m³. While H_2S concentration in treatment T1 increased significantly compared to T0 ($P < 0.05$), starting from day 2 and peaking on day 8 with a value of about 220 mg/m³. After that, the H_2S concentration gradually decreased but remained higher than the control group until the end of the study period. In particular, from day 10th to day 14th, H_2S concentration in T1 increases again, especially on days 12th and 13th. For treatment T2, H_2S levels also increased significantly compared to T0, but the emission level was lower than that of T1. H_2S concentration in T2 peaked around day 4th with a value of about 50 mg/m³, then gradually decreased and fluctuated at a lower level than T1 until the end of the study period.

The study results showed that composting, whether composting with or without BSFL, significantly increased H_2S emissions compared to lab background conditions. The increase in H_2S emissions in treatments T1 and T2 can be explained by the decomposition of sulfur-containing organic compounds in the compost, leading to the release of H_2S gas. Notably, the H_2S concentration in T1 was significantly higher than that in T2, showing that the composting process using BSFL can increase the release of H_2S compared to composting without BSFL. This may be due to the vigorous activity of BSFL in decomposing organic matter, leading to faster and greater release of H_2S. However, these high emissions levels can negatively affect the environment and human health, as H_2S is a toxic gas with an unpleasant odor and can cause many health problems if exposed to high concentrations.

In contrast to available data on GHG and NH_3 emissions via organic waste valorization using BSFL, the published articles provide limited information regarding sulfur compound emissions. Michishita et al. (2023) found that the presence of BSFL led to a notable reduction in the emission of smelly sulfur compounds like dimethyl disulfide and dimethyl trisulfide, which are commonly generated as a result of methionine and cysteine breakdown by *Lactobacillus* and *Enterococcus* bacteria. These findings were very dissimilar from those of our study. The discrepancy might be due to the different experimental conditions.

H_2S is a well-known malodorous gas that is commonly produced in the process of composting organic waste. Several factors, such as moisture content, aeration, and porosity of composts, can be controlled while composting to reduce the generation and release of odor smells (Zhang et al., 2013). The ideal moisture content for developing the composting process was 40 - 60%

(Zhang et al., 2013). Nonetheless, the substrate's moisture level in this study (72 - 85%) was higher than the recommended range, as indicated above. Moreover, the odor gas formation in BSFL composting is typically attributed to poor oxygen transfer from insufficient aeration.

3.3.3. The CO_2 emissions

Figure 3C shows the CO_2 concentration (%) during the experiment. During 14 days of monitoring, the results showed a clear difference in CO_2 emission levels between treatments. The concentration of CO_2 in the control group remained very low, ranging from 0 to 0.4% throughout the study period. Levels of CO_2 in T1 and T2 increased sharply from the first day and finally became relatively stable at approximately 2.5% for the remainder of the study period. These were significantly higher emission levels than the control group, demonstrating the organic decomposition activity in both treatments.

Carbon dioxide is the most significant GHG and is the primary emission generated during the rearing process of BSFL from organic materials (Boakye-Yiadom et al., 2022). Several studies have assessed the CO_2 emissions generated during the rearing of BSFL with different substrates (Pang et al., 2020a; Pang et al., 2020b; Lindberg et al., 2022). Most research indicates that CO_2 levels demonstrated low emissions in the early days, which gradually increased, culminating in peak emission rates during the mid-treatment phase, and a steady decrease in the later stages can be attributed to the stabilization of the substrate and a decline in the metabolic activities of both the bacteria and BSFL (Chen et al., 2019; Pang et al., 2020a).

Compared to these works, our result showed different CO_2 emission patterns. It could be due to a difference in the feeding regime (amount of feed, feeding frequency). In our study, 1,000 7-DOLs were fed five times with a feeding rate of 500 mg ww/larva per day (a feed amount of 2,5 kg ww). In the study of Chen et al. (2019), 450 3-DOLs were fed one time with a feed amount of 160 g dw, while in the study of Pang et al. (2020a; 2020b) 1,600 - 1,800 3-DOLs were fed one time with a feed amount of 1 - 1,2 kg ww.

Several factors, such as the C/N ratio, moisture content, pH, and batch feeding time, may influence the rate of CO_2 emissions during the composting process of BSFL (Boakye-Yiadom et al., 2022). Pang et al. (2020b) reported that with an increasing C/N ratio of the substrate, the CO_2 emissions in BSFL composting were increased. As stated above, an increase in substrate moisture content was negatively associated with emissions of CO_2 (Chen et al., 2019). For pH effects, the emissions of CO_2 were found to be minimal under extreme pH conditions of 3.0 and 11.0, while they peaked at the optimal pH levels of 5.0 and 7.0 (Pang et al., 2020a). Zhang et al. (2021) observed that an increase in batch feeding frequency led to increased CO_2 emissions.

4. Conclusions

The waste reduction rate in the BSFL treatment (74.3%) was approximately twice as high as without BSFL (38.7%). The pH and moisture content of both treatments showed a similar trend. The CO_2 and H_2S emissions in T1 were higher than those in T2, while NH_3 levels released in T2 (414 - 2541 mg/m^3) were relatively higher than in T1 (414 - 2268

mg/m^3). Temperature affects the metabolic activities of BSFL and the microorganisms and gas emissions during composting. Therefore, temperature monitoring should be considered in future studies. Management and control of these gas emissions are necessary to ensure that the composting process does not adversely affect the environment and public health. This suggests that further research is needed to determine the optimal conditions to maximize the environmental benefits of using BSFL in composting.

Conflict of interest

The authors declare that there is no conflict of interest regarding the publication of this paper.

References

Arabzadeh, G., Delisle-Houde, M., Tweddell, R. J., Deschamps, M. H., Dorais, M., Lebeuf, Y., Derome, N., & Vandenberg, G. (2022). Diet composition influences growth performance, bioconversion of black soldier fly larvae: agronomic value and in vitro biofungicidal activity of derived frass. *Agronomy* 12(8), 1765. https://doi.org/10.3390/agronomy12081765.

Barrington, S., Choinière, D., Trigui, M., & Knight, W. (2002). Effect of carbon source on compost nitrogen and carbon losses. *Bioresource Technology* 83(3), 189-194. https://doi.org/10.1016/S0960-8524(01)00229-2.

Boakye-Yiadom, K. A., Ilari, A., & Duca, D. (2022). Greenhouse gas emissions and life cycle assessment on the black soldier fly (*Hermetia illucens* L.). *Sustainability* 14(16), 10456. https://doi.org/10.3390/su141610456.

Coudron, C. L., Berrens, S., Van Peer, M., Deruytter, D., Claeys, J., & Van Miert, S. (2024). Ammonia emissions related to black soldier fly larvae during growth on different diets. *Journal of Insects as Food and Feed* 10(2024), 1469-1483. https://doi.org/10.1163/23524588-00001049.

Chen, J., Hou, D., Pang, W., Nowar, E. E., Tomberlin, J. K., Hu, R., Chen, H., Xie, J., Zhang, J., Yu, Z., & Li, Q. (2019). Effect of moisture content on greenhouse gas and NH_3 emissions from pig manure converted by black soldier fly. *Science of The Total Environment* 697, 133840. https://doi.org/10.1016/j.scitotenv.2019.133840.

Ebeneezar, S., Tejpal, C. S., Jeena, N. S., Summaya, R., Chandrasekar, S., Sayooj, P., & Vijayagopal, P. (2021). Nutritional evaluation, bioconversion performance and phylogenetic assessment of black soldier fly (Hermetia illucens, Linn. 1758) larvae valorized from food waste. *Environmental Technology and Innovation* 23, 101783. https://doi.org/10.1016/j.eti.2021.101783.

Giannetto, A., Oliva, S., Ceccon Lanes, C. F., de Araújo Pedron, F., Savastano, D., Baviera, C., Parrino, V., Lo Paro, G., Spanò, N. C., Cappello, T., Maisano, M., Mauceri, A., & Fasulo, S. (2020). *Hermetia illucens* (Diptera: Stratiomydae) larvae and prepupae: Biomass production, fatty acid profile and expression of key genes involved in lipid metabolism. *Journal of Biotechnology* 307, 44-54. https://doi.org/10.1016/j.jbiotec.2019.10.015.

Guo, R., Li, G., Jiang, T., Schuchardt, F., Chen, T., Zhao, Y., & Shen, Y. (2012). Effect of aeration rate, C/N ratio and moisture content on the stability and maturity of compost. *Bioresource Technology* 112, 171-178. https://doi.org/10.1016/j.biortech.2012.02.099.

GV (The Government of Vietnam). (2022). Decree No. 46/2022/ND-CP dated on July 13, 2022: Amendments to some articles of the Government's Decree No. 13/2020/ND-CP dated January 21, 2020 on elaboration of the law on animal husbandry. Ha Noi, Vietnam. Retrieved June 1, 2024, from https://datafiles.

chinhphu.vn/cpp/files/vbpq/2022/07/46-nd.signed.pdf.

Huis, A. V. (2020). Insects as food and feed, a new emerging agricultural sector: a review. *Journal of Insects as Food and Feed* 6(1), 27-44. https://doi.org/10.3920/JIFF2019.0017.

Jiang, T., Schuchardt, F., Li, G. X., Guo, R., & Luo, Y. M. (2013). Gaseous emission during the composting of pig feces from Chinese Ganqinfen system. *Chemosphere* 90(4), 1545-1551. https://doi.org/10.1016/j.chemosphere.2012.08.056.

Koerkamp, P. W. G. G. (1994). Review on emissions of ammonia from housing systems for laying hens in relation to sources, processes, building design and manure handling. *Journal of Agricultural Engineering Research* 59(2), 73-87. https://doi.org/10.1006/jaer.1994.1065.

Lalander, C., Diener, S., Zurbrügg, C., & Vinnerås, B. (2019). Effects of feedstock on larval development and process efficiency in waste treatment with black soldier fly (*Hermetia illucens*). *Journal of Cleaner Production* 208, 211-219. https://doi.org/10.1016/j.jclepro.2018.10.017.

Lindberg, L., Ermolaev, E., Vinnerås, B., & Lalander, C. (2022). Process efficiency and greenhouse gas emissions in black soldier fly larvae composting of fruit and vegetable waste with and without pre-treatment. *Journal of Cleaner Production* 338, 130552. https://doi.org/10.1016/j.jclepro.2022.130552.

Lopes, I. G., Lalander, C., Vidotti, R. M., & Vinnerås, B. (2020). Using *Hermetia illucens* larvae to process biowaste from aquaculture production. *Journal of Cleaner Production* 251, 119753. https://doi.org/10.1016/j.jclepro.2019.119753.

Ma, J., Lei, Y., Rehman, K. u., Yu, Z., Zhang, J., Li, W., Li, Q., Tomberlin, J. K., & Zheng, L. (2018). Dynamic effects of initial pH of substrate on biological growth and metamorphosis of black soldier fly (Diptera: Stratiomyidae). *Environmental Entomology* 47(1), 159-165. https://doi.org/10.1093/ee/nvx186.

Meneguz, M., Gasco, L., & Tomberlin, J. K. (2018). Impact of pH and feeding system on black soldier fly (*Hermetia illucens*, L; Diptera: Stratiomyidae) larval development. *PLos One* 13(8), e0202591-e0202591. https://doi.org/10.1371%2Fjournal.pone.0202591.

Michishita, R., Shimoda, M., Furukawa, S., & Uehara, T. (2023). Inoculation with black soldier fly larvae alters the microbiome and volatile organic compound profile of decomposing food waste. *Scientific Reports* 13(1), 4297. https://doi.org/10.1038/s41598-023-31388-z.

MOH (Ministry of Health). (1989). Branch standard No. 52 TCN 353-89/BYT: Air quality - Baryta absorption method for determination of carbon dioxide content. Retrieved June 20, 2024, from https://caselaw.vn/van-ban-phap-luat/259575-tieu-chuan-nganh-52-tcn-352-1989-ve-cacbon-oxyt-nam-1989-tinh-trang-hieu-luc-khong-xac-dinh.

Nguyen, T. L., & Cao, T. S. (2024). Current situation of agricultural by-products and management solutions in Vietnam. In *Proceedings of Agricultural and Rural Environment and Sustainable Development* (159-168). Ha Noi, Vietnam: Vietnam National University of Agriculture.

Oonincx, D. G. A. B., van Broekhoven, S., van Huis, A., & van Loon, J. J. A. (2015). Feed conversion, survival and development, and composition of four insect species on diets composed of food by-products. *PLos One* 10 (12), e0144601. https://doi.org/10.1371/journal.pone.0144601.

Pang, W., Hou, D., Chen, J., Nowar, E. E., Li, Z., Hu, R., Tomberlin, J. K., Yu, Z., Li, Q., & Wang, S. (2020a). Reducing greenhouse gas emissions

and enhancing carbon and nitrogen conversion in food wastes by the black soldier fly. *Journal of Environmental Management* 260, 110066. https://doi.org/10.1016/j.jenvman.2020.110066.

Pang, W., Hou, D., Nowar, E. E., Chen, H., Zhang, J., Zhang, G., Li, Q., & Wang, S. (2020b). The influence on carbon, nitrogen recycling, and greenhouse gas emissions under different C/N ratios by black soldier fly. *Environmental Science and Pollution Research* 27(34), 42767-42777. https://doi.org/10.1007/s11356-020-09909-4.

RIBE (Research Institute for Biotechnology and Environment). (2017). *Research on black soldier fly - feeding and management in Vietnam* (research report). Nong Lam University, Ho Chi Minh City, Vietnam.

VS (Vietnam Standards). (1995). Standard No. TCVN 5293 : 1995: Air quality - Indophenol method for determination of ammonia content. Retrieved June 20, 2024, from https://caselaw.vn/van-ban-phap-luat/258473-tieu-chuan-viet-nam-tcvn-5293-1995-st-sev-5299-80-ve-chat-luong-khong-khi-phuong-phap-indophenol-xac-dinh-ham-luong-amoniac-nam-1995.

Wang, Y. S., & Shelomi, M. (2017). Review of black soldier fly (*Hermetia illucens*) as animal feed and human food. *Foods* 6(10), 91. https://doi.org/10.3390/foods6100091.

WHO (World Health Organization). (1981). *Hydrogen sulfide*. Geneva, Switzerland: IPCS International Programme on Chemical Safety.

Yang, F., Li, G., Shi, H., & Wang, Y. (2015). Effects of phosphogypsum and superphosphate on compost maturity and gaseous emissions during kitchen waste composting. *Waste Management* 36, 70-76. https://doi.org/10.1016/j.wasman.2014.11.012.

Yang, S. (2019). *Explanation of an industrial application of black soldier fly converting food waste into valuable products*. Retrieved June 22, 2024, from https://www.evoconsys.com/blog/explanation-of-an-industrial-application-of-black-soldier-fly-converting-food-waste-into-valuable-products.

Zhang, H., Schuchardt, F., Li, G., Yang, J., & Yang, Q. (2013). Emission of volatile sulfur compounds during composting of municipal solid waste (MSW). *Waste Management* 33(4), 957-963. https://doi.org/10.1016/j.wasman.2012.11.008.

Zhang, X., Li, Z., Nowar, E. E., Chen, J., Pang, W., Hou, D., Hu, R., Jiang, H., Zhang, J., & Li, Q. (2021). Effect of batch feeding times on greenhouse gas and NH_3 emissions during meat and bone meal bioconversion by black soldier fly larvae. *Waste and Biomass Valorization* 12(7), 3889-3897. https://doi.org/10.1007/s12649-020-01277-x.

Antimicrobial activity of cashew nut testa extract (*Anacardium occidentale* L.)

Phuong T. Nguyen, Luyen T. L. Nguyen, Mai T. T. Bui, Hau L. M. Nguyen, & Huan T. Phan*
Faculty of Chemical Engineering and Food Technology, Nong Lam University, Ho Chi Minh City, Vietnam

ARTICLE INFO

Research Paper

Received: August 27, 2024
Revised: October 10, 2024
Accepted: October 31, 2024

Keywords

Anacardium occidentale L. testa
Antibacterial activity
MIC
Phytochemical screening
Polyphenols

***Corresponding author**

Phan Tai Huan
Email: pthuan@hcmuaf.edu.vn

ABSTRACT

The cashew nut (*Anacardium occidentale* L.) testa, commonly considered as a by-product of cashew processing, is rich in polyphenols. This research investigated the antimicrobial effects of the cashew nut testa extracts prepared using a mixture of 0.22% cellulase and pectinase (1:1, v/v) with a ratio of raw material to solvent of 1:55 (v/v), an extraction temperature of 49°C and pH 4.0 for 60 min. Phytochemical screening revealed the presence of various phenolic compounds in the testa extract, including saponins, coumarins, triterpenoids, tannins, flavonoids, and alkaloids. The extract's antimicrobial efficacy was assessed against 4 bacterial strains associated with food poisoning: *Bacillus cereus, Staphylococcus aureus*, *Shigella* spp., and *Salmonella typhimurium*. Remarkably, the extract demonstrated inhibitory action against *Staphylococcus aureus*, producing an inhibition zone diameter of 1.00 mm at a concentration of 25 mg/mL and the largest diameter of 12.93 mm at 800 mg/mL. The Minimum Inhibitory Concentration (MIC) values were determined as follows: 200 mg/mL for *Salmonella typhimurium*, 100 mg/mL for both *B. cereus* and *Shigella* spp., and 25 mg/mL for *Staphylococcus aureus*.

Cited as: Nguyen, P. T., Nguyen, L. T. L., Bui, M. T. T., Nguyen, H. L. M., & Phan, H. T. (2024). Antimicrobial activity of cashew nut testa extract (*Anacardium occidentale* L.). *The Journal of Agriculture and Development* 23(Special issue 2), 155-165.

1. Introduction

Food spoilage and its etiological agents have been prevented using chemical preservatives for a long time (Mostafa et al., 2012). Although these chemical preservatives have demonstrated effectiveness in preventing foodborne diseases and controlling outbreaks, their repeated use has led to the accumulation of chemical residues in the food and feed chain, the development of microbial resistance to these chemicals, and adverse side effects on human health (Harris et al., 2018). For this reason, current food processing trends focus on using natural compounds, which are considered safe alternatives and satisfy the consumer preferences for more "green foods". Manufacturers have been searching for safer

natural alternatives like phytochemicals (such as polyphenols, including flavonoids, and essential oils rich in terpenoids, such as carotenoids) (Gutiérrez-del-Río et al., 2021).

Cashew (*Anacardium occidentale* L.) is a member of the *Anacardium* genus of the Anacardiaceae family. It is native to Brazil but is now widely grown in many tropical countries such as Mozambique, Tanzania, Kenya, Indonesia, Thailand, India, and Vietnam (Lubi & Thachil, 2000; Paramashivappa et al., 2001; Das et al., 2004). The cashew apple fruit includes two parts: the true fruit and the false fruit. The false fruit comprises 90% of the whole fruit's weight but is usually discarded during harvest. The true fruit consists of three main parts: the nutshell, testa, and kernel. The testa is considered waste in the cashew nut processing industry (Sruthi & Naidu, 2023). Currently, this by-product is often partially used as animal feed or as fuel for furnaces. Testa constitutes about 1 - 3% of the total weight of cashew nuts and contains biologically active compounds such as (+)-catechin, (-)-epicatechin, epigallocatechin, epigallocatechin gallate, gallic acid, syringic acid, and p-coumaric acid (Sruthi & Naidu, 2023). These compounds exhibit antimicrobial activity against human pathogens (Markus et al., 2017).

There are many methods to extract polyphenols, such as solid-liquid extraction (SLE), pressurized liquid extraction (PLE), ultrasonic-assisted extraction (UAE), microwave-assisted extraction (MAE), and supercritical extraction (SCE) (Ajila et al., 2011). However, in this study, a mixture of cellulase and pectinase, an efficient and eco-friendly method, was used to extract phenolic compounds. Additionally, the disk-diffusion assay was also used in this study. It offers many advantages over other methods, including simplicity, low cost, the ability to test enormous numbers of microorganisms and antimicrobial agents, and the ease of interpreting results provided (Balouiri et al., 2016). The objective of this study was to evaluate the effect of the extraction conditions on total polyphenol content (TPC) and reveal the presence of various phenolic compounds within the cashew nut testa extract. Particularly, the evaluation of the antimicrobial activity of the extract against four bacterial strains: *Bacillus cereus*, *Staphylococcus aureus*, *Shigella* spp., and *Salmonella typhimurium*, respectively, was carried out.

2. Materials and Methods

2.1. Materials

Organic cashew nut testa (CNT) was provided by Hanfimex Group, Binh Phuoc branch. The raw testa included hard shells, broken kernels, and testa, which were products of cashew processing. The raw testa was removed from the broken kernels and hard shells, and the testa was retained. After that, the raw testa was dried at 45°C to a moisture content below 10%, pulverized, and sieved through a 0.5 mm screen to obtain a fine powder. Finally, CNT was packed in silver zip bags and stored in the fridge at 8°C for further use (Figure 1).

Figure 1. Cashew nut testa powders.

2.2. Chemicals

Folin-Ciocalteu reagents were supplied by Merck (Darmstadt, Germany). Standard gallic acid was purchased from Sigma-Aldrich (USA). Enzyme pectinase (P) (4130 U/g) and cellulase (C) (endoglucanase, 774 U/g) were purchased from Novozymes in Singapore. The buffer was a mixture of sodium phosphate monobasic dihydrate (Merck, Germany) and citric acid monohydrate (Fisher, USA). Mueller-Hilton agar (MHA, Merck, Germany) was used as the antibacterial medium. Tryptone Soya Agar (TSA, Merck, Germany) and Tryptone Soya Broth (TSB, Merck, Germany) were used as the culture medium, and Gentamicin (Merck, Germany). Qualitative chemicals, including ethanol (C_2H_5OH), ferric chloride ($FeCl_3$), sulfuric acid (H_2SO_4), chloroform ($CHCl_3$), potassium iodide (KI), and ammonium hydroxide (NH_4OH), all met analytical standards. All other chemicals used were of analytical grade. Analytical water was obtained by a Milli-Q filtration system (Millipore, Bedford, Massachusetts, USA).

2.3. Cashew nut testa extraction preparation

2.3.1. Preparation of sample for phytochemical screening

The qualitative analysis of bioactive compounds in cashew nut testa (CNT) such as saponins, coumarins, triterpenoids, tannins, flavonoids, alkaloids, and phenolic compounds was carried out using methods referenced from studies by Godghate & Sawant (2013), Iqbal et al. (2015), and Singh & Kumar (2017). Firstly, 20 g of cashew nut testa powder sample was prepared and subjected to magnetic stirring extraction using distilled water and absolute 80% ethanol as extract solvents. The extraction was carried out under a vacuum and protected from light, with each solvent having a volume of 200 mL and an extraction time of 48 h. The resulting extract was then vacuum filtered to obtain a pure liquid, which was stored in the fridge at about 4°C until further used. The qualitative results were considered positive when the basic identification reaction for each chemical group was clearly expressed and stable for a certain period. The level of positivity was determined through complementary chemical reactions.

2.3.2. Preparation of cashew nut testa extract

Cashew nut testa was extracted at a temperature of 49°C and pH = 4 for 60 min with a mixture of the C:P enzyme (ratio 1:1) with a concentration of 0.22% and a ratio of CNT: solvent was 1:55 (g/mL), (Dao, 2023). Firstly, the Erlenmeyer flask containing 54 mL of buffer solution (pH = 4) was heated up to 49°C . Then, it was added 1g of cashew nut testa powder and 1 mL of a mixture of C:P enzyme (0.22%). After that, the flask was incubated for 60 min. Then, the temperature of the flask was increased to 90°C and kept for 5 min. After inactivating the mixture of C : P enzyme, the flask was cooled in a cold-water bath (about 10°C). The extract mixture was filtered by vacuum filtration to obtain a clear amber-colored solution. The extract was stored in a dark glass bottle to protect it from light and was placed in the fridge at 8°C for further used.

2.3.3. Preparation of freeze-dried powder of CNT extract

The CNT extract at a concentration of 3.2 - 3.4° Brix was poured into the vials with the appropriate sample amount. The vial was covered with a food wrap and poked at least 5 holes to let the steam escape and limit the liquid overflow into the machine during the drying process. After that, the sample was frozen and placed in the drying rack. The freeze-drying process started when the vacuum reached below 4 mmHg. After 72 h of drying, the lyophilisates were collected and stored in silver zip bags with added silica desiccant to protect them from light as well as moisture and were placed in the fridge at about 8°C for further used.

2.4. Qualitative phytochemical analysis

2.4.1. Saponins

Five mL extract of CNT was mixed with 20 mL of distilled water and then it was agitated in a graduated cylinder for 15 min. The formation of foam indicated the presence of saponin in the sample (Godghate & Sawant, 2013).

2.4.2. Coumarins

Three mL of NaOH 10% was added to 2 mL of aqueous extract of CNT. The yellow colour was formed that showed the presence of coumarins in the sample (Godghate & Sawant, 2013).

2.4.3. Triterpenoids

One mL of the extract of CNT was treated with 1 mL of chloroform and filtered. The filtrate was added with a few drops of concentrated sulphuric acid, shaken, and allowed to stand. If the lower layer turns red, a steroid is present. A golden yellow layer at the bottom indicated the presence of triterpenoids in the sample (Singh & Kumar, 2017).

2.4.4. Tannins

One mL of CNT extract was taken and treated with 1 mL of 10% alcoholic ferric chloride solution. The formation of a blue or greenish colour showed the presence of tannins in the sample (Iqbal et al., 2015).

2.4.5. Flavonoids

The CNT extract was treated with a NaOH 10% solution. The formation of an intense yellow color was observed, indicating the presence of flavonoids in the sample (Godghate & Sawant, 2013).

2.4.6. Alkaloids

Wagner's reagent was formed from a mixture of 2 g of potassium iodide and 1.27 g of iodine, which were dissolved in distilled water to make the final volume 100 mL. Two mL of Wagner's reagent was mixed well with 2 mL of filtrate. The appearance of a brown color indicated the presence of alkaloids in the sample (Iqbal et al., 2015).

2.5. Total phenolic content (TPC)

Determination of the total phenolic content was carried out using the Folin-Ciocalteu test. Firstly, 0.1 mL of the cashew sample diluted with 1.8 mL of Folin-Ciocalteu reagent (10%, v/v) was shaken well and left for 5 min. Then add 1.2 mL of 15% Na_2CO_3 to the solution and make up to 10 mL with distilled water. The mixture was kept in the dark for 90 min, with the absorbance measured at 734 nm in a PhotoLab 6600 UV-Vis spectrophotometer (Jenway 7300, England). A standard curve was generated using different concentrations of gallic acid (R^2 = 0.9983) and distilled water was used as a control. The results were expressed in grams of gallic acid equivalents (GAE) per kilogram of dry weight (DW) (Nguyen et al., 2021).

2.6. Antimicrobial activity test

2.6.1. Disc diffusion assay

The assay was carried out using the disk diffusion method (Balachandran et al., 2013). Four strains of food bacterial pathogens *Bacillus cereus* ATCC 11178, *Staphylococcus aureus* ATCC 6538, *Salmonella typhimurium* ATCC 14028, and *Shigella* spp., were identified by the Quality Measurement Standards Technical Center 3 (QUATEST 3) in Ho Chi Minh City. The Muller-Hinton agar (MHA) plates were inoculated using a sterile swab with bacterial suspensions equal to 0.5 McFarland turbidity. The final concentration of the bacterial suspension was 1.5×10^8 CFU/mL. The lyophylisates of CNT extracts were suspended in distilled water. Standard blank

disks 6.0 mm diameter were placed on media and inoculated with 20 µL of the extract solution. The plates were incubated at 37°C for 24 h. The zone of inhibition was measured. The distilled water was used as a negative control.

2.6.2. Minimum inhibitory concentration (MICs)

The MIC was determined using the sample dilution method. The lyophilisates of cashew nut testa extract were suspended in distilled water at different concentrations of 800, 400, 200, 100, 50, and 25 mg/mL and further fractionated through a sterile membrane. The turbidity of the microbial suspension was adjusted to McFarland 0.5, equivalent to 1.5 x 10^8 CFU/mL. The bacteria were then spread onto MHA agar plates using a sterile cotton swab and allowed to dry. Next, 10 µL of each sample concentration was pipetted onto a sterile paper disc (diameter = 6 mm), dried, and placed on the agar surface with evenly spread bacteria. The paper disc was lightly pressed to secure it onto the agar surface. The positive control was the antibiotic gentamicin, while distilled water was the negative control.

2.7. Statistical analysis

Experiments were arranged with one random factor and three repetitions. The raw data was collected and processed using Microsoft Excel 2020. Statistical analysis was performed using Statgraphics Centurion XVI software (Statpoint Technologies Inc., USA), and differences among groups were analyzed using one-way ANOVA variance analysis, followed by the Multiple Range Test. The criterion for statistical significance was set at $P < 0.05$. The results were shown as mean and standard deviation (Mean ± SD), the differences in mean values were determined using one-way ANOVA at $P < 0.05$ significance level.

3. Results and Discussion

3.1. Qualitative bioactive compounds of cashew nut testa extraction

The qualitative analysis of bioactive compounds in CNT was carried out using water. The qualitative results of bioactive compounds in cashew nut testa extract are presented in Table 1.

Table 1. The results of the qualitative phytochemical compounds from extract of cashew nut testa by water and ethanol

Phytochemical compound	Chemical test	Indicator	Results
Saponins	Froth test	Foam 1 cm form that lasted for 10 min	+
Triterpenoids	Salkowski test	Appearance of red-brown colour	+
Tannins	Braemer's test	Greenish grey	+
Flavonoids	Ammonium test	A layer of yellow color-ation at the bottom	+
Alkaloids	Wagner's test	Formation of brown precipitate	+
Coumarins	Three mL of 10% NaOH was added to 2 mL of aqueous extract of CNT.	Formation of yellow colour	+

Results (+) are means of the presence of phytochemical compounds; CNT: Cashew nut testa.

According to Godghate & Sawant (2013), the presence of foam up to 1 cm above the mixture for 2 - 3 min was indicative of the presence of saponins (Figure 2a). The control sample (test tube No. 0) showed no observable phenomenon. However, the sample extracted with water (test tube No. 1) produced a thin layer of foam that lasted for 10 min. Similarly, the sample extracted with ethanol (test tube No. 2) also formed a thin layer of foam that lasted for 10 min, but it also caused turbidity due to the excess ethanol reacting with water. This indicates that saponin was present in both samples of extract, with clear positive results.

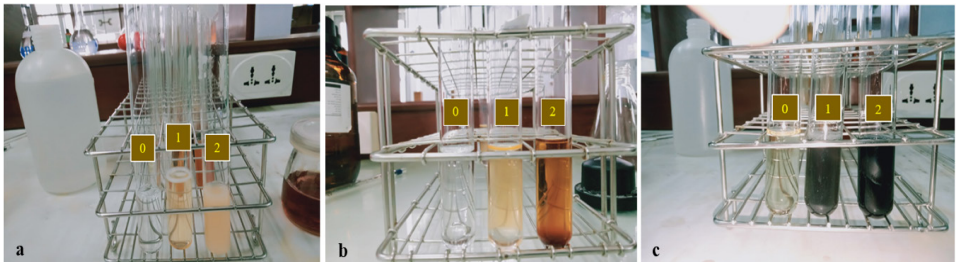

Figure 2. Results of test for saponins (a), triterpenoids (b) and tannins (c) in cashew nut testa. extract. Test tube No. 0 contained the control sample, test tube No. 1 contained the sample extracted with water, and test tube No. 2 contained the sample extracted with ethanol.

The results in Figure 2b show a separation between water and non-polar solvent (test tube No. 0), and a separation of light yellow (test tube No. 1) and brownish yellow at the bottom (test tube No. 2). These are indicators of the presence of triterpenoids in the extract.

Figure 2c showed a colour change in the control sample due to the colour of the reagent (test tube No. 0), green appeared in the sample extracted with water (test tube No. 1) and grey-blue appeared in the sample extracted with ethanol (test tube No. 2). These are indicators showing the presence of tannins in the extract. In Figure 3a, sample zero did not show any colour change, but samples 1 and 2 showed a change from clear yellow to dark yellow and from brownish yellow to dark brown, respectively. This result indicated the presence of flavonoids in both extracts.

Upon observation of Figure 3b, it was evident that sample zero contained a yellow colour, which was the colour of the reagent. Sample 1 showed a subtle colour change, while sample 2 changed from a light brown to a dark brown and became opaque. These changes indicated the presence of alkaloids in both extracts. Based on these indicators, it can be concluded that both extracts contain alkaloids.

Figure 3. Results of test for flavonoids (a), alkaloids (b) and coumarins (c) in cashew nut testa extract. Test tube No. 0 contained the control sample, test tube No. 1 contained the sample extracted with water, and test tube No. 2 contained the sample extracted with ethanol.

Figure 3c showed that sample zero did not exhibit any change, while samples 1 and 2 showed cloudiness at stage A, which gradually decreased at stage B. This indicated the presence of coumarins in both extracts.

In short, the findings indicated that all six bioactive compounds were detected in various samples of cashew nut testa extracted with either water or ethanol. The components found in CNT extracts, including alkaloids, flavonoids, tannins, saponins, triterpenoids, and coumarins, were the primary phenolic compounds that have also been found in extracts of numerous other plants.

Qualitative analysis of some bioactive components of the methanolic leaf extract of *M. citrifolia* (Aishatu et al., 2020) showed the presence of tannins, steroids, saponins, flavonoids, and alkaloids. These results agreed with the findings of preliminary phytochemical screening of crude plant extracts from *Ephedra intermedia* indigenous to Balochistan (Gul et al., 2017). The phytochemical analysis showed that the *Ephedra intermedia* plant extract contains a mixture of phytochemicals such as reducing sugars, cardiac glycoside, phenolic compounds, flavonoids, and alkaloids (Gul et al., 2017). Additionally, a wide variety of bioactive compounds such as alkaloids, saponins, coumarins, flavonoids, terpenoids, and tannins were found to be present in the leaves of *Annona squamosa* Linn. *(custard apple)* (Nguyen et al., 2020).

The extract contained most of the polyphenols present in the CNT. These are important polyphenols in plant cells. According to Abbas et al. (2017), they play a role in fighting pathogens from microorganisms, preventing harmful oxidation reactions, and protecting plants from the effects of ultraviolet radiation. In addition, polyphenols also have a positive effect in the treatment of diseases related to the cardiovascular system, nerves, cancer, osteoporosis, and diabetes (D'Archivio et al., 2007).

3.2. Total phenolic content of CNT extracts

In this study, the total phenolic content (TPC) of the cashew nut testa extract was determined. The results revealed a TPC of 240.06 ± 1.03 mg GAE/g DW, which was also similar to some other studies. Studies have shown that CNC (cashew nut shell) contains a significant amount of phenolic compounds, as evaluated by Mazzetto et al. (2008) in their study on ethanol extracts directly obtained from the seed coat. The concentration of total phenols in these extracts was found to be approximately 185.44 mg/gallic acid equivalent (GAE). This result is consistent with the findings of Kamath & Rajini (2007), who also used ethanol to extract phenolic compounds from the seed coat. They observed a higher total phenolic content (243 mg/GAE) when the extraction was performed under stirring at 37°C for 3 h, compared to the ethanolic extract at room temperature. These results suggest that the cashew nut shell is a rich source of phenolic compounds, which could potentially be explored for their antibacterial activity against pathogenic strains.

3.3. Antimicrobial activity

The antibacterial activity of the CNT extract was evaluated using the disc diffusion method, as indicated by the antibacterial rings around the test paper circle. Results are presented in Figure 4.

Figure 4 shows that Gentamicin has a strong antibacterial ability against 4 tested bacterial strains. Specifically, Gentamicin is more sensitive to G+ bacteria such as *S. aureus*, and *B. cereus* than to G– bacteria such as *S. typhimurium*, *Shigella* spp.

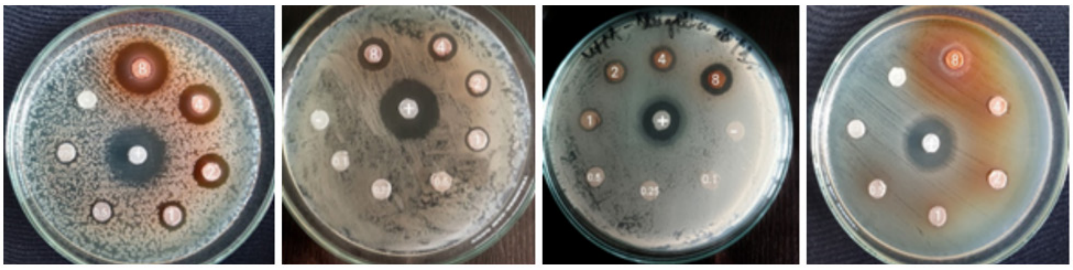

A) B) C) D)

Figure 4. Antimicrobial activity of the phenolic compounds on food-borne pathogens (A) *Shigella* spp. (B) *B. cereus* (C) *S. aureus* (D) *S. typhimurium*.

Additionally, Table 2 showed the antibacterial activity of CNT extract against *S. typhimurium, B. cereus, Shigella* spp., and *S. aureus* were found in the range of 25 - 200 mg/mL. The highest zone of inhibition was obtained for *S. aureus* and the lowest for *S. typhimurium*. Based on the antibacterial activity of the CNT extract, the minimum inhibitory concentration (MIC) values were performed using the broth dilution microplate method. The CNT extract controlled the growth of *S. aureus* with MIC of 25 mg/mL, *B. cereus* and *Shigella* spp. with MIC of 100 mg/mL, and *S. typhymurium* with MIC of 200 mg/mL. The maximum inhibition zone diameter was exhibited by CNT extract against *Staphylococcus aureus* (12.93 mm), *Bacillus cereus* (7.67 mm), *Shigella* spp. (7.08 mm), and *Salmonella typhimurium* (3.93 mm) at 800 mg/mL concentration.

Table 2. Antibacterial activities profile of cashew nut testa extract

Concentration of cashew nut testa extract (mg/mL)	*Diameter of inhibition zone (mm)*			
	Bacillus cereus	*Salmonella typhimurium*	*Staphylococcus aureus*	*Shigella* spp.
Gentamycin (1 mg/mL)	$14.17^{a} \pm 0.14$	$9.67^{a} \pm 0.01$	$15.00^{a} \pm 0.04$	$11.17^{a} \pm 0.14$
800S	$7.67^{b} \pm 0.14$	$3.93^{b} \pm 0.05$	$12.93^{b} \pm 0.03$	$7.08^{b} \pm 0.14$
400	$4.42^{c} \pm 0.14$	$1.79^{c} \pm 0.04$	$8.77^{c} \pm 0.03$	$4.08^{c} \pm 0.14$
200	$3.50^{d} \pm 0.00$	$0.67^{d} \pm 0.02$	$5.66^{d} \pm 0.03$	$2.83^{d} \pm 0.14$
100	$2.33^{e} \pm 0.14$	-	$2.66^{e} \pm 0.03$	$1.50^{e} \pm 0.00$
50	-	-	$1.77^{f} \pm 0.03$	-
25	-	-	$1.00^{g} \pm 0.03$	-
10	-	-	-	-
Distilled water	-	-	-	-

$^{a-g}$values are means of three replicates, and those with different letters within the same column are the difference is statistically significant; "–": Resistance.

The antibacterial ability of cashew nut testa extract may come from bioactive compounds such as tannins, catechins, saponins, and coumarins (Oliveira et al., 2015). According to Farha et al. (2020), tannins are natural compounds that have the potential to replace antibiotics due to their good antibacterial ability. Tannins inhibit bacterial growth through the following mechanisms: tannins form complexes with iron from the environment so that bacteria cannot use iron; inactivate enzymes involved in cell wall synthesis, inhibiting bacterial cell wall synthesis; bind directly to the peptidoglycan layer and destroy the integrity of the cell wall; form hydrogen bonds with membrane proteins, leading to changes in the permeability of the cell membrane, causing the membrane to denature and be destroyed (Dong et al., 2018; Salehi et al., 2019).

4. Conclusions

This study's findings revealed the presence of various phytochemical compounds in the cashew nut testa extract, including saponins, coumarins, triterpenoids, tannins, flavonoids, and alkaloids, as determined through phytochemical screening. The antimicrobial results demonstrated that the CNT extracts had significant antimicrobial efficacy against four bacterial strains known for causing food poisoning: *Bacillus cereus*, *Staphylococcus aureus*, *Shigella* spp., and *Salmonella typhimurium*. Notably, the extract showed inhibitory action against *Staphylococcus aureus*, with an inhibition zone diameter of 1.00 mm at a concentration of 25 mg/mL and the largest diameter of 12.93 mm at 800 mg/mL. The Minimum Inhibitory Concentration (MIC) values were determined to be 200 mg/mL for *Salmonella typhimurium*, 100 mg/mL for both *B. cereus* and *Shigella* spp., and 25 mg/mL for *Staphylococcus aureus*. However, the antibacterial activity of the extract was only evident at a high concentration of 800 mg/mL. Therefore, the antibacterial results of this study may not apply to food preservation in practical settings. Nevertheless, our findings are crucial as a foundation for further research on cashew nut testa and other similar materials.

Conflict of interest

The authors declare no conflict of interest.

Acknowledgements

This research was financed by Project B2022 - NLS- 02 (Vietnam's Ministry of Education and Training). We would like to thank Anh Dang Thi Ngoc, Mi Nguyen Diem and Hue Do Thi Kim for their support in preparing cashew nut testa extracts and antibacterial test samples.

References

Abbas, M., Saeed, F., Anjum, F. M., Afzaal, M., Tufail, T., Bashir, M. S., Ishtiaq, A., Hussain, S., & Suleria, H. A. R. (2017). Natural polyphenols: An overview. *International Journal of Food Properties* 20(8), 1689-1699. https://doi.org/10.1080/10942912.2016.1220393.

Ajila, C. M., Brar, S. K., Verma, M., Tyagi, R. D., Godbout, S., & Valéro, J. R. (2011). Extraction and analysis of polyphenols: recent trends. *Critical Reviews in Biotechnology* 31(3), 227-249. https://doi.org/10.3109/07388551.2010.513677.

Balachandran, C., Duraipandiyan, V., Balakrishna, K., Sundaram, R. L., Vijayakumar, A., Ignacimuthu, S., & Al-Dhabi, N. A. (2013). Synthesis and medicinal properties of plant-derived

vilangin. *Environmental Chemistry Letters* 11, 303-308. https://doi.org/10.1007/s10311-013-0408-4.

Balouiri, M., Sadiki, M., & Ibnsouda, S. K. (2016). Methods for in vitro evaluating antimicrobial activity: A review. *Journal of Pharmaceutical Analysis* 6(2), 71-79. https://doi.org/10.1016/j.jpha.2015.11.005.

Dao, T. M. T. (2024). *Optimizing the process of extracting polyphenol from cashew nut testa using a mixture of cellulase and pectinase enzymes* (Unpublished master's thesis). Nong Lam University, Ho Chi Minh City , Vietnam

D'Archivio, M., Filesi, C., Benedetto, R. D., Gargiulo, R., Giovannini, C., & Masella, R. (2007). Polyphenols, dietary sources and bioavailability. *Annali-Istituto Superiore di Sanita* 43(4), 348.

Das, P., Sreelatha, T., & Ganesh, A. (2004). Bio oil from pyrolysis of cashew nut shell-characterisation and related properties. *Biomass and Bioenergy* 27(3), 265-275. https://doi.org/10.1016/j.biombioe.2003.12.001.

Dong, G., Liu, H., Yu, X., Zhang, X., Lu, H., Zhou, T., & Cao, J. (2018). Antimicrobial and anti-biofilm activity of tannic acid against Staphylococcus aureus. *Natural Product Research* 32(18), 2225-2228. https://doi.org/10.1080/14786419.2017.1366485.

Farha, A. K., Yang, Q. Q., Kim, G., Li, H. B., Zhu, F., Liu, H. Y., Gan, R. Y., & Corke, H. (2020). Tannins as an alternative to antibiotics. *Food Bioscience* 38, 100751. https://doi.org/10.1016/j.fbio.2020.100751.

Godghate, A., & Sawant, R. (2013). Qualitative phytochemical analysis of chloroform extract of leaves of *Adhatoda vasica* Nees. *Rasayan Journal of Chemistry* 6(2), 107-110.

Gul, R., Jan, S. U., Faridullah, S., Sherani, S., & Jahan, N. (2017). Preliminary phytochemical screening, quantitative analysis of alkaloids, and antioxidant activity of crude plant extracts from *Ephedra intermedia* indigenous to Balochistan. *The Scientific World Journal* 2017(1), 5873648. https://doi.org/10.1155/2017/5873648.

Gutiérrez-del-Río, I., López-Ibáñez, S., Magadán-Corpas, P., Fernández-Calleja, L., Pérez-Valero, Á., Tuñón-Granda, M., Miguélez, E. M., Villar, C. J., & Lombó, F. (2021). Terpenoids and polyphenols as natural antioxidant agents in food preservation. *Antioxidants* 10(8), 1264. https://doi.org/10.3390/antiox10081264.

Harris, S. J., Cormican, M., & Cummins, E. (2012). Antimicrobial residues and antimicrobial-resistant bacteria: impact on the microbial environment and risk to human health-A review. *Human and Ecological Risk Assessment: An International Journal* 18(4), 767-809. https://doi.org/10.1080/10807039.2012.688702.

Iqbal, E., Salim, K. A., & Lim, L. B. (2015). Phytochemical screening, total phenolics and antioxidant activities of bark and leaf extracts *of Goniothalamus velutinus* (Airy Shaw) from Brunei Darussalam. *Journal of King Saud University-Science* 27(3), 224-232. https://doi.org/10.1016/j.jksus.2015.02.003.

Kamath, V., & Rajini, P. S. (2007). The efficacy of cashew nut (*Anacardium occidentale* L.) skin extract as a free radical scavenger. *Food Chemistry* 103(2), 428-433.

Lubi, M. C., & Thachil, E. T. (2000). Cashew nut shell liquid (CNSL)-A versatile monomer for polymer synthesis. *Designed Monomers and Polymers* 3(2), 123-153. https://doi.org/10.1163/156855500300142834.

Markus, J., Wang, D., Kim, Y. J., Ahn, S., Mathiyalagan, R., Wang, C., & Yang, D. C. (2017). Biosynthesis, characterization, and bioactivities evaluation

of silver and gold nanoparticles mediated by the roots of Chinese herbal *Angelica pubescens* Maxim. *Nanoscale Research Letters* 12, 1-12. https://doi.org/10.1186/s11671-017-1833-2.

Mazzetto, S. E., Lomonaco, D., & Mele, G. (2008). Cashew nut oil: Opportunities and challenges in the context of sustainable industrial development. *Quimica Nova* 32(3), 732-741. https://doi.org/10.1590/S0100-40422009000300017.

Mostafa, A. A., Al-Askar, A. A., Almaary, K. S., Dawoud, T. M., Sholkamy, E. N., & Bakri, M. M. (2018). Antimicrobial activity of some plant extracts against bacterial strains causing food poisoning diseases. *Saudi Journal of Biological Sciences* 25(2), 361-366.

Nguyen, M. T., Nguyen, V. T., Le, V. M., Trieu, L. H., Lam, T. D., Bui, L. M., Nhan, L. T. H., & Danh, V. T. (2020). Assessment of preliminary phytochemical screening, polyphenol content, flavonoid content, and antioxidant activity of custard apple leaves (Annona squamosa Linn.). *IOP Conference Series: Materials Science and Engineering* 736(6), 062012. https://doi.org/10.1088/1757-899X/736/6/062012.

Nguyen, T. T., Tran, T. P. N., Phan, T. H., Tran, T. A. T., & Nguyen, T. T. (2021). Physicochemical properties, antioxidant and antibacterial activities of spray-dried powder and custard apple peel extract (*Annona squamosa L.*). *Journal of Science and Technology-IUH* 49(01), 57-66.

Oliveira, N. F., Leal, R. S., & Dantas, T. N. C. (2015). The importance of the cashew nut (*Anacardium occidentale* L.) coat: A review. *American International Journal of Contemporary Scientific Research* 2(8), 09-41.

Paramashivappa, R., Kumar, P. P., Vithayathil, P. J., & Rao, A. S. (2001). Novel method for isolation of major phenolic constituents from cashew (*Anacardium occidentale* L.) nut shell liquid. *Journal of Agricultural and Food Chemistry* 49(5), 2548-2551. https://doi.org/10.1021/jf001222j.

Salehi, B., Gültekin-Özgüven, M., Kırkın, C., Özçelik, B., Morais-Braga, M. F. B., Carneiro J. N. P., Bezerra, C. F., Silva, T. G., Coutinho, H. D. M., Amina, B., Armstrong, L., Selamoglu, Z., Sevindik, M., Yousaf, Z., Sharifi-Rad, J., Muddathir, A. M., Devkota, H. P., Martorell, M., Jugran, A. K., Martins, N., & Cho, W. C. (2019). Anacardium plants: chemical, nutritional composition and biotechnological applications. *Biomolecules* 9(9), 465. https://doi.org/10.3390/biom9090465.

Singh, V., & Kumar, R. (2017). Study of phytochemical analysis and antioxidant activity of *Allium sativum* of Bundelkhand region. *International Journal of Life-Sciences Scientific Research* 3(6), 1451-1458. http://dx.doi.org/10.21276/ijlssr.2017.3.6.4.

Sruthi, P., & Naidu, M. M. (2023). Cashew nut (*Anacardium occidentale* L.) testa as a potential source of bioactive compounds: A review on its functional properties and valorization. *Food Chemistry Advances* 3, 100390. https://doi.org/10.1016/j.focha.2023.100390.

Effect of gelatin, fermentation temperature, starter culture ratio on physicochemical properties of peanut kefir

Dung T. N. Dang
Faculty of Chemical and Food Technology, HCMC of Univeristy of Technology and Education, Ho Chi Minh City, Vietnam

ARTICLE INFO

Research Paper

Received: August 21, 2024
Revised: November 02, 2024
Accepted: November 15, 2024

Keywords

Rheology
SEM
Shear stress
Viscosity

***Corresponding author**

Dang Thi Ngoc Dung
Email:
dzungdang@hcmute.edu.vn

ABSTRACT

Peanuts *(Arachis hypogaea)* are highly nutritious exerting health benefits such as preventing malnutrition, reducing heart disorders, and potentially prevent certain types of cancer. Kefir is one of the fermented dairy products containing probiotics and renowned for its beneficial effects on human health. This study aimed to evaluate the effects of gelatin concentration, fermentation temperature, and starter culture ratios on pH, the rheological properties, texture properties, and SEM (scanning electron microscope) of peanut kefir. The rheological properties of Peanut kefir exhibited pseudo-plastic behavior ($0 < \eta < 1$) and weak gel properties. Peanut kefir's rheological characteristics (viscosity, shear stress) and texture properties (hardness, adhesiveness, adhesive force) changed with gelatin content, fermentation temperature, and starter culture ratio. The FTIR spectrum of the gel peanut kefir sample was similar to that of the control sample. The optimal conditions for producing peanut kefir were 0.5% gelatin content, fermentation temperature of 25°C for 13 h, and a 5% starter culture ratio, resulting in a smooth kefir surface structure and a well-bound kefir gel. The SEM images revealed that the experimental sample exhibited a stable gel texture and no layer separation compared to the control sample. Generally, gelatin content, fermentation temperature, and starter culture ratio significantly influenced the quality of peanut kefir.

Cited as: Dang, D. T. N. (2024). Effect of gelatin, fermentation temperature, starter culture ratio on physicochemical properties of peanut kefir. *The Journal of Agriculture and Development* 23(Special issue 2), 166-182.

1. Introduction

Kefir is a fermented dairy product containing probiotics, and it can be fermented by kefir grains (Saygili et al., 2022; Bourrie et al., 2023). Kefir grain, a natural starting culture, comprises several lactic acid bacteria, acetic acid bacteria, and yeasts encased in a polysaccharide matrix (Stadie et al., 2013). Kefir shows its beneficial effects on human health (Egea et al., 2022). Kefir grains' microbiota generates fatty acids, peptides, organic acids, and bacteriocins that can bind mycotoxin and have antibacterial and antifungal properties (González-Orozco et al., 2022). In addition to its antibacterial, antimutagenic, anticarcinogenic, wound-healing, cholesterol-lowering, allergy, and lactose intolerance-preventing qualities, traditional kefir is good for the immune and digestive/gastrointestinal systems. Moreover, studies using kefir have shown promise in promoting increased colon *bifidobacteria* and glycemic control because it has high α-glucosidase inhibitory activity and balances intestinal microbiota (Egea et al., 2022). Kefir's distinct flavor is derived from a complex microecological environment that is created by the breakdown of lactose, protein, and fat in milk into galactose, lactic acid, exopolysaccharides, vitamins, free amino acids, free fatty acids, volatile alcohols, aldehydes, ketones, and esters (Xiao et al., 2023). Lactic and acetic acid-producing bacteria, lactose fermentation, and alcoholic yeast produce these compounds (González-Orozco et al., 2022; Xiao et al., 2023).

Peanuts are a legume belonging to the family *Fabaceae*, the genus *Arachis*, and the scientific name *Arachis hypogaea*, originating in Central and South America (Settaluri et al., 2012). They are widely grown in India, South America, China and elsewhere. Peanuts are considered an important nutritional source because they are a rich source of protein and essential amino acids, which can help prevent malnutrition, reduced heart disorders, certain types of cancer (Syed et al., 2021). Furthermore, peanuts contain rich compounds of lipids (Dwivedi et al., 2014) and carbohydrates, capable of supplementing the energy needs of the human body (Settaluri et al., 2012). Furthermore, recent research has shown the importance of the phytonutrient content of peanuts, including phytosterols, phenolic acids, isoflavonoids, and resveratrol, which may improve general health and wellness (Dwivedi et al., 2014).

Kefir is a popular fermented milk product worldwide; however, it is fermented from plant milk and has yet to be popular. Kefir is a new product in the Vietnamese market and is less popular than yogurt. The ultimate chemical-physical qualities and sensory quality of kefir are determined by fermentation parameters, which include temperature, time, starter culture ratio, and gelatine content. Research indicates that rheological and textural characteristics significantly impact kefir quality; nevertheless, there is little research on the subject, particularly regarding nut kefir.

This study examined the effects of gelatin concentration, fermentation temperature, and kefir culture ratio on pH value and peanut kefir's rheological-textural properties. Based on the rheological behaviors of *peanut kefir*, manufacturers will choose suitable methods, techniques, and equipment for the production process.

2. Materials and Methods

2.1. Raw materials

Sucrose and mature peanut seeds were purchased from Coop supermarket. Peanuts had characteristic color, no strange smell, no mold or weevils, and an oval shape of about 4 ÷ 10 mm. Gelatin was obtained from Louis Francois, France. Kefir starter culture with 6.8 x 10^{10} CFU/g was purchased from Yogourmet, France. Chemical materials were purchased from China's Xilong Scientific Co., Ltd.

Figure 1. Peanut seeds.

2.2. Research methods

2.2.1. Preparing peanut milk

The peanuts (Figure 1) were cleaned and soaked in water for 5 h. Then, they were crushed using a blender (Philips HR3041/00, Holland) and filtered through a clean muslin cloth to remove residual hull particles. The solution was homogenized at 7000 rpm in 10 min (T18 digital ULTRA-TURRAX® – IKA, Germany). Milk from the separated peanuts was pasteurized at 85°C for 10 **min**, cooled at 25°C quickly, and stored at 4°C.

2.2.2. Preparing kefir culture

Kefir grains were obtained from commercial kefir grains with identified lactic acid bacteria strains such as *Lactococcus cremoris*, *Streptococcus cremoris*, *Lactobacillus plantarum*, and the yeast (*Saccharomyces cerevisiae)*. Kefir strains were commercial strains activated in unsweetened fresh cow's milk at 5 g/1000 mL (w/v). The inoculated culture containing commercial strains was incubated at 37°C for 24 h under sterile conditions. Afterward, the kefir culture was kept at 4°C for later use.

2.2.3. Preparing peanut kefir

Peanut milk (containing 9% total solids) mixed with 3% (w/v) sucrose. Subsequently, gelatin was added to the mixture at concentrations of 0.3, 0.5, and 0.7% (w/v). The mixture was heated at 85°C for 5 min, then cooled to 25°C. Kefir culture was added with the ratio of 1, 3, 5, 7, and 9% (v/v) of the peanut milk. The inoculum was poured into 100 mL sterilized glass bottles and incubated at 23, 25, 27, and 29°C until pH = 4.6 was reached.

2.3. Methods

pH: The pH value of kefir samples was measured every hour of incubation using a previously calibrated digital pH meter (HANNA). pH meter was calibrated with a pH buffer of 7.00 and a pH of 4.00 before the kefir samples were measured; the sample's pH was determined by immersing the probe directly into a homogenized kefir sample.

Determination of protein content: Protein content was determined according to the method of Mæhre et al. (2018).

Determination of fat content: Fat content was determined based on the research method of AOAC 905.02 (2000).

Dynamic rheology measurements

The experiment was based on the method given by Gul et al. (2018). HAAKE RheoStress

RS600, USA, viscoelastic measurements were taken in a controlled strain rheometer. The plates were set up in a parallel geometric configuration (PP35, ø = 20 mm) with a measuring gap of 0.5 mm. The shear stress, and apparent viscosity test was performed at 25°C with shear rates from 0.01 ÷ 100s^{1}. As a result, Ostawwld - de Waele equations can be used to fit each set of data as follows: η_{app} = K. γ (n-1).

Whereas η_{app}: apparent viscosity (Pas); k: consistency coefficient (Pa sn); γ: shear sweep (1/s); n: flow behavior index.

Textural properties

The textural characteristics of peanut kefir samples were analyzed using the Texture Analyzer, CT3TM (BROOKFIELD, USA). The textural characteristics such as hardness (g. force), adhesiveness (mJ), and adhesive force (g. force/s) were measured using a spreadability probe with a cylinder 12.7 mm at 25 ± 1°C. The equipment was set to 0.5 mm/s test speed, 10 mm distance, and trigger force = 5 g. The instrument software examined the textural data (force vs. time) and parameters. The tests were done in triplicates, and the results were expressed as mean standard ± error.

Fourier transform infrared spectroscopy (FTIR)

The determination of FTIR was based on the research method of Chen et al. (2015). The TIR analysis aimed to identify the functional groups in kefir products. Before measuring the infrared spectrum, the samples were deep-frozen and freeze-dried for 24 h to collect dried kefir powder. FTIR spectra of kefir samples were recorded by scanning the transmittance from wavenumbers 4000 ÷ 400 cm^{-1} with a resolution of 4 cm^{-1}.

Scanning electron microscope (SEM)

Measuring kefir microstructure with SEM followed a method described by (Xiao et al., 2023) using an SEM-type TS1000PLUS (Hitachi, Japan) with 100-time magnification and 10 kV. The control sample (CS) was used to compare the differences in microstructure images of the studied peanut kefir.

2.4. Data analysis

All experiments were repeated three times. Data were analyzed and statistically processed using the ANOVA test on the Origin 2024b software platform.

3. Results and Discussion

Table 1 shows the means of the chemical composition of peanut milk samples used to produce kefir.

Table 1. Chemical composition of peanut milk

No.	Criteria	Content (g/100 mL)
1	Protein	8.2 ± 0.19
2	Lipid	13.65 ± 0.26
3	Carbohydrate	24.4 ± 0.54

Mean value from triplicate means± standard deviation.

According to Diarra et al. (2005), the quality assessment of peanut milk revealed a protein content of at least 8%, indicating its high quality. The protein analysis of the experimental samples yielded a protein content of 8.2%. Therefore, the protein content of peanut milk samples was suitable for kefir fermentation. In addition, peanut's protein content is significant for fermented products' physical and structural properties. Therefore, the peanut milk not only meets the quality criteria for further studies but also improves the structure of the finished peanut kefir product for further studies.

The effect of added gelatin content on and rheological - textural properties

Gelation addition may improve the quality of the kefir. The results showed a significant improvement in the gel texture of kefir products with added gelatin; the product did not dehydrate and prevent water separation; the gel network formed had a smooth texture; and viscosity tended to increase compared to CS (Figure 2). In particular, with samples supplemented with higher gelatin content, the coagulated gel blocks formed in the product had good adhesiveness, did not break, and the amount of whey separated was also less.

Gelatin was one of the most critical factors influencing kefir's rheological properties (Said, 2020). As a thixotropic gel, yogurt's shear thickening qualities lead its viscosity to frequently reduce during mixing, recover some of its previous structure, and then increase when shearing stops. The steady-state rheological behavior of peanut kefir at selected gelatin levels (0, 0.3, 0.5, 0.7%) is shown in Figure 2a. In contrast, the effect of gelatin levels on the apparent viscosity behavior is shown in Figure 2b. The Ostawwld - de Waele model explained the rheological behavior of kefir well.

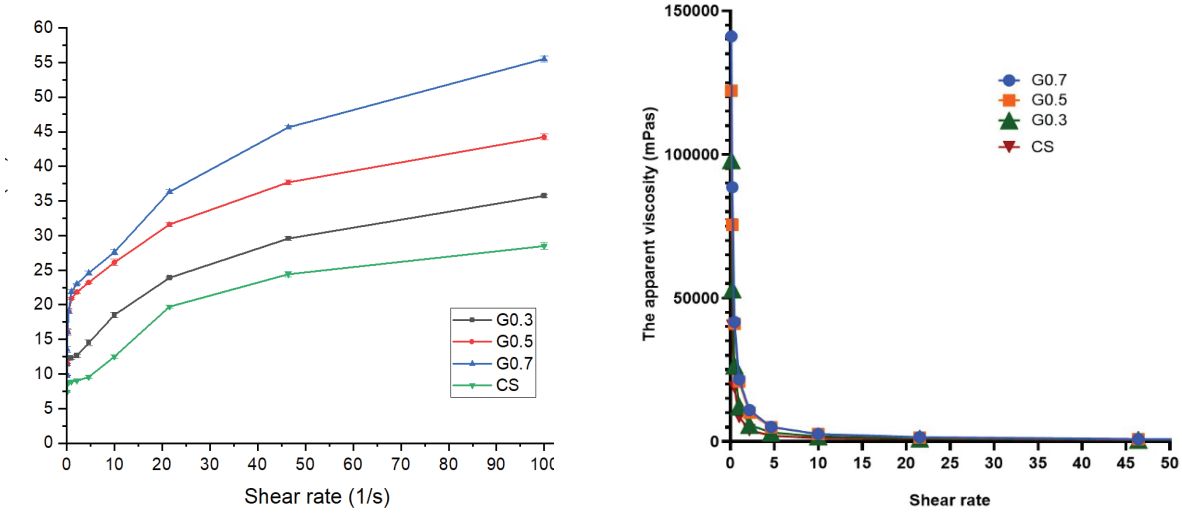

Figure 2. (a) Shear stress at various gelatin levels: 0, 0.3, 0.5, 0.7%; and (b) the apparent viscosity of peanut kefir at various gelatin levels: 0, 0.3, 0.5, 0.7%.

The flow curves of the shear stress variation with shear rate show that all samples exhibit an exponent of $0 < \eta < 1$, demonstrating that peanut kefir samples have non-Newtonian and pseudo-liquid properties (Guénard-Lampron et al., 2020). Increasing the amount of added gelatin increases the shear stress value, with the gelatin ratio being 0.3% (τ = 35.74 Pa) < 0.5% (τ = 44.22 Pa) < 0.7% (τ = 55.51 Pa) at a shear rate 100 (s^{-1}) (Figure 2). Additionally, it has been established that protein network stability requires the unfolding and rearrangement of secondary structure, aided by forming disulfide bridges, hydrogen bonds (Luo et al., 2019), and hydrophobic interactions, making the protein block tighter and requiring greater shear force (Ahmed et al., 2019). The shear stress with added gelatin increased in the early stages, then gradually stabilized, and

gelatin developed a solid three-dimensional network in fermented yogurt (Ares et al., 2007). The higher the stress, the higher their resistance to shear force (Frengova et al., 2002). Therefore, the results showed that the investigated samples were consistent with the Ostawald-de Waele rheological model. The samples' viscosity curves with shear rates from 1 ÷ 100 s^{-1} were similar; the apparent viscosity at the shear rate ranges from 0 ÷ 20s^{-1} decreased sharply, then gradually decreased to a constant value. Specifically, sample G0.7's apparent viscosity at the shear rate range from 0 ÷ 20 (s^{-1}) decreased from 141100 mPas to 1578 mPas. According to Figure 2b, kefir samples with added gelatin had a higher viscosity than CS. CS had an apparent viscosity of 284.7 mPas, and samples G0.3, G0.5, and G0.7 had an apparent viscosity, respectively, 357.4, mPas, 442.2 mPas and 472.3 mPas at a shear rate of 100 s^{-1}. Pang et al. (2019a) stated that adding 0.1 ÷ 1% gelatin affects the structure and rheology of peanut yogurt. The increase in viscosity upon adding gelatin is reportedly due to interactions between gelatin and milk proteins.

Studies have shown that adding a stabilizer (gelatin or other hydrocolloids) that acts as a thickener or gelling agent (Said, 2020) can help achieve good texture and stability (Supavititpatana et al., 2008).

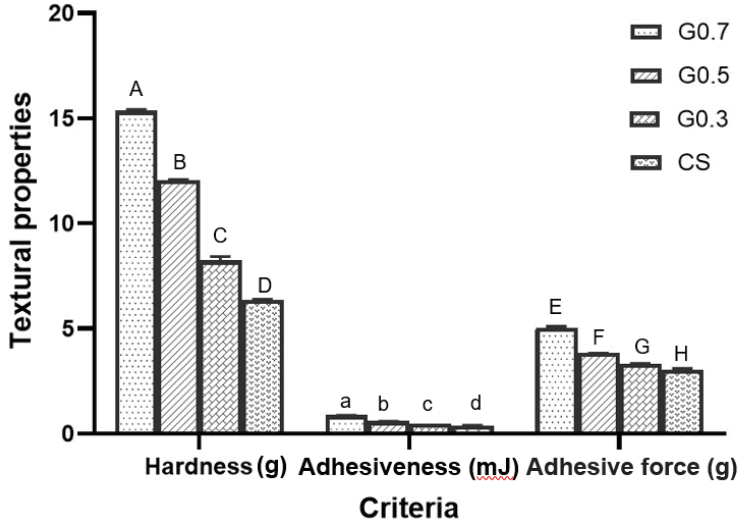

Figure 3. Effect of gelatin levels on peanut kefir's hardness, adhesiveness, and adhesive force. Mean value from triplicate means ± standard deviation. Different letters are significantly different ($P < 0.05$).

The results of the study on the effect of gelatin concentration (from 0.3, 0.5, and 0.7%) on the hardness, adhesion, and cohesive force of peanut kefir showed that the hardness increased by 46.67% and the adhesion increased by 16.27% between the G0.7 and G0.3. Figure 3 shows that all samples' hardness, adhesiveness, and adhesive force values were from 8.23 to 15.35 g, 0.45 to 0.87 mJ, and 3.33 to 5.04 g, respectively. The highest hardness, adhesiveness, and adhesive force of G0.7 were 15.35 g, 0.87 mJ, and 5.04 g; the lowest values of G0.3 were 8.23 g, 0.49 mJ, and 3.33 g, respectively. The CS showed that the gel texture was too soft, and hardness could not be determined. It was explained by the fact that gelatin contributes to stabilizing the structure

of kefir (Said, 2020) due to its ability to cut polysaccharide chains into short chains, thus increasing the gelation ability and contributing to the stability of the gel state. The gelatin ratio increased, and the firmness of kefir increased. G0.5 had a relatively harmonious firmness, making it a smooth structure suitable for kefir product properties.

The effect of fermentation temperature on pH, fermentation time, and rheological properties

The rheological characteristics are crucial in identifying various interactions in the recently developed kefir formulation (Saygili et al., 2022). The temperature at which kefir is incubated impacts its rheological characteristics (Dimitreli & Antoniou, 2011).

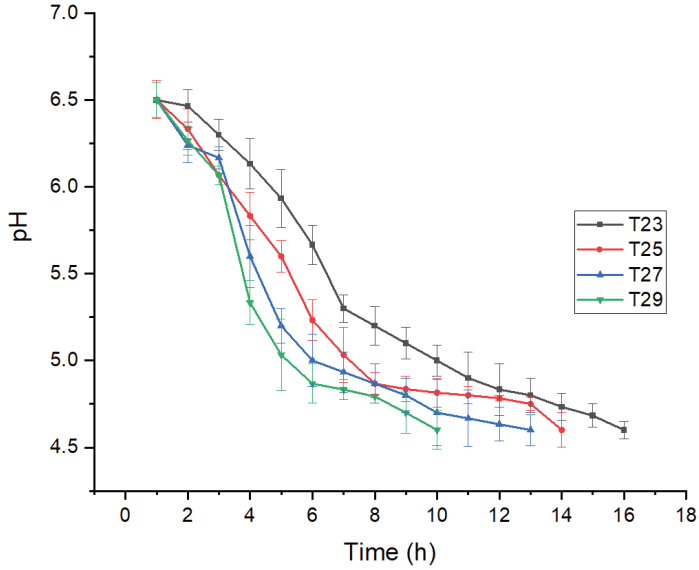

Figure 4. Various fermentation temperatures (23, 25, 27, 29°C) affect Peanut kefir's pH and fermentation time. Mean value from triplicate means ± standard deviation.

Figure 4 shows that the pH decreased while the acidity increased over fermentation time. When the fermentation temperature increases, the samples' fermentation time is different; the higher the temperature, the shorter the fermentation time. The T29 has the lowest time (10 h), with pH = 4.59; T23 has the longest fermentation time (16 h), with pH = 4.61. Fermentation temperature affects the fermentation process, as low temperature decreases the number or strength of hydrophobic bonds inside the protein gel. This result is entirely consistent with the research results of Nguyen et al. (2017) when studying the influence of ingredients (milk, gelatin, and kefir) on the quality of fruit yogurt, confirmed that the same proportion of microorganisms, fermentation temperature increases, fermentation time decreases. Lopes et al. (2019) stated that fermentation temperature significantly affects gel formation and acidification rate. High fermentation temperatures increase the ability to separate layers and weaken the protein network, thereby reducing gel hardness, viscosity smoothness, and sensory properties. Therefore, it makes the gel network susceptible to rearrangements, and these changes can lead to greater whey separation; besides, high fermentation temperatures cause rapid coagulation formation but easily lead to dehydration because acidification occurs

too quickly, and protein molecules are dense, reducing water-holding capacity (Mellema et al., 2002). The creation of acid content in kefir products depends on the growth of microorganisms and fermentation ability. The research survey and similar studies show that the peanut kefir fermentation temperature of T25 is suitable for the 13-h fermentation time, and the gel structure is stable.

Fermentation temperature is one of the critical factors influencing peanut kefir rheology. The steady-state rheological behavior of peanut kefir at selected gelatin levels (23, 25, 27, 29°C) is shown in Figure 5a. In contrast, the effect of gelatin substitution on the apparent viscosity behavior is shown in Figure 5b. The Ostawwld – de waele model explained the rheological behavior of kefir well.

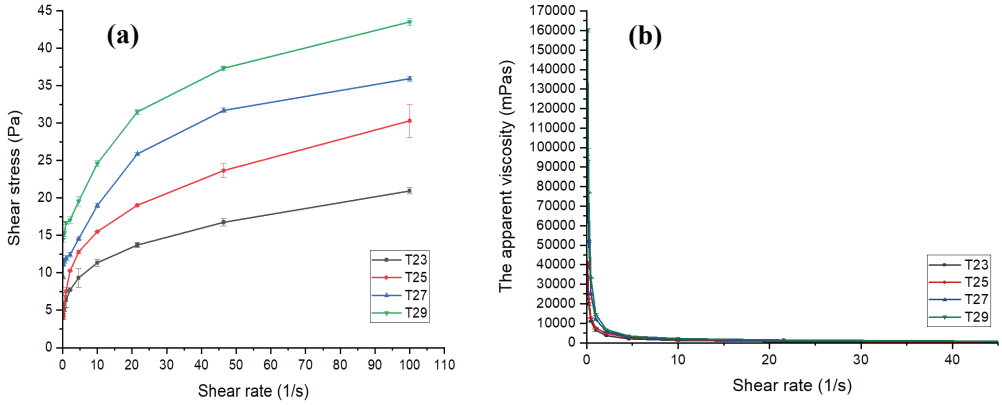

Figure 5. (a) Shear stress at various fermentation temperature; and (b) The apparent viscosity of kefir at various fermentation temperature: 23; 25; 27; 29oC. Mean value from triplicate means ± standard deviation.

According to Figure 5a, the peanut kefir samples surveyed are all pseudo-liquid because $0 < \eta < 1$. The samples tend to withstand low shear stress at a specific low shear rate, with T23 having a shear stress of 3.92 Pa at a shear rate of 0.9969 s^{-1}. After that, the increased the shear rate leads to a gradual increase in shear stress, and at a certain point, when shear rate continues to increase, the shear stress remains constant (Figure 5a). However, there are some differences in shear stress between the samples when changing the shear rate from 0 ÷ 100s^{-1}. When increasing the fermentation temperature from 23°C to 29°C, shear stress, according to the kefir's shear rate, gradually increases from 20.93 Pas to 43.51 Pas at a shear rate of 100s^{-1}; in contrast, the viscosity decreases because the water hol capacity decreases as the shear rate increases. According to Saygili et al. (2022), examining the apparent viscosity values of fermented cow's milk, it was determined that the viscosity values also increased with increasing fermentation temperature. Li et al. (2014) stated that the fermentation process of soy milk products has reduced viscosity with increasing shear stress because water molecules are well dispersed in the network structure. Besides, polysaccharides contribute to fermented milk products' increased viscosity and pseudo-liquid properties due to their ability to bind water and interact with proteins (Dimitreli & Antoniou, 2011). Bensmira and Jiang (2012) suggested that increasing fermentation temperature promotes hydrophobic interactions and creates

stronger gels. Besides, Man (2010) said that the kefir fermentation process is at its optimal temperature of 23 ÷ 25°C, the appropriate temperature for lactic bacteria and yeast to grow well. Low fermentation temperatures require longer fermentation times, affecting research performance, so we chose a kefir fermentation temperature of 25°C as the appropriate temperature for further research.

The effect of kefir culture ratio on pH, fermentation time, rheological properties, and SEM

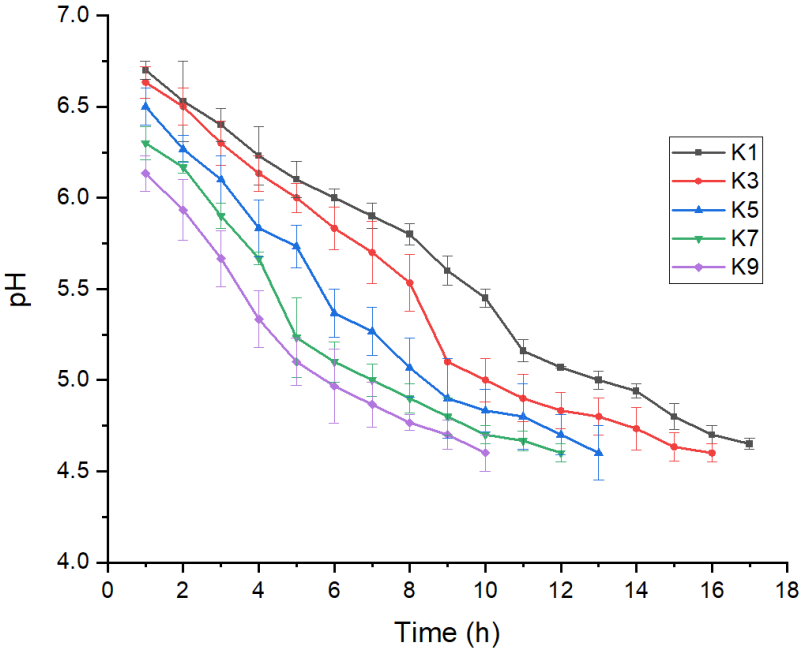

Figure 6. pH and fermentation time with various kefir culture ratios: 1, 3, 5, 7, 9%. Mean value from triplicate means ± standard deviation.

Figure 6 shows that the pH of kefir samples decreased over fermentation time with starter culture ratios. The pH in the first five h of K1, K3, and K5 decreased slowly, from 6.8 to 5.7. From 5 ÷ 10 h, pH decreased rapidly. After 10 h, the pH of the samples continued to decrease (K1 reached 4.65 at 17 h, K3 reached 4.6 at 16 h, and K5 reached 4.6 at 13 h). The pH in the first 5 h of K7 and K9 fermentation decreased rapidly, from 6.8 to 5.2 and 5.1. After 5 h, the pH of the samples continued to decrease slowly (K7's pH reached 4.6 with 12 h, and K9's pH reached 4.6 with 10 h). Figure 6 shows that increasing the kefir culture ratio, the fermentation time between samples is different; the fermentation end time of K9 is at least 10 h, pH = 4.6, and K1 has the longest fermentation time, 18 h with pH = 4.6. The kefir culture ratio increases, and the fermentation time decreases. However, the shorter the fermentation time, the more holes and water separation in the sample. When the microbial density is higher, the process of converting lactose into lactic acid occurs faster; the amount of acid formed increases, reducing the pH of the product and quickly reaching the end of the fermentation process (pH = 4.6), thereby shortening the fermentation time. Currently, the curd will not be durable, affecting the structure and feel of the product. The kefir culture ratio affects the pH value and acidity, showing that a higher kefir

culture ratio reduces fermentation time. The acidity of kefir may be developed due to organic acids; acid production in kefir products depends on microbial growth and fermentation capacity (Saygili et al., 2022). Research results show that a starter culture ratio of 5% has the most stable change in pH.

Changes in shear stress according to the shear rate of kefir samples with different kefir culture ratios (1, 3, 5, 7, 9%) are presented in Figure 7.

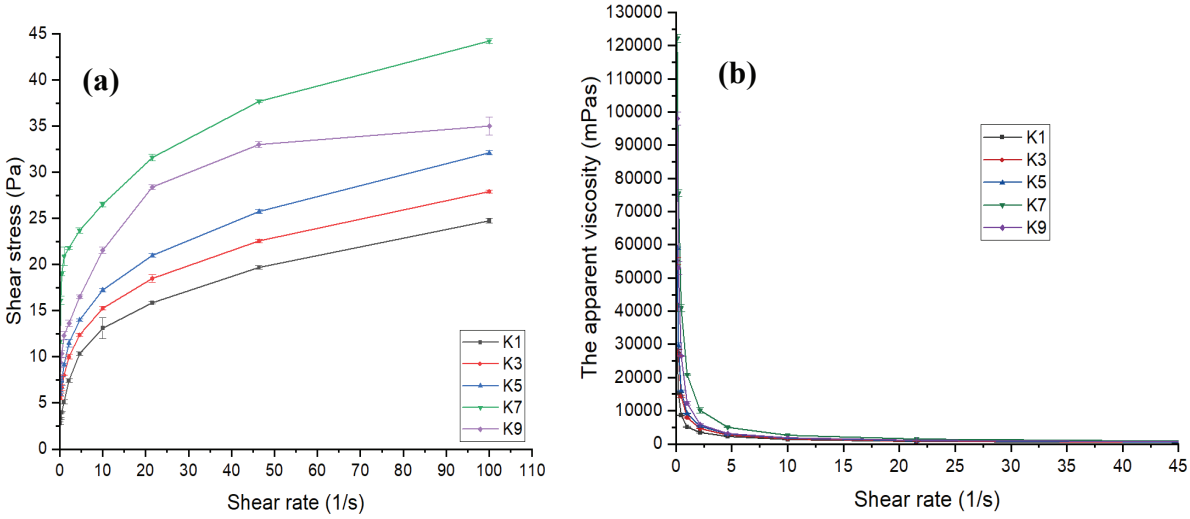

Figure 7. (a) Shear stress at various kefir culture ratios: 1, 3, 5, 7, 9%; and (b) The apparent viscosity of kefir at various kefir culture ratios: 1, 3, 5, 7, 9%. Mean value from triplicate means± standard deviation.

Figure 7 shows that the flow curve of the change in shear stress with the shear rate of the peanut kefir samples all shows an exponent of $0 < \eta < 1$, indicating that the samples are in pseudo-liquid form (Guénard-Lampron et al., 2020). Samples tend to increase the shear stress according to the shear rate from $0 \div 46s^{-1}$; K1's shear stress was 13.09 Pas at $10s^{-1}$; then, the shear rate continues to increase, the constant shear stress from the shear rate of $46 \div 100s^{-1}$, K1's shear stress was 21.98 to 22.87 Pa.

The K7 has the highest viscosity, leading to higher shear stress than the other samples. The fermentation process takes place too quickly, and the pH suddenly drops quickly, causing the protein in peanut milk to coagulate; the curd will not be stable, affecting the texture of the product. The apparent viscosity depends significantly on the existence and development of microorganisms. The highest viscosity of K7 was 442.2 mPas, and the lowest viscosity of K1 was 247.4 mPas, at $100s^{-1}$. Too high a kefir culture ratio will cause the gel structure to become loose, quickly causing layer separation and significantly affecting viscosity. K9 created acidification too quickly, reducing water retention. The decrease in viscosity was independent of the fermentation parameters and the source of the kefir starter microflora in the present study; this decrease can be explained by the hydrolysis of EPS into its monomers by glycol hydrolases (Purwandari et al., 2007). Structure scanning electron microscope of samples in Figure 8.

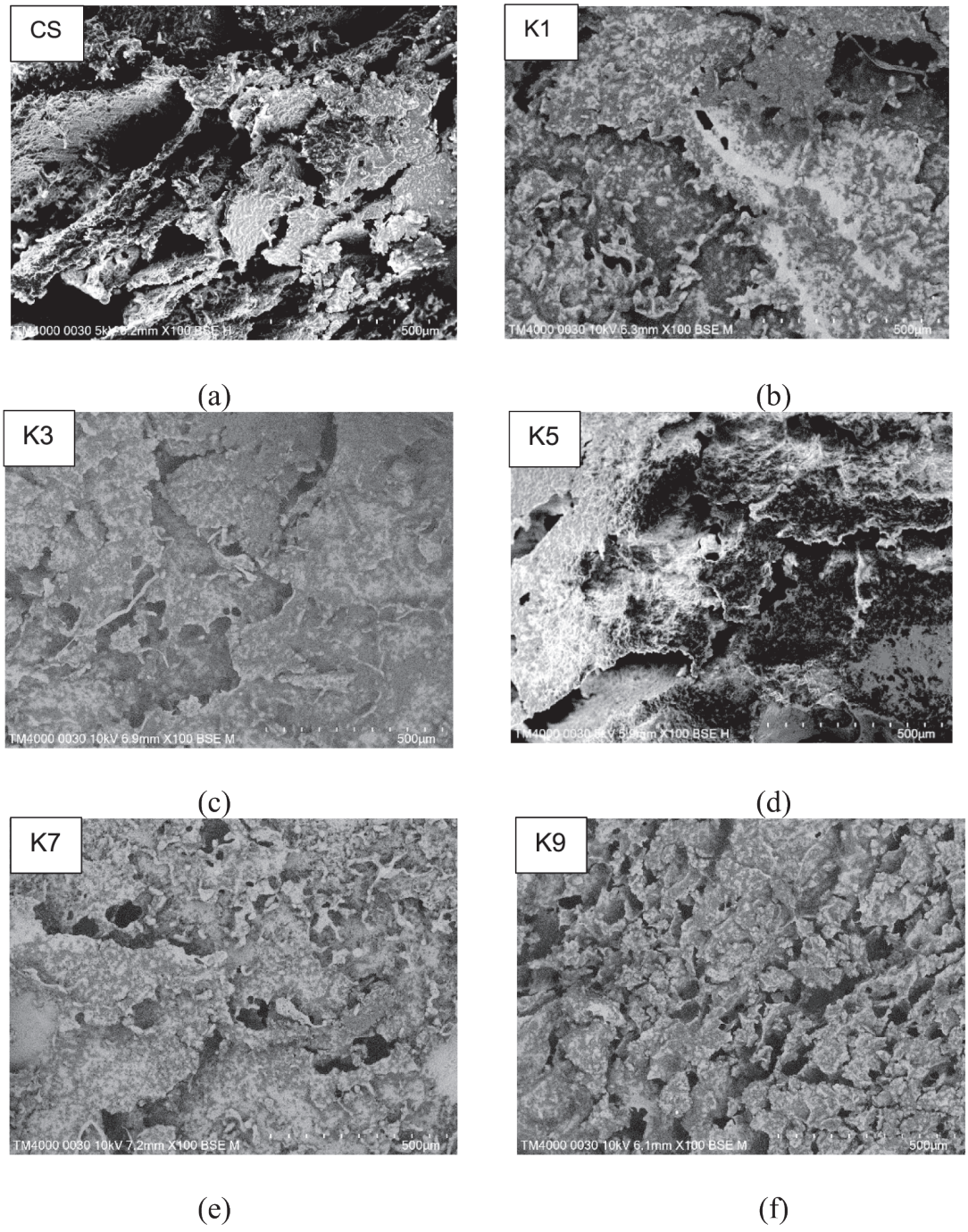

Figure 8. The SEM micrographs of kefir samples at various kefir culture ratios: 0, 1, 3, 5, 7, and 9% under a magnification of 100. (a) CS with 0% kefir culture ratio; (b) K1 with 1% kefir culture ratio; (c) K3 with 3% kefir culture ratio; (d) K5 with 5% kefir culture ratio; (e) K7 with 7% kefir culture ratio; (f) K9 with 9% kefir culture ratio.

The sample's SEM showed that a weak cheese structure had formed, the pores were spread out unevenly, and the cross-linking between kefir protein clusters was very strong, making tiny chains. K5 has the most uniformly distributed kefir product structure. The tight bonds in the gel network created a gel surface structure with very few holes; the structure of kefir was not dehydrated, the structure was tight, and the protein was evenly distributed. Therefore, after freezing and freeze-drying, the gel network did not create grooves and was not significantly broken. For CS, each gel block can be seen, but the gel network structure was uneven, porous, and had a water separation phenomenon; the gel network forms grooved and was broken, creating many holes; EPS exists in the pores in the gel network due to incompatibility with proteins (Hassan et al., 2003). K1 showed that, although the structure was tighter and fewer grooves appeared, the kefir structure was uneven and porous. K3 had an improved kefir structure, which was more uniform and less porous, but grooves still appeared. K7 had tight bonds with each other and minor porosity, proving that the structure of kefir was tight and had uniform protein mass. The gel network was also tighter; no grooves were created, and the gel network was not broken. K7 showed that the structure was much tighter and more uniform, but more grooves appeared, possibly because the pH rapidly decreased when the kefir culture ratio was increased. Acidity increases, causing the protein blocks to thicken, but the gel network is broken. K9 had a slightly looser structure, and the gel network was strongly destroyed. Shiva Dadkhah et al. (2011) stated that the kefir rate affected the pH value and the acidity, affecting the gel structure and network. The acidity of kefir products depended on the growth of microorganisms and fermentation ability. According to Hassan et al. (2003), EPS may exist in the pores in the network due to protein incompatibility. During the acidification stage, the incompatibility between EPS and peanut protein can cause phase separation, disrupting the formation and consolidation of the gel network and causing high protein retention, which reduces gel strength. Therefore, the structure is less dense (Pang et al., 2019b). However, if the fermentation process takes place too quickly, the sudden pH decrease quickly causes the peanut milk protein to coagulate. The curd will not be durable, affecting the structure and feel of the product. With the inoculum ratio of 5%, the structure is the tightest, less porous, and does not appear.

Some criteria for finished peanut kefir are in Table 2, the spectra of CS and study kefir samples are shown in Figure 8.

Table 2. Chemical properties for peanut kefir

No.	Criteria (%)	K5
1	Carbohydrate	22.12 ± 0.93
2	Lipid	8.46 ± 0.33
3	Protein	4.09 ± 0.21
4	Ash	0.61 ± 0.08

Mean value from triplicate means ± standard deviation.

According to Codex Standard 243-2003, the quality of kefir yogurt requires a protein content of not less than 2.7% and a fat content of less than 10%. This result shows that our peanut kefir research sample meets the nutritional value criteria.

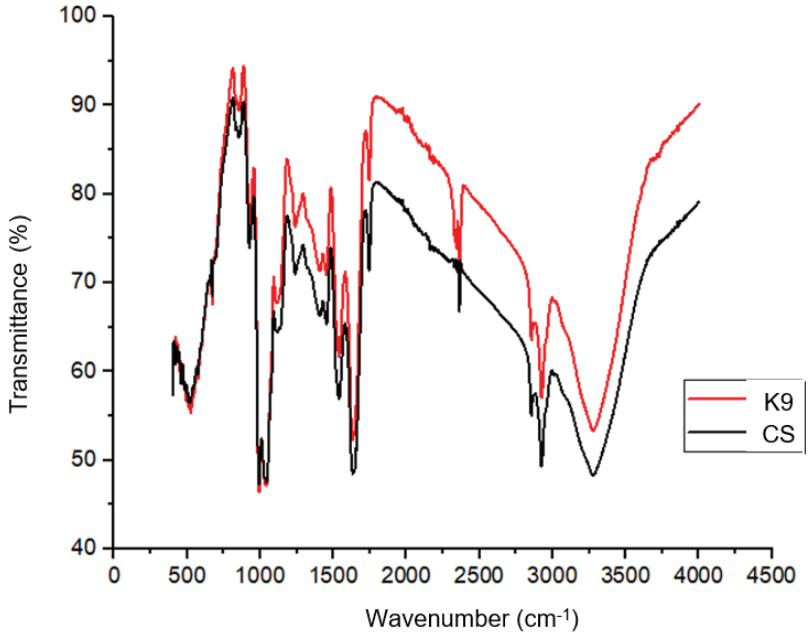

Figure 9. Fourier transform infrared spectroscopy (FTIR) spectra of the control sample (CS) and research sample (K5).

Figure 9 shows the wavelengths the functional groups of kefir samples absorb the most. Analysis related to the concentration regions of functional groups representing the presence of proteins was amide I (1600 ÷ 1800 cm^{-1}), amide II (1470 ÷ 1570 cm^{-1}), amide III (1250 ÷ 1350 cm^{-1}), and amide A (3300 ÷ 3500 cm^{-1}), which were the peaks of the amide infrared absorption characteristics. The protein leading band was the amide I band with the most vital absorption; the peak was obtained at 1744.54 cm^{-1} for both samples. It was related to the C=O stretching vibration (80%), the stretching vibration of the C-N bond (10%), and the hydrogen bond associated with COO- in the range between 1600 and 1800 cm^{-1} (Temiz & Çakmak, 2018; Vaishanavi & Preetha, 2021). In the amide II region, the maximum absorption at 1453.58 cm^{-1} arises from the bending vibration of the N–H group (60%), the stretching vibration of the CN group (30%), and the C–C stretching vibration (10%) (Long et al., 2015). In the amide III region, the most prominent absorption peak was at 1239.04 cm^{-1}; the vibrations existing in this region were mainly related to the bending in the vibrational plane of CN and NH groups in the amide or the vibrations of CH_2 groups (Temiz & Çakmak, 2018). The FTIR spectrum shows peanut protein was found in the higher range from 853.35 to 1042.10 cm^{-1}, and the lower range was 2924.28 to 3609.05 cm^{-1}. In the amide A region (3300 ÷ 3500 cm^{-1}), the absorption of these two peaks reaching a maximum at 3279.6 cm^{-1} was due to the presence of this related to the extended NH group bond and the interaction with each other by the O–H bond. The region in 3000 ÷ 3500 cm^{-1} was also due to molecular chains interacting by intra-and intermolecular hydrogen bonds (Salari et al., 2019). In addition, 900 ÷ 1200 cm^{-1} was dominated by polysaccharides related to the vibration of the characteristic C–O group and aromatic N–O compounds. In particular, there was a peak at the wave number 925.664 cm^{-1} related to additional sucrose (Mechmeche et al., 2019). The shape of the spectra of the two kefir samples was similar, indicating that gelatin was added to the sample without any change in

nutritional composition. During heating, the protein underwent structural changes related to disrupting hydrogen bonds in the molecules that stabilize the α-helical structure (Tian et al., 2020). Botelho et al. (2014) stated that FTIR to determine the nutritional characteristics of fermented soy kefir, which showed a peak in the amide I was 1629 cm^{-1}, the amide II region at 1419 cm^{-1}; our research result was 1744.54 cm^{-1}, and 1453.58 cm^{-1}, respectively. In the amide III region, the peak was 1239.04 cm^{-1}, and the peak was 3279.60 cm^{-1} - there is a prolonged N-H group bond of amide A. Therefore, K5 had no change in chemical groups in the kefir product.

4. Conclusions

The current study describes the effects of gelatin concentration, fermentation temperature, and kefir culture ratio on peanut kefir's pH, textural properties, and rheological properties. The study found that gelatin content increased the hardness, adhesiveness, and adhesive force compared to unaided gelatin content. Moreover, the results indicated that the suitable gelatin content, fermentation temperature, and kefir culture ratio for peanut kefir was 0.5% gelatin content, and fermentation temperature was 25°C with an added kefir culture ratio of 5%. The peanut kefir product has carbohydrate content (22.12 ± 0.93%), lipid content (8.46 ± 0.33), protein content (4.09 ± 0.21%), ash content (0.61 ± 0.08%) with peanut kefir's rheological behavior was a pseudo-liquid form.

Conflict of interest

The authors have no relevant financial or non-financial interests to disclose.

Acknowledgements

Thank you, HCMUTE, for supporting facilities to the author to finish the research. The author sincerely thanks Ms. Son Thi Ve Ry and Ms. Mai Ngoc Son Tuyen for their assistance with data processing.

References

Ahmed, J., Mulla, M., Al-Ruwaih, N., & Arfat, Y. A. (2019). Effect of high-pressure treatment prior to enzymatic hydrolysis on rheological, thermal, and antioxidant properties of lentil protein isolate. *Legume Science* 1(1), e10. https://doi.org/10.1002/leg3.10.

AOAC (Association of Official Analytical Chemists). (2000). *Official methods of analysis* (17th ed.). Maryland, USA: AOAC Intl.

Ares, G., Gonçalvez, D., Pérez, C., Reolón, G., Segura, N., Lema, P., & Gámbaro, A. (2007). Influence of gelatin and starch on the instrumental and sensory texture of stirred yogurt. *International Journal of Dairy Technology* 60(4), 263-269. https://doi.org/10.1111/j.1471-0307.2007.00346.x.

Bensmira, M., & Jiang, B. (2012). Effect of some operating variables on the microstructure and physical properties of a novel Kefir formulation. *Journal of Food Engineering* 108(4), 579-584. https://doi.org/10.1016/j.jfoodeng.2011.07.025.

Botelho, P. S., Maciel, M. I. S., Bueno, L. A., Marques, M. D. F. F., Marques, D. N., & Silva, T. M. S. (2014). Characterisation of a new exopolysaccharide obtained from of fermented kefir grains in soymilk. *Carbohydrate Polymers* 107(1), 1-6. https://doi.org/10.1016/j.carbpol.2014.02.036.

Bourrie, B. C. T., Diether, N., Dias, R. P., Nam, S. L., De La Mata, A. P., Forgie, A. J., Gaur, G., Harynuk, J. J., Gänzle, M., Cotter, P. D., & Willing, B. P. (2023). Use of reconstituted kefir consortia to

determine the impact of microbial composition on kefir metabolite profiles. *Food Research International* 173(Pt.2), 113467. https://doi.org/10.1016/j.foodres.2023.113467.

Chen, Z., Shi, J., Yang, X., Nan, B., Liu, Y., & Wang, Z. (2015). Chemical and physical characteristics and antioxidant activities of the exopolysaccharide produced by Tibetan kefir grains during milk fermentation. *International Dairy Journal*, *43*, 15–21. https://doi.org/10.1016/j.idairyj.2014.10.004.

Diarra, K., Nong, Z. G., & Jie, C. (2005). Peanut milk and peanut milk based products production: A review. *Critical Reviews in Food Science and Nutrition*, *45*(5), 405–423. https://doi.org/10.1080/10408390590967685

Dimitreli, G., & Antoniou, K. D. (2011). Effect of incubation temperature and caseinates on the rheological behaviour of Kefir. *Procedia Food Science* 1, 583-588. https://doi.org/10.1016/j.profoo.2011.09.088.

Dwivedi, S., Puppala, N., Maleki, S., Ozias-Akins, P., & Ortiz, R. (2014). Peanut improvement for human health. In Janick, J. (Ed.). *Plant breeding reviews: Volume 38* (1st ed., 143-186). New Jersey, USA: John Wiley & Sons. https://doi.org/10.1002/9781118916865.ch04.

Egea, M. B., Dos Santos, D. C., de Oliveira Filho, J. G., da Costa Ores, J., Takeuchi, K. P., & Lemes, A. C. (2022). A review of nondairy kefir products: Their characteristics and potential human health benefits. *Critical Reviews in Food Science and Nutrition* 62(6), 1536-1552. https://doi.org/10.1080/10408398.2020.1844140.

Frengova, G. I., Simova, E. D., Beshkova, D. M., & Simov, Z. I. (2002). Exopolysaccharides produced by lactic acid bacteria of kefir grains. *Zeitschrift Für Naturforschung C* 57(9-10), 805-810. https://doi.org/10.1515/znc-2002-9-1009.

González-Orozco, B. D., García-Cano, I., Jiménez-Flores, R., & Alvárez, V. B. (2022). Invited review: Milk kefir microbiota - direct and indirect antimicrobial effects. *Journal of Dairy Science* 105(5), 3703-3715. https://doi.org/10.3168/jds.2021-21382.

Guénard-Lampron, V., Bosc, V., St-Gelais, D., Villeneuve, S., & Turgeon, S. L. (2020). How do smoothing conditions and storage time change syneresis, rheological and microstructural properties of nonfat stirred acid milk gel? *International Dairy Journal* 109, 104780. https://doi.org/10.1016/j.idairyj.2020.104780.

Gul, O., Atalar, I., Mortas, M., & Dervisoglu, M. (2018). Rheological, textural, colour and sensorial properties of kefir produced with buffalo milk using kefir grains and starter culture: A comparison with cows' milk kefir. *International Journal of Dairy Technology* 71(S1), 73-80. https://doi.org/10.1111/1471-0307.12503.

Hassan, A. N., Ipsen, R., Janzen, T., & Qvist, K. B. (2003). Microstructure and rheology of yogurt made with cultures differing only in their ability to produce exopolysaccharides. *Journal of Dairy Science* 86(5), 1632-1638. https://doi.org/10.3168/jds.S0022-0302(03)73748-5.

Li, C., Li, W., Chen, X., Feng, M., Rui, X., Jiang, M., & Dong, M. (2014). Microbiological, physicochemical and rheological properties of fermented soymilk produced with exopolysaccharide (EPS) producing lactic acid bacteria strains. *LWT - Food Science and Technology*, *57*(2), 477–485. https://doi.org/10.1016/j.lwt.2014.02.025

Long, H. G., Ji, Y., Pan, B. H., Sun, W. Z., Li, T. Y., & Qin, X. G. (2015). Characterization of thermal denaturation structure and morphology of soy glycinin by FTIR and SEM. *International Journal of Food Properties* 18(4), 763-774. https://doi.org/10.1080/10942912.2014.908206.

Lopes, R. P., Mota, M. J., Pinto, C. A., Sousa, S., Silva, J. A. L. D., Gomes, A. M., Delgadillo, I., & Saraiva, J. A. (2019). Physicochemical and microbial changes in yogurts produced under different pressure and temperature conditions. *LWT* 99, 423-430. https://doi.org/10.1016/j.lwt.2018.09.074.

Luo, W. Y., Liu, Q. X., & Pang, H. Z. (2019). Tribo-rheological properties of acid milk gels with different types of gelatin: Effect of concentration. *Journal of Dairy Science* 102(9), 7849-7862. https://doi.org/10.3168/jds.2019-16305.

Man, L.V.V. (2010). *Textbook of technology for manufacturing dairy products and mixed drinks*. Ho Chi Minh City, Vietnam: Ho Chi Minh City National University publishing House.

Mæhre, H., Dalheim, L., Edvinsen, G., Elvevoll, E., & Jensen, I.-J. (2018). Protein determination-method matters. *Foods*, *7*(1), 5. https://doi.org/10.3390/foods7010005.

Mechmeche, M., Ksontini, H., Hamdi, M., & Kachouri, F. (2019). Production of bioactive peptides in tomato seed protein isolate fermented by water kefir culture: Optimization of the fermentation conditions. *International Journal of Peptide Research and Therapeutics* 25(1), 137-150. https://doi.org/10.1007/s10989-017-9655-8.

Mellema, M., Walstra, P., Van Opheusden, J. H. J., & Van Vliet, T. (2002). Effects of structural rearrangements on the rheology of rennet-induced casein particle gels. *Advances in Colloid and Interface Science* 98(1), 25-50. https://doi.org/10.1016/S0001-8686(01)00089-6.

Nguyen, P. T. M., Kravchuk, O., Bhandari, B., & Prakash, S. (2017). Effect of different hydrocolloids on texture, rheology, tribology and sensory perception of texture and mouthfeel of low-fat pot-set yoghurt. *Food Hydrocolloids 72*, 90-104. https://doi.org/10.1016/j.foodhyd.2017.05.035

Pang, H. Z., Cao, N. J., Zheng, M. Y., Luo, W. Y., Liu, Q. X., & Xiao, L. (2019a). Effects of different types of hydrocolloids on texture and rheological properties of soymilk yogurt. *Food and Fermentation Industries* 45(3), 1-6. https://doi.org/10.13995/j.cnki.11-1802/ts.018305.

Pang, H. Z., Xu, L. R., Zhu, Y., Li, H., Bansal, N., & Liu, Q. X. (2019b). Comparison of rheological, tribological, and microstructural properties of soymilk gels acidified with glucono-δ-lactone or culture. *Food Research International* 121, 798-805. https://doi.org/10.1016/j.foodres.2018.12.062.

Purwandari, U., Shah, N. P., & Vasiljevic, T. (2007). Effects of exopolysaccharide-producing strains of Streptococcus thermophilus on technological and rheological properties of set-type yoghurt. *International Dairy Journal* 17(11), 1344-1352. https://doi.org/10.1016/j.idairyj.2007.01.018.

Said, M. I. (2020). Role and function of gelatin in the development of the food and non-food industry: A review. *IOP Conference Series: Earth and Environmental Science* 492(1), 012086. https://doi.org/10.1088/1755-1315/492/1/012086.

Salari, M., Khiabani, M. S., Mokarram, R. R., Ghanbarzadeh, B., & Kafil, H. S. (2019). Preparation and characterization of cellulose nanocrystals from bacterial cellulose produced in sugar beet molasses and cheese whey media. *International Journal of Biological Macromolecules* 122, 280-288. https://doi.org/10.1016/j.ijbiomac.2018.10.136.

Saygili, D., Döner, D., İÇiEr, F., & Karagözlü, C. (2022). Rheological properties and microbiological characteristics of kefir produced from different milk types. *Food Science and Technology* 42, e32520. https://doi.org/10.1590/fst.32520.

Settaluri, V. S., Kandala, C. V. K., Puppala, N., & Sundaram, J. (2012). Peanuts and their

nutritional aspects - A review. *Food and Nutrition Sciences* 3(12), 1644-1650. http://dx.doi.org/10.4236/fns.2012.312215.

Shiva Dadkhah, R. P., Mahnaz Mazaheri Assadib and Ali Moghimic. (2011). Kefir production from soymilk. *Annals of Biological Research*, 293-299.

Supavititpatana, P., Wirjantoro, T. I., Apichartsrangkoon, A., & Raviyan, P. (2008). Addition of gelatin enhanced gelation of corn-milk yogurt. *Food Chemistry* 106(1), 211-216. https://doi.org/10.1016/j.foodchem.2007.05.058.

Syed, F., Arif, S., Ahmed, I., & Khalid, N. (2021). Groundnut (peanut) (*Arachis hypogaea*). In Tanwar, B., & Goyal, A. (Eds.). *Oilseeds: Health attributes and food applications* (93-122). Beach Road, Singapore: Springer. https://doi.org/10.1007/978-981-15-4194-0_4.

Temiz, H., & Çakmak, E. (2018). The effect of microbial transglutaminase on probiotic fermented milk produced using a mixture of bovine milk and soy drink. *International Journal of Dairy Technology* 71(4), 906-920. https://doi.org/10.1111/1471-0307.12521.

Tian, R., Feng, R. J., Huang, G., Tian, B., Zhang, Y., Jiang, Z. L., & Sui, N. X. (2020). Ultrasound driven conformational and physicochemical changes of soy protein hydrolysates. *Ultrasonics Sonochemistry* 68, 105202. https://doi.org/10.1016/j.ultsonch.2020.105202.

Xiao, R., Liu, M., Tian, Q., Hui, M., Shi, X., & Hou, G. X. (2023). Physical and chemical properties, structural characterization and nutritional analysis of kefir yoghurt. *Frontiers in Microbiology* 13, 1107092. https://doi.org/10.3389/fmicb.2022.1107092.

Detection of Zucchini yellow mosaic virus infecting pumpkin using realtime RT-PCR

Nhi H. Lu[1], Toan Q. Truong[2], & Biet V. Huynh[1,2*]

[1]Faculty of Biological Sciences, Nong Lam University, Ho Chi Minh City, Vietnam

[2]Research Institute for Biotechnology and Environment, Nong Lam University, Ho Chi Minh City, Vietnam

ARTICLE INFO

Research Paper

Received: August 31, 2024
Revised: November 02, 2024
Accepted: November 22, 2024

Keywords

Curcubita moschata
Realtime RT-PCR
Yellow mosaic
ZYMV

***Corresponding author**

Huynh Van Biet
Email: hvbiet@hcmuaf.edu.vn

ABSTRACT

Zucchini yellow mosaic virus (ZYMV) is a significant pathogen causing yellow mosaic disease in *Cucurbitaceae*. It can spread rapidly from infected plants to healthy ones or through contaminated seed sources, leading to a substantial reduction in the yield and quality of pumpkins after harvest. Currently, there is no effective treatment to eliminate this virus, making seed screening prior to planting and the removal of symptomatic plants the most effective control methods. In this study, a 214 bp target gene of the ZYMV was amplified using specific primers, then cloned into the pJET1.2 vector and transformed into *Escherichia coli* JM109. A realtime RT-PCR procedure was developed to detect and quantify ZYMV utilizing a primer pair designed for a 164 bp product. The standard curve was established with the equation y = -3.417x + 49.605 and correlation coefficient R^2 = 0.9969 for quantifying the ZYMV virus. The realtime RT-PCR was built with qualitative results corresponding to the PCR method. Additionally, the procedure quantified test samples with viral loads ranging from 7.1 x 10^6 to 8.5 x 10^9 copies/µL.

Cited as: Lu, N. H., Truong, T. Q., & Huynh, B. V. (2024). Detection of Zucchini yellow mosaic virus infecting pumpkin using realtime RT-PCR. *The Journal of Agriculture and Development* 23(Special issue 2), 183-192.

1. Introduction

Pumpkin (*Cucurbita moschata*) originates from Southern Mexico - Central America and is widely cultivated around the world, especially in subtropical areas such as Asia, America, and Africa (Lim, 2012). Often referred to as a "golden food", pumpkin is rich in vitamins and nutrients essential for human health. However, hot, dry weather or erratic rainfall can lead to infections by harmful diseases, including wilt (caused by *Pseudomonas solanacearum*), anthracnose (caused by *Colletotrichum lagenarium*), powdery mildew (caused by *Erysiphe cichoracearum*), leaf mosaic (caused by Squash mosaic virus), and yellow mosaic (caused by Zucchini yellow mosaic virus). Among them, yellow mosaic disease is particularly impactful, significantly reducing

both productivity and fruit quality a disease that significantly reduces productivity and fruit quality. The earlier the disease manifests, the lower the pumpkin yield at harvest. Research by Moradi et al. (2019) indicates that Zucchini yellow mosaic virus (ZYMV) is one of the most diverse strains of Potyvirus, capable of causing yield losses of up to 100%. This disease is primarily transmitted by aphids. Common symptoms include swollen leaves, yellow spots, reduced size, swollen buds, few fruits and deformed fruits, lumps, spots, cracks, reducing productivity and shelf life. Some symptoms may not be visibly apparent and can only be detected through molecular testing. However, in Vietnam, research on pumpkin diseases has been limited. Common diagnostic methods include ELISA, PCR, and realtime RT-PCR. While ELISA is simple and user-friendly, it lacks high sensitivity and can be time-consuming (Hu et al., 1993). The PCR is also widely used to diagnose viral diseases but this method is only capable of qualitative function and cannot detect virus-infected samples at low concentrations. Currently, the realtime RT-PCR method is considered optimal, as it can accurately quantify and detect pathogens at low concentrations with a quick turnaround time. Therefore, developing a realtime RT-PCR process for detecting the ZYMV is essential for early pathogen detection and timely prevention, helping to reduce the damage caused by this pathogen to farmers.

2. Materials and Methods

2.1. Materials

Pumpkin leaf samples were randomly collected from gardens in Tay Ninh province. After collection, leaf samples were stored at -20^{o} C until used for extraction. Each sample is placed in a separate bag and labeled with its corresponding name.

The RNA control sample for the ZYMV virus was provided by the Molecular Biology Laboratory at the Research Institute for Biotechnology and Environment, Nong Lam University, Ho Chi Minh City, Vietnam. *Escherichia coli JM109* virus strain was used for gene cloning.

2.2. RNA extraction and synthesizing cDNA from RNA

Total RNA was extracted from 50 mg of leaf sample using the EZ-10 Spin Column Plant RNA Miniprep Kit (Biobasic) following the manufacturer's protocol. The purity of RNA was assessed by measuring the optical density (OD) at 260 nm and 280 nm using a spectrophotometer (Biodrop, UK).

cDNA synthesis reactions were carried out according to the manufacturer's instructions for the SensiFAST™ cDNA Synthesis Kit (Bioline, UK). The reaction was conducted in a PCR machine (Applied Biosystems 2720 Thermal Cycler), the following thermal cycling conditions: 25°C for 10 min, 42°C for 15 min, 48°C for 15 min, and 85°C for 5 min.

2.3. Primers used in the study

Primers used for realtime RT-PCR to detect ZYMV virus were designed using Primer3 software to amplify a 164 bp gene segment (Table 1).

Table 1. Primers information

Primer name	Sequence 5' – 3'	Size (bp)	Source
ZYMVF	CATACATGCCGAGGTATGGTTT	214	Aguiar et al. (2019)
ZYMVR	GTGTGCCGTTCAGTGTCTT		
ZYMVF new	GGCTCGATACGCTTTCGACTT	164	This study
ZYMVR new	TGTGCCGTTCAGTGTCTTCG		
pJET1.2-F	CGACTCACTATAGGGAGAGCCGC	118	CloneJET ™ PCR Cloning Kit
pJET1.2-R	AAGAAC ATCGATTTTCCATGGCAG		

The sequence of primers was checked for the non-specific binding in NCBI Primer Blast tool. This primer pair had a high specificity to only pair with ZYMV (Figure 1).

	Sequence (5'->3')	Length	Tm	GC%	Self complementarity	Self 3' complementarity
Forward primer	GGCTCGATACGCTTTCGACTT	21	60.80	52.38	6.00	1.00
Reverse primer	TGTGCCGTTCAGTGTCTTCG	20	60.87	55.00	3.00	2.00

Products on target templates

>LC781588.1 Zucchini yellow mosaic virus OGC3 gene for coat protein, partial cds

```
product length = 164
Forward primer  1    GGCTCGATACGCTTTCGACTT  21
Template        419  ......................  439

Reverse primer  1    TGTGCCGTTCAGTGTCTTCG  20
Template        582  ......................  563
```

>LC781584.1 Zucchini yellow mosaic virus OGC5 gene for coat protein, partial cds

```
product length = 164
Forward primer  1    GGCTCGATACGCTTTCGACTT  21
Template        428  ......................  448

Reverse primer  1    TGTGCCGTTCAGTGTCTTCG  20
Template        591  ......................  572
```

>OP771419.1 Zucchini yellow mosaic virus isolate BY01 coat protein gene, partial cds

```
product length = 164
Forward primer  1   GGCTCGATACGCTTTCGACTT  21
Template        78  ......................  98

Reverse primer  1    TGTGCCGTTCAGTGTCTTCG  20
Template        241  ......................  222
```

Figure 1. The result of the primer was compared to the target sequences by using Primer Blast tool on NCBI Genbank.

2.4. PCR reaction process

The reaction was conducted in a total volume of 25 µL, comprising 12.5 µL of MyTaq Mix (2X) (Bioline, UK), 9.5 µL of nuclease-free water (Bio Basic, Canada), 0.5 µL (10 µM) of each forward and reverse primer, and 2 µL of the cDNA sample. The reaction was performed in a PCR machine (Applied Biosystems 2720 Thermal Cycler) and included three stages: Stage 1 with 94°C for 5 min, stage 2 consist of 35 cycles with 95°C for 30 sec, 52°C for 1 min 30 sec, 72°C for 2 min, stage 3 with 72°C for 8 min and hold at 4°C.

The amplified gene segment was sequenced at Nam Khoa Trading and Service Company Limited in Ho Chi Minh City. The sequencing results were then compared with the ZYMV virus sequences published on GenBank (NCBI).

2.5. Procedure for creating plasmid clones carrying target genes

The target gene segment of ZYMV virus was inserted into vector pJET1.2 according to the instructions of CloneJET ™ PCR Cloning Kit (Thermo Scientific). Following the insertion, the vector is transformed into *E. coli* JM109 bacteria using the chemical transformation method (Sambrook, 2001). After completing the cloning steps, the bacteria were cultured in an Luria-Bertani (LB) medium supplemented with 50 mg/L of Ampicillin.

After 24 h of bacterial culture, colonies growing on solid LB medium were selected for PCR reactions using the pJET1.2 primer pair (Table 1), following the instructions of the CloneJET PCR Cloning Kit (Thermo Scientific). The PCR products were then analyzed by electrophoresis.

The plasmid DNA sample obtained after amplification was sent for sequencing at Nam Khoa Trading and Service Company Limited, Ho Chi Minh City. Sequencing results were compared with the ZYMV virus sequence Prior to cloning, as well as with sequences published on GenBank.

2.6. Generation of a standard curve

Each reaction has a total volume of 10 µL, including 5 µL SensiFAST SYBR® Lo-ROX Kit (2X), 3.6 µL of nuclease-free water (Bio Basic, Canada), 0.2 µL (10 µM) of each forward and reverse primer, and 1 µL of the cDNA sample. Realtime RT-PCR reaction was performed using an Applied Biosystem 7500 Realtime PCR machine (Applied Biosystem, USA). The reaction comprised two stages: Stage 1: 95°C for 2 min, Stage 2: 40 cycles: 95°C for 15 sec, 60°C for 35 sec.

Plasmid DNA copy number was calculated using the formula (Staroscik, 2004):

$$\text{Number of copies} = \frac{6{,}022 \times 10^{23} \times C}{650 \times 10^{9} \times L}$$

Where: C is the DNA amount (ng), L is the length of the DNA (bp)

The plasmid DNA sample was diluted with nuclease-free water. Two parameters were used to evaluate the stability of the standard curve: the correlation coefficient R2 and amplification efficiency (PCR efficiency) E%. An R2 coefficient of 0.99 or higher indicates high linearity of the standard curve. The E% is accepted in the range of 90% to 110% and is calculated using the formula: E% = (E – 1) 100%; $E = 10^{-1/\text{slope}}$. The allowable slope of the standard curve ranges from -3.58 to -3.1, with an ideal slope of = -3.32. The standard curve can be expressed as Y = aX + b, where Y is the threshold cycle (ct) and X is the logarithm of the copy number, a is the slope, and b is the y-intercept.

2.7. Evaluation of the specificity of the Realtime RT-PCR

The cDNA of other *Potyvirus* including DsMV (Dasheen mosaic virus), PRSV (Papaya ringspot virus) and ChiVMV (Chilli veinal mottle virus) were tested with ZYMV primer to verify the specificity of the RT-PCR assay.

2.8. Applying the ZYMV virus detection process on samples collected from the field

Field samples were randomly collected to detect and quantify the level of infection. Samples were obtained from 2 gardens: garden 1 in Chau Thanh district, Tay Ninh city, and garden 2 in Ninh Son district, Tay Ninh city. The composition and thermal cycling conditions of the reaction were consistent those used to

generate the standard curve. The copy number of ZYMV - infected samples was determined using this standard curve.

3. Results and Discussion

3.1. PCR reaction results

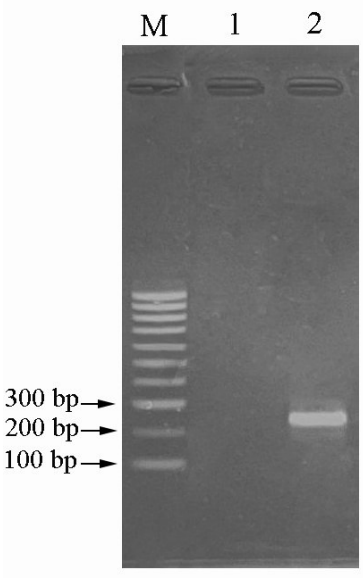

Figure 2. The electrophoresis results of the PCR product for the target gene segment using the primer pair Zucchini yellow mosaic virus F/R . M: DNA ladder, Well 1: negative control, Well 2: positive control.

The electrophoresis result (Figure 2) indicated that the sample in well 2 was positioned near the 200 bp band of the DNA ladder, corresponding to the amplification of the 214 bp gene segment (Aguiar et al., 2019). A comparison of the obtained sequence with ZYMV virus sequences published on GenBank revealed that the amplified gene segment is 99.07% similar to the ZYMV virus gene sequence with accession number DQ925448.1 (Ha et al., 2008). This confirms that the PCR reaction established in this study successfully amplified the correct gene segment of the ZYMV virus.

3.2. Cloning a bacterial strain carrying the ZYMV gene

Figure 3. White colonies grow on Luria-Bertani medium.

To confirm that the colonies growing on the culture medium (Figure 3) contain the target gene segment, PCR will be conducted using the primer pair pJET1.2. The initial size of the target gene segment was 214 bp. While the amplified plasmid DNA will measure 332 bp (which includes 118 bp from the pJET1.2 vector). The electrophoresis results (Figure 4) indicated that the vector containing the target gene segment has been successfully transformed into the bacteria.

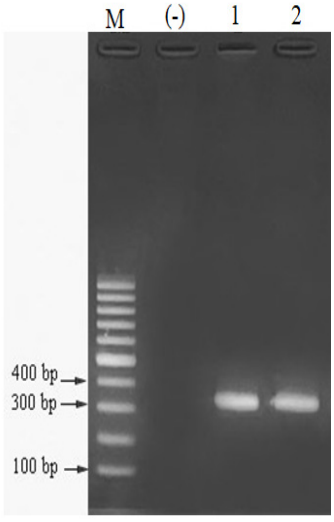

Figure 4. Electrophoresis result of PCR colonies with primer pair pJET1.2 (M: DNA ladder, (-): negative control, well 1: colony sample).

The sequencing results of the plasmid DNA sample, after successful cloning, show a 100% similarity with the gene sequence prior to insertion into the vector, and a 99.07% similarity with the ZYMV virus sequence (accession number DQ 925448.1) published in GenBank (Ha et al., 2008). This confirms that the gene segment inserted into the plasmid corresponds to the ZYMV virus gene.

3.3. Realtime RT-PCR reaction results

3.3.1. Generation of a standard curve

The correlation coefficient R^2 of the plasmid DNA sample is 0.9969 (Figure 5), which is with the acceptable limit (R^2 0.99), indicating that standard curve has high linearity, this supports accurate dilution calculations and pipetting of the required volumes. The standard curve equation is given by y = -3.417x + 49.605. The PCR reaction efficiency (E%) is 96.18%, and the slope is -3.417, both of which fall within the acceptable range. The standard curve was constructed based on the Ct threshold cycle value, using five standard points corresponding to five diluted concentrations of plasmid DNA, with each concentration repeated three times to enhance accuracy (Table 2). All plasmid DNA samples with concentrations of 10^9, 10^8, 10^7, 10^6, and 10^5 copies/µL were successfully amplified as shown by the amplification chart (Figure 6) and melting curve (Figure 7).

Table 2. Ct value of the reaction that amplifies the sample containing the Zucchini yellow mosaic virus gene segment

Sample (copies/µL)	Log of copies number	Threshold cycle (Ct) (Mean ± SD)	Coefficient of Variation (%)
10^9	7	18.51 ± 0.15	0.83
10^8	6	21.77 ± 0.38	1.75
10^7	5	26.18 ± 0.12	0.46
10^6	4	29.81 ± 0.43	1.43
10^5	3	33.79 ± 0.55	1.69
(-)	0	_	_

"-": negative control, "_": not detected.

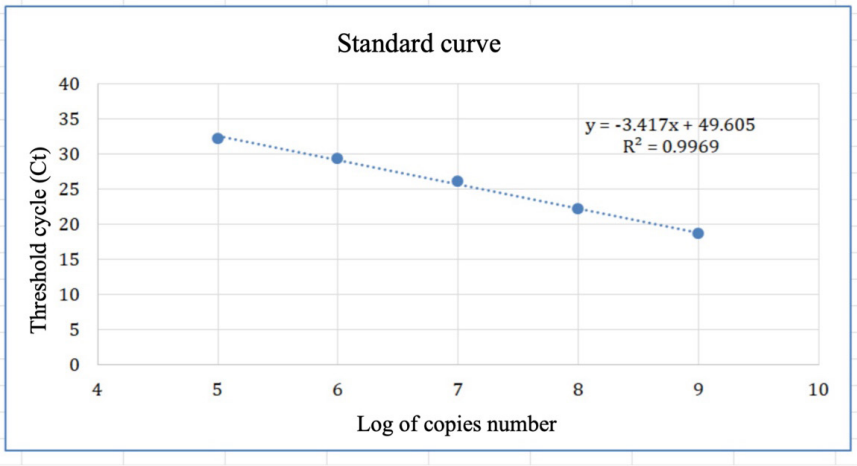

Figure 5. Standard curve generated from the plasmid containing the target gene.

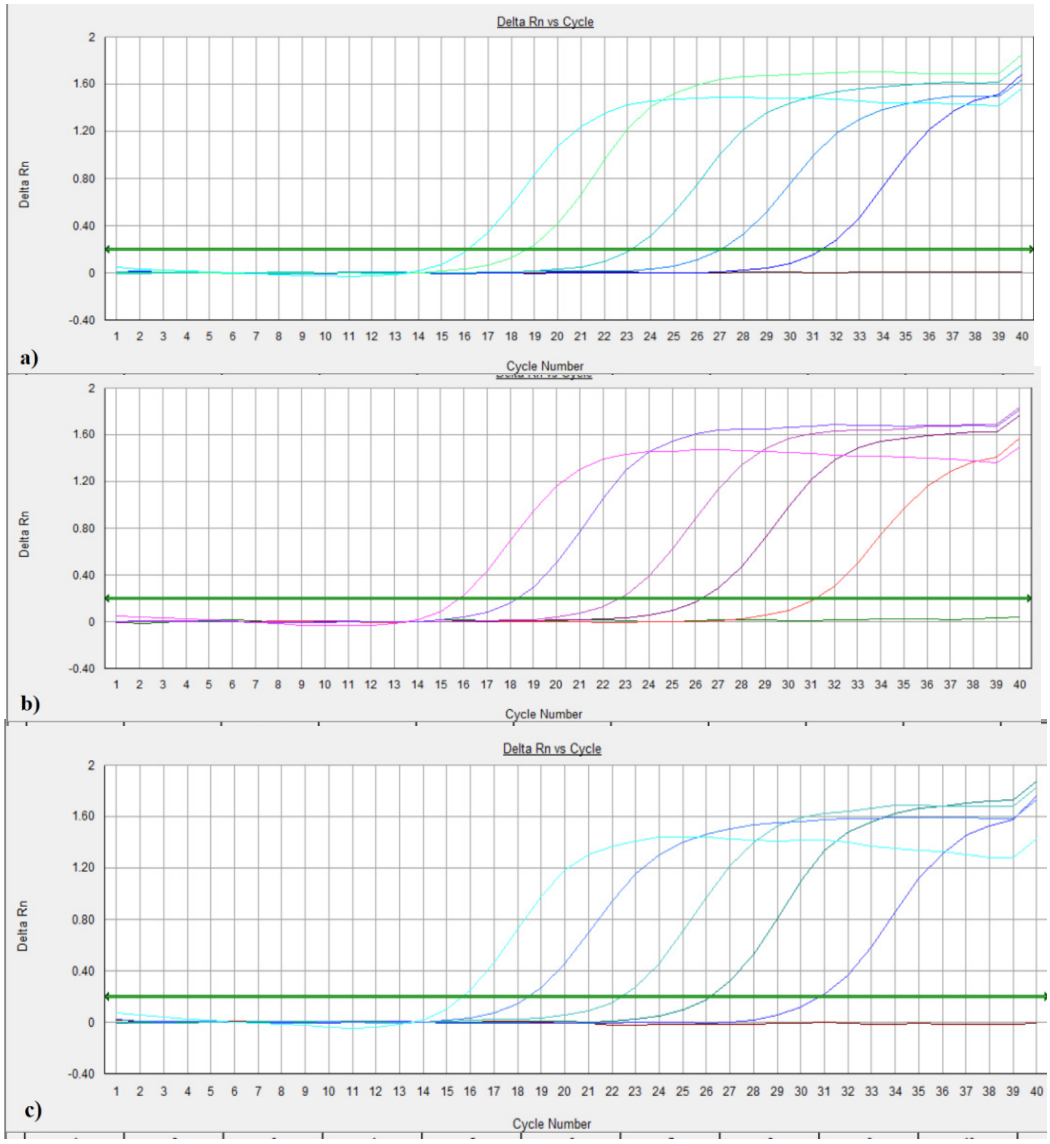

Figure 6. Amplification chart of Zucchini yellow mosaic virus gene segment based on fluorescence signal. (a): replication 1, (b): replication 2, (c): replication 3.

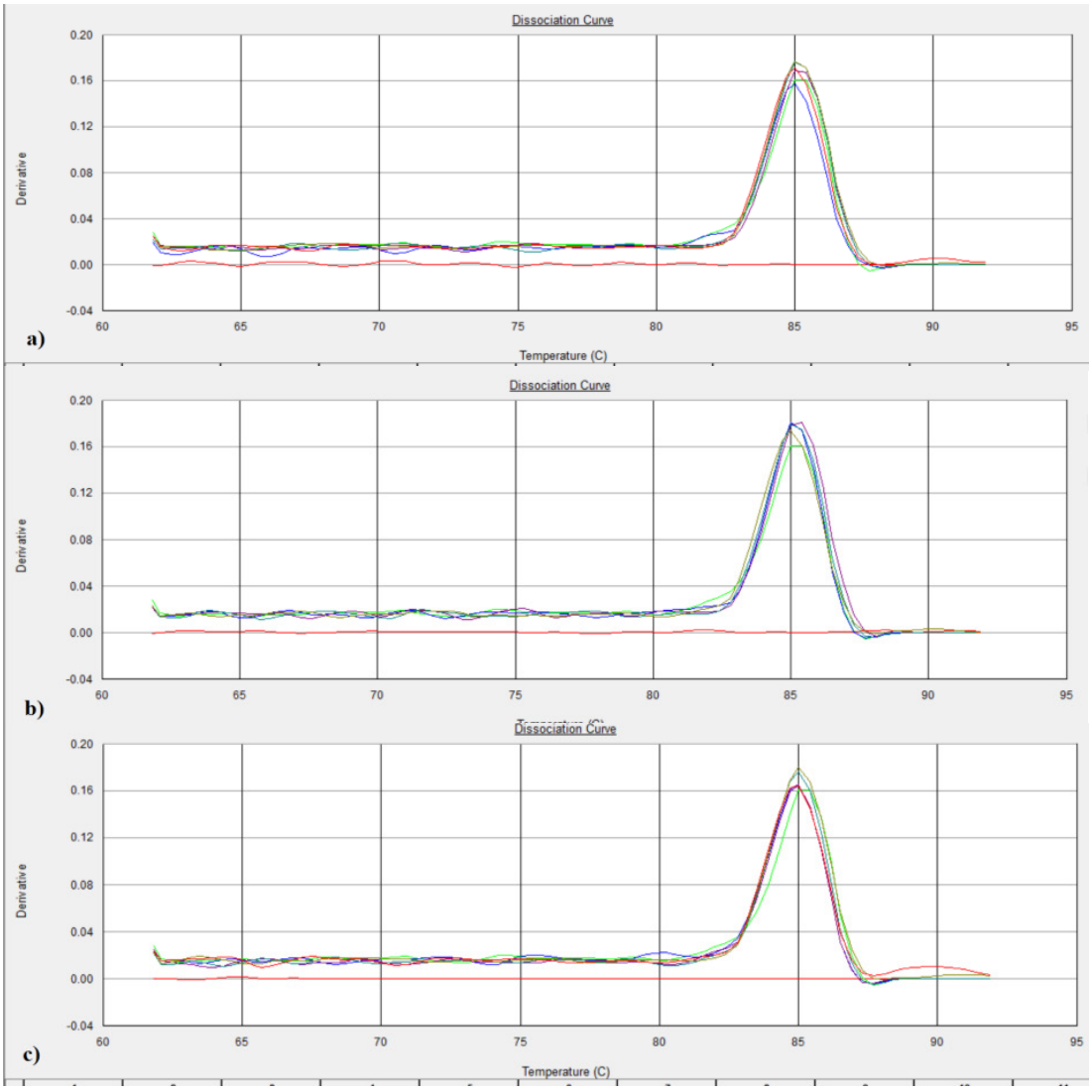

Figure 7. Melting curve diagram of Zucchini yellow mosaic virus gene fragment. (a): replication 1, (b): replication 2, (c): replication 3.

3.3.2. Evaluation of the specificity of the realtime RT-PCR

Table 3. The results for the specificity evaluation of the realtime RT-PCR

Sample	Threshold cycle (Ct)	Quantitative value (number of copies/ µL)	Qualitative
Zucchini yellow mosaic virus	18.45	1.3 x 10^9	+
Dasheen mosaic virus	_	_	-
Papaya ringspot virus	_	_	-
Chilli veinal mottle virus	_	_	-

"+": positive, "-": negative, "_": not detected.

The result in Table 3 showed that the RT-PCR assay did not detect the virulence gene in the cDNA of DsMV, PRSV, and ChiVMV. This result suggested that the primer was specified with ZYMV.

3.3.3. Diagnosis of ZYMV on field samples with realtime RT-PCR procedure

Of the 10 samples collected from garden 1, 4 were identified as positive for the ZYMV virus (Table 4). In garden 2, all 10 samples tested positive for the ZYMV virus. Notably, the quantification values for the 20 samples ranged from 7.1 x 10^6 to 8.5 x 10^9 copies/µL (Table 4).

Table 4. Threshold cycle (Ct) values of realtime RT-PCR for pumpkin leaf samples collected from the field

Garden	Sample	Realtime RT-PCR			PCR
		Ct	Quantitative value (Number of copies/µL)	Qualitative	Qualitative
	Negative control (-)	-	-	-	-
	Positive control (+)	18.45	1.3 x 10^9	+	+
Garden 1	1.1	25.48	11.5 x 10^6	+	+
	1.2	22.41	90.9 x 10^6	+	+
	1.3	16.14	6.2 x 10^9	+	+
	1.4	-	-	-	-
	1.5	-	-	-	-
	1.6	16.4	5.22 x 10^9	+	+
	1.7	-	-	-	-
	1.8	-	-	-	-
	1.9	-	-	-	-
	1.10	-	-	-	-
Garden 2	2.1	15.67	8.5 x 10^9	+	+
	2.2	26.14	7.4 x 10^6	+	+
	2.3	25.12	14.6 x 10^6	+	+
	2.4	25.44	11.8 x 10^6	+	+
	2.5	16.55	4.7 x 10^9	+	+
	2.6	23.77	36.4 x 10^6	+	+
	2.7	22.73	73.3 x 10^6	+	+
	2.8	23.17	54.5 x 10^6	+	+
	2.9	26.19	7.1 x 10^6	+	+
	2.10	24.93	16.6 x 10^6	+	+

(+): positive, (-): negative.

The qualitative results showed 100% concordance between the realtime RT-PCR method and the RT-PCR method. The results showed that the presence of ZYMV virus is quite common, causing losses in productivity and product quality during harvest, but to date there are no detailed statistics on losses caused by the disease. For the conventional RT-PCR technique, the PCR product needs to be electrophoresed to check the results, but with realtime RT-PCR technique, the amplification and quantification reactions take place at the same time, without the need for electrophoresis, which saves time and shortens the experimental steps compared to conventional RT-PCR technique. In addition, with high sensitivity, realtime RT-PCR technique can detect ZYMV virus early in the seed source or in seedlings before symptoms appear, thereby helping to eliminate pathogens early, reduce the possibility of spreading, save time, planting costs and care efforts.

4. Conclusions

The realtime RT-PCR technique demonstrated high specificity and accuracy in detecting the ZYMV virus. This diagnostic procedure was effective in quantifying the concentration of ZYMV in field-collected samples, revealing viral loads ranging from 7.1 x 10^6 to 8.5 x 10^9 copies/µL.

Conflict of interest

The author declares that there are no conflict of interest to disclose related to this manuscript.

Acknowledgements

This research was supported by the Research Institute for Biotechnology and Environment, Ho Chi Minh city Nong Lam University.

References

Aguiar, R. W. S., Martins, A. R., Nascimento, V. L., Capone, A., Melo Costa, L. T., Campos, F. S., Fidelis, R. R., Santos, G. R., Resende, R. O., & Nagata, T. (2019). Multiplex RT-PCR identification of five viruses associated with the watermelon crops in the Brazilian Cerrado. *African Journal of Microbiolog Research* 13(3), 60-69. https://doi.org/10.5897/AJMR2018.8976.

Ha, C., Revill P., Harding, R. M., Vu, M., & Dale, J. L. (2008). Identification and sequence analysis of potyviruses infecting crops in Vietnam. *Archives of Virology* 153(1), 45-60. https://doi.org/10.1007/s00705-007-1067-1.

Hu, J. S., Ferreira, S., Wang, M., & Xu, M. Q. (1993). Detection of cymbidium mosaic virus, odontoglossum ringspot virus, tomato spotted wilt virus, and potyviruses infecting orchids in Hawaii. *Plant Disease* 77(5), 464-468.

Lim, T. K. (2012). Cucurbita moschata. In Lim, T. K. (Ed.). *Edible medicinal and non-medicinal plants - Volume 2: Fruit*. Dordrecht, Netherlands: Springer. https://doi.org/10.1007/978-94-007-1764-0_41.

Moradi, Z., Mehrvar, M., & Nazifi, E. (2019). Population genetic analysis of Zucchini yellow mosaic virus based on the CI gene sequence. *Journal of Cell and Molecular Research* 10(2), 76-89. https://doi.org/10.22067/jcmr.v10i2.76133.

Sambrook, J., & Russell, D.W. (2001) *Molecular cloning: A laboratory manual* (3rd ed.). New York, USA: Cold Spring Harbor Laboratory Press.

Staroscik, A. (2004). *Calculator for determining the number of copies of a template*. Retrieved March 14, 2023, from http://cels.uri.edu/gsc/cndna.html.

Evaluating the production of freeze-dried Kefir yogurt supplements with *Cordyceps militaris*

Tran B. T. Huynh[1], Trang D. T. Le[2], & Loan T. T. Cao[1*]

[1]Faculty of Biological Sciences, Nong Lam University, Ho Chi Minh City, Vietnam

[2]Research Institute of Biotechnology and Environment, Nong Lam University, Ho Chi Minh City, Vietnam

ARTICLE INFO

Research Paper

Received: August 31, 2024
Revised: December 13, 2024
Accepted: December 18, 2024

Keywords

Cordyceps militaris
Gelatin
Kefir
Maltodextrin
Skimmed milk powder

***Corresponding author**

Cao Thi Thanh Loan
Email:
loan.caothithanh@hcmuaf.edu.vn

ABSTRACT

The research aimed to produce freeze-dried Kefir yogurt supplemented with *Cordyceps militaris*, diversifying fermented foods, while offering convenient storage, consumption options and health benefits. To enhance the structure and flavor of the product, ingredients such as maltodextrin, skimmed milk powder and gelatin were incorporated. Experiments also included the addition of sucrose to further enhance these attributes. The optimal formulation for the freeze-dried Kefir yogurt supplemented with *C. militaris* was determined as containing Kefir with 5% *C. militaris* powder, while maintaining a lactic acid bacteria (LAB) count of 7.4 × 10^7 CFU/g. This formulation also received the highest sensory scores and positive feedback on its structure, flavor, and moisture content, which remained below 5%. The study revealed that the addition of *C. militaris* powder to Kefir yogurt did not significantly impact the LAB count. In conclusion, the research successfully developed a freeze-dried Kefir yogurt enriched with *C. militaris* which contains bioactive compounds such as Cordycepin (1712 mg/kg) and Adenosine (89.9 mg/kg), contributing to yogurt's potential as a promising healthy snack.

Cited as: Huynh, T. B. T., Le, T. D. T., & Cao, L. T. T., (2024). Evaluating the production of freeze-dried Kefir yogurt supplements with *Cordyceps militaris*. *The Journal of Agriculture and Development* 23(Special issue 2), 193-202.

1. Introduction

In Vietnam, digestive-related diseases affect up to 10% of the population, and the incidence is rising. These disorders, such as constipation, diarrhea, and gastroesophageal reflux disease, can significantly impact patients' health and daily life if left untreated. The digestive system, particularly the intestines, plays a crucial role in the immune system by protecting against disease-causing agents in food. Kefir, a fermented milk drink, contains more than 30 beneficial microflora offering various health benefits including improved digestion, antibacterial effects, and antioxidant activity (Rosa et al., 2017). Despite these advantages, Kefir remains less popular in Vietnam due to its unique taste and limited awareness. Additionally, its short shelf life and temperature-sensitive storage requirements present challenges (Ho et al., 2021).

Cordyceps militaris (CM) is known for its bioactive compounds with numerous health benefits, ranging from anti-inflammatory to neuroprotective properties (Das et al., 2010). It's composed of various bioactive compounds, including adenine, polysaccharide, cordycepin, adenosine, and cordyheptapeptide (Wu et al., 2019). The CM has been shown to enhance the NK cell activity and lymphocyte proliferation and partially increased Th1 cytokine secretion. Therefore, CM is safe and effectively increased cell-mediated immunity of healthy male adults (Kang et al., 2015). However, despite the availability of various *C. militaris*, their bitter taste and aroma limit their popularity among consumers. To address these issues, combining *C. militaris* with sweet and sour Kefir yogurt, following by freeze-drying could be optimal method to improve the sensory, biological, and nutritional characteristics of the product, and making it suitable for long-term storage and easy transportation (Ho et al., 2021). Therefore, this research aimed to diversify product options and make Kefir as well as *C. militaris* more accessible to Vietnamese consumers enhancing both taste and health benefits.

2. Materials and Methods

2.1. Kefir milk

Kefir yogurt was supplied by Tracy Kefir, Viet Nam. The Kefir fermentation process used the commercial unsweetened pasteurized cow's milk (Vietnam Dairy Products Joint Stock Company, Vietnam) as the medium. Kefir grains were added to the milk at a concentration of 7% (w/v) and the mixture was thoroughly mixed to ensure even distribution of the Kefir grains and the milk. The fermentation process occurred at 22°C for 22 - 24 h. Then, the Kefir yogurt product was refrigerated at 1 - 4°C to preserve its structure and flavor.

2.2. *Cordyceps militaris* powder

Cordyceps militaris dried powder with 6 ± 0.25% moisture content, supplied by the Research Institute of Biotechnology and Environment (RIBE) at Nong Lam University, Ho Chi Minh City, Vietnam. The powder was added directly to the Kefir yogurt at concentrations of 5%, 6%, or 7% and mixed thoroughly. The particle size of dried CM powder is around 1 mm that helps it to dissolve quickly in the fermented Kefir without forming lumps. These varying concentrations were tested to evaluate potential differences in sensory quality and bacterial counts resulting from the incremental incorporation of *C. militaris* into the Kefir yogurt.

2.3. Food additives

The production of freeze-dried Kefir involves the incorporation of several food additives to maintain the overall quality of the kefir as well as the density of beneficial bacteria in the final product. Maltodextrin (MD), used as a stabilizer, is sourced from Tereos FKS in Indonesia. Skimmed milk powder (SMP), an essential component for enhancing the nutritional profile and texture is imported from New Zealand, and gelatin (G), which contributes to the structural integrity and mouthfeel of the final product, is obtained from Ewald-Germany. To determine the optimal formulation, each additive MD, SMP, and G was incorporated at three different concentrations (5%, 10%, and 15%). A control sample containing only Kefir and *Cordyceps militaris* (CM) without any additives was also prepared. All samples were then subjected to freeze-drying and subsequently evaluated based on lactic acid bacteria counts and sensory attributes.

2.4. Preparation of the freeze-dried kefir yogurt supplemented with CM

The freeze-dried yogurt was prepared followed by Doan et al (2022). Briefly, the kefir milk after fermentation (24 h) was mixed with CM powder and each additive MD, SMP, and G, respectively as described above. Finally, 10% sucrose was added to the mixture to reduce the bitterness of CM. Then, the mixture was poured into silicone molds (21 x 4 x 16 cm), placed on stainless steel trays and were placed in the freeze dryer (Harvestright, UT, USA) operating at - 30°C, and dried at 45°C, with a total drying time of 30 h (Yamaguchi et al., 2019; Ismail et al., 2020; Pham, 2022).

2.5. Lactic acid bacteria count

The lactic acid bacteria (LAB) were isolated from Kefir yogurt products using a serial dilution method. Briefly, the sample was serially diluted to 10^{-5} and 100 µL aliquots from dilution factors of 10^{-3} to 10^{-5} were spread onto MRS medium. The MRS medium consisted of 0.4% yeast extract, 0.8% beef extract, 1% peptone, 2% D-glucose, 0.2% K_2HPO_4, 0.02% $MgSO_4$, 0.004% $MnSO_4$, 0.1% Tween 80, and 0.5% sodium acetate ($C_2H_3NaO_2$), with 2% agar powder added, following the formulation by de Man et al. (1960). Uniform colonies were collected and subcultured on MRS agar at 37°C for 48 h. Colony morphology, gram staining, catalase, oxidase, urease, motility, and endospore staining were performed for preliminary identification. The LAB count is calculated using the following formula:

$$A = \frac{N}{n_1 \times V \times f_1 + ... + n_i \times V \times f_1}$$

Where:

A: The number of bacteria in 1 gram of the sample (CFU/mL).

N: The total number of colonies counted on the selected plates.

V: The volume of the sample solution inoculated onto each plate (mL).

n_i: The number of plates inoculated at the i-th dilution level.

f_i: The corresponding dilution factor.

2.6. Sensory evaluation

The sensory attributes of Kefir yogurt and freeze-dried snacks were evaluated using a 9-point hedonic scale, as described by Noel et al. (2011). Thirty consenting volunteers rated their liking or disliking of various attributes, such as appearance, aroma, taste, texture, and overall acceptability, on a scale ranging from 1 means "Dislike Extremely" to 9 means "Like Extremely". The results of the sensory tests provided valuable insights into consumer acceptance and preferences for the product.

2.7. Moisture content

The moisture content of the dried yogurt tablets was measured by drying the samples at 105°C in a forced-air drying oven (Ahn et al., 2014), until a constant weight was obtained. The moisture content was then calculated according to the Vietnamese standard TCVN 10788:2015.

$$W = \frac{M1 - M2}{M1} \times 100$$

Where:

W: Moisture content of the yogurt tablets (%);

M1: Initial weight of the yogurt tablets (g);

M2: Weight of the yogurt tablets after drying (g).

2.8. Data analysis

The data was analyzed using one-way ANOVA with Minitab 16 software to determine statistically significant differences among treatments ($\alpha = 0.05$).

3. Results and Discussion

3.1. Bacterial count in Kefir yogurt

The colonies isolated from Kefir yogurt appeared round, smooth, and milky white in color. The bacteria were Gram-positive and tested positive for catalase activity, while negative for oxidase. The isolates demonstrated the ability to utilize calcium carbonate ($CaCO_3$) but were non-motile and did not form endospores. Based on these biochemical tests, the isolated bacteria were characterized as lactic acid bacteria (LAB). After 24 h of fermentation, the LAB count in Kefir yogurt was 5.4 x 10^8 CFU/mL. Previous studies have also reported the presence of beneficial probiotic microorganisms in Kefir yogurt. For instance, Rosa et al. (2017) reported that the probiotic microorganisms in the Kefir yogurt are in range of 10^4 - 10^7 CFU/mL. In the present study, the Kefir yogurt product contained a higher number of beneficial bacteria, which is expected to promote potential positive health effects (Mijačević et al., 2001; Castellone et al., 2021).

3.2. The effect of CM powder on the quantity of LAB after mixing with Kefir yogurt

Liquid Kefir yogurt, supplemented with varying concentrations of CM, was utilized to assess the density of lactic acid bacteria (LAB). This experiment was performed prior to the freeze-drying process to investigate the impact of CM powder addition on the population of beneficial bacteria in Kefir yogurt. The results of this analysis are summarized in Table 1.

Table 1. Lactic acid bacteria (LAB) count of liquid Kefir yogurt after *Cordyceps militaris* (CM) supplementation

CM supplementation ratio in Kefir (%)	The average LAB count (Log CFU/mL)
0	$8.73^a \pm 0.01$
5	$8.72^a \pm 0.008$
6	$8.73^a \pm 0.008$
7	$8.74^a \pm 0.008$

The results are presented as the mean ± SD. Different letters in the same column indicated that values were significantly different (P < 0.05).

All four samples had a LAB count of 8 log CFU/mL, indicating potential probiotic benefits (Table 1). There was no statistically significant difference in the number of LAB observed after the addition of CM, suggesting that CM did not influence LAB density in Kefir yogurt. According to the study of Ghasempour et al. (2014), consuming 100 mL of Kefir daily offers beneficial probiotics, enzymes, and nutrients. Besides, a review by Truong et al. (2023) has shown that CM contains nucleosides, sterols, polysaccharides, and phenolic compounds that can support immunity and provide antioxidant supplementation to the body. Additionally, *C. militaris* is a valuable source of natural carotenoids, which are secondary metabolites

in the fruiting body and mycelium that may contribute to the color of the freeze-dried yogurt (Figure 1) (Lee et al., 2020). It has been shown that carotenoids possess strong antioxidant properties, which help mitigate oxidative stress and protect retinal cells from damage (Chen et al., 2022). Therefore, the evaluation of bioactive activities of these compounds in the freeze-dried Kefir yogurt is necessary in future research.

Another research by Huynh et al. (2022) found that using 0.25 to 0.5 g of CM powder did not result in any adverse effects on mice and had a liver-protective impact through the ability to reduce AST-ALT liver enzyme activity in plasma, reduce Malondialdehyde content, and inhibited hepatocellular lipid peroxidation. Based on these findings, adding 5%, 6%, and 7% CM powder to 100 mL of Kefir yogurt may provide health and digestive benefits without any adverse effects on the human body. Due to insignificant effects on density of LAB when adding CM powder to Kefir, the optimal concentration of CM powder was selected based on sensory evaluation results below.

3.3. Sensory evaluation

To determine the optimal concentration of CM to be added to Kefir yogurt before freeze-drying, a sensory evaluation was conducted. Initial samples displayed a bitter taste, attributed to the inherent bitterness of CM. Therefore, the formular of the was modified following the approach outlined by Doan et al. (2022) with 10% sucrose was incorporated. Sensory evaluation results indicated that Kefir yogurt supplemented with 5% CM powder achieved the highest sensory scores, regardless of the presence of sucrose (Table 2). Consequently, the 5% CM powder concentration was selected as the optimal ratio for Kefir yogurt production.

Table 2. Sensory evaluation (n = 30) of fresh Kefir yogurt with *Cordyceps militaris* (CM) supplement

Samples	Average score	
	Set 1: without sucrose	Set 2: add 10% sucrose
100% Kefir (Control)	$3.38^{b} \pm 0.57$	$8.04^{a} \pm 0.28$
Kefir + 5% CM	$3.98^{b} \pm 0.43$	$8.55^{a} \pm 0.22$
Kefir + 6% CM	$2.68^{b} \pm 0.37$	$7.11^{a} \pm 0.31$
Kefir + 7% CM	$2.48^{b} \pm 0.29$	$6.79^{a} \pm 0.30$

The results are presented as the mean ± SD. Different letters in the same row indicated that values were significantly different ($P < 0.05$).

3.4. Identification of optimal additive(s) for the freeze-dried Kefir yogurt supplemented with CM

The food additives were incorporated into kefir yogurt to maintain the overall quality of the kefir as well as the density of beneficial bacteria in the final product after freeze-drying. Samples containing 5% MD and 5% SMP exhibited structural damage, while those with 10% and 15% MD, SMP retained their shape (Figure 1). The yogurt sample with gelatin was shrunk and cannot maintain the shape well (G sample, Figure 1). Therefore, yogurt samples with MD and SMP supplementation were used to investigate the viability of LAB after freeze-drying.

The results showed significant differences between the control and the samples with additives, as well as variations in the effect of different additive ratios (Table 3). After supplementing with MD and SMP, there was a significant increase in the LAB quantity at all ratios. Among the three ratios of additives, the products with 15% additives showed the highest LAB count, followed by 10%, and 5%. This trend was consistent for both type of additives, MD and SMP. These results were consistent with previous studies (Reddy et al., 2009; Ismail et al., 2020), in which LAB survival was higher in Kefir spray-dried with MD compared to non-fat samples. The inclusion of 10% sugar as lyoprotective agents markedly enhanced the survival rates of both lactic acid bacteria and yeasts was also shown in the study of Chen et al. (2006). These findings also align with research by Pham (2022) on the positive impact of increased additive ratios in enhancing the survival of LAB after freeze drying Kefir yogurt.

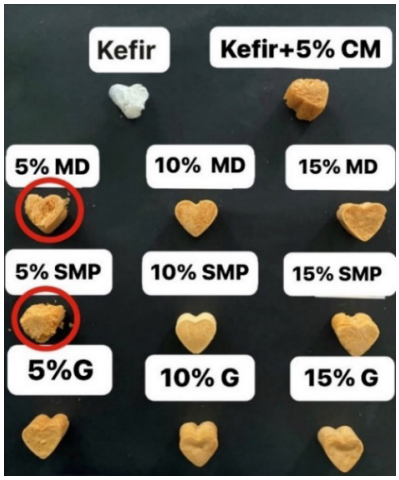

Figure 1. Freeze-dried CM-supplemented Kefir yogurt with additives.

The structural integrity of all four samples remained intact, and the LAB count was within an acceptable range as a beneficial bacterial count of at least 6 Log CFU/g is linked to positive health effects (Castellone et al., 2021). Therefore, the 10% and 15% of MD and SMP samples were selected for further testing in the next content.

Table 3. Variations in lactic acid bacteria (LAB) counts among the Kefir samples after freeze-drying

Sample	Average LAB count (Log CFU/g)
Kefir + 5% CM	$6.74^{d} \pm 0.02$
Kefir + 5% CM + 5% MD	$7.74^{c} \pm 0.01$
Kefir + 5% CM + 10% MD	$7.80^{b} \pm 0.01$
Kefir + 5% CM + 15% MD	$7.87^{a} \pm 0.01$
Kefir + 5% CM + 5% SMP	$7.75^{c} \pm 0.03$
Kefir + 5% CM + 10% SMP	$7.81^{b} \pm 0.01$
Kefir + 5% CM + 15% SMP	$7.87^{a} \pm 0.02$

The results are presented as the mean ±SD. Different letters in the same column indicated that values were significantly different (P < 0.05).

3.5. Improving the sensory taste of the freeze-dried Kefir yogurt formula supplemented with CM

After selecting the optimal ratio and type of additives to preserve structural integrity and ensure a stable LAB count in the kefir snacks, further improvement in the product's taste was identified as necessary. While the sourness of the kefir and bitterness of the CM were moderated, the product's overall flavor remained unpalatable due to the strong taste of CM powder. Following the approach used in the previous research on dried yogurt products by Doan et al. (2022), 10% sucrose was added to improve the sensory properties of freeze-dried Kefir. The moisture content and LAB viability of the sugar-added product were presented in Tables 4 and 5.

Table 4. The result average moisture content (%) of the freeze- dried Kefir

5% CM Kefir yogurt	Average moisture (%)	TCVN 7729: 2007
MD 10% + 10% Sucrose	$1.16^{d} \pm 0.02$	Pass (< 5%)
MD 15% + 10% Sucrose	$2.84^{b} \pm 0.02$	Pass (< 5%)
SMP 10% + 10% Sucrose	$2.03^{c} \pm 0.03$	Pass (< 5%)
SMP 15% + 10% Sucrose	$3.07^{a} \pm 0.02$	Pass (< 5%)

The results are presented as the mean values (± SD). Different letters in the same column indicated that values were significantly different (P < 0.05). MD: Maltodextrin; SMP: Skimmed milk powder.

3.6. LAB count after freeze-drying

Table 5. Lac tic acid bacteria (LAB) density of four freeze-dried Kefir yogurt samples

5% CM Kefir yogurt	Average LAB count (Log CFU/g)
MD 10% + 10% Sucrose	$7.80^{b} \pm 0.01$
MD 15% + 10% Sucrose	$7.87^{a} \pm 0.01$
SMP 10% + 10% Sucrose	$7.81^{b} \pm 0.01$
SMP 15% + 10% Sucrose	$7.87^{a} \pm 0.01$

The results are presented as the mean values (± SD). Different letters in the same column indicated that values were significantly different (P < 0.05). MD: Maltodextrin; SMP: Skimmed milk powder.

All four samples meet the moisture content requirements of the Vietnamese standard for heat-treated milk products TCVN 7729:2007 (Table 4). This demonstrates good preservation efficiency of freeze-dried yogurt. In addition, the results in Table 5 showed that the samples with 15% added maltodextrin and skimmed milk powder have higher LAB count than those added at 10%. However, all four samples complied with the CODEX STAN 243 - 2003 requirement for a count of at least 7 log CFU/g of beneficial bacteria (CAC, 2003). Therefore, the optimal formula for freeze-dried kefir was decided by sensory evaluation score. The results of Table 6 showed that the 15% MD with 10% sucrose freeze-dried Kefir achieved the highest sensory evaluation score of 8.62 while maintaining structural integrity.

Table 6. Sensory evaluation scores (n = 30) of freezes- dried Kefirs supplemented with *Cordyceps militaris* (CM)

Sample	Average score
MD 10% + 10% Sucrose	$7.80^{b} \pm 0.40$
MD 15% + 10% Sucrose	$8.62^{a} \pm 0.26$
SMP 10% + 10% Surcose	$7.02^{c} \pm 0.39$
SMP 15% + 10% Surcose	$6.44^{d} \pm 0.31$

The results are presented as the mean values (± SD). Different letters in the same column indicated that values were significantly different (P < 0.05). MD: Maltodextrin; SMP: Skimmed milk powder.

Through the evaluation of structural integrity and sensory scores, the 15% maltodextrin added 10% sucrose sample stood out with the best results, maintaining its structure after drying and density of beneficial LAB. Additionally, the product quality was evaluated based on cordycepin and adenosine content, yeast and mold counts. The product met the requirements of the Vietnamese Standard TCVN 7030:2002 for heat-processed dairy products, with no presence of yeast or mold detected, thereby confirming the product's safety for consumption.

The final Kefir products were sent for quantification to the Center for Analytical Services and Experimentation (CASE), concluding that the freeze-dried Kefir contained Cordycepin of 1712 mg/kg and Adenosine of 89.9 mg/kg. The results show that the inclusion of 5% CM powder in the product, using approximately 15 g, equivalent to 30 dried Kefir yogurt tablets supplemented with CM, would be sufficient to meet the body's immunity and digestive support needs based on the study Sun et al. (2014). Furthermore, the incorporation of *C. militaris* powder into Kefir yogurt could potentially enhance some beneficial effects. For example, the protective effects of *C. militaris* polysaccharide-supplemented probiotic yogurt have been demonstrated in mice, where daily consumption for 28 days led to notable improvements in liver health. Research by Han et al. (2020) showed that this supplementation significantly reduced liver damage in mice with alcoholic liver injury. The effects included a marked decrease in liver index, alanine aminotransferase (ALT) and aspartate aminotransferase (AST) activities, as well as reductions in total cholesterol (TC), triglyceride (TG), and low-density lipoprotein cholesterol (LDL-C) levels in the serum. In addition, the cordycepin in *C. militaris*, which structurally resembles adenosine, plays a critical role in DNA and RNA synthesis. As demonstrated by Thuy et al. (2021), cordycepin can integrate into the RNA and DNA structures of bacteria and viruses, interfering with nucleic acid biosynthesis and modification. This activity limits the growth of harmful microorganisms, adding another layer of health benefits to the product. Given these findings, further research is needed to explore the full bioactive potential of the developed freeze-dried Kefir yogurt supplemented with *C. militaris*, particularly in relation to its effects on liver health, microbial growth, and overall nutritional value.

4. Conclusions

The findings of this study indicate that freeze-dried Kefir yogurt could serve as a promising market alternative for the dairy industry given its high beneficial lactic acid bacteria count. The

addition of *C. militaris* powder to the Kefir yogurt did not significantly impact the LAB density, indicating compatibility between CM and Kefir yogurt. However, the structural integrity of dried Kefir yogurt was notably influenced by the choice of additives used in the formulation. Among the three tested additives, maltodextrin demonstrated superior preservation of LAB viability while also maintaining the structural integrity of freeze-dried Kefir yogurt.

Conflict of interest

All authors declare that they have no conflict of interest.

Acknowledgements

The authors express sincere gratitude to the Faculty of Biological Sciences at Nong Lam University Ho Chi Minh City for their guidance and support throughout their studies. Special thanks to Tracy Kefir Company and the Research Institute of Biotechnology and Environment, Nong Lam University Ho Chi Minh City for providing the necessary resources for study completion.

References

Ahn, J. Y., Kil, D. Y., Kong, C., & Kim, B. G. (2014). Comparison of oven-drying methods for determination of moisture content in feed ingredients. *Asian-Australasian Journal of Animal Sciences* **27(11), 1615.** https://doi.org/10.5713/ajas.2014.14305.

CAC (Codex Alimentarius Commission). (2003). Codex Standard 243-2003 for fermented milks, adopted on June 4, 2003. Retrieved October 20, 2024, from http://www.fao.org/fao-who-codexalimentarius.

Castellone, V., Bancalari, E., Rubert, J., Gatti, M., Neviani, E., & Bottari, B. (2021). Eating fermented: Health benefits of LAB-fermented foods. *Foods* 10(11), 2639. https://doi.org/10.3390/foods10112639.

Chen, B. Y., Huang, H. S., Tsai, K. J., Wu, J. L., Chang, Y. T., Chang, M. C., Lu, C. M., Yang, S. L., & Huang, H. S. (2022). Protective effect of a water-soluble carotenoid-rich extract of *Cordyceps militaris* against light-evoked functional vision deterioration in mice. *Nutrients* 14(8), 1675. https://doi.org/10.3390/nu14081675.

Chen, H. C., Lin, C. W., & Chen, M. J. (2006). The effects of freeze drying and rehydration on survival of microorganisms in kefir. *Asian-Australasian Journal of Animal Sciences* 19(1), 126-130. https://doi.org/10.5713/ajas.2006.126.

Das, S. K., Masuda, M., Sakurai, A., & Sakakibara, M. (2010). Medicinal uses of the mushroom *Cordyceps militaris*: current state and prospects. *Fitoterapia* 81(8), 961-968. https://doi.org/10.1016/j.fitote.2010.07.010.

de Man, J. D., Rogosa, D., & Sharpe, M. E. (1960). A medium for the cultivation of lactobacilli. *Journal of Applied Microbiology* 23(1), 130-135. https://doi.org/10.1111/j.1365-2672.1960.tb00188.x.

Doan, T. U. N., Nguyen T. Y. L., Hoang T. T., & Cao T. T. L. (2022). Developing freeze-dried snack bites from kefir milk. In *The 4th international Conference on Sustainable Agriculture and Environment* (16-27). Nong Lam University, Ho Chi Minh City. Retrieved April 1, 2024, from https://hcmuaf.edu.vn/data/proceedings-sae2022.pdf.

Ghasempour, M., Sefidgar, S. A. A., Moghadamnia, A. A., Ghadimi, R., Gharekhani, S., & Shirkhani, L. (2014). Comparative study of Kefir yogurt-drink and sodium fluoride mouth rinse on salivary mutans streptococci. *The Journal of Contemporary Dental Practice* 15(2), 214. https://doi.org/ 10.5005/jp-journals-10024-1517.

Han, Y., W., Liu, Y. Y., & Chen, W. (2020). Synergistic protective effects of cordyceps militaris polysaccharide supplemented yogurt on alcoholic liver injury in kunming mice. *Food*

Science 41(1), 209-214. https://doi.org/10.7506/spkx1002-6630-20181120-228.

Ho, P. H., Vu, T. T., Nguyen, C. N., & Vu, H. S. (2021). Development of freeze-dried red dragon fruit yoghurt containing probiotics. *Journal of Science and Technology: Engineering and Technology for Sustainable Development* 31(4), 014-018. https://doi.org/10.51316/jst.153.etsd.2021.31.4.3.

Huynh, N. T. D., Tri, K. N., Le, P. N. T., Nguyen, T. N. T., & Tran, C. L. (2022). Evaluation of toxicity and hepatoprotective effects of two products from *Cordyceps militaris* manufactured by Lavite Co., Ltd. *Vietnam Medical Journal* 511(2). https://doi.org/10.51298/vmj.v511i2.2142.

Ismail, E. A., Aly, A. A., & Atallah, A. A. (2020). Quality and microstructure of freeze-dried yoghurt fortified with additives as protective agents. *Heliyon* 6(10). https://doi.org/10.1016/j.heliyon.2020.e05196.

Kang, H. J., Baik, H. W., Kim, S. J., Lee, S. G., Ahn, H. Y., Park, J. S., Park, S. J., Jang, E. J., Park, S. W., Choi, J. Y., Sung, J. H., & Lee, S. M. (2015). Cordyceps militaris enhances cell-mediated immunity in healthy Korean men. *Journal of Medicinal Food* 18(10), 1164-1172. https://doi.org/10.1089/jmf.2014.3350.

Lee, C. T., Huang, K. S., Shaw, J. F., Chen, J. R., Kuo, W. S., Shen, G., Grumezescu, A. M., Holban, A. M., Wang, Y. T., & Wang, J. S. (2020). Trends in the immunomodulatory effects of Cordyceps militaris: total extracts, polysaccharides and cordycepin. *Frontiers in Pharmacology* 11, 575704. https://doi.org/10.3389/fphar.2020.575704.

Mijačević, Z., Bulajić, S., & Nedić, D. (2001). Survival and therapeutic potential of probiotic microorganisms in fermented milk. *Acta Veterinaria-Beograd* 51(5-6), 325-331.

Noel, P. L., Veeramachaneni, K., & O'Reilly, U. M. (2011). Baseline genetic programming: symbolic regression on benchmarks for sensory evaluation modeling. *Genetic Programming Theory and Practice IX*, 173-194. https://doi.org/10.1007/978-1-4614-1770-5_10.

Pham, V. T. (2022). *Optimizing the freeze-drying process for kefir milk snack bites* (Unpublished bachelor's thesis). Nong Lam University, Ho Chi Minh City, Vietnam.

Reddy, K. B. P. K., Madhu, A. N., & Prapulla, S. G. (2009). Comparative survival and evaluation of functional probiotic properties of spray-dried lactic acid bacteria. *International Journal of Dairy Technology* 62(2), 240-248. https://doi.org/10.1111/j.1471-0307.2009.00480.x.

Rosa, D. D., Dias, M. M., Grześkowiak, Ł. M., Reis, S. A., Conceição, L. L., & Maria do Carmo, G. P. (2017). Milk kefir: nutritional, microbiological and health benefits. *Nutrition Research Reviews* 30(1), 82-96. https://doi.org/10.1017/S0954422416000275.

Sun, Y., Shao, Y., Zhang, Z., Wang, L., Mariga, A. M., Pang, G., & Zhao, L. (2014). Regulation of human cytokines by Cordyceps militaris. *Journal of Food and Drug Analysis* 22(4), 463-467. https://doi.org/10.1016/j.jfda.2014.01.025.

Thuy, D. T. P., Anh, T. T. N., Thuy, N. T. T., Intaparn, P., Tapingkae, T., & Mai, N. T. (2021). Simple and efficient method for the detection and quantification of cordycepin content in cordyceps. *Chiang Mai Journal of Science* 48, 420-428. https://epg.science.cmu.ac.th/ejournal.

Truong, H. S., Le, M. K., Le, V. A., & Hoang, H. L. (2023). The effects of *Cordyceps militaris* on human health: A review. *Vietnam Medical Journal* 525(1). https://doi.org/10.51298/vmj.v525i1.5042.

Wu, X. F., Zhang, M., & Li, Z. (2019). Influence of infrared drying on the drying kinetics, bioactive compounds and flavor of *Cordyceps militaris*. *LWT - Food Science and Technology* 111, 790-798. https://doi.org/10.1016/j.lwt.2019.05.108.

Yamaguchi, S. K. F., Moreira, J. B., Costa, J. A. V., de Souza, C. K., Bertoli, S. L., & Carvalho, L. F. D. (2019). Evaluation of adding spirulina to freeze-dried yogurts before fermentation and after freeze-drying. *Industrial Biotechnology* 15(2), 89-94. https://doi.org/10.1089/ind.2018.0030.